GEOCHEMISTRY AND NOBLE GASES OF PERMAFROST GROUNDWATER AND GROUND ICE IN YUKON AND THE NORTHWEST TERRITORIES, CANADA

NICHOLAS CHARLES UTTING

Thesis submitted to the
Faculty of Graduate & Postdoctoral Studies
University of Ottawa
in partial fulfillment of the requirements for the
Ph.D. degree in Earth Sciences

Ottawa-Carleton Geoscience Centre
and
University of Ottawa
Ottawa, Canada

Thèse soumise à
Faculté des etudes supérieures et postdoctorales
Université d'Ottawa
en vue d'obtention du doctorate en
Sciences de la Terre

Centre Géoscientifique d'Ottawa-Carleton
et
Université d'Ottawa
Ottawa, Canada

Abstract:

In Canada's western Arctic, perennial discharge from permafrost watersheds is the surface manifestation of active groundwater flow systems, yet understanding the mechanisms of groundwater recharge and flow in periglacial environments remains enigmatic. This thesis addresses questions on how and where groundwater recharge occurs. Watersheds were selected in Yukon (Fishing Branch River at Bear Cave Mountain) and the Northwest Territories at latitudes spanning from continuous to discontinuous permafrost (five tributary rivers to the Mackenzie River from Wrigley to Aklavik). All are characterized by perennial flow with open water in the winter, and discharge from sedimentary formations of karstic carbonates and evaporate rocks. Determinations of groundwater contributions to discharge, mixing, recharge conditions and circulation times were made on the basis of a suite of analytical approaches involving measurements of major dissolved ions, $\delta^{18}O$, δD, $\delta^{13}C_{DIC}$, ^{3}H, noble gases and flow gauging was conducted at some sites.

The application of these tracers show that hydrogeological conditions and flow paths in permafrost terrains are surprisingly similar to those of temperate regions. Groundwater recharge was determined to be a mix of annual precipitation with contributions from snowmelt and precipitation. All systems investigated show that groundwaters have recharged through organic soils with elevated P_{CO_2}, which suggests that recharge occurs largely during summer when biological activity is high. Noble gas concentrations show that the recharge temperature was between 0 and 6 °C, which, when considered in the context of discharge temperatures, suggests that there is no significant imbalance of energy flux into the subsurface. Groundwater ages were found using the ^{3}H-^{3}He method and were dependent on flow path. By characterizing groundwater and surface water chemistry, the proportion of groundwater was found in numerous water courses.

The possible impact of ground ice formation and melting on noble gas concentrations in groundwater was considered. To assess this link, a new method to measure the noble gas composition of ground ice bodies was developed. The method can be used to determine the origin of ice, based on changes in noble gas ratios between ice

originating from compaction of snow (e.g. glacier ice) vs. ice originating from freezing of water. No significant fractionation of noble gases during groundwater freezing and ground ice formation was identified. Applied to determination of the origin of ground ice bodies, the method was shown to be both diagnostic of ice origin and un-encumbered by reactivity in the subsurface, which compromises the use of the dominant atmospheric gases (O_2 and N_2).

Résumé

Dans l'Ouest de l'Arctique canadien, la décharge pérenne dans certaines rivières en région de pergélisol est la manifestation en surface d'une circulation d'eau souterraine; cependant la compréhension des mécanismes d'écoulement et de recharge des eaux souterraines en région de pergélisol demeure énigmatique. Cette thèse s'intéresse à la question de savoir comment et où la recharge des eaux souterraines se produit. Des bassins versants ont été choisis au Yukon (Rivière Fishing Branch à Bear Cave Mountain) et dans les Territoire du Nord-Ouest à des latitudes s'étendant du pergélisol discontinu au pergélisol continu (cinq tributaires du Mackenzie entre Wrigley et Aklavik). Toutes ces rivières ont un écoulement d'eau pérenne avec des zones non gelées et une décharge dans des formations sédimentaires de roches carbonatées et d'évaporites. L'identification des contributions des eaux à la décharge, les mélanges, les conditions de recharge, et les temps de circulation ont été faits à partir d'analyses qui ont inclus les concentrations en éléments majeurs, leur valeur isotopique ($\delta^{18}O$, δD, $\delta^{13}C$, ^{3}H), ainsi que leur teneur en gaz rares. A certain des sites analysés des mesures d'écoulement ont été prises.

L'application de ces traceurs montre que les conditions hydrauliques et le chemin des écoulements en région de pergélisol sont similaires à ceux des régions tempérées. La recharge en eau souterraine a été identifiée comme étant un mélange de précipitations annuelles, avec des contributions de neige et de pluies. Tous les systèmes étudiés montrent que les eaux souterraines se sont rechargées en traversant des sols organiques avec une P_{CO_2} élevée, ce qui suggère que la recharge se produire largement durant l'été quand l'activité biologique est élevée. Cependant, les concentrations en gaz nobles montre que la température de recharge des eaux souterraines était entre 0 et 6 °C ce qui indique qu'il n'y a pas de déséquilibre de flux d'énergie à l'intérieur de la zone proche de la surface. L'âge des eaux a été déterminé par la méthode ^{3}H-^{3}He et cet âge est dépendant du chemin d'écoulement. En caractérisant les paramètres chimiques des eaux de surface et des eaux souterraines, il a été possible de trouver la contribution des eaux souterraines aux eaux surface.

Le possible impact de la formation et de la fonte de la glace souterraine sur les concentrations des gaz nobles a été considéré. Pour déterminer s'il y a un lien entre ceux-ci, une nouvelle méthode pour mesurer la concentration en gaz nobles dans les glaces souterraines a été développée. La méthode peut être utilisée pour déterminer l'origine de la glace; elle est basée sur les changements dans les rapports des gaz nobles entre la glace issue de la compaction de la neige (c'est-à-dire la glace de glacier) par opposition à la glace issue du gel de l'eau. Aucun fractionnement significatif des gaz nobles durant l'engel des eaux souterraines et la formation de glaces souterraines n'a été identifié. Appliquée à l'identification de l'origine des masses de glace enfouies, on a montré que la méthode pouvait permettre d'identifier l'origine des glaces souterraines sans qu'elle soit affectée par des réactions biologiques de sub-surface, lesquelles rendent inutilisables les gaz atmosphériques (O_2, and N_2).

Acknowledgements:

I would like to thank my thesis supervisor Dr. Ian Clark and co-supervisor Dr. Bernard Lauriol for their support, ideas and guidance over the course of this study. I'd also like to thank my thesis committee Dr. John Blenkinsop, Dr. Tom Kotzer and Dr. Michel Robin for guidance over the course of my thesis. I am grateful for the help from Dr. Ratan Mohapatra from the University of Ottawa noble gas lab for his help and guidance over the years. The staff of the G.G. Hatch isotope lab and geochemistry lab Paul Middlestead, Wendy Albi, Patricia Wickham, Ping Zhang and Monika Wilk for their help in conducting sample analysis. I should also like to thank Dr. Werner Aeschbach-Hertig (University of Heidelberg) for having me visit his lab in 2007; this visit was motivational and very enjoyable experience. I should also like to thank Neil Mochnacz (Department of Fisheries and Ocean) for the opportunity to sample with him in the Mackenzie valley and the support from DFO. I'd also like to thank Dr. Brewster Conant Jr. who participated it the same sampling campaigns and provided insights to the groundwater discharge along those rivers. I'd also like thank Dr. Denis Lacelle, for his ideas along the way.

The research in this thesis has been funded by numerous funding agencies including: NSERC, the Polar Continental Shelf Project, the Northern Scientific Training Program, the Department of Fisheries and Oceans, the Yukon Geological Survey, University of Ottawa: International Office and the University of Ottawa: Faculty of Graduate and Postdoctoral Studies.

I would also like to thank my friends for their support, and company on the endless coffee trips. I'd also like to thank my family for their continual support and encouragement. Finally I cannot thank Lieserl enough for her love, support and patience over the course of my thesis.

Chapter 1: Introduction

1.1 Introduction

The Arctic has received much attention in recent years due to increased activity in the north (e.g. oil and gas exploration) (McCracken *et al.,* 2007) and the observed and anticipated impacts of climate warming (Lawrence and Slater, 2005). These issues have resulted in initiatives such as the International Polar Year (2007-2008) and in Canada the construction of a new High Arctic Research Station (cited as PMO, 2010), which aim to better understand the changing conditions in the Arctic.

An area of permafrost research which, owing to its arcane nature, has received little attention is that of groundwater circulation in permafrost catchments, and the possible links with permafrost stability and climate variability (Zhao-ping *et al*., 2010; Muskett and Romanovsky, 2009; Frey *et al.,* 2007). If the climate continues to get warmer, permafrost could melt, resulting in a lower water table (Zhao-ping *et al*., 2010) and changes to the amount of groundwater storage (Muskett and Romanovsky, 2009). Deeper circulation of water is also likely to increase solute loading to creeks and rivers (Frey *et al.,* 2007). Additionally, the degradation of permafrost may result in new pathways for the migration of contaminants (Dyke, 2001). It is therefore timely to study groundwater in permafrost terrain to better understand where it flows and how it recharges.

Evidence for perennial groundwater discharge in permafrost catchments is found in a variety of periglacial features from open system pingos (Müller, 1959) to icings (e.g. Anisimova *et al.,* 1973; Clark and Lauriol, 1997; Hu and Pollard, 1997) and thermal groundwater springs (Michel, 1986; Clark *et al.*, 2001). However, an understanding of the fundamental hydrogeological components such as groundwater circulation rates, recharge environments, recharge rates and subsurface history are lacking. This thesis aims to build this understanding through the use of a variety of hydrological tools including aqueous geochemistry, environmental isotopes and noble gases.

1.2 **Permafrost**

Permafrost is defined as "*ground which remains at or below 0 °C for more than two consecutive years*" (NRC, 1988). Solutes in water may decrease the freezing temperature; therefore when temperatures are below 0 °C, it does not always mean the ground is frozen (French, 1996). Researchers interested in physical processes may use a different definition and refer to permafrost as "*ground that remains frozen for more than two consecutive years*". To clarify this ambiguity, the term 'perennially cryotic ground' is sometimes used to refer to ground which is below 0 °C (NRC, 1988). In this thesis, permafrost is used to refer to ground which is below 0 °C and is assumed to be frozen.

The periglacial environment refers to areas where permafrost is present (French, 1996). The periglacial environment represents about 23% of the earth's land surface (French and Shur, 2010). In locales where the mean annual air temperature is between -1 °C and -4 °C, permafrost is generally found in dry regions of peat lands, on north facing slopes and in other shaded areas. In regions where the mean annual air temperatures are between -4 °C to -8.5 °C, permafrost becomes thicker and more widespread. Where the mean annual air temperature is colder than -8.5 °C permafrost is continuous (Brown, 1971). The distribution of permafrost in Yukon and Northwest Territories (NWT) is shown in Figure 1- 1. Discontinuous permafrost tends to be metres to tens of metres thick, while continuous permafrost can be hundreds to over a thousand metres in thickness (Brown, 1971). The increase in permafrost thickness with increasing latitude is shown in Figure 1-2.

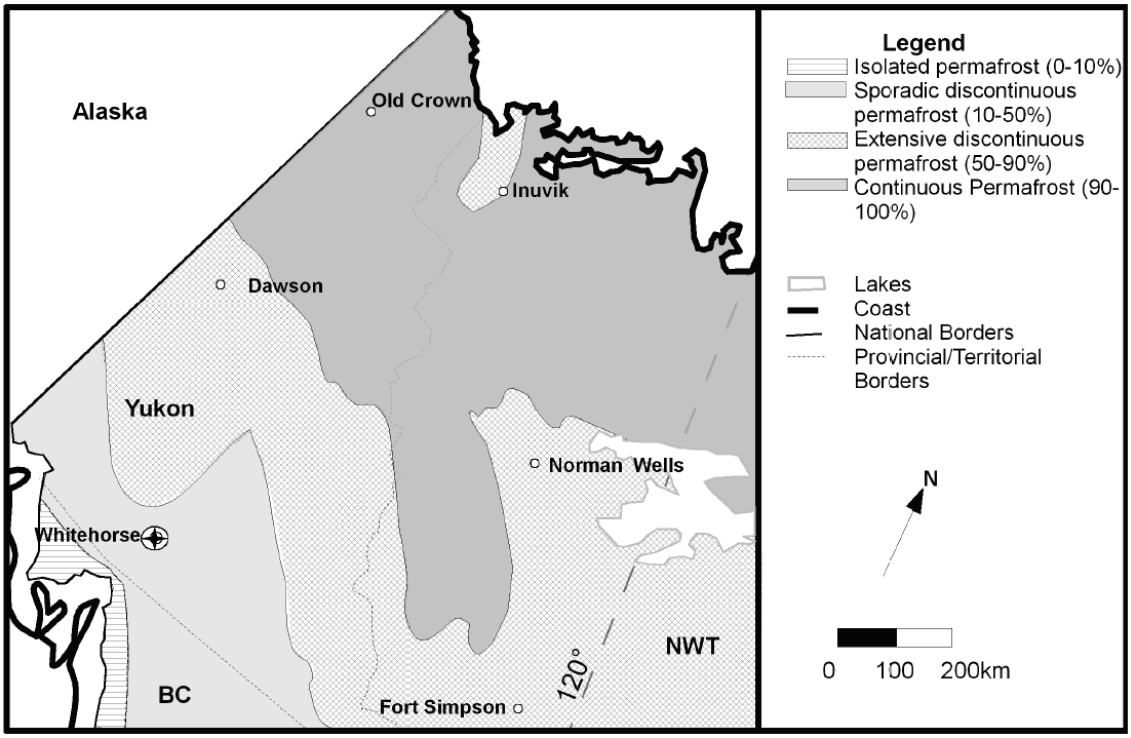

Figure 1- 1: Map of permafrost distribution in NWT and Yukon (Permafrost distribution from NRCan, 2003)

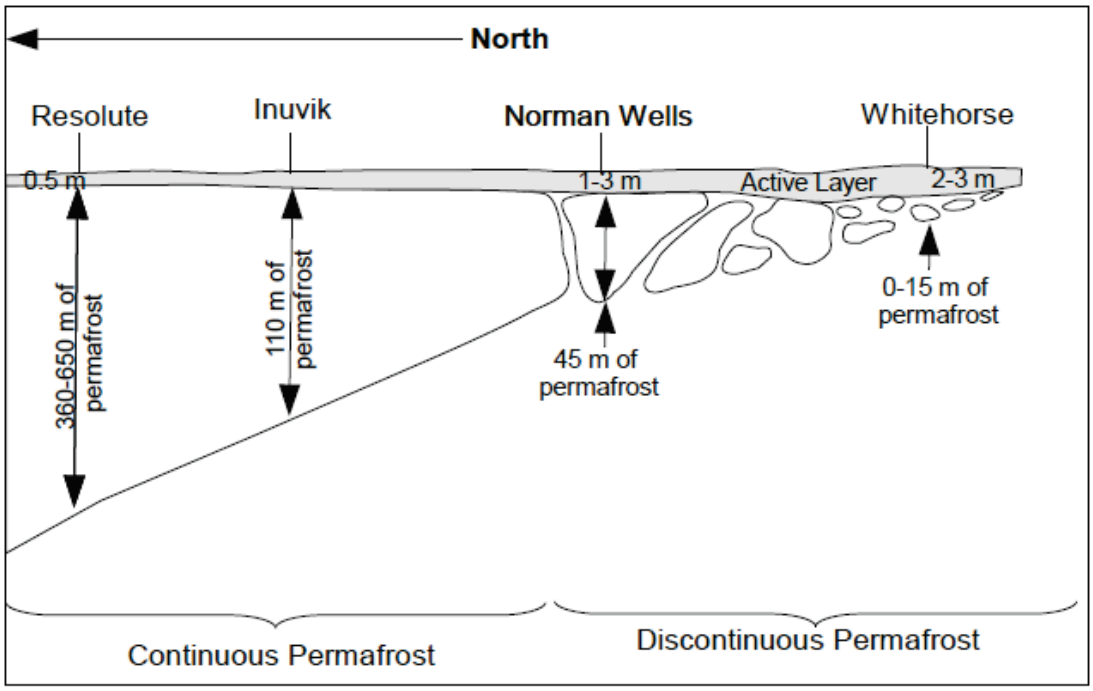

Figure 1- 2: Schematic cross section of permafrost thickness of northwestern Canada (modified from Brown, 1975; Péwé, 1982; Washburn, 1980)

1.2.1 Hydrology: Active Layer and Runoff

River discharge in permafrost basins is some combination of groundwater and runoff from within and over the active layer. The active layer is the surface layer which thaws on an annual basis and subsequently freezes at the end of the melt season (Davis, 2001). The depth at which permafrost is encountered is referred to as the permafrost table. In some cases there is a layer of ground which remains above 0 °C year-round in between the active layer and the permafrost table (Figure 1- 3). The freeze and thaw of the active layer has a profound effect on the hydrological cycle in the Arctic (e.g. Cederstrom *et al.*, 1953; Ferrians *et al.*, 1969; French, 1996). In permafrost terrain peak river discharge occurs later in the spring due to accumulations of snow and cool temperatures (Serrez and Barry, 2005).

The active layer may be only 15 cm thick in polar areas and up to 1 m thick in warmer areas (French, 1996). There may be a layer of peat within the active layer (Quinton and Marsh, 1999). In some areas the active layer has become thicker due to recent climate warming, for example from 1978 to 2006 the thickness of the active layer in northern Sweden increased at a rate of between 0.7 and 1.3 cm/yr (Akerman and Johansson, 2008). A thicker active layer may allow for greater groundwater recharge and also a change in water chemistry (Frey *et al.*, 2007). Permafrost temperatures have also been found to be increasing. In the central and northern part of the Mackenzie Valley permafrost temperatures have increased by 0.3 to 0.6 °C per decade from the mid 1980's to midway through the first decade of the 2000's and there is warming at most sites in North America (Smith *et al.*, 2005; Smith *et al.*, 2010).

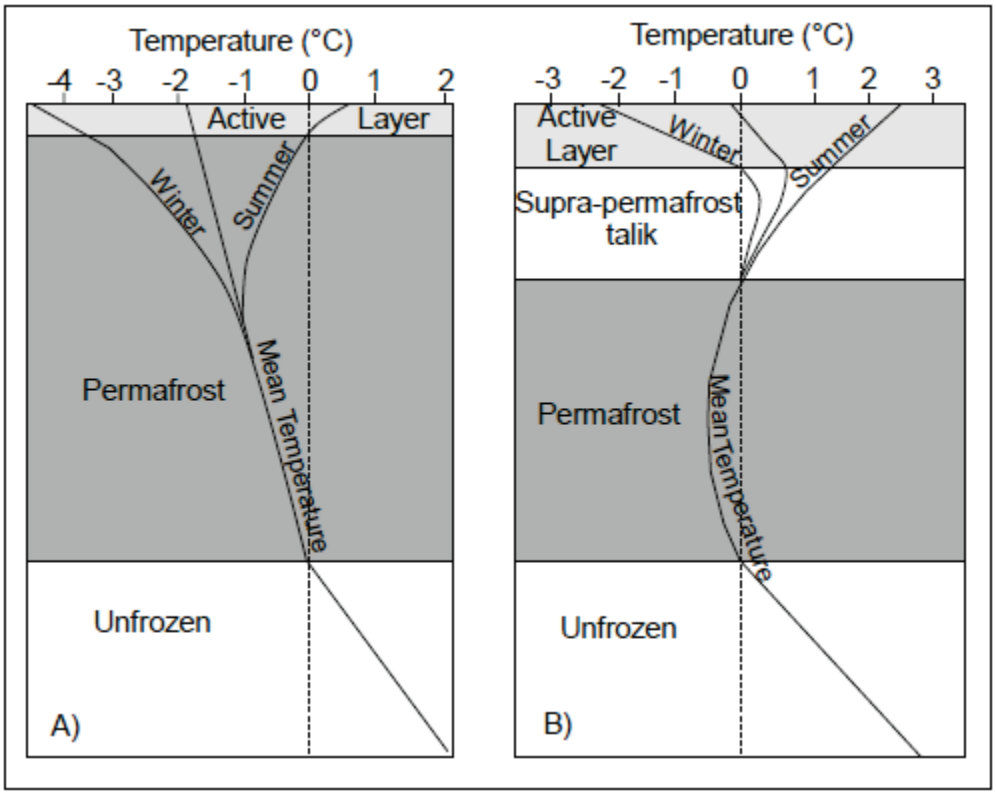

Figure 1- 3: Schematic thermal profile of permafrost ground. A) Shows ground which is perennially frozen and overlying active layer during summer. B) Shows ground where permafrost table is separated from the active layer by an unfrozen zone (Scale = not defined) (Modified from Davis, 2001).

Numerous studies have investigated the chemical and physical changes that occur in the active layer (McNamara *et al*., 1997; Hayashi *et al*., 2004; Kokelj and Burn, 2005; Quinton and Pomery, 2006). Quinton and Pomery (2006) studied some of these changes in a single watershed northeast of Inuvik. In early spring, drainage was characterized by the presence of Na^+ and Cl^- ions which was likely from dry deposition on the snow that accumulated over the winter. With more snow melt and spring precipitation there was greater dilution. As the active layer increased in thickness, interflow deepened and the pH increased, likely due to the weathering of mineral material (Quinton and Pomery, 2006). As snow disappeared, runoff interacted more with the soil and the runoff became dominated by Ca^{2+} and Mg^{2+} ions from the weathering of mineral material deeper in the soil. The solute composition and concentration changed through the melt season, but remained low compared to those of groundwater. For example, within the watershed studied by Quinton and Pomery (2006) stream water samples contained maximum Ca^{2+} and

Mg^{2+} concentrations of 11 ppm and 5 ppm respectively, which was lower than concentrations in most groundwaters sampled in permafrost terrain (e.g. Clark *et al.,* 2001; Michel, 1986). The lower total dissolved solids (TDS) of active layer waters is presumably due to the shorter residence time of water. Similar processes are observed in the Wolf Creek watershed 15 km south of Whitehorse (Carey and Quinton, 2004; 2005).

Karsted bedrock at surface can host active layer water. In Svalbard, Norway, a proglacial groundwater system flows during the summer through dissolution porosity in gypsum/anhydrite, limestone and dolomite, resulting in waters dominated by Ca^{2+}-Mg^{2+}-HCO_3^--SO_4^{2-} (Dragon and Marciniak, 2010). This shallow groundwater system freezes up each year, making it susceptible to seasonal changes in temperature and precipitation. A similar system exists along Little Fish Creek in NWT, Canada, where there are non-perennial springs of water with high Ca^{2+} and SO_4^{2-} concentrations (Clark *et al.*, 2001).

1.2.2 Groundwater and Talik

Talik is a zone in permafrost which remains unfrozen year-round and in which groundwater can flow (Muller, 1947). Taliks may exist as supra-permafrost, intra-permafrost or sub-permafrost locations (Figure 1- 4) (Tolstikhin and Tolstikhin, 1976). Different types of talik exist in different permafrost scenarios. For instance, a hydrochemical talik remains unfrozen due to water with high TDS. A hydrothermal talik is one which remains above 0 °C due to the heat imported by the water (French, 1996). Groundwater may either have latent heat from recharge or may gain heat from the earth's crust.

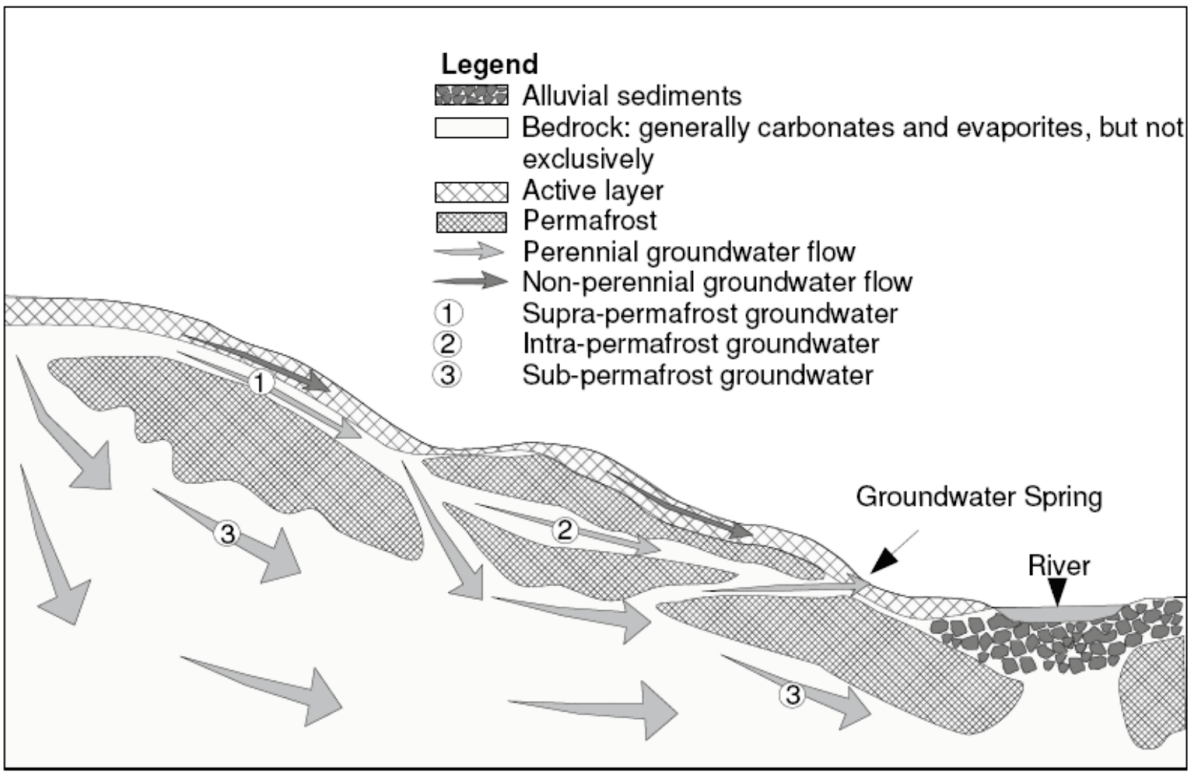

Figure 1- 4: Conceptual model of groundwater distribution in flow in permafrost terrain (Modified from French, 1996).

Groundwater flow in permafrost often occurs in karst with recharge occurring by diffuse flow or through dolines (Ford and Williams, 2007). Karstic groundwater systems are known in numerous areas of northwestern Canada such as along the Firth River in northern Yukon (Clark and Lauriol, 1997), rivers in the Norman Wells region of the NWT (Michel, 1986), the Nahanni River (Brook and Ford, 1980), and near Great Bear Lake, NWT (Van Everdigen, 1981). In northeastern Canada, groundwater drainage occurs in permafrost on Akpatok Island (Lauriol and Gray, 1990). In Alaska, there are groundwater-fed streams on the northern coast near Prudhoe Bay (Craig and McCart, 1975). Many of these systems were established when the climate was warmer prior to glaciation, however they are able to persist under the colder present conditions (Ford and Williams, 2007). In northeastern Russia, groundwater flows in sedimentary rocks, but unfortunately much of the literature on these locales is in Russian (Glotov, 2009).

On the island of Svalbard permafrost is 100 to 400m; however groundwater recharge occurs sub-glacially (Haldorsen and Heim, 1999; Haldorsen *et al.,* 2010). Glacier

area and melt is climate dependant, as such subglacial recharge is also climate dependent. The west Lovébreen glacier has shrunk since the Little Ice Age resulting in a decrease in groundwater recharge and discharge. If the glacier continues to decrease in size, the discharge zone may freeze up (Haldorsen and Heim, 1999).

In the Canadian Rockies near the Columbia Ice Fields, there is sporadic alpine permafrost. In this area there is groundwater flow through the extensive Castleguard karst system (Ford, 1983). In the Canadian High Arctic, evidence for groundwater flow seems rare, except on Axel Heiberg Island (McKay *et al.,* 2005; Omelon *et al.,* 2006 and Pollard, 2005). The water discharging from these springs is a mixture of water which recharged subglacially and water from a talik below a lake. The water flows through dissolution porosity in evaporite rocks resulting in brine groundwater with high TDS. Grasby *et al.* (2003) describe perennial springs discharging supraglacially on Ellesmere Island.

Permafrost groundwater flow in bedrock tends to occur in soluble sedimentary rocks such as carbonates and evaporites. There are large parts of the Arctic in Canada and Scandinavia which are underlain by less soluble igneous and metamorphic rocks. As these rocks are less soluble, the dissolution porosity does not develop restricting groundwater flow. In general, Scandinavia is warmer and permafrost is far less extensive than at similar latitudes in North America (IPA, 2010). In discontinuous permafrost, there may be greater opportunities for groundwater flow in other rock types. For example on the northeastern coast of Russia, there is groundwater flow in some fractured and porous volcanic rocks (Glotov and Glotova, 2008).

Taliks also may exist in unconsolidated sediments; this often occurs beneath rivers (French, 1996). The morphology and size of such taliks are dependent on the size of the river and local distribution of permafrost. For example, beneath the Eagle River borehole data show that talik has a sharp boundary and ranges from 20 m to over 34 m in depth (Crampton, 1979). Under the Sagavanirktok River in Alaska, ground penetrating radar was used to determine that in winter, the talik was 50 m wide but only 1 m thick (Arcone *et al*., 1998).

Cool groundwater discharge may freeze soon after reaching the surface. If a river freezes to the bottom and there is groundwater discharge, water pressure will build up and crack the ice. When groundwater overflows to the surface during the winter months, a thick layer of ice forms known as an Icing (english), Aufeis (german), Naledi (russian) and Glacage (french). Icings were first described in Russia (Wrangel, 1841; Anisimova *et al.,* 1973), and have since been described in many polar areas for example the Brooks Range, Alaska (Yoshikawa *et al*., 2007); pro-glacially in Svalbard (Bennett *et al.*, 1998); in Finland (McFadden, 1990); and in Iceland (Venzke, 1988). In Canada icings have also been observed in numerous areas. A large icing is found on the Firth River, Yukon, where 12% of basin groundwater discharge is trapped. In central Yukon, icings form in the North Fork Pass area (Hu and Pollard, 1997). In the Canadian High Arctic, icings form at the Axel Heiberg Island springs (Pollard, 2005) and in the Akshayuk Pass area of southern Baffin Island (Lacelle *et al.,* 2006).

Where groundwater discharges at a sufficiently high rate, the water may not freeze immediately and open water persists year-round, for example, the Fishing Branch River, Yukon discussed in Chapter 4. Perennially open water is most often caused by discharging thermal waters. Such waters have been studied along Little Fish Creek, (Clark *et al.,* 2001) as well as some rivers in the Norman Wells region of the NWT (Michel, 1986), MacArthur Hot Springs (Yukon) (van Everdingen, 1974). In Chapter 3 of this thesis, both thermal and non-thermal groundwaters are studied in the Mackenzie River Basin from rivers with open water.

1.2.3 Ground Ice and Cave Ice

Hydrology in permafrost regions also involves the formation and degradation of ground ice. Permafrost degradation in ice-rich terrain may cause retrogressive thaw slumps (Lantuit and Pollard, 2008; Lacelle *et al.*, 2010). The melting of massive ground ice bodies may result in thaw slumps (French, 1996). Slumps may be triggered by undercutting erosion due to stream or wave action, or by active layer failure, or by an increase in precipitation. Slumps generally stabilize 30 to 50 years after the initial perturbation (French

and Egginton, 1973). Slumps can expose sediments which have been frozen and not exposed to weathering for thousands of years.

Cryostratigraphy is the study of the sedimentological features of frozen ground (French and Shur, 2010). The expansion of water during freezing results in processes in frozen ground being different to non-frozen ground. Ice below ground may be invisible at the surface for example pore ice. Ice below ground may also form small hills as is the case with pingo ice. Large ground ice bodies originate from buried surface ice or have an intrasedimental origin (Mackay, 1989).

Intrasedimental ice may form by injection of groundwater or by ice nucleation in the subsurface (French and Shur, 2010; Mackay and Dallimore, 1992). The most common form of injection ice is vein ice. Intrasedimental ice may exist as a single vein about 1 cm in width or as a thick wedge shaped body between 0.5 -4 m thick (French and Shur, 2010). These ice bodies grow by cryosuction, where a zone of ice forms as the freezing of water creates a concentration gradient which moves towards the frozen front, continually creating suction. Alternatively, ground ice may originate as glacial ice, which was buried during an advance or a buried snow bank covered by windblown sediments (Lacelle *et al.,* 2007; Lacelle *et al.,* 2009b).

Karst plays an important role in the flow of groundwater in permafrost; however in some areas there is ice in caves. The ice formations that exist in some caves may be seasonal or perennial (Ford and Williams, 2007) and may form from either inflowing groundwaters or from atmospherically-derived vapour. Ice flowstone and ice stalagmites may form from dripping water (Ford and Williams, 2007; Lacelle *et al.*, 2009a). Condensation from circulation of summer air can build up cave ice formations, in some cases forming ice plugs that may completely block cave passages. Alternatively ice may form from the alteration of hoar frost, or may develop from freezing of summer waters over top winter ice (Lauriol, 1968; Lauriol and Clark, 1993).

1.3 **Knowledge gaps**

There remain gaps in the understanding of permafrost groundwaters in the Arctic. Woo *et al.* (2000), Woo and Marsh (2005) and Woo *et al.* (2008), provide summaries of recent research progress in permafrost hydrology from 1995 until 2008, including their assessment of the state of permafrost groundwater research: "*There has also been an unplanned neglect on the groundwater aspects, which has left a large void since the 1980s.*" (Woo and Marsh, 2005). The research which has been conducted on groundwater has focused on several areas of interest. For example, Clark and Lauriol (1997) and Hu and Pollard (1997) look at the formation of icings. The discharge of saline groundwater in the High Arctic on Axel Heiberg has been the focus of numerous publications (e.g. Andersen *et al.,* 2002; Heldman *et al.,* 2005 and Pollard, 2005). Clark *et al.* (2001) also focus on a special case with the study of thermal groundwater's along Little Fish Creek, NWT. Another geographic area of focus has been the North Slope of Alaska where several studies have looked at the sources of groundwater and the formation of icings (Hinzman *et al.,* 2003; McNamara *et al.,* 1997; Yoshikawa *et al.,* 2007). The Woo *et al.* (2008) summary cites eight groundwater articles, of which there is a geographic focus on three areas, with two of these areas being characterized by what are likely unusual flow systems (e.g. thermal springs and non-thermal saline springs).

Concerns over the impact of climate change mean questions that had previously been ignored now have relevance. For example, is there evidence that warm recharging groundwater may cause permafrost degradation? What methods can best determine the temperature of groundwater recharge? Previous research has proposed mechanisms for groundwater recharge in permafrost terrain; however can these be further refined using newer geochemical techniques and more extensive sampling? Some groundwater ages have been previously determined in permafrost, however can newer methods (e.g. ^{3}H-^{3}He) be used to further refine these and better estimate flow rates? Although groundwater discharge has been characterized along many rivers in the Yukon and NWT, only a few studies (e.g. Clark and Lauriol, 1997; Clark *et al.,* 2001) have determine relative or absolute contributions of bedrock groundwater to Arctic rivers.

Recent studies on ground ice have exploited the ratios of N_2/Ar and O_2/Ar gases as a way of determining the origin of ice bodies in Yukon and NWT (e.g. Cardyn *et al.*, 2007; Lacelle *et al.*, 2007; Lacelle *et al.,* 2009b; St. Jean *et al.,* 2011). This method has been found to be compromised by alteration of the gas ratios by microorganisms living in the ice matrix consuming and/or producing O_2, N_2 and CO_2 (Radtke *et al*., 2010) (for more detail, see 2.3.2 Entrapped Gases in Ground Ice). This thesis explores the use of noble gas ratios as an alternative method to determine the origin of ice.

These research questions are summarized on a schematic cross section of permafrost terrain (Figure 1- 5). This diagram highlights some of the unknowns and questions that this thesis aims to answer.

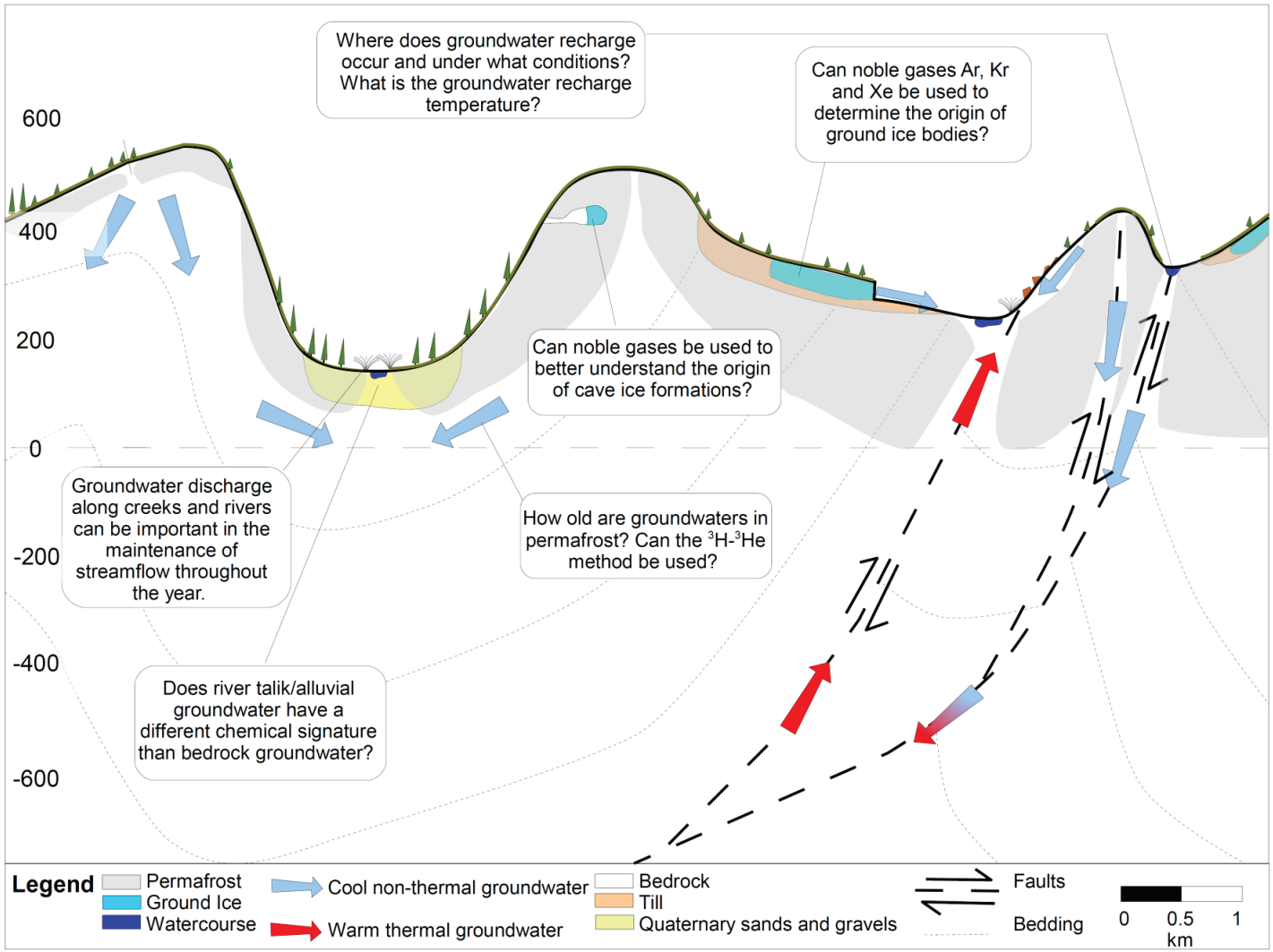

Figure 1- 5: Schematic diagram of groundwater and ground ice in permafrost in Yukon and Northwest Territories and some of the main questions that this thesis aims to answer.

1.4 **Objectives**

This thesis aims to fill the knowledge gaps outlined above and to test new geochemical methods in the study of permafrost hydrogeology and Quaternary history. A predominant theme is the use of noble gases and geochemical methods to study groundwater and ground ice. Three main objectives are:

i) To isolate the major ion geochemical signatures of different water sources contributing to selected Arctic creeks and rivers with the focus on distinguishing groundwater from surface runoff. The concentrations of Cl^- and SO_4^{2-} ions are assumed to be conservative and used to calculate the relative and absolute amounts of groundwater in watercourses.

ii) To use chemical and isotopic methods to determine the recharge environment:
   a. Use $\delta^{13}C_{DIC}$ and P_{CO2} to determine if groundwater recharge occurred under open or closed conditions with respect to the supply of CO_2, and investigate weathering of carbonate bedrock in recharge areas.
   b. Use $\delta^{18}O$- δD to determine the precipitation sources of groundwater (eg. snow melt vs. summer rains).
   c. Use noble gas concentrations (Ne, Ar, Kr and Xe) to determine recharge temperatures.
   d. Evaluate groundwater circulation rates, based on the ^3H-^3He dating method.

iii) Ground ice may have an intrasedimental origin or buried origin. The different origins relate to different formational processes (accumulations of snow vs. freezing of water). These processes impart different gas ratios. This thesis aims to determine the effectiveness of using noble gas ratios (δAr/Xe, δKr/Xe) in determining the origin of ground ice.

These objectives are studied in three areas of Yukon and NWT, presented in Chapters 3, 4 and 5.

- Chapter 3 is an overview of hydrogeochemistry and groundwater discharge of springs in the Mackenzie River Basin, NWT. This chapter uses geochemistry and noble gases to determine recharge conditions, groundwater age and relative proportions of groundwater in the studied watercourses.
- Chapter 4 is a multi-year watershed case study of the Fishing Branch River where groundwater discharges all year. This chapter uses geochemistry and noble gases to determine recharge conditions, groundwater age, and the absolute amount of groundwater discharge. Using the groundwater discharge the groundwater recharge rate is estimated. This chapter has been submitted as a paper to the journal Permafrost and Periglacial Processes.
- Chapter 5 is a study of using noble gases to determine the origin of ground ice bodies. The noble gas ratios were measured in the ground ice bodies and compared to the expected ratios in ice formed from water vs. ice formed from the compaction of snow. This chapter will be submitted as a paper to the journal Quaternary Research.

1.5 Statement of Original Contribution

This thesis applies isotopic and geochemical methods to groundwater in permafrost where there has been limited research and also develops new application for these methods. The major original contributions and findings of this work are:

- To the knowledge of the author this is the first study using the noble gas recharge temperature method to groundwaters in permafrost terrains and the first to use tritium helium dating to groundwaters in permafrost terrains.
- This study looks at a larger geographic area than many other studies, with samples being collected over a large area of Yukon and NWT, as opposed to single watersheds. The wide focus of this research allows for general conclusions on groundwater recharge in permafrost to be made, for example that recharge occurs through organic soils during summer and often occurs at higher elevations.
- This study pioneers the use of noble gases as a method for determining the origin of ground ice bodies.

Chapter 2: Methods

2.1 Introduction

Numerous geochemical and isotopic methods have been used together with physical hydrological measurements in permafrost watersheds (e.g. Clark *et al.*, 2001; Hayashi *et al.*, 2004, Quinton and Pomery, 2006). These studies used geochemistry and isotopes to determine the sources of water over time and were combined with physical measurements to determine absolute values of flow. For this study of groundwater and ground ice in permafrost watersheds of the northwest Yukon and NWT, new approaches of study were applied along with established ones. These were based on noble gas concentrations, dissolved inorganic carbon (DIC, $\delta^{13}C$, P_{CO_2}), pH, $\delta^{18}O$, δD, together with stream discharge measurements and temperature logging. In this chapter the theory of the methods used is presented. Additional detail for specific applications is provided in the chapter in which the method is used, as well as in Appendix B.

2.2 Physical Methods

2.2.1 River Flow

Flow was measured at a variety of locations along the Fishing Branch River (Chapter 4) in order to determine incremental increases in flow from groundwater discharge. This has been done using the area-velocity method (Dingman, 2002). A transect is made of a water course at perpendicular to flow. Water depth and velocity are measured approximately 20 times at set intervals across the channel. The depths, and flow velocities are used to determine the volume of water per unit time.

2.2.2 Traditional Cryostratigraphic Methods

The morphology of ground ice bodies is dependent on the origin of the ground ice body. Traditional cryostratigraphic methods focus on using the morphology of ice and surrounding sediments to determine the origin of the ice body (French and Shur, 2010). For example, the shape of an ice wedge in cross section is diagnostic of its formation, while buried glacier ice may have layers of sediment embedded in it (Klassen and Shilts, 1987).

Although buried glacier ice may contain sediment, the same can be true for segregated ice which has formed in place. This ambiguity has lead researchers to look for other ways of determining the origin of ground ice bodies, as discussed later in section 2.3.2.

2.3 Geochemical and Isotopic Methods

Physical methods for the study of ground ice and groundwater can be complemented by the use of geochemical and isotopic methods. In the study of groundwaters, geochemistry can be applied to various applications including the determination of weathering rates, flow path and groundwater mixing components (e.g. Appelo and Postma, 1993; Clark *et al.*, 2001). Chemical tracers have also been used in the study of ground ice (Leibman, 1996).

The stable isotopes $\delta^{13}C$, $\delta^{18}O$ and δD have increasingly been used in the study of groundwater recharge and the origin of ground ice bodies. The use of these isotopes focuses on how they are fractionated by biological, chemical and physical reactions. δD-$\delta^{18}O$ are measured in water. The ratios of these isotopes in precipitation and subsequently in groundwater are largely dependent on fractionation during evaporation and condensation. For meteoric precipitation, the average slope of the $\delta^{18}O$ vs. δD regression is 8.13 with a deuterium excess of 10.8‰ (Equation 2- 1). In temperate regions, groundwater has $\delta^{18}O$ and δD values close to the mean annual average for $\delta^{18}O$ and δD found in precipitation in a given area. This may differ for permafrost regions due to a potential discrimination against winter precipitation which may be lost to surface runoff before groundwater recharge can occur.

Equation 2- 1: $\delta D = 8.13\delta^{18}O + 10.8$ (Rozanski *et al.,* 1993)

A groundwater that deviates from the local average and meteoric water line has been altered by fractionation processes (Clark and Fritz, 1997). For example, if a groundwater has an isotopic signature that is depleted compared to the mean annual isotopic composition and plots along the regression slope, this may indicate recharge at a higher elevation. If water plots to the right of the local meteoric water line on a graph of $\delta^{18}O$ and δD, this indicates the water may have underdone evaporation prior to recharge.

Fractionation also occurs during freezing and can be exploited in determining the origin of massive ice bodies (Lorrain and Demeur, 1985; Mackay and Dallimore, 1992; Lacelle *et al.,* 2004). This method exploits the isotopic differences between meteoric precipitation and isotope fractionation that occurs during freezing of water. Firnified ice (transformation of snow to ice as on a glacier) will yield δD - $\delta^{18}O$ values which plot near the local meteoric waterline. Freezing of liquid water causes isotopic fractionation resulting in a different slope and deuterium excess. If the slope of the regression is less than 7, the ice likely formed from freezing of liquid water as opposed to compaction of snow (glacier ice, buried snowbank) (Lacelle and Clark, 2011).

There is variability in the deuterium excess with different formation processes; the value d (deuterium excess, Equation 2- 2) is plotted against the value of δD. Compacted meteoric precipitation will have a slope of 0.019, while if water freezes under Rayleigh fractionation, the slope is expected to be -0.295 (Lacelle and Clark, 2011). However, due to variability in freezing processes under Rayleigh fractionation, the slope can be similar to the slope of samples with meteoric origins, and therefore this has not been found to be a very reliable method of determining the origin of ice bodies (Lacelle and Clark, 2011).

Equation 2- 2: $d = \delta D - 8\delta^{18}O$

In groundwaters δD and $\delta^{18}O$ provide information on the source of recharging water and the evolution of that water. Measurements of $\delta^{13}C_{DIC}$ are complementary to this and provide information on recharge conditions, CO_2 uptake in the soils and weathering. The decay of organic matter in soil produces CO_2 which is in turn dissolved by recharging groundwater (Clark and Fritz, 1997). Water that dissolves CO_2 in most soils will have an initial $\delta^{13}C_{DIC}$ value of ~ -23‰. The dissolution of CO_2 in water results in fractionation of ^{13}C as do the reactions between H_2CO_3, HCO_3^- and CO_3^{2-}. The acidity in the water is then consumed during weathering. If the minerals weathered are marine carbonates, they typically that have a $\delta^{13}C$ of around 0‰, which results in enrichment of the $\delta^{13}C_{DIC}$ value. During open system weathering there is a continual supply of CO_2 and the resulting water will have a $\delta^{13}C_{DIC}$ between -15 ‰ and -18 ‰. In closed system weathering water dissolves CO_2 during recharge and subsequently weathers carbonate minerals along the flow path, the

resulting $\delta^{13}C_{DIC}$ will be approximately -12‰. Because water which recharges through soil is more acidic due to the dissolution of CO_2, this water may in turn dissolve more carbonate material. If the partial pressure of CO_2 decreases, for example after groundwater discharge, CO_2 may degas, resulting in calcite super-saturation.

2.3.1 Gases in Geochemistry

Gases dissolved in water and entrapped in ice have received increased attention in recent years due to the unique information they may provide on groundwater and ice origin. In groundwaters, dissolved gases may provide information about chemical and biological reactions (e.g. oxidation, methanogenesis) (Appelo and Postma, 1993). Alternatively, some gases may be added to water by radioactive decay either from isotopes in water or rock (e.g. $^{3}H \rightarrow ^{3}He$, $^{235,238}U$ and $^{232}Th \rightarrow ^{4}He$)(Ballentine and Burnard, 2002). Quaternary geologists have found that occluded gases can be useful in determining the origin of ground ice (Cardyn *et al.*, 2007).

2.3.2 Entrapped Gases in Ground Ice

Occluded gases can be used in determining whether ground ice bodies formed from snow or liquid water. This method exploits the differences in solubilities of different gases in water resulting in gas ratios different from those in atmospheric air (Cardyn *et al.*, 2007). Subsurface ice may originate from snow (buried glacier ice, buried snow bank) or the freezing of water (injection ice). The ratios of gases in the ice will reflect whether the ice originated from snow or liquid water. Several studies have used N_2/Ar and O_2/Ar as a way of determining the origin of ice bodies in Yukon and NWT (e.g. Cardyn *et al.*, 2007; Lacelle *et al.*, 2007; Lacelle *et al.,* 2009b; St. Jean *et al.,* 2010). The preceding studies have successfully used these gases; however, it was found that some ice samples appear to deviate from the two-component mixing line between ice from air-equilibrated water and atmospheric air. These deviations have been linked to microorganisms living in the ice matrix consuming and/or producing O_2, N_2 and CO_2 (Radtke *et al*., 2010). While such reactions provide data on the geochemical and biological environment of the ice, they

compromise the use of these gas ratios as a method of distinguishing firnified ice (glaciers, snowbanks) from ice derived from the direct freezing of water.

Noble gases are inert and therefore affected only by physical processes. Some previous studies have analysed noble gas concentration in glaciers (e.g. Serveringhaus *et al.*, 2003; Serveringhaus and Battle, 2006; Ahn *et al.*, 2009). Ahn *et al.* (2009) exploited the greater solubility of Xe relative to Ar in water to identify glacier melt layers from non-melted layers. Chapter 5 presents a novel method to determine the origin of ground ice bodies using Ar, Kr and Xe. The method complements other tools for characterizing ground ice in assessing ice genesis and mechanisms of emplacement.

2.4 **Noble Gases**

There are six noble gases: helium, neon, argon, krypton, xenon and radon, in order of atomic number. This study focused on the first five. Radon is radioactive with a short half-life and not used in this research. These gases are non-reactive as they have complete outer electron shells. The noble gases make up less than one percent of the atmosphere (Table 2- 1) and each has several different isotopes. Some of these isotopes are the product of radioactive decay. The applications of these gases include groundwater studies, dating of geologic samples, and analysis of meteorite samples in cosmochemistry studies (for general review: Porcelli *et al.,* 2002). The low concentrations of these elements mean the analysis is complicated and expensive. In this study, noble gases have been used to determine groundwater recharge temperatures, groundwater circulation rates and the origin of ground ice formations.

Table 2- 1: Atmospheric concentration of Noble gases. (from Andrews, 1992)

Element/Isotope	Volume in Atmosphere (%)	Mol % of isotope
^{3}He	6.8E–10	1.4E–04
^{4}He	5.2E–04	100
Total helium	*5.2E–4 (partial pressure = 5.239E^{-6} atm)*	
^{20}Ne	1.7E–03	91.05
^{21}Ne	4.7E–07	0.01
^{22}Ne	1.6E–04	8.94
Total neon	*1.8E–3 (partial pressure = 1.818E–5 atm)*	
^{36}Ar	3.2E–03	0.33
^{38}Ar	5.9E–04	0.06
^{40}Ar	9.3E–01	99.6
Total argon	*9.3E–1 (partial pressure = 9.34E–3 atm)*	
^{78}Kr	4.0E–07	0.35
^{80}Kr	2.6E–06	2.27
^{82}Kr	1.3E–05	11.56
^{83}Kr	1.3E–05	11.55
^{84}Kr	6.5E–05	56.9
^{86}Kr	2.0E–05	17.37
Total krypton	*1.1E–4 (partial pressure = 1.139E–6 atm)*	
^{124}Xe	8.30E-09	0.1
^{126}Xe	7.70E-09	0.09
^{128}Xe	1.70E-07	1.92
^{129}Xe	2.30E-06	26.44
^{130}Xe	3.50E-07	4.08
^{131}Xe	1.80E-06	21.18
^{132}Xe	2.30E-06	26.89
^{134}Xe	9.00E-07	10.44
^{136}Xe	7.60E-07	8.89
Total Xenon	*8.6E-6 (partial pressure = 8.6E-8 atm)*	

There has been limited research applying noble gas methods in permafrost terrain. Greene *et al.* (2008) used noble gas concentrations to determine the origin of deep groundwaters in the Con Min, NWT. Waters were found to have originated from the mixing of evaporated Devonian sea water with glacial melt water. The Con Mine study

provides insights into deep groundwaters beneath permafrost, however it provides little insight into shallow younger waters. Dissolved gases were used to determine the origin of groundwater discharging from saline groundwater springs on Axel Heiberg Island (79°N) (Mckay *et al.*, 2005). These springs were believed to recharge either from lake water or subglacial melt water. The ratio of N_2/Ar in lake water is 37, while the atmospheric ratio is 82. This analysis indicated that groundwater was a 1:1 mix of lake water and melted glacial water that circulated beneath deep permafrost.

2.4.1 Noble gases: Recharge temperature

The solubility of noble gases in water is dependent on temperature, pressure and salinity. Most groundwaters are fresh enough that the salinity can be ignored (Mazor, 1991). The amount of gas dissolved in water can be determined using Equation 2- 3.

Equation 2- 3: $C_{(ccstp/cc)} = B_{(ccstp/cc/atm)} \cdot P_{(atm)}$

Where $C_{(ccstp/cc)}$ is the concentration of gas in water at standard temperature and pressure, $B_{(ccspt/cc/atm)}$ is the Bunsen coefficient at a given temperature and $P_{(atm)}$ is the partial pressure of the gas in atmospheres. The Bunsen coefficient is the volume of gas at 0°C which can be absorbed by a volume of liquid at a given temperature with a partial pressure of 1 atmosphere. If the recharge elevation is approximately known, the atmospheric pressure can be found, and the only variable which can affect gas solubility is temperature (Mazor, 1991)(Figure 2- 1). Once groundwater enters the saturated zone, there is no longer any exchange of noble gases with the atmosphere, therefore concentration and isotopic ratios are conserved. Groundwater recharge is, in most cases, a slow process, meaning the noble gas temperature is representative of the mean annual temperature (Stute *et al.*, 1995). Determining groundwater temperature from noble gas concentrations involves using the concentrations of multiple gases, ideally neon, argon, krypton and xenon (Kipfer *et al.,* 2002). Helium is not used in these calculations as its concentration is affected by the products of radioactive decay (Kipfer *et al.,* 2002). The concentration of xenon is the most sensitive to temperature and the lighter gases are progressively less sensitive to temperature.

When determining groundwater recharge temperature the concentration of xenon cannot simply be converted to temperature. While biological and chemical reactions do not alter noble gas concentrations, they can be altered by physical processes (Kipfer *et al.,* 2002). The most important process is the addition of excess air. During recharge, water often dissolves more air than is calculated for air-equilibrated water using the Bunsen solubility equation. This happens when bubbles are forced into solution due to processes like water table changes. High excess air may be attributed to large water table changes (Manning and Caine, 2007), while undersaturation may be linked to groundwater pumping (Aeschbach-Hertig *et al.*, 2008). Neon solubility is less sensitive to temperature changes than argon, krypton or xenon. The neon concentrations can be used to correct for excess air. The amount of excess air can then be subtracted from the other gases so that a recharge temperature may be calculated (Figure 2- 2).

The addition of excess air means the system is not at equilibrium and the gas concentrations may subsequently change due to different processes. Three models exist to explain these processes: i) unfractionated excess air, ii) partial re-equilibrium with the atmosphere iii) close-system equilibrium with entrapped air (Kipfer *et al.,* 2002). Un-fractionated excess air has atmospheric gas composition. In the partial re-equilibrium model, air is entrapped and dissolved; however, being supersaturated in air there is diffusive gas loss. Under the closed systems equilibrium model there is partial dissolution of gas bubbles, which alters the gas ratios in the excess air component. For an expanded explanation of these processes see Kipfer *et al.* (2002).

To accurately determine recharge temperature from noble gas concentrations, the preceding processes can be taken into account using an inverse modeling approach (Aeschbach-Hertig *et al.,* 1999). In this thesis the author has used the MatLab program Noble 90 (Peeters *et al.,* 2003) to model temperature, excess air and fractionation to find the best fit. The noble gas concentrations and constraining physical parameters (i.e. recharge elevation) are inputs into the modeling software. The software iteratively minimizes χ^2, the error-weighted sum of the model-data deviations of the individual noble gases, which at the same time provides a measure of the goodness of the achieved fit.

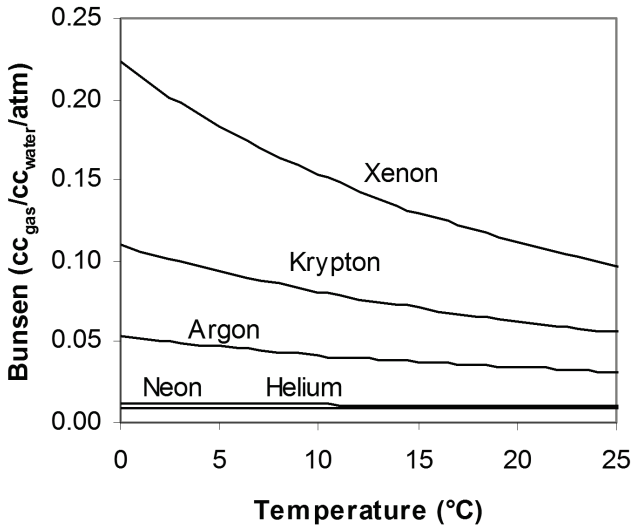

Figure 2- 1: Solubility of noble gases in water vs. temperature (Weiss, 1970; 1971; 1978 and Clever, 1979).

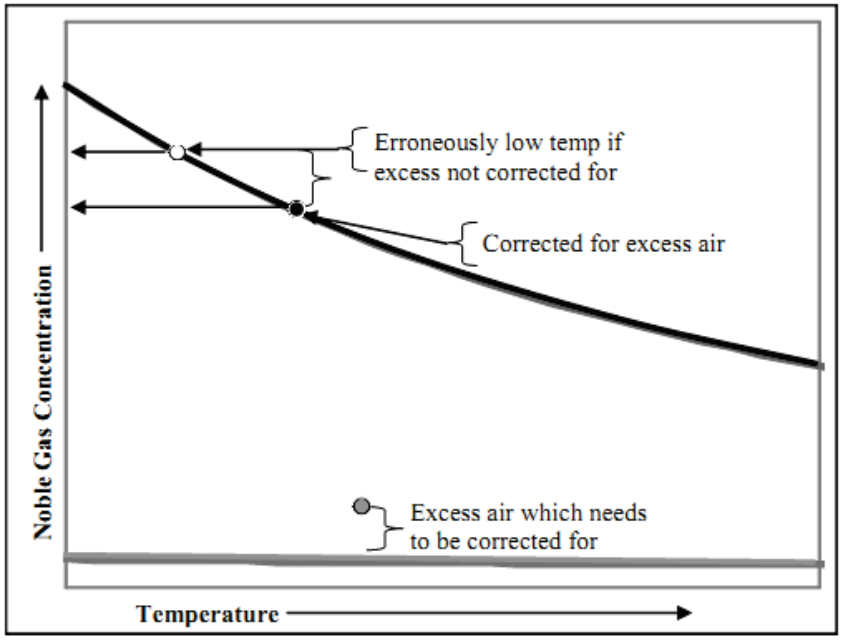

Figure 2- 2: Diagram of excess air and noble gas temperatures. Black curve shows concentrations of xenon vs. temperature, while grey curve shows neon vs. temperature. Grey circle is a sample neon value, which falls above the neon concentrations for air equilibrated water. Hollow circle is a sample Xe concentration which is un-corrected for excess air. The amount of excess air is determined from the neon and is removed from the Xe concentration to determine a value which is corrected for excess air.

As the noble gas recharge temperature is generally the same as the mean annual air temperature of recharge location, numerous studies have used groundwater recharge temperatures in conjunction with dating methods to determine paleoclimate (Clark *et al.,* 1998; Stute *et al.,* 1995; Aeschbach-Hertig *et al.,* 2002). The preceding three studies sampled waters from aquifers in North America and found temperatures 4 to 9 °C colder at the last glacial maximum compared to the Holocene. Although groundwater recharge temperature is commonly the same as mean annual air temperature, it may deviate due to different surface factors like water table depth, precipitation rates, vegetation and most importantly snow cover (Farrera *et al.,* 1999). Cey (2009) examined differences between recharge temperature and mean annual air temperature and found that groundwater recharge temperature can be significantly higher than the mean annual air temperature. This difference can be attributed to snow which acts as an insulator from cold winter air and the limited groundwater recharge during frozen periods.

2.4.2 Noble Gases: Groundwater Dating

As with dating of rocks and organic matter, radioactive decay systems can be used to determine groundwater age (Kipfer *et al.,* 2002). Old groundwaters can be dated using accumulations of ^{4}He from the decay of uranium and thorium and ^{40}Ar from the decay of potassium (Lippmann *et al.,* 2003). This method is suitable for waters in the order of millions of years old. Groundwaters of intermediate age (up to about 30 000 years) can be dated using ^{14}C dating (Clark and Fritz, 1997). Modern waters can be dated using the decay of tritium ^{3}H to ^{3}He. Tritium occurs naturally in precipitation with background levels of between 3.4 to 15 TU depending on latitude (Kaufman and Libby, 1954; Brown, 1961). This background is due to the bombardment of ^{14}N by neutrons from cosmic rays which produces ^{3}H and ^{12}C. The testing of thermonuclear bombs in the 1960's increased the amount of tritium in the atmosphere by orders of magnitude. Atmospheric testing reached a peak in 1963 with maximum concentrations between 5000 and 6000 TU (Figure 2-3)(IAEA, 2010). As tritium input was variable over time, it was found that it could be used as a tracer of groundwater age. Tritium decays to ^{3}He, with a half-life of 12.3 years (Clark and Fritz, 1997). As tritium levels in precipitation have decreased back to near background,

tritium concentrations have been coupled with their decay product to date waters instead of relying on the bomb peak. As tritium concentrations decrease in water, ^{3}He concentrations increase (Figure 2- 4). Based on this decay system, groundwater age can be determined using Equation 2- 4.

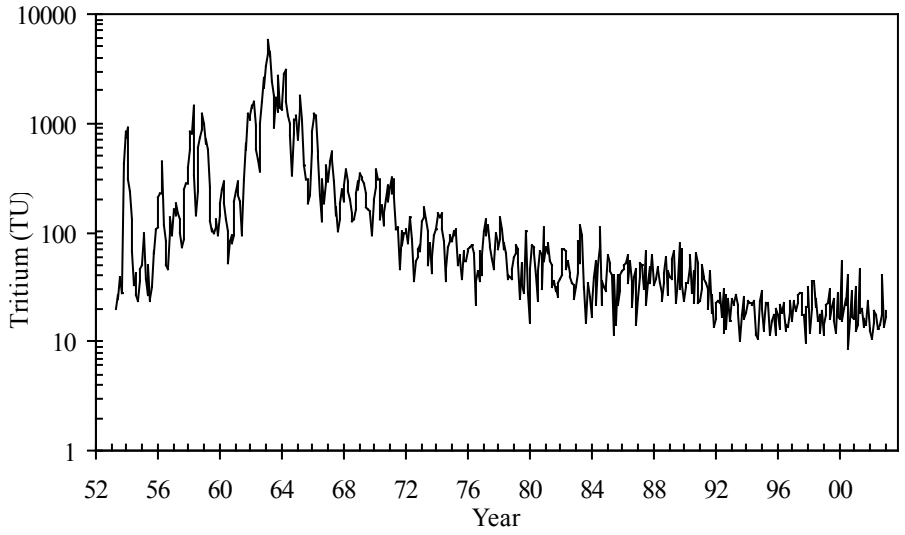

Figure 2- 3: Tritium in precipitation collected in Ottawa from 1952 to 2004 (from IAEA: GNIP database www.IAEA.org).

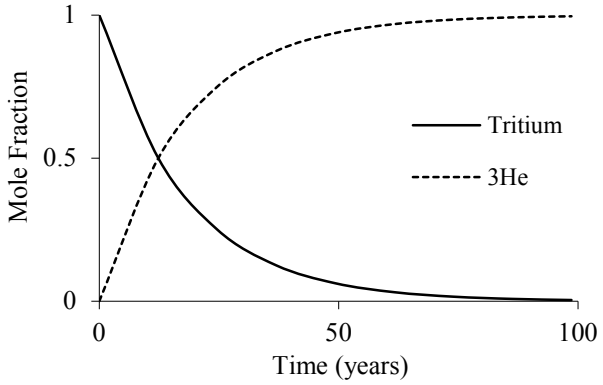

Figure 2- 4: Mole fractions of tritium and ^{3}He over 100 years.

Equation 2- 4: $$t = \frac{1}{\lambda}\ln\left(1+\frac{^{3}He}{^{3}H}\right) = \frac{12.3}{\ln 2}\cdot\ln\left(1+\frac{^{3}He}{^{3}H}\right)$$ (Clark and Fritz, 1997).

To calculate Equation 2- 4 accurately, it is necessary to account for all sources of ^{3}He. The amount of ^{3}He in air-equilibrated water is calculated based on the atmospheric ratio. The decay of uranium and thorium which produces ^{4}He imparts a neutron flux which

produces a variable amount of ^{3}He. Equation 2- 5 accounts for the various sources of ^{3}He where: R is the ^{3}He/^{4}He ratio of different components; the subscript "m" denotes measured; while "eq" stands for equilibrium; "ex" denotes excess; "ter" is for crustal sources; and L_{ex} is the He/Ne of the excess air component (Kipfer *et al.,* 2002).

Equation 2- 5:

$$^3He_{Tri} = {}^4He_m (R_m - R_{ter}) - {}^4He_{eq} (R_{eq} - R_{ter}) - L_{ex} (Ne_m - Ne_{eq}) (R_{ex} - R_{ter})$$

2.4.3 Sample Collection

Noble gases have been analysed from ice and groundwater. Gases have been collected from groundwater using both water-filled copper tubes as well as gas-filled diffusion samplers. Copper tube samples were collected in 3/8" tubes, approximately 35 cm long. Sampling was conducted by pumping the sample groundwater through these tubes and when possible a pipe cleaner brush was used to remove bubbles from the interior of tubes. This process helps ensure that there is no air contamination in samples. Tubes were then either crimped closed or clamped closed, to isolate the sample from the atmosphere. At sites where repeat visits were possible diffusion samplers were used.

Diffusion samplers have two 10 cm ¼'' copper tubes at each end connected by 10 cm of silicon tubing which is permeable to non-polar gases. The silicon tubing is filled with glass beads to reduce the internal volume of gas that must be exchanged. The samplers are placed in the groundwater to be sampled and left for 3 days or more (time depends on volume of sampler and length of silicon). Over time the gas in the sampler equilibrates with the gases in the water (Manning *et al*., 2003). Samplers are then removed and clamped or crimped closed. In the lab the concentration of gas in the copper tube is measured. To determine the concentration of gas in the sampled groundwater the pressure of the gas inside the tube is determined from the ideal gas law (Equation 2- 6) and the Bunsen coefficient is used to determine the concentration of gas in cc_{stp}/cc_{H2O} (cc_{stp}/cc_{H2O} :cubic centimetres of gas at STP/cubic centimetre of water)(Equation 2- 7) (Weiss, 1970; 1971; 1978 and Clever, 1979).

Equation 2- 6 $$P = \frac{nRT}{V} = \frac{(cc_{stp}/22.414L/mol)\cdot(0.082058atm\cdot L/mol/K)\cdot(T_{spirng}+273.15)}{V}$$

Equation 2- 7 $$cc_{STP}/cc_{H2O} = B\cdot P$$

2.4.4 Sample Analysis

Noble gas concentrations and ratios are determined by mass spectroscopy. Noble gas analysis is complicated by their low concentrations and their presence in air. The analysis of helium, neon, argon, krypton and xenon is therefore performed under high vacuum conditions. The gas is cleaned and cryogenically separated prior to being analysed in the mass spectrometer. In this study noble gas analysis has been conducted on three different noble gas analysis lines.

University of Ottawa: Isotope Dilution using a Quadrupole Mass Spectrometer

In a quadrupole mass spectrometer there are four parallel metal rods. Opposing rods are connected electrically and a radio frequency and direct current are applied to them. A magnetic field is produced and the quadrapole acts as a mass filter (March and Todd, 2005). The advantage of this type of instrument is cost. The disadvantage is that masses cannot be resolved with the same precision as a magnetic sector mass spectrometer and peak highs are less stable. To measuring noble gas concentrations it is only necessary to resolve 1 atomic mass unit separation. Using a spike of rare isotopes means that the ratios of peaks can be measured, which are more stable than the absolute peak heights. The isotopic ratio of the spike is provided by the manufacturer of the spike. The volume of gas in each spike aliquot was determined by measuring air standards with a known volume. The noble gas line used in this study is based on the design of Poole *et al.* (1997) and is mostly described in Battye (2002) and Greene (2005). The design of the line uses has been slightly modified and is described in Appendix B. This noble gas line was used for the measurement of Ar and Kr concentrations in water in Chapter 3, and the measurement of Ar, Kr and Xe in ice in Chapter 5.

University of Ottawa: Helium-Neon Magnetic Sector Noble Gas Mass Spectrometer

At the University of Ottawa samples were analysed for helium and neon concentrations and isotopes using a MAP 215-50. The methods used on this instrument are described in the relevant chapters as these methods have been improved over the course of this study. This instrument was used for select measurements of He and Ne in Chapter 3 and Chapter 4.

University of Heidelberg: Noble Gas Magnetic Sector Mass Spectrometre

A six week research visit was made to the Department of Environmental Physics, University of Heidelberg, Germany. In Heidelberg a GV 5400 mass spectrometer was used for the measurement of He through Xe. The measurements obtained by this instrument are presented in Chapter 4.

2.5 Summary

The methods described above are applied to different problems and settings in the next three chapters. Chapters 3 and 4 apply these methods to groundwater studies. Major ion geochemistry is used to determine proportions of groundwater in the rivers studied. Absolute groundwater discharge amounts were determined in Chapter 4 using river flow measurements associated with water chemistry. The DIC and $^{13}C_{DIC}$ are used to determine groundwater recharge conditions. The stable isotopes δD and $\delta^{18}O$ are used to determine if groundwater recharge occurred either at higher elevations or if it displays a seasonal bias. Noble gases are used to determine the temperature of groundwater recharge and groundwater age. The focus of Chapter 5 is to apply noble gas methods to the determination of the origin of ground ice bodies. This novel method exploits the difference in the gas solubilities to be able to determine ice originating from snow vs. ice originating from freezing of liquid water.

Chapter 3: Groundwater Contribution to Discharge in Permafrost Watersheds: Tributaries of the Northern Mackenzie River, NWT, Canada

3.1 Introduction

In periglacial environments, the presence of permafrost has a profound effect on the hydrological cycle (e.g. Cederstrom *et al.*, 1953; Ferrians *et al.*, 1969). The reduction of infiltration imposed by frozen ground results in greater runoff and a reduction of seasonal water flow and storage in talik, which greatly alters the generation of streamflow in permafrost watersheds (Woo and Steer, 1983; McNamara *et al.*, 1997). Infiltration of precipitation during the melt season to the active layer can reduce surface runoff and buffer the discharge response to precipitation (Carey and Quinton, 2004). Due to the fact that there are unfrozen zones in the permafrost, groundwater recharge may occur, as it does in the Mackenzie Valley where there are groundwater systems that flow perennially in limestone and evaporite rocks. The discharge from these groundwater systems keeps sections of these rivers ice-free in winter.

This chapter examines the hydrogeology of numerous watersheds in western NWT, Canada using geochemical methods. The objectives are to quantify the role of groundwater in streamflow generation and to determine recharge conditions. Based on the results, a conceptual model of groundwater circulation in permafrost watersheds is developed.

3.2 Background

In the near surface permafrost environment, water may run off overland, through unfrozen organic soils, as interflow, or through saturated soils in the active layer (Quinton and Pomery, 2006; Carey and Woo, 2000). As there is water flow in the active layer, ions in the soils may become leached (Kokelj and Burn, 2005). During snowmelt, creek discharge will increase, while TDS and pH will decrease (Carey and Quinton, 2004). This water may contain dissolved material that was deposited on the snow over the winter. For example, the first drainage of snow near Inuvik is characterized by waters with low Na^+

(1.9 ppm) and Cl^- (4.4 ppm) concentrations originating from dry deposition on snow (Quinton and Pomery, 2006). As the active layer begins to thaw, water can infiltrate and weather mineral material (Quinton and Pomery, 2006). This weathering may lead to an increase in the pH of water.

In permafrost terrain, perennial groundwater may flow in supra-permafrost, intra-permafrost or sub-permafrost aquifers. However, determining where groundwater flow occurs is difficult (French, 1996). As in temperate regions, groundwater in permafrost terrain may be thermal or non-thermal. Traditionally, a thermal groundwater is classified as one which is significantly warmer than the mean annual air temperature (White, 1957). To be consistent with previous research, in this study thermal groundwaters are those which are > 5 °C and non-thermal are those < 5 °C at discharge (Michel, 1978). Non-thermal waters (< 5 °C) may be associated with supra-permafrost, intra-permafrost or sub-permafrost groundwater flow. Thermal waters are associated with sub permafrost flow. Groundwater flow in permafrost regions most often occurs in karsted rocks where enhanced flow through karst openings increases transport of heat into the subsurface and prevents freezing (Ford and Williams, 2007). Karst has been found to drain a large amount of water in permafrost regions, such as from spring snowmelt (van Everdingen, 1981) and seasonal precipitation (Clark and Lauriol, 1997).

Permafrost catchments draining the central part of the Mackenzie Valley east of Norman Wells host groundwater springs which were extensively studied by Michel, (1977; 1986). Three main groundwater component end-members were identified: Na^+-Cl^-, Ca^{2+}-SO_4^- and Ca^{2+}-Mg^{2+}-HCO_3^-. The Na^+-Cl^- end member is associated with deep thermal groundwaters. The Ca^{2+}-SO_4^- and Ca^{2+}-Mg^{2+}-HCO_3 end members are generally associated with non-thermal waters. The Bear Rock Formation (Devonian) was found to be the primary sub-permafrost aquifer. There is also groundwater flow in the Mt. Kindle Formation, the Franklin Mountain Formation and the Saline River Formation. Groundwater recharge was found to occur mostly in the Franklin Mountains through karsted limestones and evaporites. The Ca^{2+}-SO_4^- end member was attributed to the dissolution of anhydrite from the Bear Rock Formation, as supported by the ^{34}S signature. Moreover, δD and $\delta^{18}O$ results indicate groundwater is depleted relative to mean annual precipitation and this may

be the result of snowmelt. Groundwater ages were estimated using tritium and ^{14}C and were found to range from less than 15 years to over 10 000 years depending on the flow system.

Along Little Fish Creek, in the Richardson Mountains, groundwater springs discharge 16 °C water with high total dissolved solids (3200 mg/l). Based on temperature and TDS, this groundwater was determined to have a deep flow path related to faulting in the region (Mutch and McCart, 1974). A more extensive study incorporated sampling along the river in 1997 along with other time-series samples collected between 1992 and 1997. Three water sources were found to contribute to creek discharge: deep thermal groundwater, shallow non-perennial groundwater and perennial runoff / active layer discharge (Clark *et al*., 2001).

3.3 **Sampling Sites**

The study area is located within a geographic area of about 80 000 km^2 ranging from 63° N to 68° N and 123 °W to 136 °W (Figure 3- 1). Sites with perennial groundwater discharge were selected. This groundwater discharge may support the spawning and overwintering of fish (N. Mochnacz-Department of Fisheries and Ocean- personal communication, 2008). Water chemistry samples were collected from 19 rivers (shown in Figure 3- 1). Seven creeks and rivers that were sampled more extensively (White Sand Creek, Hodgson Creek, Smith Creek, Canyon Creek, Gibson Creek, Gayna River and Little Fish Creek) based on the presence of groundwater springs. Herein these rivers are referred to as the primary rivers.

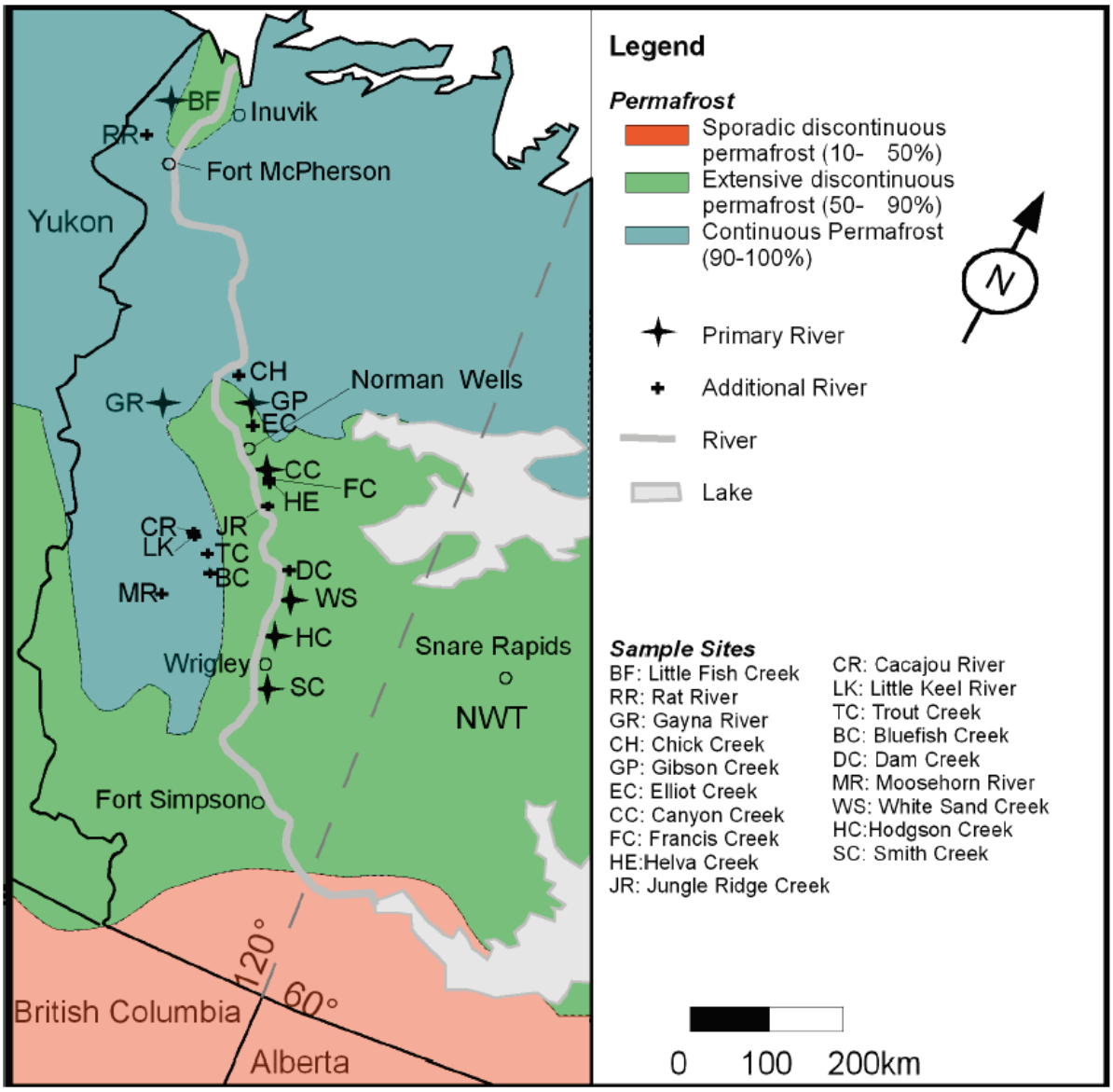

Figure 3- 1: Sampling sites and distribution of permafrost in Yukon and the Northwest Territories (Permafrost distribution from NRCan, 2003).

The studied watersheds range in size from 10 to 1500 km^2. Little Fish Creek Watershed is ~ 300 km^2 and over the year river flow ranges from ~2.2 to 1050 m^3/s, with thermal groundwater discharge estimated at 1.6 m^3/s (Clark *et al.,* 2001). Flow has not been measured on the other water courses. Estimates provided here are based on the author's experience with flow gauging. Smith Creek watershed is ~85 km^2 and winter flow is estimated at 0.01 to 0.1 m^3/s (4 to 37 mm annual recharge over the basin). Gibson Creek watershed is ~10 km^2 and winter flow is estimated at 0.01 m^3/s (32 mm annual recharge over the basin). White Sand Creek watershed is ~205 km^2 and winter flow at the midstream

site visited was less than 0.01 m^3/s (3 mm annual recharge over for the basin upstream of this site ~95 km^2). Hodgson Creek watershed is ~220 km^2 and winter flow at the site visited was less than 0.01 m^3/s (5 mm annual recharge over for the basin upstream of this site ~70 km^2). Canyon Creek watershed is ~75 km^2 and winter flow is estimated at 0.1 m^3/s (42 mm annual recharge over the basin). Gayna River watershed is ~1500 km^2 and winter flow is estimated at 1 to 5 m^3/s (21 to 105 mm annual recharge over the basin).

The closest meteorological station in the southern portion of the study area is located in Forth Simpson (61°50' N, 121°19' W), 175 km south-east of Smith Creek. Fort Simpson has an average annual air temperature of -3.2 °C and receives annually an average of 369 mm of precipitation (Figure 3- 2). In the middle part of the study area is Norman Wells (65°17' N, 126°43' W), which has a mean annual air temperature of -5.5 °C and receives an average of 290.7 mm of precipitation per year. Inuvik (68°18' N, 133°28' W), the northernmost meteorological station (100 km east of Little Fish Creek) has a mean annual air temperature of -8.8 °C and receives an average 248 mm of precipitation annually (Environment Canada, 2010). These differences in climate conditions result in different vegetation. In the central Mackenzie Valley the sampling sites are surrounded by coniferous forest (see Figure 3- 3) while near Little Fish Creek there are fewer trees, with areas of tundra steppe type vegetation and open rock slopes (see Little Fish Creek Figure 3-3). This difference is due to the higher latitude of Little Fish Creek.

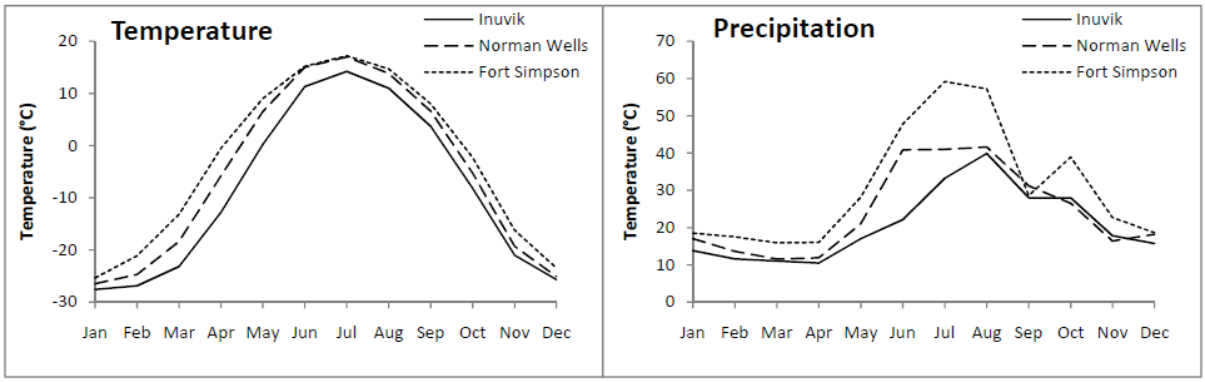

Figure 3- 2: Graphs of mean monthly precipitation and temperature (from 1971 to 2000) through the year from Inuvik (68 m.a.s.l.), Norman Wells (73 m.a.s.l.) and Fort Simpson (169 m.a.s.l.) (data from Environment Canada, 2010)

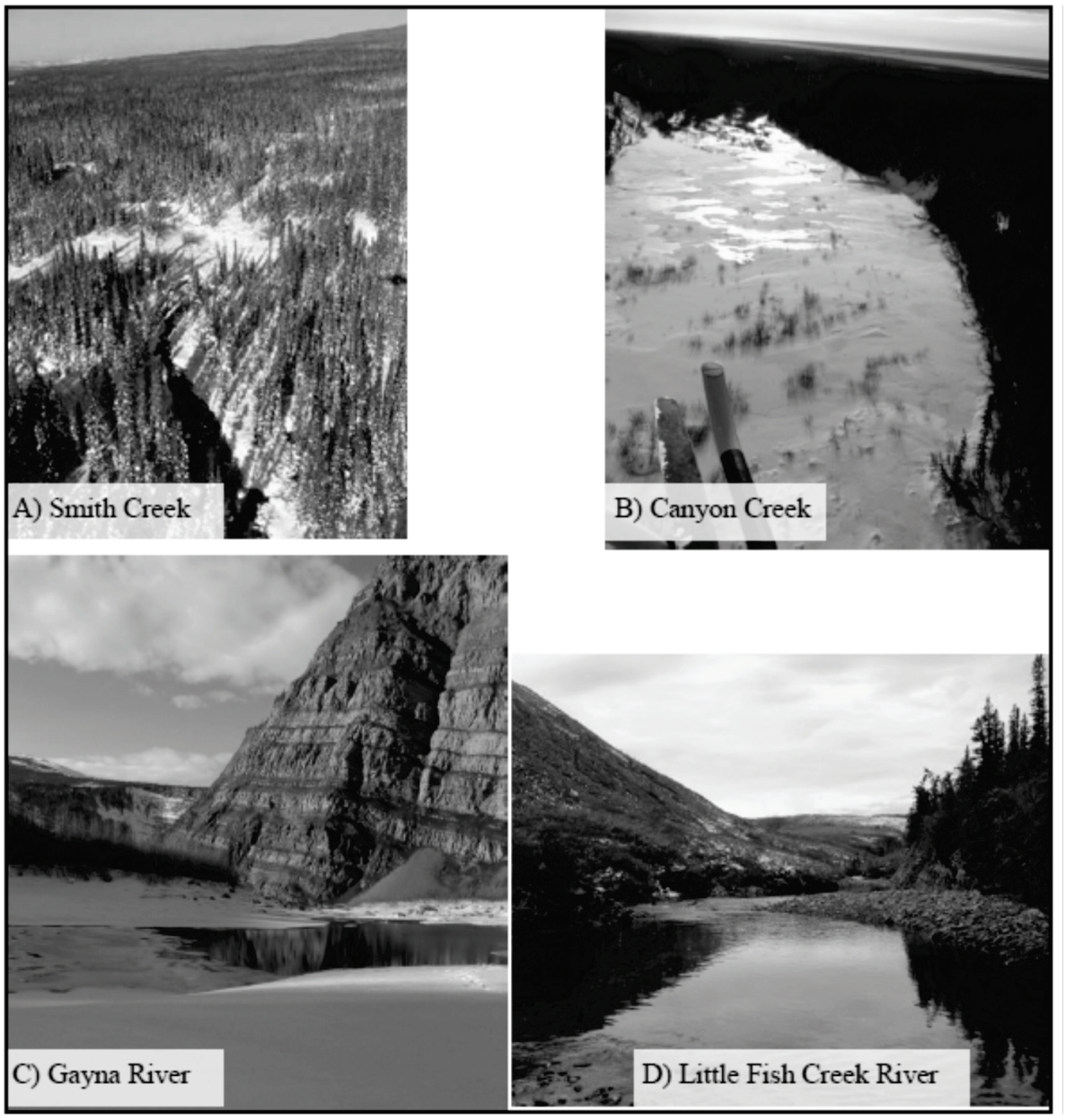

Figure 3- 3: A) View of Smith Creek and groundwater pools from helicopter. Creek is about 2-3 m across. (March 2008) B) View of Canyon Creek from helicopter showing wide river channel with icings. (March 2008) C) Gayna River, near sampling site, groundwater spring located behind photographer. Open water is present upstream, however ends soon downstream (March 2008). D) Little Fish Creek in upper reaches. (September 2008).

The southern part of the study area is located in extensive discontinuous permafrost which progressively becomes continuous permafrost in the northern part of the study area (NRCan, 2003, Figure 3- 1). Permafrost is also colder in the northern part of the study area. The mean annual ground temperature (MAGT) of permafrost is measured at the depth

where temperature does not change during the year. The MAGT of the southern sampling sites (Smith Creek, White Sand Creek and Hodgson Creek) is >0 to -2 °C (Smith *et al.*, 2010). The MAGT of the sites near Norman Wells (Canyon Creek, Gibson Creek and Gayna River) is 0 to -2 °C. Near Little Fish Creek the MAGT is -2 to -5 °C. In the central and southern part of the study area (Smith Creek, White Sand Creek, Hodgson Creek, Canyon Creek, Gayna River and Gibson Creek) permafrost ranges in thickness from <10 m to 100 m (Smith and Burgess, 2002). Near Little Fish Creek permafrost is 100 to 200 m in thickness.

All of the water courses studied have headwaters in mountainous terrain and flow into the Mackenzie River. The relief of NWT and Yukon is shown in Figure 3- 4. The study sections of Canyon Creek, Hodgson Creek, Smith Creek and White Sand Creek range in elevation from 100 - 300 m.a.s.l. The headwaters of these creeks are in mountainous terrain up to 800 m.a.s.l. Gibson Creek sampling sites are located at 120 m.a.s.l. and the surrounding hills are up to 400 m.a.s.l. The sample sites on Gayna River are at 275 m.a.s.l. and the surrounding mountain tops are 900 - 1300 m.a.s.l. The Little Fish Creek sampling sites range from 270 to 370 m.a.s.l. and the surrounding mountains are up to about 700 m.a.s.l. Photos from Smith Creek, Canyon Creek, Gayna River and Little Fish Creek are shown in Figure 3- 3. The topography of each of the primary rivers and locations of sampling sites are shown in Figure 3- 5 to Figure 3- 8.

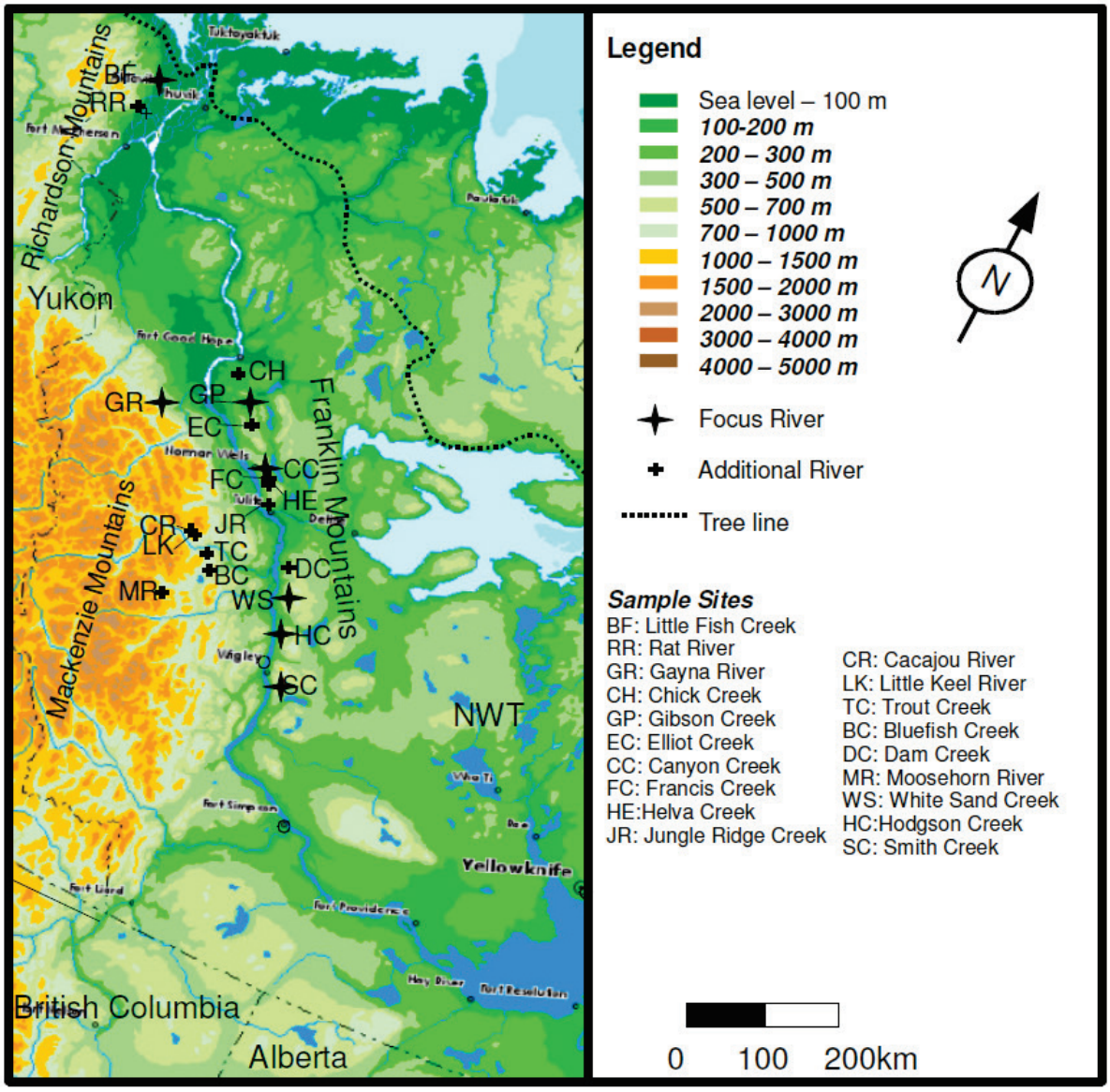

Figure 3- 4: Relief of NWT and mountain ranges (Relief and tree line from NRCan, 2003)

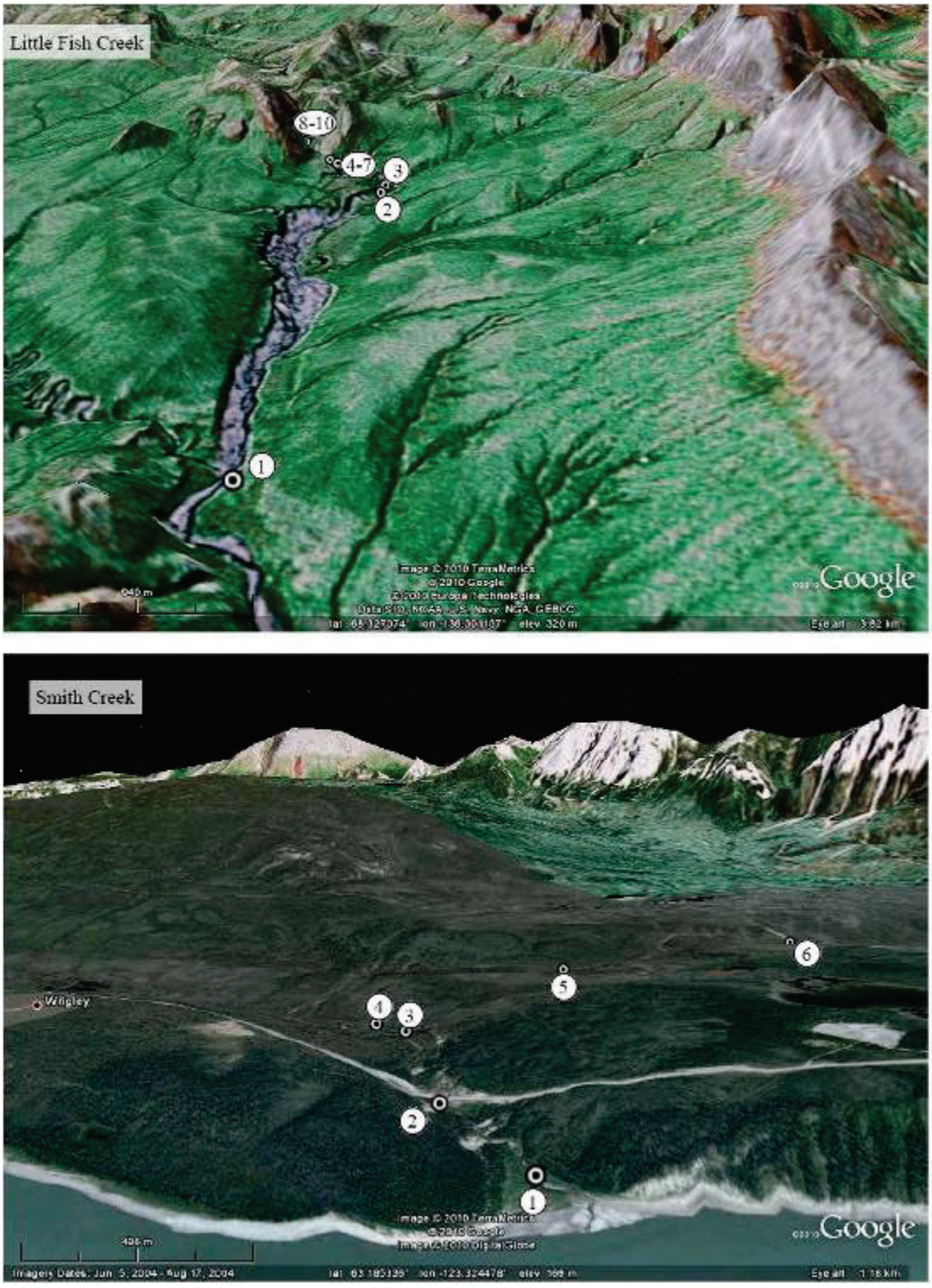

Figure 3- 5: Satellite image draped over topography and sample sites along Smith Creek and Little Fish Creek. (From Google Earth).

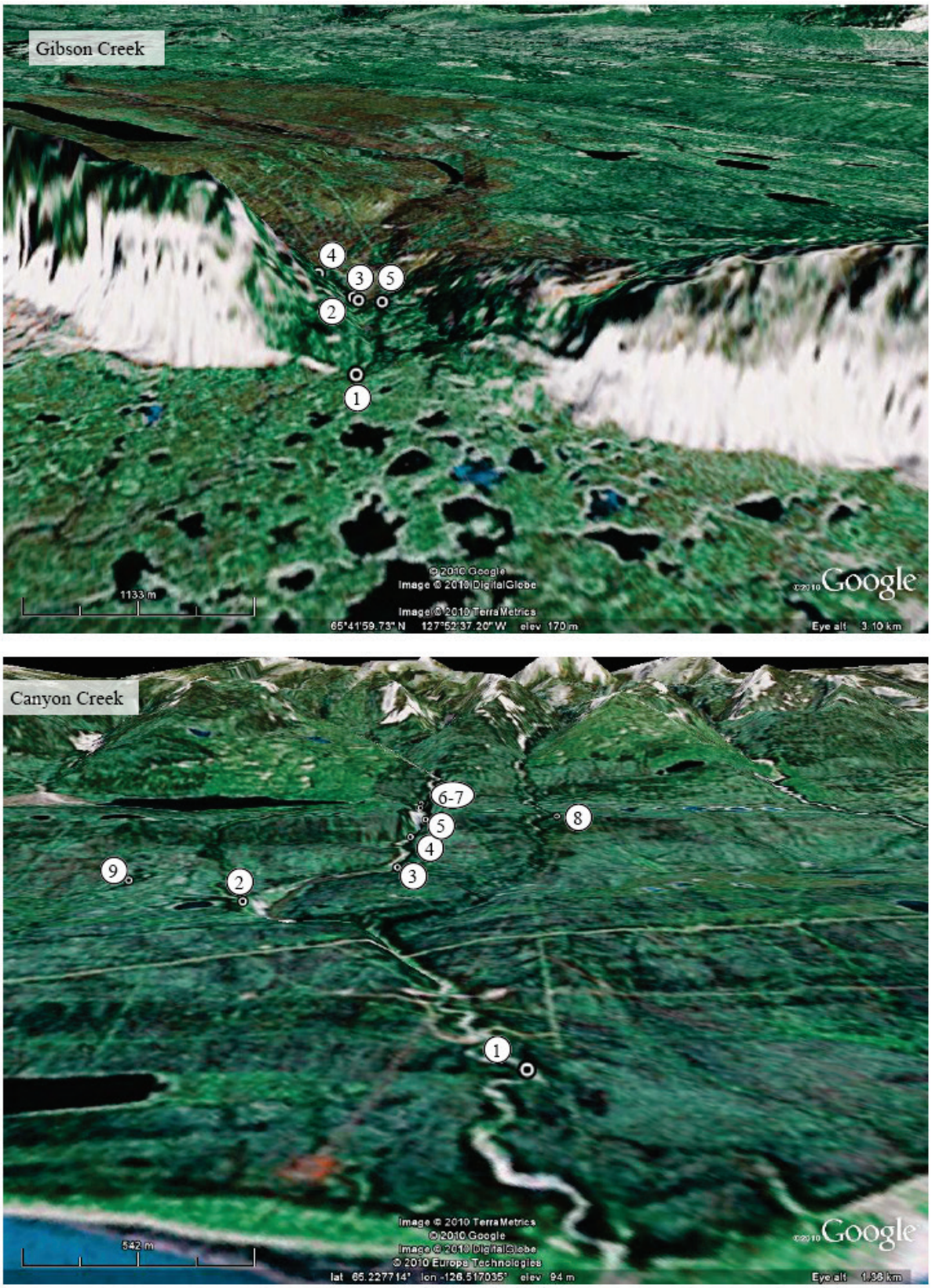

Figure 3- 6: Satellite image draped over topography and sample sites along Gibson Creek and Canyon Creek. (From Google Earth).

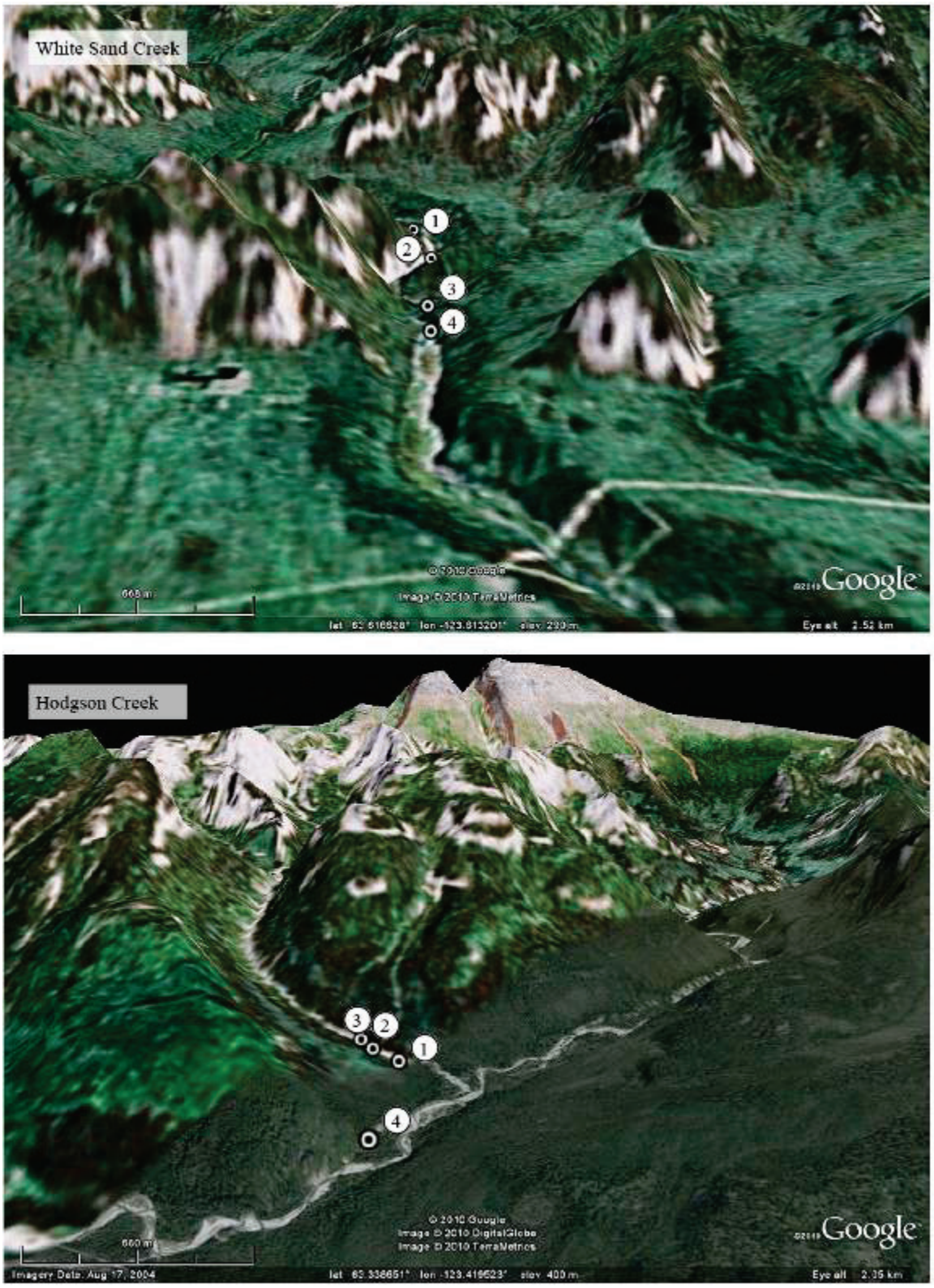

Figure 3- 7: Satellite image draped over topography and sample sites along White Sand Creek and Hodgson Creek. (From Google Earth).

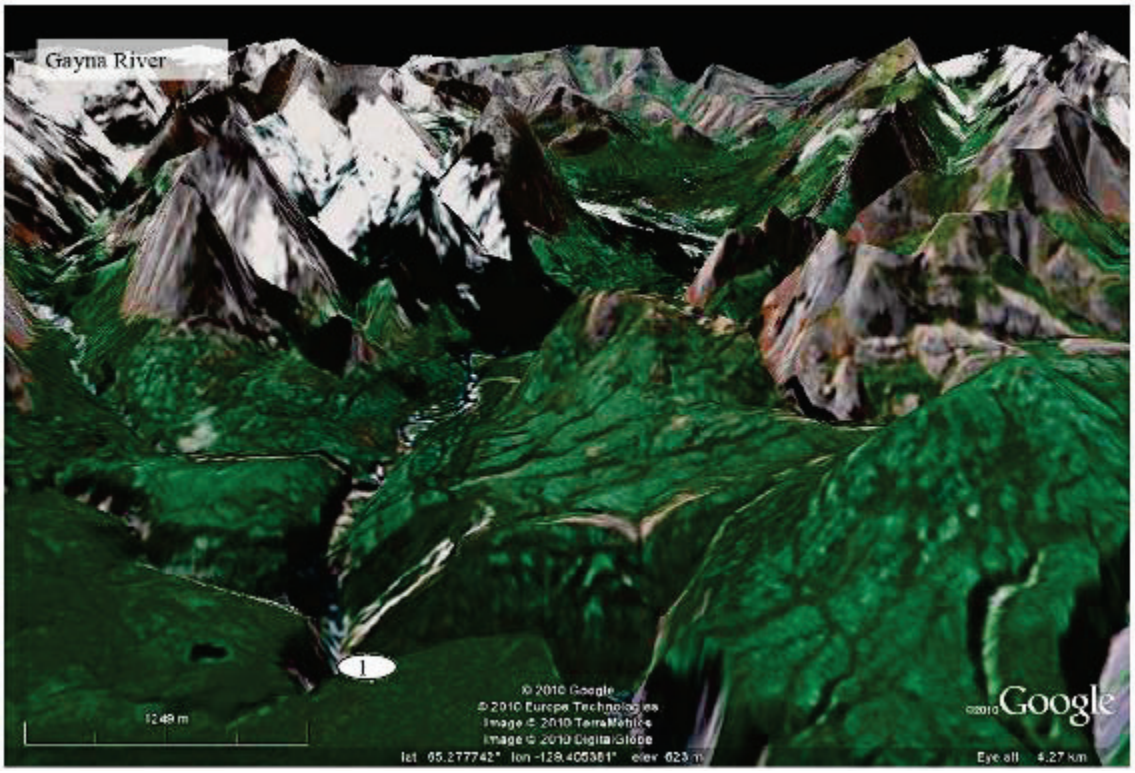

Figure 3- 8: Satellite image draped over topography and sample sites along the Gayna River. (From Google Earth).

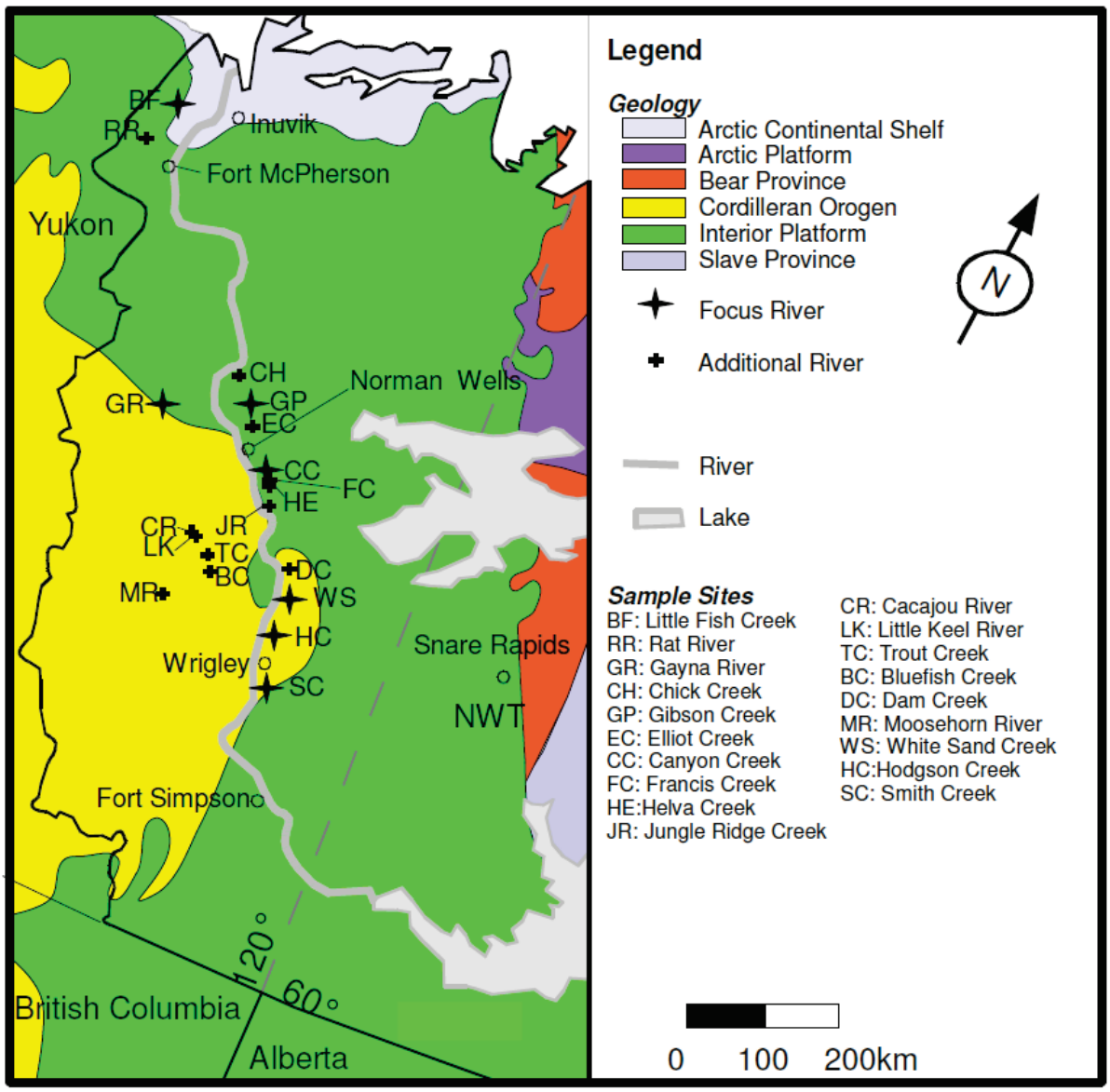

Figure 3- 9: Regional map of sampling location's geologic provinces (Geological Information from NRCan, 2004)

The water courses studied are located in either the Interior Platform or the Cordilleran orogen geologic provinces of Canada (NRCan, 2004, Figure 3- 9). In the central Mackenzie Valley there is a succession of Cambrian to Upper Devonian rocks which host groundwater flow (Michel, 1977; 1986). Along the east side of the Mackenzie, these formations generally dip to the west, with more extensive faulting to the east in the Franklin Mountains (Douglas and Norris, 1973;Walter, 1981). The Middle Devonian Bear Rock Formation is composed of gypsum and brecciated dolomite which has high porosity and permeability making it the most important aquifer on the east side of the river (Michel,

1986). The Gayna River is located on the east side of the Mackenzie and is underlain by the same geologic units, however these dip east with some local folds and faults. The watersheds are shown on geologic maps of White Sand Creek, Hodgson Creek and Smith creek in Figure 3- 11, and Gayna River, Canyon Creek and Gibson Creek in Figure 3- 12.

Karsted formations are primary aquifers along the east side of the Mackenzie River. Sinkholes in the Franklin Mountain Formation and the Mount Kindle Formation may allow for groundwater recharge (van Everdingen, 1981). Karst also forms in the Bear Rock Formation on both the east and west side of the Mackenzie and plays an important role in the drainage of water (Hamilton and Ford, 2002). Karstification process has been occurring since at least the Cretaceous soon after deposition but may have slowed during the Pleistocene glaciations (van Everdingen, 1981).

The sampling sites were glaciated by the Laurentide ice sheet at the glacial maximum (Duk-Rodkin, 1993). Ice in the region was relatively thin and did not deposit much till (Hamilton and Ford, 2002). Glacial deposits consist of rolling and hummocky moraines (Hughes *et al.,* 1973). The Quaternary deposits onlap onto the Franklin Mountains. Stream valleys have fluvial gravel deposits from high flow periods.

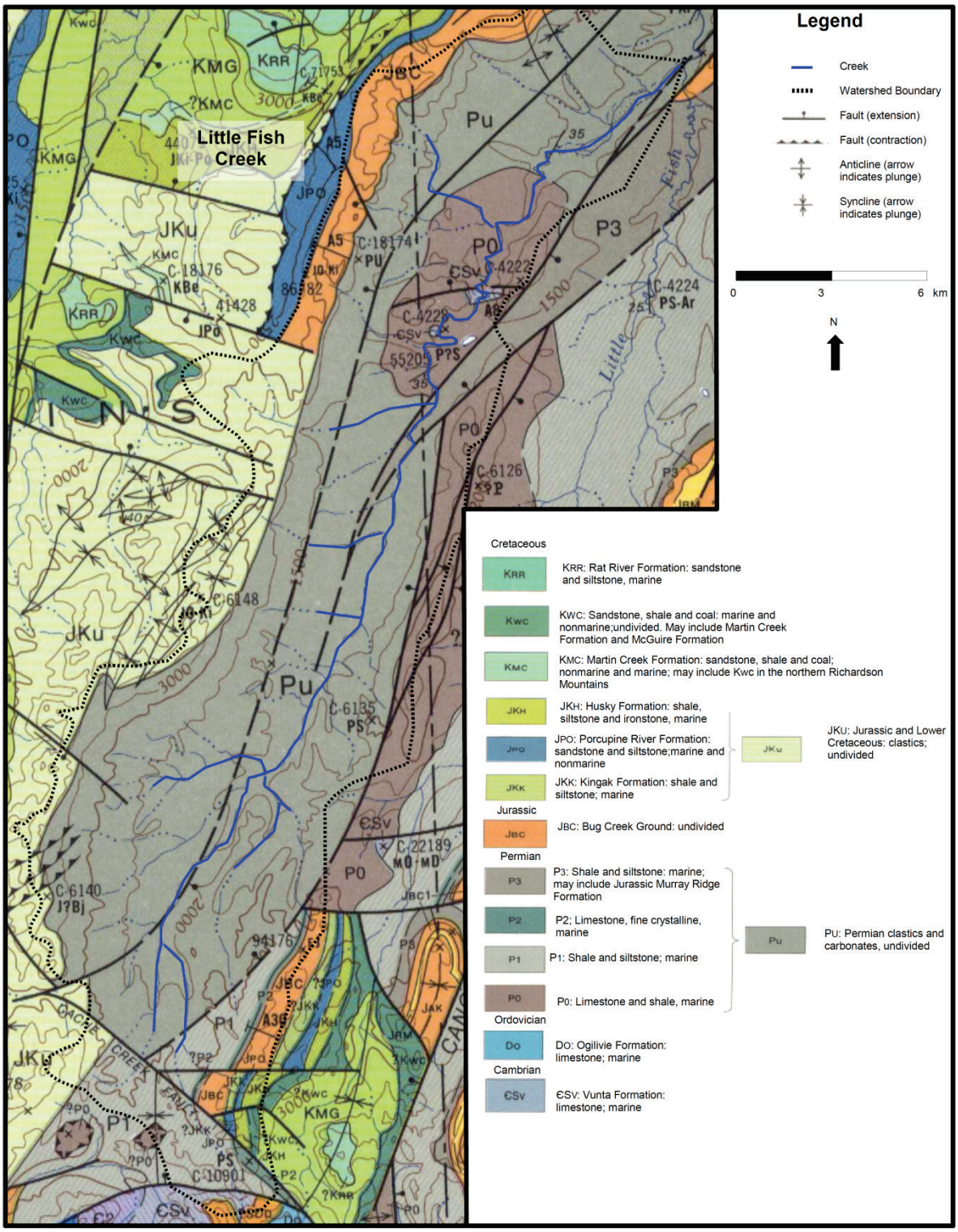

Figure 3- 10: Geological map with outline of Little Fish Creek watershed (geological basemap from: Norris, 1977)

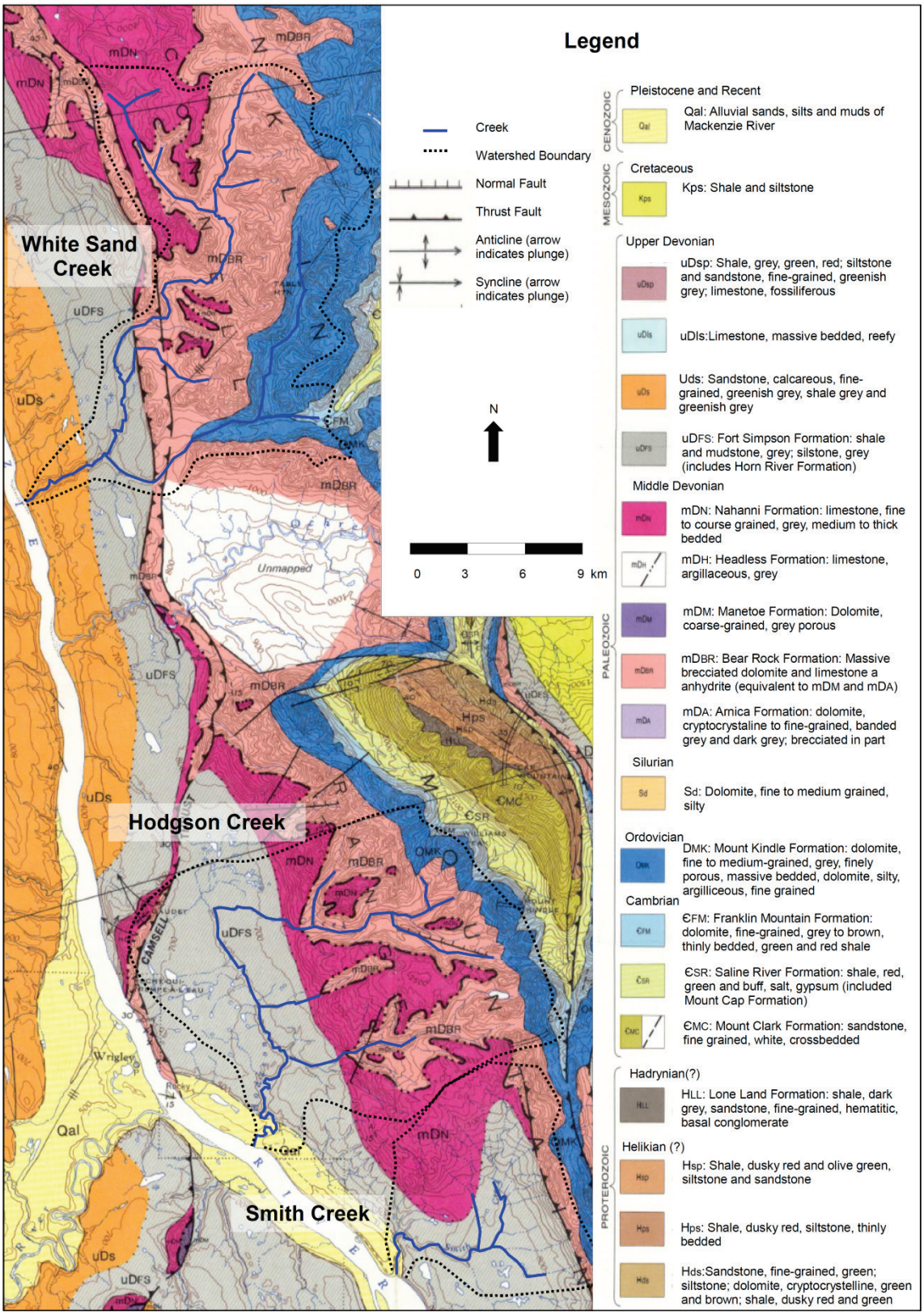

Figure 3- 11: Geological map with outlines of White Sand Creek, Hodgson Creek and Smith Creek watersheds. (geological basemap from: Douglas and Norris, 1973)

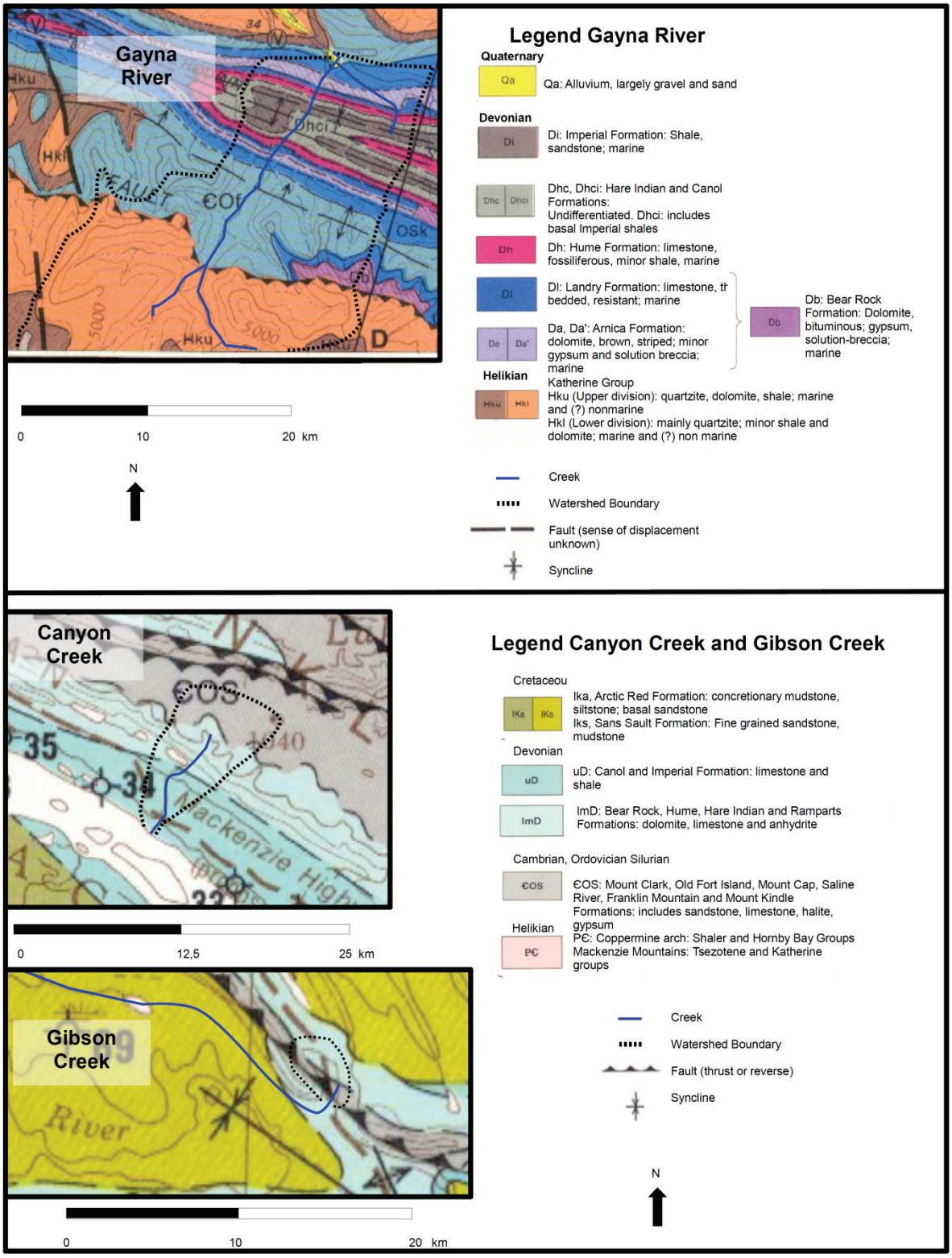

Figure 3- 12: Geological map with outlines of Gayna River, Canyon Creek and Gibson Creek watersheds (geological basemap for Gayna River from Aitken and Cook, 1974, Canyon Creek and Gibson Creek from Walter, 1981)

3.4 **Methods**

Groundwater sampling sites were selected along rivers where there is known perennial groundwater discharge (Mutch and McCart, 1974; Michel, 1977; Michel, 1986; Clark *et al.,* 2001). This study includes water samples collected during numerous excursions along selected rivers. From August 16 to September 4, 2007 Department of Fisheries and Oceans (DFO) personnel collected 24 water samples as part of a regional programme along Gayna River, Gibson, Hodgson, Whites Sand and Smith Creeks. From March 3 to 6, 2008, (winter), activities were focused on identifying and sampling open water zones along five creeks and one river. From June 26 to July 2, 2008 (summer), attention was focused on collecting material from upstream and downstream of known discharge zones, determined from the winter reconnaissance work. The June sampling exercise captured early flow conditions. From September 20 to 23, 2008 (fall), samples were collected along Little Fish, upstream and downstream of a groundwater discharge zone in order to refine the research previously conducted on this reach by Clark *et al.* (2001). The fall sampling exercise on Little Fish Creek included the river at both baseflow and higher river discharge after heavy rains.

Water temperature, pH and electrical conductivity were measured in the field except for those samples collected in August and September 2007 and June 2008, as they were collected by DFO personnel who did not have the necessary equipment. The electrical conductivity and pH of these samples were measured once returned to the lab. The pH was measured using a Hanna Instruments HI 9025 while temperature and conductivity were measured using a WTW COND 330i. In the field, samples were collected using single 250 mL HDPE bottles. They were kept cool and in the dark and were filtered within 24 hours of sampling through 0.45 μm filters. The filtrate filled three 30 ml HDPE bottles for cation, anion and $\delta^{18}O$ and δD analysis as well as three 40 mL amber TraceClean vials with septa caps for dissolved organic and inorganic carbon. August - September 2007 and June 2008 samples were filtered once returned to the University of Ottawa. While it is not ideal to have such a delay as mineral precipitates may form, this is unlikely with most samples. $\delta^{13}C_{DIC}$ and $\delta^{13}C_{DOC}$ were not analysed from these sampling trips as such a delay would affect these results.

Major ion geochemistry was analysed for all samples. Samples from the primary rivers and the Rat River were also analysed for δD and $\delta^{18}O$, dissolved organic and inorganic carbon (DOC, DIC). Water samples collected in March 2008 and September 2008 were analysed for $\delta^{13}C$ isotopes. Major ion geochemistry analysis was conducted at the University of Ottawa, Department of Earth Science geochemistry lab. Cations were measured using inductively coupled plasma emission spectroscopy (ICP-ES) and anions were measured by ion chromatography. Four anion samples from Smith Creek were believed to have precipitated a sulphate mineral prior to anion analysis, thereby reducing the total amount of SO_4^{2-} in solution. To correct for this, the value of SO_4^{2-} in these samples was found using the elemental sulphur concentrations from acidified samples. Since cation samples were acidified, calcium and other cations which may have precipitated with SO_4^{2-} would have dissolved and thus been included in the measurement. Samples for which this calculation was performed are listed in Appendix B. DOC, DIC and $\delta^{13}C$ isotope samples were analysed at the University of Ottawa Hatch Isotope lab. DIC and DOC are measured using an OI Analytical Aurora Model 1030W TIC-TOC Analyser. Bicarbonate was then calculated from the DIC measurements and pH. Ratios of $^{18}O/^{16}O$ and D/H were determined by CO_2 and H_2 gas equilibrium methods respectively. To determine D/H of, water samples are equilibrated with H_2 gas at 25 °C and the ratio of D/H of the gas phase was measured (analytical reproducibility of ±1.5‰). The $^{18}O/^{16}O$ ratio of the water samples was determined on CO_2 isotopically equilibrated with the water at 25 °C (analytical reproducibility of ±0.1‰). Measurements of $^{18}O/^{16}O$ and D/H were conducted on a Finnigan Mat Delta+ XP isotope mass spectrometer at the G.G. Hatch Laboratory (University of Ottawa). Isotope ratios are presented in δ notation in parts per thousand difference of $^{18}O/^{16}O$ or D/H in a sample with respect to Vienna Standard Mean Ocean Water (VSMOW).

Noble gas samples were collected using $3/8^{th}$ inch copper tubes attached to a small hand pump used to pass water through sample tubes. Efforts were made to pump lightly to avoid any potential degassing of samples during this process. Sample tubes were then clamped closed. Analyses of helium isotopes and neon concentrations were conducted on a MAP 215-50 noble gas mass spectrometer using standard noble gas extraction and analysis techniques (Mohapatra and Murty, 2000). The sample inlet section was evacuated to

8×10^{-3} Torr prior to opening the sample. Water samples were opened and water flowed into a glass bulb to degas. The water was then frozen with liquid nitrogen to reduce vapour pressure. Gas was subsequently purified with a series of traps and getters. Samples were processed using the following steps for 10 minutes each: a liquid nitrogen cooled charcoal trap that traps gases heavier than mass ~25 atomic mass units, a liquid nitrogen cooled aerogel (a silica compound produced by NASA) trap that traps gases heavier than mass ~25 atomic mass units (R. Mohapatra, personal communication, 2010), a titanium getter to sorb N_2, O_2, CO_2 and CO and decompose hydrocarbons (Mohapatra, 1998), a second liquid nitrogen cooled charcoal trap, a second titanium getter, and a SAES (ST 707) getter to remove H_2, CO and N_2 (SAES, 2010). The remaining sample contains only He, Ne and residual Ar. The sample was then let into the mass spectrometer for analysis with a third -180 °C charcoal trap adjacent to the source to remove any remaining argon.

The analysis of argon and krypton was conducted using an isotope dilution noble gas line with a quadrupole mass spectrometer based on the design of Poole *et al.* (1997). The specific line is mostly described in Battye (2002) and Greene (2005) (full description in Appendix A). The spike is composed of rare noble gas isotopes: ^{3}He (99.99%), ^{22}Ne (99.9%), ^{36}Ar (99.7%), ^{78}Kr (68.9%) and ^{136}Xe (100%) where percentages represent the relative percent of the rare noble gas isotope within the spike with respect to the other isotopes of the same element. Once connected to the line, samples are degassed and water vapour is trapped in a U-tube cooled with ethanol to -30 °C. Reactive gases are then removed using a hot titanium getter pump at 600 ˚C. An aliquot of gas is then let into the mass spectrometer for argon analysis. The ratio of ^{36}Ar/^{40}Ar is measured, which is used to determine gas concentrations. Kr-Xe is then cryogenically separated from Ar and other gases in the line by trapping on charcoal at -78 ˚C, and then heating the trap to release Kr and Xe to the quadrupole where the ratio of ^{78}Kr/^{84}Kr and ^{136}Xe/^{132}Xe are measured. Xenon was included in the initial measurements; however during the analysis of groundwater samples the Xe signal was too weak. This weak signal may be the result of the U-tube vapour trap that was based on the design used by Kulongoski and Hilton (2002) and Sano and Takahata (2005). It is postulated that the U-tube did not trap all water vapour. The ineffective trapping of water vapour may have overwhelmed the getter resulting in the high background and weak xenon signal. This weak xenon signal resulted in measurements

which were not valid. Of the noble gases, xenon is the most sensitive to the water temperature at recharge and valid xenon concentration would have helped constrain groundwater recharge temperatures. This problem did not affect the xenon values presented in the other chapters of this thesis as this U-tube was not used.

3.5 **Results and Interpretation:**

3.5.1 Major Ion Geochemistry

Surface Water

The variability of surface water chemistry is related to the variability in groundwater chemistry and watershed geology. River water is composed of overland runoff, active layer drainage and groundwater. The variations in these three components result in a range of TDS in surface water from 287 ppm in June 2008 along Smith Creek to 1749 ppm in September 2008 along Little Fish Creek. Typically, the groundwater component contributes the greater amount of TDS (from 371 to 2817 ppm). Where groundwater has higher TDS the surface water subsequently has higher TDS. During low flow conditions the creeks and rivers had higher TDS relative to the other sampling events. There is no trend of increasing salinity from north to south that might indicate greater groundwater contributions to the south. This is attributed to the limitations of point sampling on each river and to the varied geology. In general, the geochemistry of watershed discharge in this area is dominated by the dissolution of limestone and anhydrite. In March 2008 creek waters had higher TDS as they were at low flow conditions with significant groundwater components. In June 2008 creek waters had lower TDS due to the dilution of snowmelt.

It is necessary to distinguish the components of surface water to be able to calculate the contribution of groundwater to these water courses, which will be discussed further in the section *Determining Groundwater Contributions Using Major Ion Chemistry*. In this study, overland runoff and active layer drainage are combined and referred to as runoff. General observations are made below about overland runoff and groundwater; this is followed by a more detailed discussion of these components along the various rivers in the section below entitled *Groundwater and Surface Water Chemistry of the Primary Rivers*.

Runoff

Because runoff could not be measured directly, the composition of runoff for each river was estimated from water samples containing the lowest TDS. These low TDS waters are a mix of active layer water and overland runoff, but as mentioned previously are combined. The lowest TDS samples were collected during the June sampling with exception of Little Fish Creek. Runoff was sampled directly by Clark *et al.* (2001) and these values were used here. Due to the variable surface conditions, temperature of runoff was variable. The pH of runoff water was generally greater than that of groundwater. It is also noted that runoff water had higher DOC concentrations than groundwater. The samples with the lowest TDS are plotted in Figure 3- 13 and Figure 3- 14. The TDS of this runoff component varies from 257 ppm to 482 ppm.

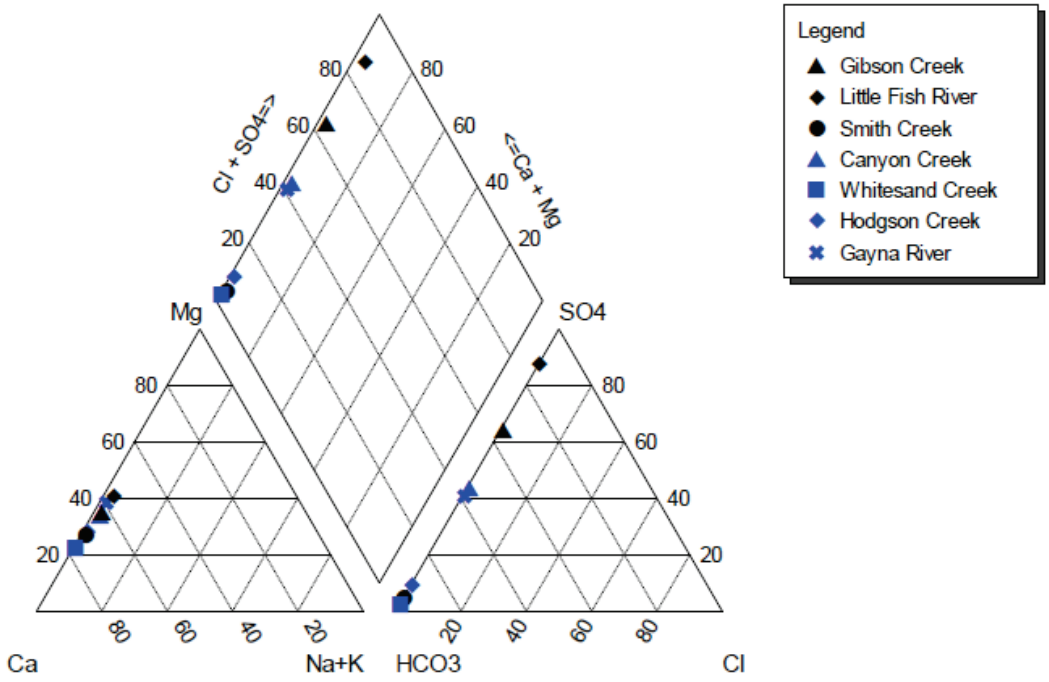

Figure 3- 13: Piper plot of lowest TDS surface water samples.

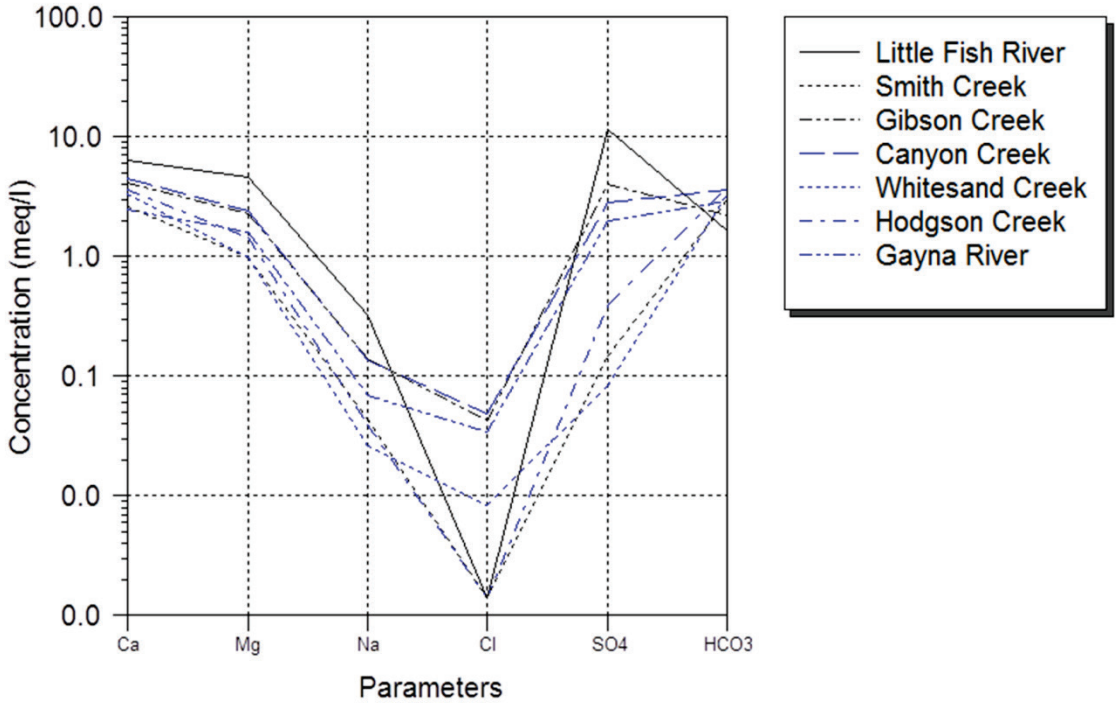

Figure 3- 14: Schoeller diagram of lowest TDS surface water samples.

Groundwater

Although the sampled groundwaters originated from similar geologic formations, there is a large amount of variability in water chemistry (Figure 3- 15). The groundwater springs sampled along the primary rivers generally have higher total dissolved solids than the local surface water. Groundwater samples were collected from Gibson Creek, Gayna Creek, Smith Creek, White Sand Creek, Hodgson Creek and Canyon Creek in March 2008 and along Little Fish Creek in September 2008. The temperature and TDS of groundwater samples are listed in Table 3- 1. Based on the TDS and temperature, groundwaters are divided into two types, warm thermal groundwaters that are > 5°C with a TDS of > 1000 ppm and non-thermal groundwaters with a temperature of < 5°C and TDS of < 1000 ppm. A piper plot of all samples is shown in Figure 3- 15; this illustrates the variability in water chemistry (full results in Appendix B). Not only is there a large range in the relative proportions of different ions, but also a wide range of absolute concentrations with over an order of magnitude in variability for many major ions (Figure 3- 16). Groundwater samples from each of the seven primary rivers are described below.

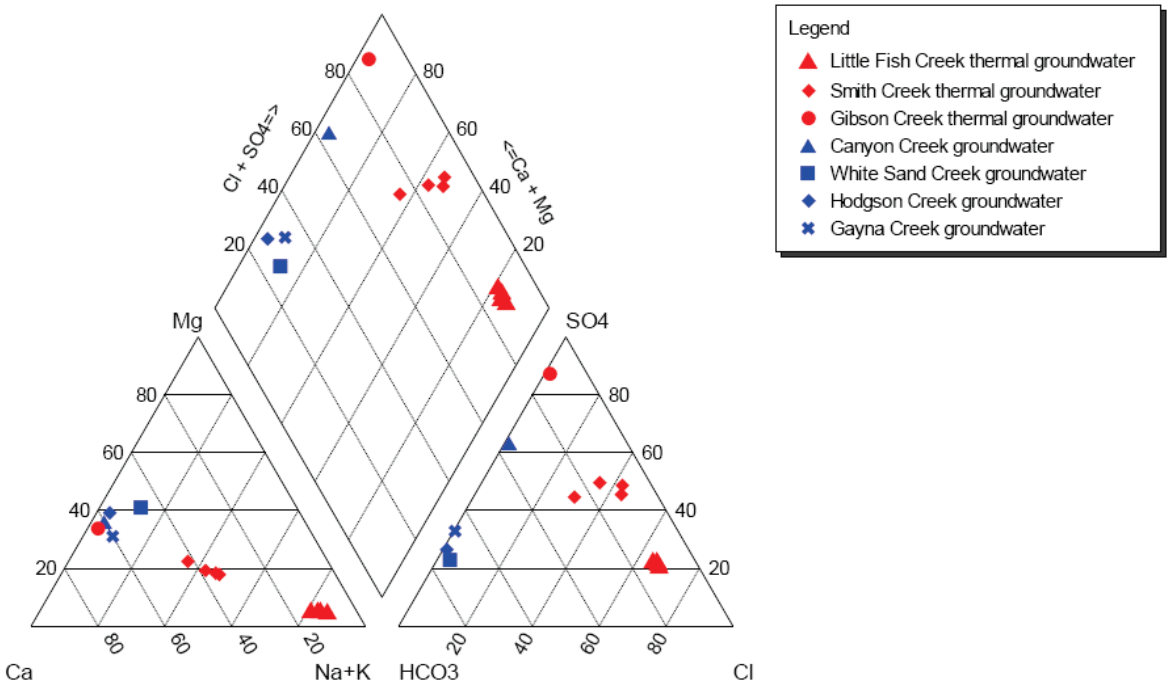

Figure 3- 15: Piper plot of groundwater samples. Red symbols represent thermal groundwaters and blue symbols are non-thermal groundwaters.

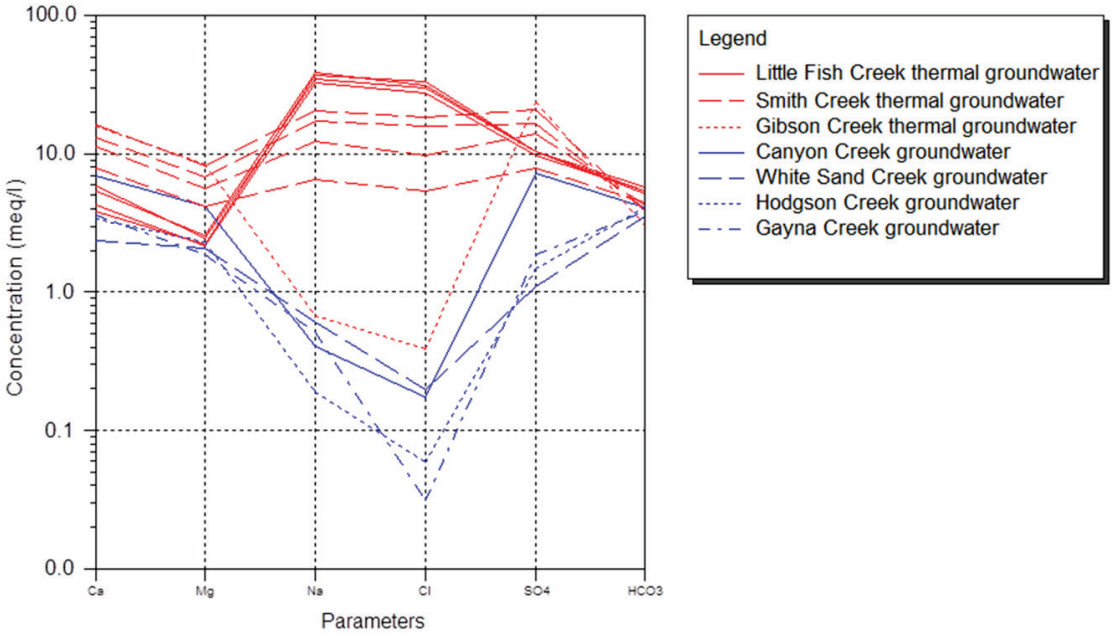

Figure 3- 16: Schoeller diagram of geochemistry from groundwater springs. Red lines represent thermal groundwaters and blue lines are non-thermal groundwaters.

Groundwater and Surface Water Chemistry of the Primary Rivers

Little Fish Creek:

Thermal groundwater discharges from numerous spring vents with a maximum temperature of 15.9 °C and TDS of 3012 ppm. The relative proportions of ions are illustrated in Figure 3- 17. The dominant ions in water are Na^+ (848 ppm) and Cl^- (1182 ppm) with an average molar ratio of Na/Cl of 1.17 ± 0.05 (n = 4). The Na^+ and Cl^- may be from marine-derived porewater (modern seawater = 0.89) (Clark *et al.*, 2001). There is more Na^+ than expected, which may be the result of cation exchange occurring with clay minerals in the shale bedrock. The relatively high SO_4^{2-} concentrations are likely the result of weathering of shale that is abundant in the regional geology (Figure 3- 10)(Norris, 1977).

During the September 2008 sampling campaign, the lowest TDS water was sampled from the creek upstream of the groundwater springs at site 10 (Figure 3- 5). This water had a TDS of 846 ppm and was dominated by Ca^{2+} (128 ppm), Mg^{2+} (56 ppm), and SO_4^{2-} (551 ppm). This water is likely from the shallow non-perennial groundwater system proposed by Clark *et al.* (2001), but with higher concentrations of Ca^{2+} and SO_4^{2-}. Supra-permafrost drainage waters which were noted by Clark *et al.* (2001) were not directly sampled in this study.

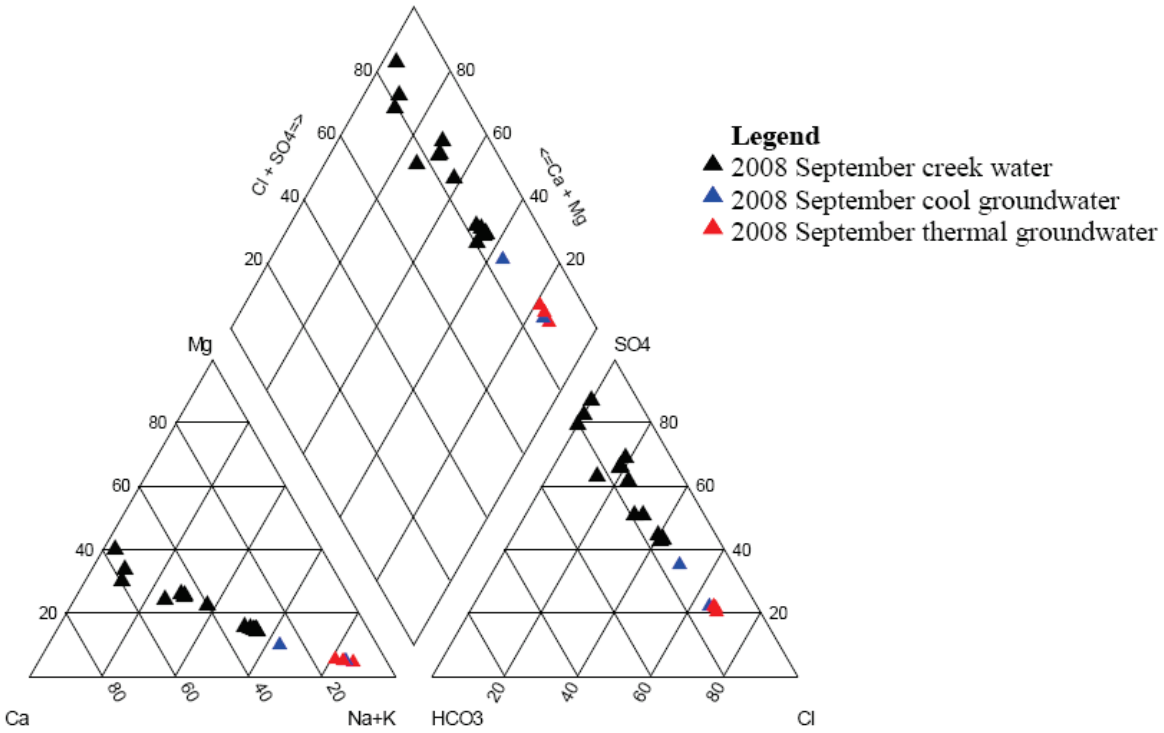

Figure 3- 17: Piper plot of major ion geochemistry from Little Fish Creek water samples.

Smith Creek:

Thermal groundwater discharges into three pools and along the creek. The groundwater had a maximum temperature of 13.8 °C and TDS of 2817 ppm. The relative proportions of major ions are illustrated in Figure 3- 18. Water chemistry is dominated by Na^+ (472 ppm) and Cl^- (651 ppm) ions that have an average molar Na/Cl value of 1.20 ± 0.05 (n = 4). The Na^+ and Cl^- were attributed to the dissolution of halite by Michel (1977) due to the presence of halite in the local geology (Figure 3- 11). The excess Na^+ was attributed to cation exchange in shales. Groundwater discharge occurs through the Fort Simpson Formation; however the Na-Cl composition and $\delta^{34}S$ suggest that most of the groundwater flow path is through the Bear Rock Formation and Saline River Formation (Michel, 1977; Michel, 1986).

During the March 2008 sampling campaign, the river water at the most upstream sampling site had an electrical conductivity of 887 µS/cm. The water sample collected at this most upstream location was found to contain thermal groundwater. The water sample

was collected near the creek bank, while the TDS was measured further into the stream channel. After sampling was conducted, it was not noted until later that there was a small thermal spring vent in the stream channel near where the water sample was taken. At the time re-sampling was not possible due to limited time and extreme cold winter conditions. For this reason the electrical conductivity was used in calculations. During the June 2008 sampling campaign, the lowest TDS water was sampled at site 6 (Figure 3- 5); this sample was taken to be representative of runoff at this location. The June sample had a TDS of 257 ppm and was dominated by Ca^{2+} (52 ppm), Mg^{2+} (12 ppm), and HCO_3^- (182 ppm) ions.

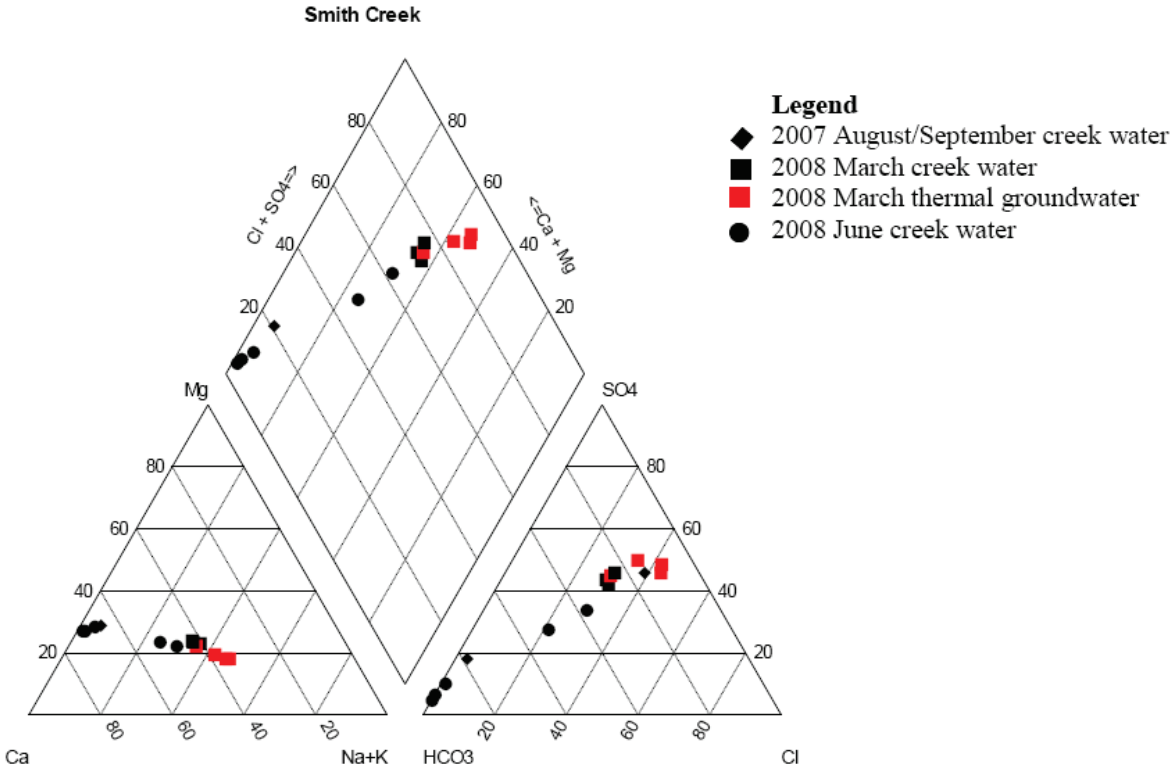

Figure 3- 18: Piper plot of major ion geochemistry from Smith Creek water samples.

Gibson Creek:

Thermal groundwater discharges into a large pool where the maximum recorded temperature was 8.2 °C and TDS was 1769 ppm. The relative proportions of ions are illustrated in Figure 3- 19. These groundwaters are dominated by Ca^{2+} (316 ppm), Mg^{2+}

(102 ppm) and SO_4^{2-} (1127 ppm) which likely originate from the weathering of anhydrite and dolomite in the Bear Rock Formation (Figure 3- 12) (Michel, 1977).

The lowest TDS water was collected in June 2008 from site 2 (Figure 3- 6); this sample was taken to be representative of runoff at this location. This sample had a TDS of 415 ppm and was dominated by Ca^{2+} (82 ppm), Mg^{2+} (27 ppm), HCO_3 (130 ppm) and SO_4^{2-} (190 ppm).

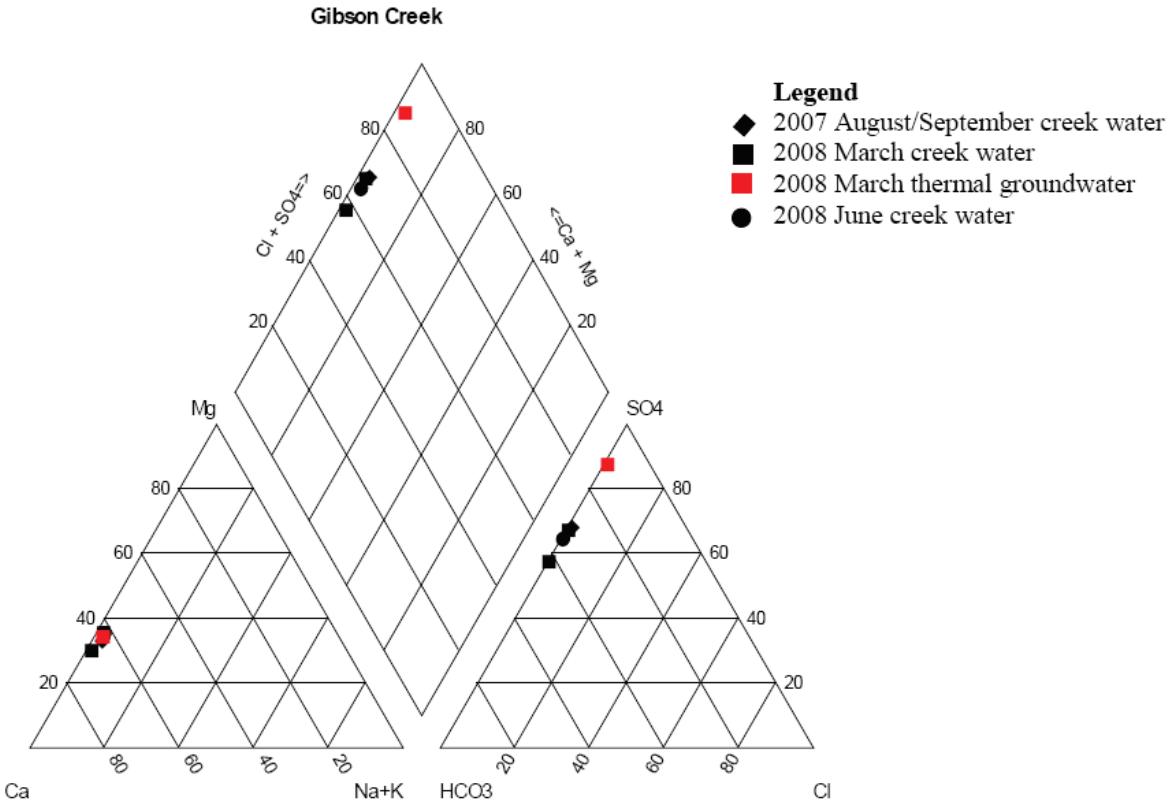

Figure 3- 19: Piper plot of major ion geochemistry from Gibson Creek water samples.

White Sand Creek, Hodgson Creek, Canyon Creek and Gayna River:

Cool groundwater that discharges along these rivers had temperatures ranging from 0.5°C to 3.8 °C and TDS ranging from 371 ppm to 811 ppm. The relative proportions of ions are illustrated in Figure 3- 20 and Figure 3- 21. Along White Sand Creek, Hodgson Creek and Gayna Creeks, groundwater was dominated by Ca^{2+}, Mg and HCO_3^- ions. Ca^{2+}, Mg^{2+} and HCO_3^- in these groundwaters were attributed to the weathering of calcite and

dolomite during recharge (Figure 3- 11 and Figure 3- 12) (Michel, 1977). In the Franklin Mountains east of the Mackenzie, there are karst sinkholes in the Franklin Mountain Formation and the Mount Kindle Formation, where dissolution of Ca^{2+}, Mg^{2+} and HCO_3^- are expected to occur (Van Everdingen, 1981). Canyon Creek groundwater had similar characteristics but with higher SO_4^{2-} concentrations. The SO_4^{2-} and some of the Ca^{2+} were attributed to the dissolution of anhydrite in the Bear Rock Formation that is composed of brecciated dolomite and gypsum, which has high porosity and permeability.

Samples taken in June 2008 and September 2007 from these four rivers had the lowest TDS and therefore were considered to be representative of runoff at the locations specified below. In June 2008, the lowest TDS sample from White Sand Creek was from site 3 (Figure 3- 7).This water had a TDS of 288 ppm and was dominated by Ca^{2+} (67 ppm), Mg^{2+} (12 ppm) and HCO_3^- (202 ppm). Along Hodgson Creek, the lowest TDS was from site 2. This sample was almost identical to the sample from site 1 (Figure 3- 7), having a TDS of 348 ppm and being dominated by Ca^{2+} (73 ppm), Mg^{2+} (17 ppm) and HCO_3^- (234 ppm). Along Canyon Creek, the lowest TDS was from site 5 (Figure 3- 6). This water had a TDS of 482 ppm and was dominated by Ca^{2+} (89 ppm), Mg^{2+} (28 ppm) and HCO_3^- (221 ppm). In September 2007 along Gayna River, the lowest TDS was from site 2 (Figure 3- 8). This water had a TDS of 345 ppm and was dominated by Ca^{2+} (49 ppm), Mg^{2+} (19 ppm) and HCO_3^- (176 ppm).

The chemistry of the groundwater and surface runoff along these rivers is variable. This is illustrated in the piper plots shown in Figure 3- 20 and Figure 3- 21. Generally, these surface waters have been classified as being dominated by Ca^{2+} and HCO_3^-, however some have higher proportion of SO_4^{2-}. Surface water along different creeks is different as there are different geological formations outcropping along these rivers.

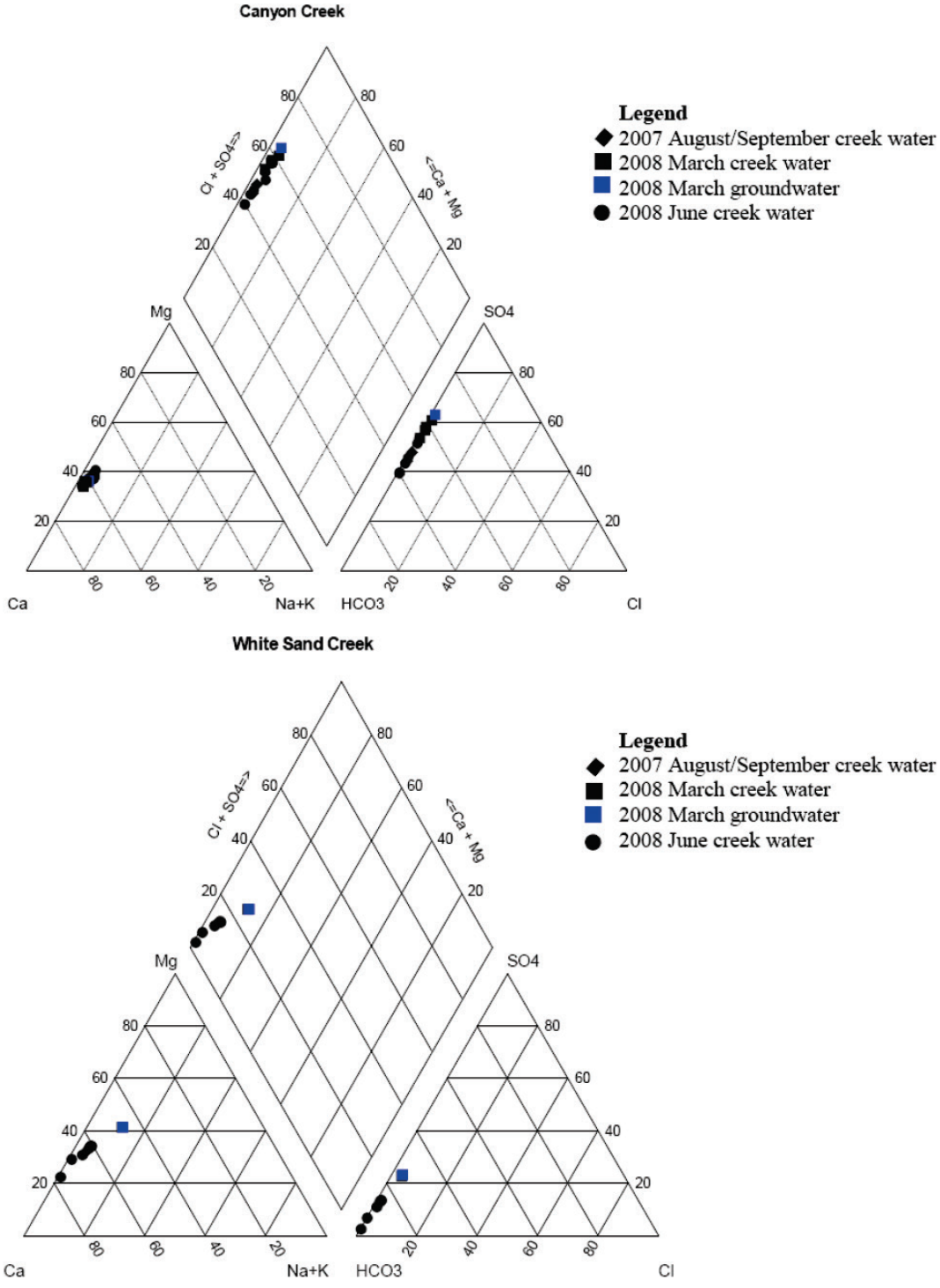

Figure 3- 20: Piper plot of major ion geochemistry from Canyon Creek and White Sand Creek water samples.

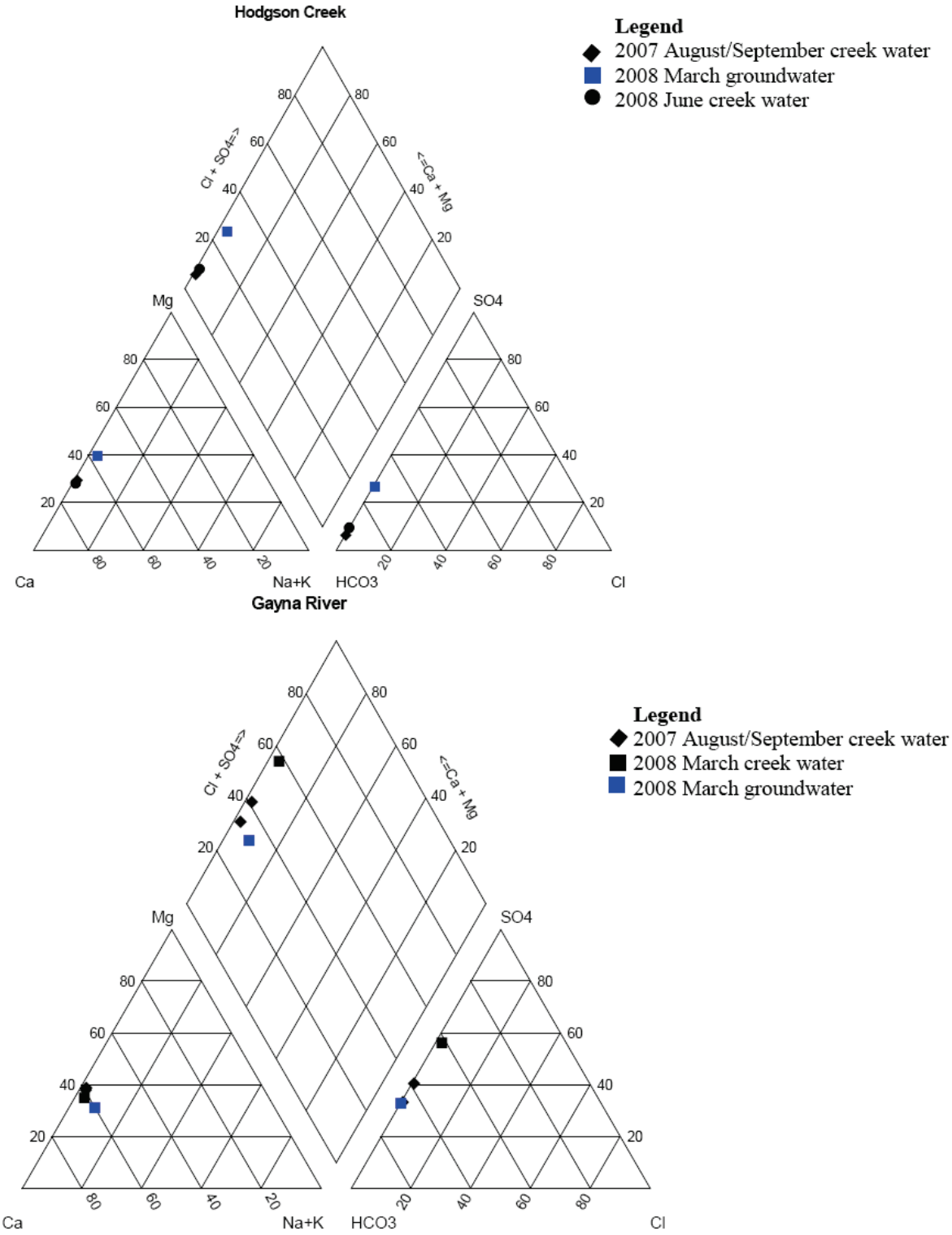

Figure 3- 21: Piper plot of major ion geochemistry from Hodgson Creek and Gayna River water samples.

Table 3- 1: Summary of data from groundwater springs along primary river including: total dissolved solids, local geologic formation, the dominant ions in groundwater from those sites as well as likely mineral sources of these ions. (Geological formation information compiled from, Aitken and Cook, 1974, Douglas and Norris, 1973; Norris, 1977, Norris, 1985 and Walter, 1981).

River	Temp. (°C)	TDS (ppm)	Geologic Formation	Dominant Ions	Likely Mineral Sources
Non-Thermal:					
Canyon	0.5	811	Devonian carbonates including Bear Rock Fm.	Ca^{2+}-Mg^{2+}-HCO_3^--SO_4^{2-}	Dolomite, calcite, anhydrite
Hodgson	2.2	428	Devonian: Bear Rock Fm.	Ca^{2+}-Mg^{2+}-HCO_3^-	Dolomite, calcite
White Sand	3.8	371	Devonian: Bear Rock Fm.	Ca^{2+}-Mg^{2+}-HCO_3^-	Dolomite, calcite
Gayna	3.1	437	Devonian: Bear Rock Fm.	Ca^{2+}-Mg^{2+}-HCO_3^-	Dolomite, calcite
Thermal:					
Little Fish	15.9	3012	Discharge from a fault in Permian limestone	Na^+-Cl^--Ca^{2+}-Mg^{2+}-HCO_3^-	Calcite, dolomite, shale
Smith	13.8	2817	At surface quaternary alluvial sediments, close to the contact with the Devonian Fort Smith Formation which is composed of shale mudstone and siltstone.	Ca^{2+}-Mg^{2+}-SO_4^{2-}-HCO_3^-	Dolomite, calcite, anhydrite
Gibson	8.2	1767	Discharge where a thrust fault reaches the surface.	Ca^{2+}-Mg^{2+}-SO_4^{2-}	Anhydrite, dolomite

3.5.2 Determining Groundwater Contributions Using Major Ion Chemistry

The characterization of groundwater and surface water chemistry was used to determine the relative contributions of groundwater to river water discharge. The relative groundwater contributions have been determined for four rivers: Little Fish Creek, Smith Creek, Canyon Creek and White Sand Creek.

Where two end-members have been isolated, only one chemical parameter of the end-members is needed for the calculation of groundwater proportions. In general a conservative water constituent is used (e.g. Cl^-), however where electrical conductivity values were more representative these were used. The values of the chemical constituents for each end-member are used in Equation 3- 1.

Equation 3- 1: $[F_B] = \frac{(S - A)}{(B - A)}$

Where S is the value for the sample, A is the value of one end-member (e.g. surface water), B is the value of the other end-member (e.g. Groundwater) and F_B is the proportion of end-member B in the sample water.

The proportion of end-members in three-component mixing is found using two chemical parameters for each end-member. In this study Cl^- and SO_4^{2-} are assumed to be conservative and so were chosen as the chemical parameters to un-mix river waters. Three end-member mixing is done by combining Equation 3- 2, Equation 3- 3 and Equation 3- 4. Equation 3- 2 indicates percent concentration of each end-member (x, y, z) that is represented per unit of water (represented as 1). Equation 3- 3 and Equation 3- 4 are mass balance equations where the concentration of the given chemical parameter in each end-member is weighted by the percent contribution of each end-member and then summed to give the total concentration of a given chemical parameter in the sample. These three equations are combined to solve for the proportion of each end-member in a given sample. Equation 3- 2 is shown with x as the only unknown in Equation 3- 5.

Equation 3- 2: $1 = x + y + z$

Equation 3- 3: $\mathrm{Cl}_{\mathrm{sample}} = x\mathrm{Cl}_{\mathrm{x}} + y\mathrm{Cl}_{\mathrm{y}} + z\mathrm{Cl}_{\mathrm{z}}$

Equation 3- 4: $SO_{4\,\mathrm{sample}} = xSO_{4\mathrm{x}} + ySO_{4\mathrm{y}} + zSO_{4\mathrm{z}}$

Equation 3- 5: $$\mathrm{x} = \frac{1 - \frac{\mathrm{SO}_{4\mathrm{sample}} - \mathrm{SO}_{4\mathrm{y}}}{\mathrm{SO}_{4\mathrm{z}} - \mathrm{SO}_{4\mathrm{y}}} - \frac{\mathrm{Cl}_{\mathrm{sample}} - \mathrm{Cl}_{\mathrm{z}}}{\mathrm{Cl}_{\mathrm{y}} - \mathrm{Cl}_{\mathrm{z}}}}{1 - \frac{\mathrm{SO}_{4\mathrm{x}} - \mathrm{SO}_{4\mathrm{y}}}{\mathrm{SO}_{4\mathrm{z}} - \mathrm{SO}_{4\mathrm{y}}} - \frac{\mathrm{Cl}_{\mathrm{x}} - \mathrm{Cl}_{\mathrm{z}}}{\mathrm{Cl}_{\mathrm{y}} - \mathrm{Cl}_{\mathrm{z}}}}$$

Little Fish Creek (on the Big Fish River):

Clark *et al*. (2001) identified three end-member components to river flow: deep thermal groundwater, shallow non-perennial groundwater and surface runoff/ active layer drainage. It was found that the amount of discharge from the shallow groundwater systems

varied throughout the year, and that there was no shallow groundwater discharge in midwinter. This aquifer is referred to a shallow non-perennial groundwater system.

Sampling was conducted on September 20th, and September 22nd 2008 at locations shown on Figure 3- 22-A. Between the two days of sampling was a major precipitation event which changed river level significantly. Water samples from the thermal groundwater springs have high Cl^- (1200 ppm) and SO_4^{2-} (500 ppm) concentrations (see Figure 3- 22-B, complete results in Appendix B). Creek water samples were taken before and after the rains at sites 9 (upstream) and 3 (downstream). At site 9, prior to the rain, the Cl^- concentration was 75 ppm and the SO_4^{2-} was 482 ppm. After the rain, the Cl^- concentration was below the detection limit of 0.1ppm and the SO_4^{2-} was 518 ppm. Downstream at site 3, prior to the rain Cl^- concentration was 360 ppm and the SO_4^{2-} was 519 ppm. After the rain the Cl^- concentration was 107 ppm and the SO_4^{2-} was 524 ppm. The rain event decreases the concentrations of Cl^- but increases the concentrations of SO_4^{2-}.

Sampling site 10 is the most upstream and is located at the confluence of two tributaries. Both of these creeks had Cl^- concentrations below the detection limit (<0.12 ppm) and high SO_4^{2-} (551 and 628 ppm, respectively). Discharge from the two upstream tributaries is interpreted to be derived from the shallow non-perennial aquifer. This water had higher SO_4^{2-} concentrations than the shallow springs sampled in 1996 that had an average concentration of 174 ppm for Cl^- and 198 ppm for SO_4^{2-}.

Based on the sampling conducted, the end-members for groundwater mixing calculations of Little Fish Creek have been revised from those used by Clark *et al*. (2001). Mixing calculations have been performed using the values listed in Table 3- 2, with the results plotted vs. distance upstream from the most downstream sampling site in Figure 3- 22-C. Mixing calculations were conducted using the chemical compositions determined in this study for thermal groundwater and non-perennial groundwater and the runoff composition was used from Clark *et al.* (2001). Groundwater proportions were also re-calculated using these revised end-members for the values presented in Clark *et al.* (2001). Prior to the rain event in September 2008, thermal groundwater contributed 33% of river flow, while after the heavy rain it decreases to 9% due to dilution (Figure 3- 22-C). In

June, during the spring freshet, thermal groundwater makes up about the same percentage of river flow as after the heavy rain. Discharge from the thermal groundwater springs is probably roughly the same through the year. Thermal groundwater represents roughly the same amount of water in the river during the June 1997 and September 2008 sampling, indicating river flow is roughly the same during both samplings.

Figure 3- 22-C shows the proportions of river water from thermal groundwater and shallow groundwater. June, 1997 values from Clark *et al.* (2001) are recalculated using the new end members and shown with green triangles with blue outline. In September 2008, the amount of both thermal groundwater and shallow groundwater is shown with the blue diamonds before the rain event and squares after the rain event. In September, groundwater represents a larger proportion of river flow compared to June. In June 1997 the majority of river flow that is not from deep groundwater is from surface runoff and active layer drainage, while in September 2008 there is a much larger proportion of shallow groundwater. After the large rain event, the shallow groundwater system is likely flushed, resulting in a higher estimate of this component of flow.

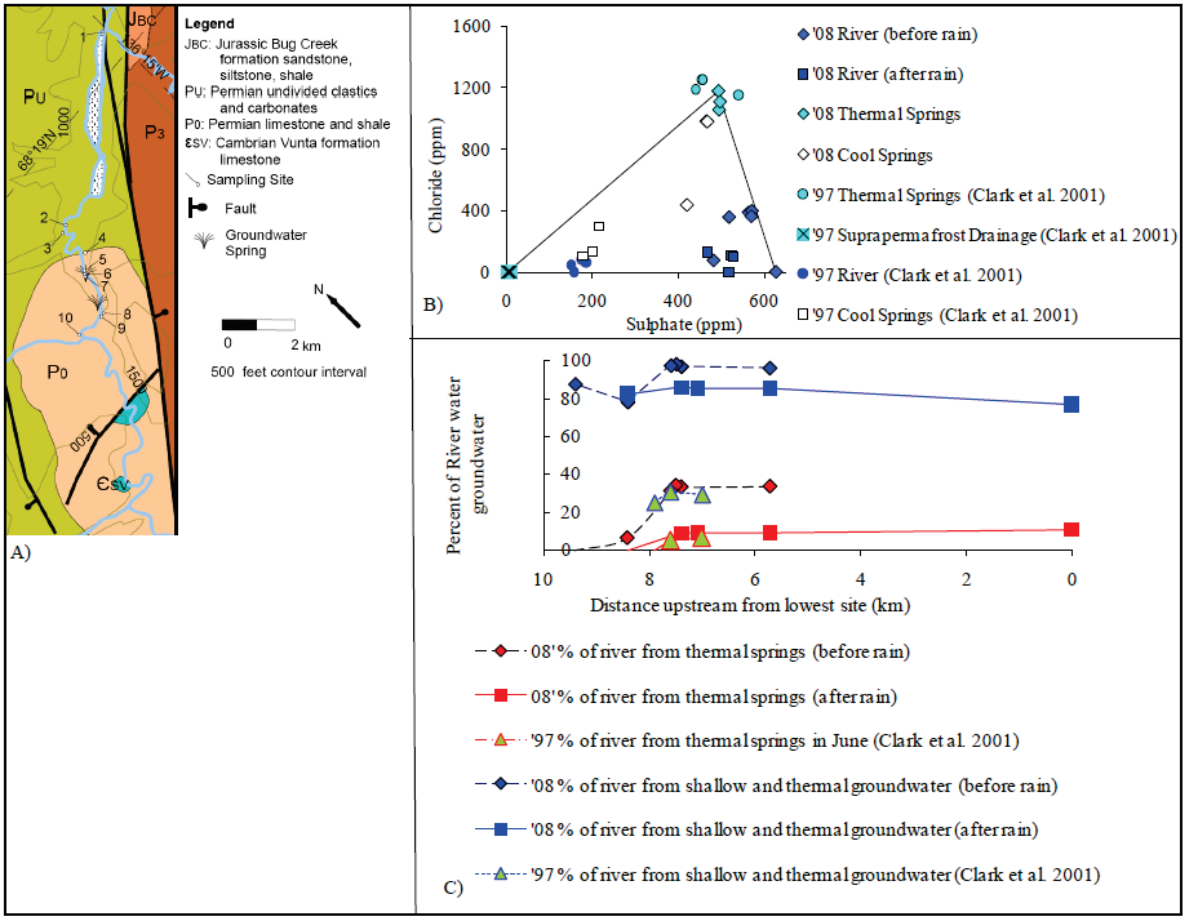

Figure 3- 22: a) Bedrock geology and sampling sites along Little Fish Creek. Geological information from Norris (1977) b) Cl^- vs. SO_4^{2-} of water samples (includes data from Clark *et al.* 2001) c) Proportion of thermal groundwater and shallow groundwater as percent of river flow vs. the distance from the most downstream sampling site (Site number 1).

Table 3- 2: End-member water compositions. Runoff composition from Clark *et al.* (2001)

	Chloride ppm	Sulphate
Shallow Groundwater	1	628
Run off	0.1	0.1
Thermal Groundwater	1191	494

Smith Creek

During field sampling the electrical conductivity was measured; the results of this measurement suggested that there are at least two water sources in Smith Creek. Based on the electrical conductivity, it was found that groundwater has high TDS while creek water had much lower TDS. Samples were collected upstream and downstream of groundwater discharge (site 3) at the sampling sites shown in Figure 3- 23-A.

The mixing of groundwater and surface water is shown with Cl^- vs. SO_4^{2-} in Figure 3- 23-B. The trend is mostly linear; however, at low concentrations it is evident that there are more than two end-members (Figure 3- 23-B see zoom-in insert). In June 2008, the most upstream samples had the lowest concentrations of chloride and sulphate and they also had the lowest ratios of Cl^-/SO_4^{2-}. This lower Cl^-/SO_4^{2-} slope suggests that there is a third river water component that is interpreted to be shallow groundwater. The geochemical composition of the shallow aquifer was found by completing the mixing triangle shown in Figure 3- 23-B. The different end-members have been used to determine the relative amounts of thermal groundwater in the creek in March and June.

Creek water mixing calculations were conducted using the EC values for the March 2008 sampling. This was done as the most upstream water sample was not truly representative of creek water as it was collected too close to a thermal spring. At this same upstream site EC was measured towards the middle of the creek channel and was found to be representative of creek water. For the June 2008 sampling, the proportion of deep thermal groundwater in the creek has been calculated from a two end-member mixing calculation using sample conductivity as well as a three end-member calculation using

concentrations of sulphate and chloride (Figure 3- 23-B). The end-member values used in these calculations are shown in Table 3- **3** with the results of this calculation shown in Figure 3- 23-C. In March 2008, bedrock groundwater makes up 34% of discharge at the most downstream site. In June 2008, the creek is comprised of only 8% groundwater. This dilution is presumably due to an increase in creek flow in the spring caused by rain and snowmelt.

Although it is evident that there are three end-members, the runoff end-member and shallow groundwater end-member are very similar. Because of the similarity between the two end-members, a slight shift in the concentrations will have a large change to the outcome of the proportions of these two end-members. Due to the remaining uncertainties, the proportions of shallow groundwater and runoff are not calculated. Despite this uncertainty, the proportion of thermal groundwater is consistent if calculated using conductivity or chemistry (Figure 3- 23-C).

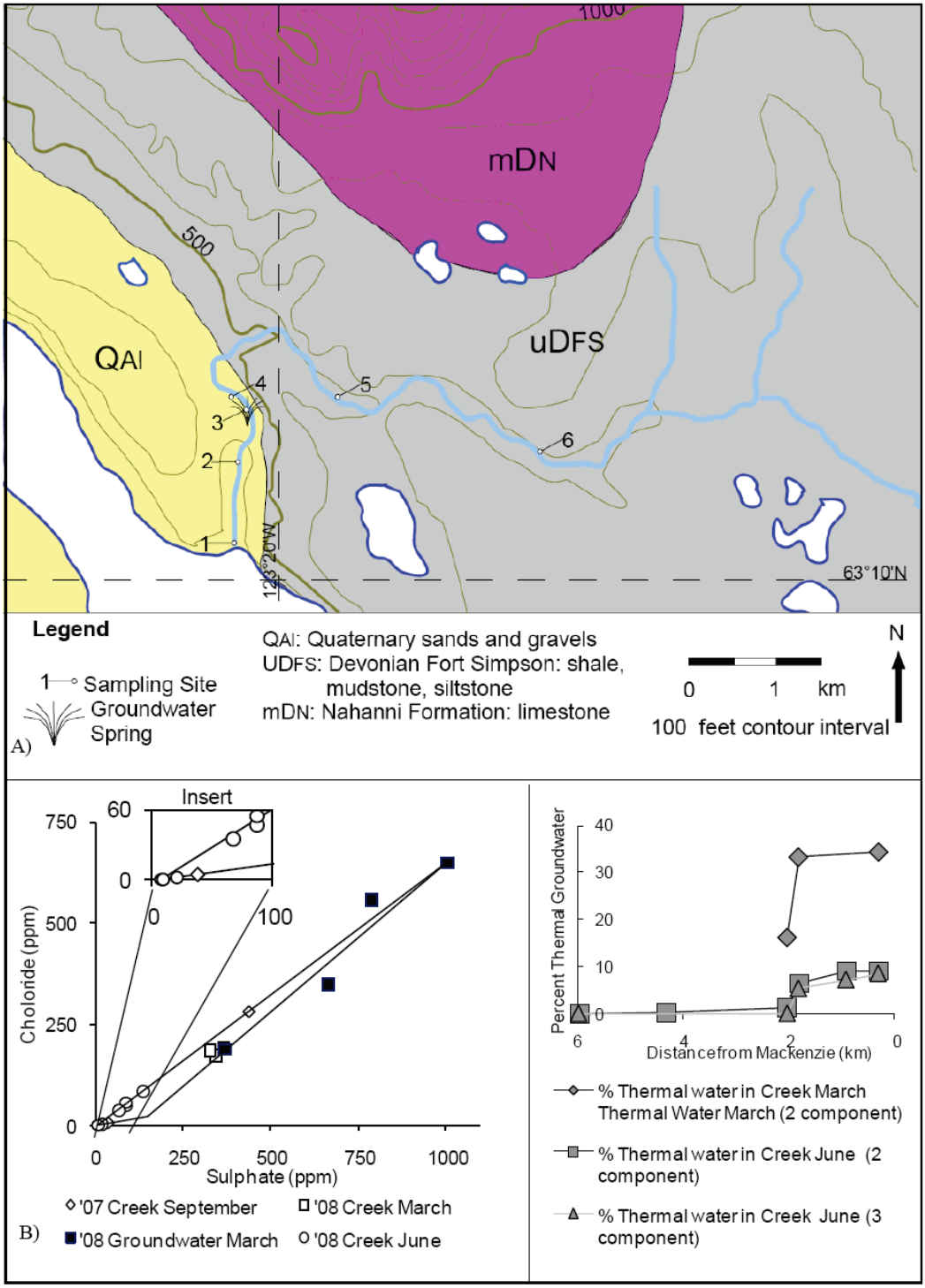

Figure 3- 23: Sampling locations and major geological units near Smith Creek, NWT (Geological information from Douglas and Norris 1973) b) Cl^- vs. SO_4^2 of water samples from Smith Creek. Three component mixing triangle shown with zoomed-in insert to show samples with lower Cl^- and SO_4^{2-} concentrations. c) Proportion of thermal groundwater as a percent of river flow vs. distance from the Mackenzie River. Two component mixing was calculated with electrical conductivity and three component was done with Cl^- and SO_4^{2-} concentrations.

Table 3- 3: End-member water compositions.

	Chloride ppm	Sulphate	Conductivity uS/cm
Shallow Groundwater	20	150	
Runoff	0	7.8	307
Thermal Groundwater	651	1006	3880

Canyon Creek

Along Canyon Creek, groundwater discharge is less evident and only one small spring was found, at site 1 (Figure 3- 24-A). Water sampled at this groundwater spring in March 2008 had higher concentrations of Cl^- and SO_4^{2-} than surface water samples from the creek that were sampled at this time (Figure 3- 24-B). This groundwater discharges through alluvial gravels, but is likely derived from a bedrock aquifer. The major ion chemistry of this groundwater is similar to the other non-thermal groundwaters in the region indicating it likely flows in a similar aquifer. In general, the March 2008 surface water had higher solute concentrations than the June 2008 samples. Samples collected along Canyon Creek in March 2008 show approximately two-component mixing, presumably between bedrock groundwater and a shallow groundwater. In June 2008, river water appears to be primarily a mix of runoff and the proposed shallow groundwater. Based on the mixing end-members in Figure 3- 24-B, Cl^- and SO_4^{2-} composition of the end-member waters are calculated and shown in Table 3- 4. Using these end-members, river water un-mixing calculations were performed. At the most downstream site in March 89 %, of creek water is groundwater derived (Figure 3- 24-C). In March, the upstream section of the creek was determined to have 22 % groundwater while in June, this section had 0 % groundwater. In June, there is typically significant snow melt and rain that greatly dilutes the groundwater signal.

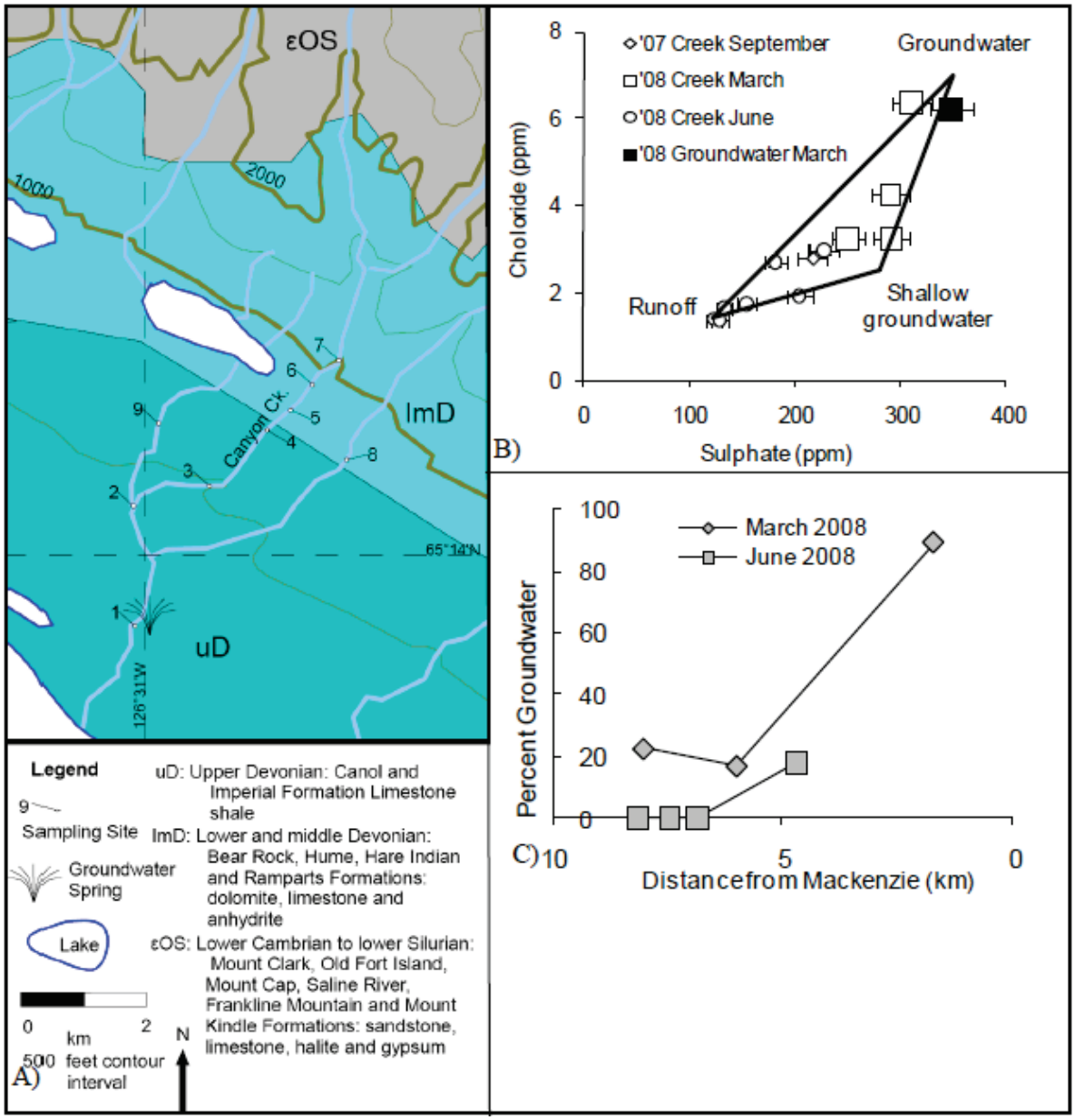

Figure 3- 24: A) Geology and sampling locations along Canyon Creek. (Geology from Walter, 1981) B) Cl^- vs. SO_4^{2-} concentrations from Canyon Creek and mixing triangle indicating three end-members. C) Proportions of bedrock groundwater as a percent of river flow vs. distance from the Mackenzie River.

Table 3- 4: End-member water compositions.

	Chloride ppm	Sulphate
Shallow Groundwater	2.5	280
Run off	1	1
Bedrock Groundwater	7	350

White Sand Creek:

During the March 2008 sampling one groundwater sample and one creek water sample beside the spring were collected. The creek was interpreted to be 100% groundwater at that time (site 3, Figure 3- 25-A). In June 2008, samples were collected upstream and downstream of this discharge location. Cl^- and SO_4^{2-} are used as a tracer of water sources (Figure 3- 25-B). The lowest concentrations represent runoff, while the highest are groundwater. A third end-member is interpreted to exist which has higher sulphate than runoff and lower chloride than the groundwater and is construed to be water from a shallow aquifer. The chemical composition of these three end-members is listed in Table 3- 5. These compositions were used to perform creek water mixing calculations from the June samples and the relative proportions of bedrock groundwater in the creek at this time are shown in Figure 3- 25-C. At the most downstream site in June, there is 22% groundwater.

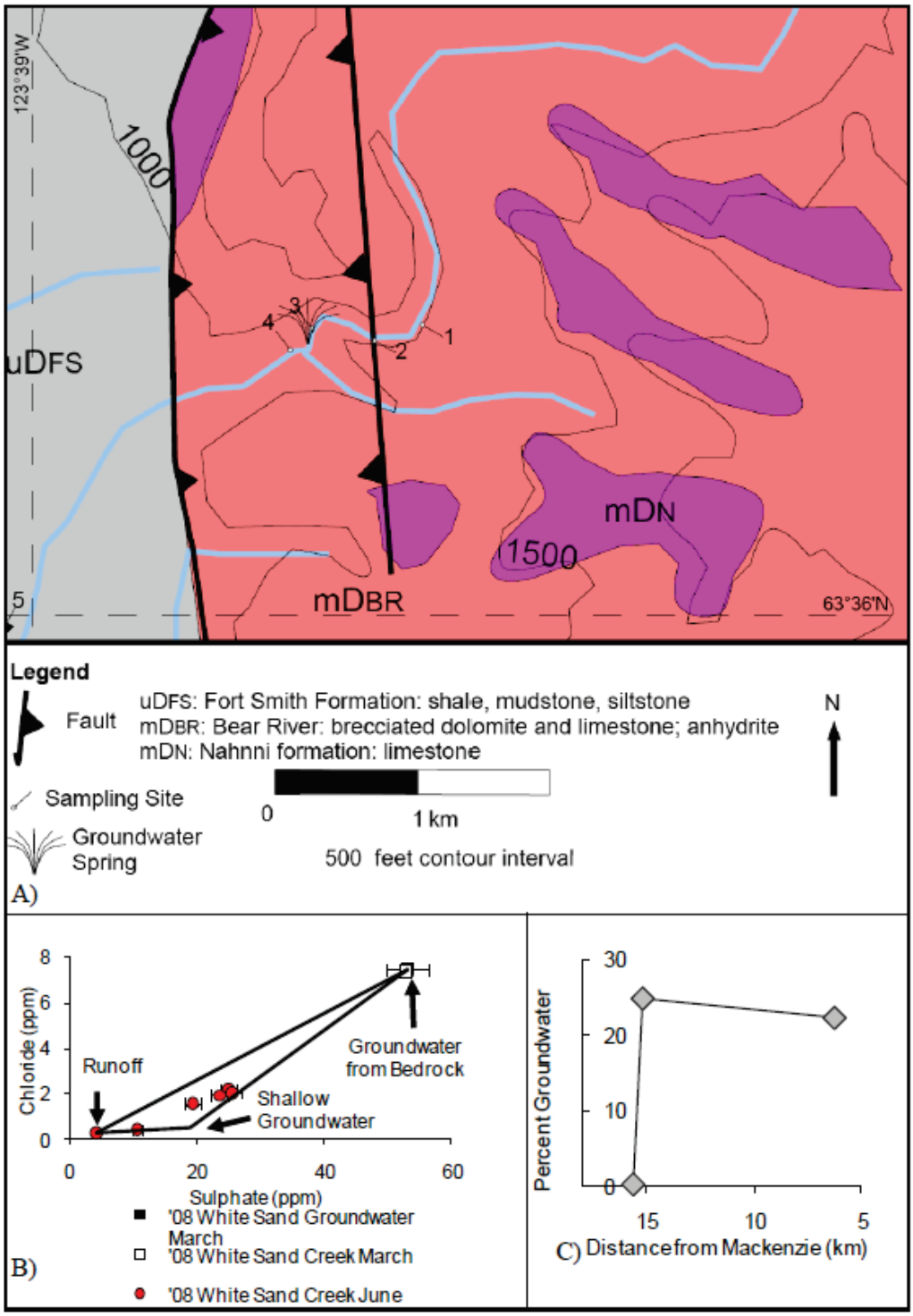

Figure 3- 25: A) Geology and sampling locations along White Sand Creek (Geological information from Douglas and Norris, 1973) B) Cl^- and SO_4^{2-} from White Sand Creek and mixing triangle indicating three end-members. C) Proportions of bedrock groundwater as a percent of river flow vs. distance from the Mackenzie River.

Table 3- 5: End-member water compositions.

	Chloride ppm	Sulphate
Shallow Groundwater	0.5	19
Run off	0.3	4.1
Bedrock Groundwater	7.5	53.2

3.5.3 Groundwater Recharge: DIC, Calcite Saturation Index and ^{13}C

The concentrations and isotopic ratios of dissolved organic carbon (DIC) can be used to determine recharge conditions. In most cases during recharge, water dissolves CO_2 from the soil where it is produced from the decomposition of organic matter (Clark and Fritz, 1997). The initial $\delta^{13}C_{DIC}$ signal in the water from the dissolved CO_2 in soil is typically ~-23‰ for C3 vegetation (Clark and Fritz, 1997). CO_2 in groundwater may also originate from other sources resulting in a different isotopic signature. For example CO_2 from C3 vegetation like sugar cane and corn produces CO_2 with a $\delta^{13}C$ -9‰ (Vogel, 1993). Other sources of CO_2 have unique $\delta^{13}C$ signatures, for example mantle CO_2 generally has a $\delta^{13}C$ between -5 and -7‰ (Hoefs, 2009). In Yukon and NWT soil CO_2 is assumed to be primarily from the decomposition of C3 vegetation. The acidity in the water is then consumed during weathering of carbonates that have a $\delta^{13}C$ of 0‰, which enriches the DIC, providing dissolution takes place under closed system conditions. Open system conditions dominate under unsaturated conditions where there is a continual supply of CO_2. Under such conditions there is equilibrium between soil CO_2 and DIC as such the $\delta^{13}C_{DIC}$ is determined by the pH. Under open system conditions, the final $\delta^{13}C$ is generally between -15 ‰ and -18 ‰. If water dissolves CO_2 during recharge, then weathers carbonate minerals along its flow path, as in closed system weathering, the end $\delta^{13}C_{DIC}$ will be close to -12‰. Greater enrichments can be generated through continued exchange between DIC and the carbonate matrix, and through incongruent dissolution of dolomite. Due to the greater partial pressure of CO_2 in soil, water dissolves more CO_2 in soil than it would under atmospheric air conditions, resulting in this more enriched $\delta^{13}C_{DIC}$ signal. If water recharges through soil and dissolves a greater amount of CO_2, the water may in turn dissolve more carbonate material. If the partial pressures of CO_2 decrease, for example after groundwater

discharge, the CO_2 may degas resulting in calcite super-saturation. Dissolved inorganic carbon was measured in all water samples. Samples from March 2008, September 2008 and August 2009 were also measured for $\delta^{13}C_{DIC}$. The calcite saturation index was calculated using WAT4 software (Ball, 1988). Groundwater samples are near calcite saturation with indices of -0.136 to 0.366. Surface water was often supersaturated in calcite, and had saturation indices of -0.771 to 1.25. Figure 3- 26-A to G shows these trends on a graph of DIC vs. pH of water samples. Along with samples the saturation curves of calcite and dolomite are shown as well as the open and closed system weathering trajectories for initial soil P_{CO2} values of $10^{-1.5}$ and $10^{-2.5}$ atm. At the surface, there is lower confining pressure and CO_2 may degas during flow resulting in calcite super-saturation of surface waters.

Most samples have P_{CO2} values between 10^{-2} and 10^{-3} atm, which are consistent with recharge through organic soil. P_{CO2} values of 10^{-2} atm reflect open system recharge, and P_{CO2} values of 10^{-3} may reflect open or closed system conditions. The $\delta^{13}C_{DIC}$ of the groundwaters ranged from -2.8 ‰ to -12.8 ‰. Along Little Fish Creek, the average $\delta^{13}C_{DIC}$ is -3.8‰ which is more enriched than the other groundwaters. The enrichment could be related to incongruent dissolution of dolomite along the flow path (Clark and Fritz, 1997). Groundwater from Smith Creek, Gibson Creek, Canyon Creek, White Sand Creek, Hodgson Creek and Gayna Creek had $\delta^{13}C_{DIC}$ values ranging from -7.4 to -12.8 ‰. These $\delta^{13}C_{DIC}$ are consistent with closed system weathering of carbonate rocks by CO_2 derived from soil. It is possible that there was minor exchange with the atmosphere resulting in some of the slightly more enriched values.

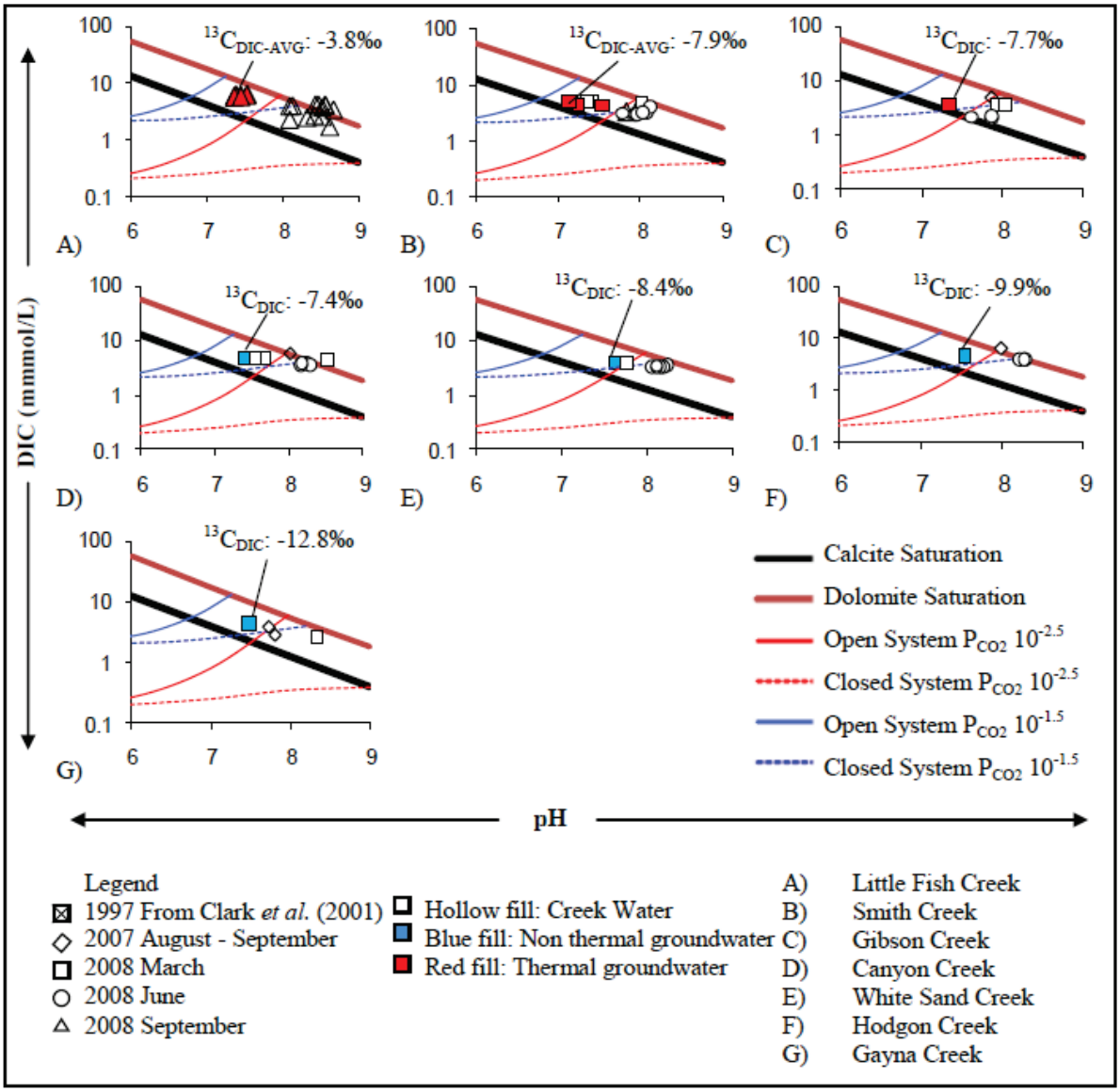

Figure 3- 26: DIC (mmol/L) vs. pH of water samples plotted with curves for calcite and dolomite saturation as well as open and closed system P_{CO2} evolution curves. Ca^{2+} and Mg^{2+} activity are equal to DIC activity. The average $\delta^{13}C_{DIC}$ values are listed for groundwaters (A to G).

3.5.4 Groundwater Recharge: Oxygen and Deuterium

δD and $\delta^{18}O$ were measured from the seven primary rivers and the Rat River. All samples with the exception of those from Little Fish Creek were compared to the meteoric water line from Fort Simpson, ($\delta D = 7.6\delta^{18}O$ - 2‰, Hayashi *et al.,* 2004). Little Fish Creek samples were compared to the meteoric water line from Inuvik ($\delta D = 7.2\delta^{18}O$ – 5.5‰ determined from IAEA GNIP database).

Groundwater

Little Fish Creek: δD and $\delta^{18}O$ results from Little Fish Creek are shown in Figure 3- 27-A with additional data from Clark *et al*. (2001). During the September 2008 sampling, thermal groundwaters had lower δD and $\delta^{18}O$ values compared to those of the river water. There was heavy rain and snow during the middle of the fall 2008 Little Fish Creek sampling campaign. Prior to the rain event, the δD and $\delta^{18}O$ composition of the river decreased progressively downstream. After the rain event there was too much scatter in the data to see a trend. Little Fish Creek thermal groundwater had an average δD of -165.0 ± 2.3‰ and an average $\delta^{18}O$ of -21.70 ± 0.2‰. These values are consistent with those of Clark *et al.* (2001) indicating stable long term discharge of thermal groundwater. The two most upstream creek water samples are interpreted to be from shallow groundwater; these waters have δD of -161.5 ± 2.2 ‰ and an average $\delta^{18}O$ of -21.2 ± 0.1‰.

Smith Creek: δD and $\delta^{18}O$ results from Smith Creek are shown in Figure 3- 27-B. Smith Creek thermal groundwater had an average δD of -179.7 ± 1.6‰ and $\delta^{18}O$ of -23.1 ± 0.1‰. During the March sampling the most enriched creek water was 1.6‰ more enriched in $\delta^{18}O$ relative to thermal groundwater. It is proposed that the more enriched water in the creek is shallow groundwater; this is consistent with groundwater mixing calculations. This enrichment suggests a greater recharge elevation for thermal groundwater. To the east of Smith Creek, the mountains have elevations between 700 and 800 m.a.s.l.. There is a 600 m elevation difference between the tops of those mountains and the groundwater springs. To correct for the change in elevation a depletion of -0.3‰/100 m of elevation gain is expected (Bortomali *et al*., 1979). Using this depletion factor, recharge from 600 m higher would be up to 1.8 ‰ more depleted.

Gibson Creek: δD and $\delta^{18}O$ results from Gibson Creek are shown in Figure 3- 27-C. In March 2008 groundwater was 0.9 ‰ more depleted than the most depleted surface water. This depletion may be the result of groundwater recharging at a higher elevation in the mountains to the east, however these mountains are further away than those near Smith Creek.

Canyon Creek: δD and $\delta^{18}O$ results from Canyon Creek are shown in Figure 3- 27-D. In March 2008, groundwater had a similar isotopic composition to surface waters and likely recharge nearby at similar elevation. In June, surface waters are more enriched.

White Sand Creek: δD and $\delta^{18}O$ results from White Sand Creek are shown in Figure 3- 27-E. In March 2008 groundwater had a similar isotopic composition to that of surface water. At this time all creek water was interpreted to be from groundwater. In June 2008, surface waters are more enriched.

Hodgson Creek: δD and $\delta^{18}O$ results from Hodgson Creek are shown in Figure 3- 27-F. Groundwater was only sampled in March 2008. In June 2008, surface water samples were enriched relative to the groundwater.

Gayna River: δD and $\delta^{18}O$ results from Gayna Creek are shown in Figure 3- 27-G. In March 2008 groundwater is 0.6 ‰ depleted relative to surface water collected at this site. As with Smith Creek and Gibson Creek, this depletion is likely due to recharge at a higher elevation.

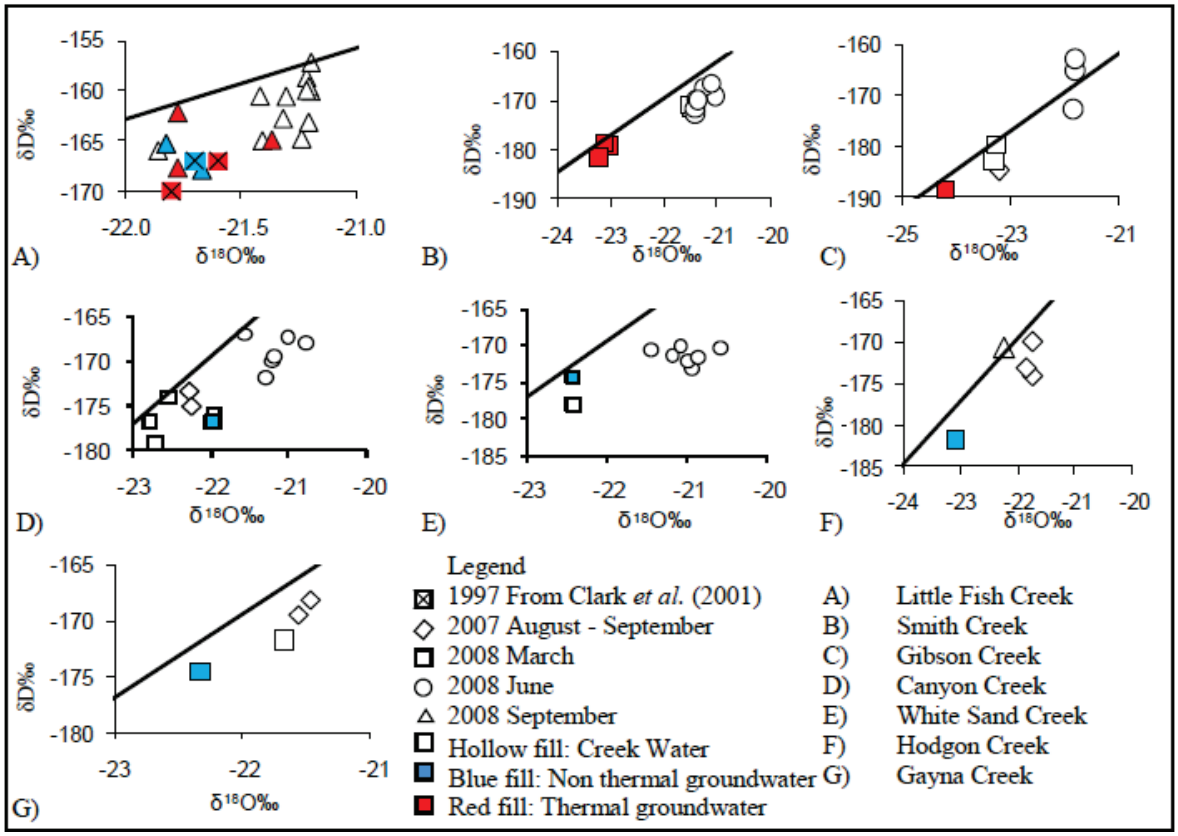

Figure 3- 27: δ D vs. $\delta^{18}O$ isotope results for water samples (Meteoric water for Little Fish Creek from Inuvik, based on IAEA GNIP database and meteoric water line for Fort Simpson, Hayashi *et al.,* 2004).

Groundwater samples were collected over 5° of latitude. It is expected that groundwater will be more isotopically depleted at higher latitudes as precipitation is more depleted (Clark and Fritz, 1997). From the seven groundwater springs sampled, there is no clear relationship with latitude (Figure 3- 28). This is likely the result of variable permafrost distributions that affect where precipitation may recharge as well as variable elevations through the catchments.

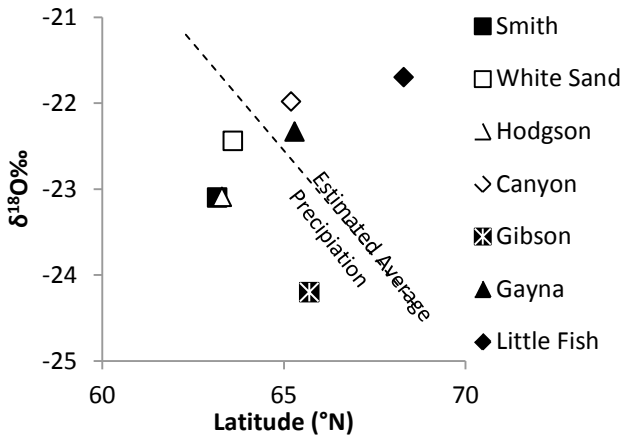

Figure 3- 28: $\delta^{18}O$ (‰) vs. latitude (°N) of groundwater samples and trend line of expected precipitation based on precipitation from Inuvik and Yellowknife (Birks *et al.,* 2003).

Surface Water

Figure 3- 29 shows δD and $\delta^{18}O$ of groundwater and surface water collected in creeks during March 2008, June 2008 and September 2008. March and June samplings included samples from White Sand Creek, Hodgson Creek, Smith Creek, Gayna Creek, Gibson Creek and Canyon Creek. In March, surface water samples fall close to the local meteoric water line. In June samples tend to fall to the right of the local meteoric water line. This shift is interpreted to be due to evaporation of surface waters. In September 2008 samples were collected from Little Fish Creek and the Rat River. These samples fall along the local meteoric water line, however they are slightly more enriched than winter samples.

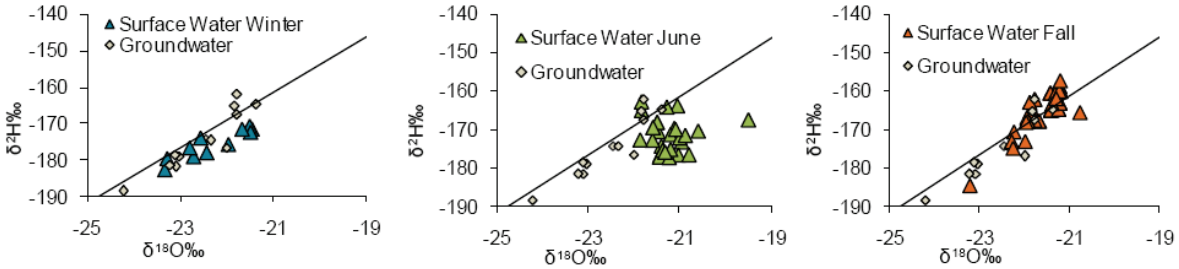

Figure 3- 29: δ D vs. $\delta^{18}O$ isotope results for water samples (Meteoric water line for Fort Simpson, Hayashi *et al.,* 2004).

3.5.5 Groundwater Recharge and Residence Time: Noble Gases

Noble gas samples were collected from springs on Smith Creek, Little Fish Creek (2 springs), Gayna River and White Sand Creek. Samples have been analysed for ^{3}He, ^{4}He, Ne, Ar, and Kr concentrations.

Groundwater recharge temperature

Recharge temperatures of the groundwater springs have been estimated using the inverse modeling approach introduced by Aeschbach-Hertig *et al.* (1999). The approach uses the concentrations of gases as well as constraining physical parameters as inputs. Different models exist to describe dissolved noble gases in groundwater as a result of equilibrium and excess air incorporation (Kipfer *et al*., 2002). The MatLab program Noble 90 (Peeters *et al.*, 2003) was used to model the noble gas concentrations and to vary the model parameters including temperature, excess air, and fractionation to find the best fit for the observed concentrations. The program minimises χ^2, the error-weighted sum of the model – data deviations of the individual noble gases, which at the same time provides a measure of the goodness of the achieved fit (Aeschbach-Hertig *et al.,* 1999).

Due to changes in pressure, recharge elevation is a necessary input to constrain the noble gas model. For sites on the east side of the Mackenzie River, recharge occurs in the Franklin Mountains where bedrock is exposed at the surface, however elevation is variable (Michel, 1986). Gayna Creek and Little Fish Creek are likely recharged in similar ways with recharge occurring on the slopes of the local mountains. Estimates of recharge elevation are given in Table 3- 7 with the modelled noble gas results. The results in Table 3- 7 were modelled under closed system equilibrium with excess air and temperature being modified to find the best fit.

The calculations return groundwater recharge temperatures between 0 and 11.9 °C (Table 3- 7). The relatively large errors on these measurements are attributed to calculating the temperatures without Xe. As mentioned in the methods section, xenon was included in original measurements, however due to technical problems these results are not included. The temperature calculated from Smith Creek had a large error which was due to

calculating the age with only Ar and Kr. This was done as the Ne concentration was very low, and likely not correct. Little Fish Creek thermal groundwater returns a recharge temperature of 5.7 ± 1.5 °C, which suggests recharge may occur only during the warmest part of the summer. Groundwater samples from Gayna River and White Sand Creek return recharge temperatures between 0 and 1.3 °C which is realistic for these systems.

Table 3- 6: Noble gas results. R/R_a is $(^3He/^4He_{sample})/(^3He/^4He_{air})$. BFF08-9-HS and BFF08-6HS are springs along Little Fish Creek.

	He (cc/g)		$^3He/^4He$		R/R_a	Ne (cc/g)		Ar (cc/g)		Kr (cc/g)	
	$x10^{-7}$	±	$x10^{-8}$	±		$x10^{-7}$	±	$x10^{-4}$	±	$x10^{-7}$	±
Little Fish Creek (BFF08-9-HS)	237	21	6.20	0.83	0.04	3.98	0.36				
Little Fish Creek (BFF08-6-HS)	216	19	6.39	0.81	0.05	2.31	0.21	5.17	0.26	0.89	0.04
Smith	15.40	1.37	3.01	0.39	0.02	0.16	0.01	6.19	0.31	1.12	0.06
White Sand	1.25	0.11	110.00	13.70	0.78	1.55	0.14	5.67	0.28		
Gayna	1.38	0.12	103.00	12.90	0.74	2.50	0.22	5.56	0.28	1.04	0.05
Gayna Duplicate	0.88	0.08	110.00	13.90	0.79	1.78	0.16	6.82	0.34	1.18	0.06

Table 3- 7: Noble gas age calculations and modelling results. ** Ne value from Smith Creek omitted during modelling.

	Groundwater Temperature	Estimated Recharge Elevation	χ^2	Recharge Temperature	±	He (cc/g)		ΔNe	A	±	^3H	^3He from ^3H	^3H-^3He Age	±
	(°C)	m a.s.l.		(°C)	(°C)	$x10^{-7}$	±	%	(ccSTP/g)		(TU)	(TU)	(years)	
Little Fish Creek (BFF08-9-HS)	15.0	800				237	21				6.3		<60	
Little Fish Creek (BFF08-6-HS)	15.9	800	19.3	5.7	1.5	216	19	31	3.3	1.2	7.0		<60	
Smith *	10.3	1000	0.00	11.9	5.4	15.4	1.4	324.4*	31.3	6.7	<0.8		>60	
White Sand	3.8	1500	34.3	0.0	2.8	1.25	0.11	0	0.0	0.9	8.6	39.0	30.4	2.6
Gayna	3.1	700	12.4	1.3	1.4	1.38	0.12	31	3.5	1.3	9.2	25.7	23.6	2.2
Gayna Duplicate	3.1	700	47.2	0.0	1.5	0.88	0.08	0	0.0	0.93	9.2	19.5	20.2	2.1

** Temperature modelling calculations omitted Ne value as likely erroneous value

^3H-^3He: Groundwater residence time

Helium concentrations and isotope ratios are dependent on the groundwater flow path and groundwater age (Kipfer *et al.,* 2002). Samples from Little Fish Creek and Smith Creek thermal springs had high helium concentrations reflecting a deep groundwater flow path and generally longer residence time. Groundwater from cool springs along White Sand Creek and Gayna River had lower helium concentrations reflecting a shallower groundwater flow path. The amounts of geogenic helium in the thermal waters was variable and likely related to different flow path depths, geology and residence times. Figure 3- 30

shows $^{3}He/^{4}He$ vs. Ne/He of the noble gas samples. The high proportion of crustal helium from Little Fish Creek and Smith Creek groundwaters is evident by the very low Ne/He. Smith Creek water had tritium concentrations below the detection limit (<0.8 TU) and a $^{3}He/^{4}He$ of 3.01 ± 0.14 x 10^{-8} which is close to the average crustal value (~2.0 x10^{-8}) (Kipfer *et al.,* 2002). Little Fish Creek water had tritium concentrations 6.5 ± 0.5 TU and had a $^{3}He/^{4}He$ value of 6.30 ± 0.13 x 10^{-8}. Samples from White Sand Creek and Gayna Rivers had tritium concentrations of 8.6 ± 0.8 and 9.2 ± 0.8 TU respectively and $^{3}He/^{4}He$ of 1.01 ± 0.14 x 10^{-6} and 1.03± 0.13 x 10^{-6}. The concentrations and ratios were used to determine the groundwater residence time of samples with measureable tritium.

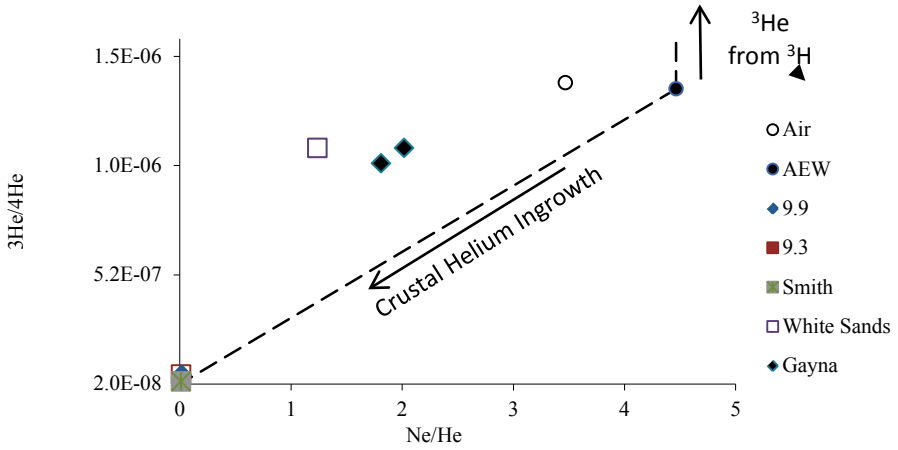

Figure 3- 30: $^{3}He/^{4}He$ vs. Ne/He of noble gas samples. Air represents atmospheric air, AEW is air equilibrated water while ^{3}He from ^{3}H is the signal of in-growth if the addition of helium is only from tritium. Gas ratios follow the crustal helium in-growth line if only crustal sources of helium are added.

Where suitable, groundwater ages were determined using ^{3}H-^{3}He dating. The amount of ^{3}He which is from ^{3}H is determined by accounting for other sources of ^{3}He such as excess air and crustal helium. This is calculated in Equation 3- 6:

Equation 3- 6: $$^{3}He_{Tri} = {}^{4}He_{m}\left(R_{m} - R_{ter}\right) - {}^{4}He_{eq}\left(R_{eq} - R_{ter}\right) - L_{ex}\left(Ne_{m} - Ne_{eq}\right)\left(R_{ex} - R_{ter}\right)$$

where R_m is the measured $^{3}He/^{4}He$, R_{eq} is the $^{3}He/^{4}He$ for atmospheric equilibrium (1.38 x 10^{-6}), R_{ex} is the $^{3}He/^{4}He$ for excess air (1.40 x 10^{-6}), R_{ter} is the $^{3}He/^{4}He$ from crustal sources, L_{ex} is the He/Ne of the excess air component (2.88 x 10^{-1}), Ne_m is the measured neon and Ne_{eq} is the equilibrium concentration of neon at recharge (Kipfer *et al.,* 2002). In this case,

the $^3He/^4He$ value from Smith Creek ($3.01 \pm 0.39 \times 10^{-8}$) is used as for R_{ter} this water contains no tritium and is likely purely a crustal signal. The value of $^3He_{tri}$ obtained from Equation 3- 6 is used in Equation 3- 7 to determine groundwater residence time:

Equation 3- 7: $$t = \frac{1}{\lambda}\ln\left(1+\frac{^3He}{^3H}\right) = \frac{12.3}{\ln 2}\cdot\ln\left(1+\frac{^3He}{^3H}\right)$$

where 12.3 years is the half-life of tritium, $^3He_{Tri}$ is from tritium, and $^3H_{TU}$ is tritium in water. The results of Equation 3- 7 are listed in listed in Table 3- 7.

Groundwater circulation rates are highly variable for the different flow systems. Smith Creek groundwater has no measurable tritium (< 0.8 TU) and a crustal helium signature. This water recharged prior to the 1950's and is classified as submodern. Smith Creek thermal water had the second highest crustal helium concentrations and was the second warmest spring sampled. Little Fish Creek groundwater contains measurable tritium 6.7 ± 0.5 TU and had the highest helium of samples measured and was the warmest water. Due to the very high helium, the correction for crustal helium has a high influence on the resulting age. If the value of 3.01×10^{-8} for $^3He/^4He$ from Smith Creek is used to correct for crustal helium in the Little Fish Creek samples the calculated ages are around 65 years. Groundwater which recharged 65 years ago would not have 6.7 ± 0.5 TU remaining. Because of the Little Fish Creek groundwaters have very high crustal helium, the correction for this introduces significant error and the calculated age is of little meaning. As there is tritium in the water the maximum age of this water is likely on the order of 50 years. The non-thermal groundwaters contain less crustal helium and have been dated successfully with the ^3H-^3He method. Groundwater sampled along White Sand Creek was determined to have a groundwater age of 30.5 ± 2.7 years. Groundwater sampled along Gayna Creek was dated at 23.8 ± 2.4 years (duplicate 20.3 ± 2.2). The original tritium in these waters was calculated and these waters fall close to historical input values (Figure 3- 31).

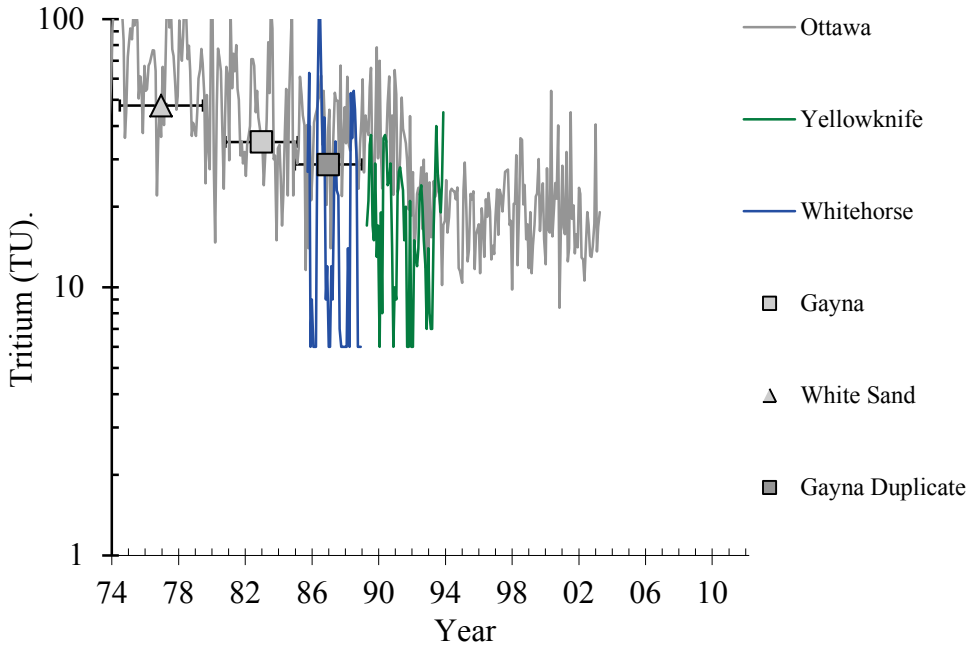

Figure 3- 31: Original tritium concentrations plotted vs. recharge year (calculated from the age), plotted with historical tritium record from Ottawa, Canada (from IAEA: GNIP database www.IAEA.org).

3.6 **Discussion:**

3.6.1 Groundwater Recharge

Within the watersheds studied, the measurements of δD, $\delta^{18}O$, $\delta^{13}C_{DIC}$, Ne, Ar and Kr were used to provide information on groundwater recharge. As δD and $\delta^{18}O$ are dependent on temperature, they provide insights to recharge elevation and potentially the sources of recharge throughout the year (snow melt vs. summer rainfall). The bedrock groundwaters from Gayna River, Smith Creek and Gibson Creek were depleted relative to the creek water at the time of sampling (March 2008).

Some bedrock groundwaters recharge at higher elevation, while other bedrock aquifers do not display an elevation-related depletion. The depletion of the bedrock groundwater compared to the creek water for $\delta^{18}O$ was 0.6‰ for Gayna Creek, 1.6‰ for Smith Creek and 0.9‰ for Gibson Creek during the March 2008 sampling. To estimate if elevation can account for these differences, a correction of -0.3 ‰/100m increase in

elevation was used (Bortolami *et al*., 1979). This correction represents a mid-range literature value. Following this depletion rate, bedrock groundwater recharge is estimated to be 200 m higher for Gayna Creek, 530 m higher for Smith Creek and 300 m higher for Gibson Creek. The thermal groundwater along Little Fish Creek is depleted by 3.5 ‰ for δD and 0.5 ‰ for $\delta^{18}O$ compared to the most upstream creek water which is interpreted to be shallow groundwater. This depletion suggests groundwater is recharged at about 150 m higher elevation; this is consistent with previous research (Clark *et al.,* 2001). Previous research on groundwaters along the east side of the Mackenzie River (Smith Creek, White Sand Creek, Canyon Creek, Hodgson Creek and Gibson Creek) proposed that recharge was dominated by snow melt that recharges in temporary lakes in the Franklin Mountains (Michel, 1977). To add insights to recharge from lakes or through soils at higher elevations, the DIC system, and in particular, $\delta^{13}C_{DIC}$ was used.

Measurements of $\delta^{13}C_{DIC}$ were used to determine if recharge occurs in organic soils and if it is under open or closed system conditions. Groundwaters have P_{CO2} values between 10^{-2} and 10^{-3} atm with the CO_2 derived from organic soils. The $\delta^{13}C_{DIC}$ of groundwater from White Sand Creek, Smith Creek, Hodgson Creek, Canyon Creek, Gibson Creek and Gayna River ranges from -7.4 to -12.8 ‰. This range of $\delta^{13}C_{DIC}$ is interpreted to be derived from the dissolution of soil CO_2 and the subsequent weathering of marine carbonates under closed system conditions. These processes occur in a similar way in non-permafrost watersheds (Clark and Fritz, 1997). The groundwater from Little Fish Creek has average $\delta^{13}C_{DIC}$ values of -3.8 ‰, which is more enriched than groundwater from other creeks. This enrichment may be the result of incongruent dissolution of dolomite (Clark and Fritz, 1997). Although dolomite rocks are not present in the local watershed, they do exist in the region (Norris, 1977). These waters likely flow along faults, and may interact with dolomite rocks at depth. The dissolution of dolomite is the likely source of Mg in the thermal groundwater (27 to 31 ppm). If water has reached calcite saturation but has not reached dolomite saturation, incongruent dissolution of dolomite may occur which can result in $^{13}C_{DIC}$ enrichment.

The calculated recharge temperatures from White Sand Creek, Gayna River, and Little Fish Creek were 0.0 ± 2.8 °C, 1.3 ± 1.4 °C and 5.7 ± 1.5 °C. The Smith Creek

groundwater sample was excluded from this discussion as the error on the calculated temperature was high. White Sand Creek groundwater had a recharge temperature of 0.0 ± 2.8 °C and discharge temperature of 3.8 °C. Gayna River groundwater had a recharge temperature of 1.3 ± 1.4 °C and discharge temperature of 3.1 °C. These two samples suggest that groundwater has warmed up very slightly along the flow path; however with only two samples and such a small difference between them, minimal interpretation is appropriate. The higher recharge temperature of Little Fish Creek (5.7 ± 1.5 °C) may indicate that recharge does not happen until later in the summer when soils are warmer.

Based on the noble gas results and the δD, $\delta^{18}O$ and $^{13}C_{DIC}$ of groundwater, it is proposed that groundwater recharge to the central Mackenzie Valley sites occurs through soils at upper elevations in the catchments. This is similar to the mountain-front recharge model applied to arid regions (Wilson and Guan, 2004). In arid regions there is limited groundwater recharge in the valleys due to reduced precipitation, while in the study area, permafrost in the valleys reduces groundwater infiltration. In the Central Mackenzie Valley, thermal inversions are common in winter (Eley, 1974). These thermal inversions have been linked to elevated ground temperatures and possibly thinner permafrost just below the tree line elevation in the mountains on the east side of the Mackenzie River (~550 m.a.s.l.) (Taylor *et al.,* 1998). If zones of thinner permafrost exist just below the tree line, they may act as recharge zones. Recharge water appears to represent precipitation from the entire year. However recharge may be from variable elevations. Michel (1977; 1986) proposed that recharge may occur from draining of ephemeral lakes underlain by karst in the Franklin Mountains. There is abundant karst in the Franklin Mountains and there is likely recharge in karst, however $^{13}C_{DIC}$ values indicate recharge through organic soils. Recharge must happen during the summer when soils are producing CO_2, and when groundwater temperatures are >0 °C; this water may subsequently flow into karst.

3.6.2 Groundwater Flow

The extent of permafrost limits groundwater recharge and flow tends to occur in formations with large porosity (Michel, 1977). Where permafrost is colder, the size of pores and cavities necessary for groundwater recharge increases. Larger pores and fissures mean

the water-rock interaction is reduced per unit volume of water, resulting in less cooling of water. In the central Mackenzie Valley, the mean annual ground temperatures (MAGT) range from -2 °C to > 0 °C, with permafrost thickness ranging from <10 m to 100 m (Smith and Burgess, 2002; Smith *et al.*, 2010). The temperature of permafrost varying with depth near Norman Wells is shown in Figure 3- 32, which presents temperature data from the borehole "Canyon Creek 2A" from September 2008 (Data courtesy S. Smith – Geological Survey of Canada - personal communication, 2010). Although there are many shallow boreholes measuring temperature in the Mackenzie valley, "Canyon Creek 2A" is one of few publicly available which are instrumented to the base of permafrost in this area. This borehole shows that the base of permafrost at this location is 23 m below ground and that the coldest temperature of permafrost at this site is -0.33 ± 0.1 °C. In areas where the MAGT is near 0 °C, the flow of water is greatly reduced, however there may still be some groundwater flow (Burt and Williams, 1976). Freezing temperature of the groundwater may also be depressed by pore pressure and dissolved solutes (van Everdingen, 1976).

In the central Mackenzie Valley, permafrost is between -2 °C and 0 °C, and is tens of metres thick (Smith and Burgess, 2002; Smith *et al.*, 2010). This permafrost likely reduces groundwater recharge but does not completely block it. In the sampled groundwaters, the noble gas groundwater recharge temperatures are similar to discharge temperatures. White Sand Creek groundwater temperature was 3.8 °C and the noble gas recharge temperature was 0.0 ± 2.8 °C. Gayna River groundwater temperature was 3.1 °C and the noble gas recharge temperature was 1.3 ± 1.4 °C. White Sand Creek groundwater was found to be 30.4 ± 2.6 yrs and Gayna River groundwater was found to be 23.6 ± 2.2 yrs. To maintain a relatively warm temperature, it is proposed that water may move more quickly through the upper, colder regions of the flow path, resulting in less heat loss and subsequently flows through aquifers at temperatures similar to the recharge temperature. The "Canyon Creek 2A" borehole shows that at 23 m below the ground surface there is no permafrost at this location and groundwater may flow freely. Although there are numerous permafrost monitoring boreholes in the area, "Canyon Creek 2A" is the only one of this depth. Once water infiltrates into this unfrozen zone it flows as it would in non-permafrost terrain. Because the noble gas data cannot determine temperature variations along the flowpath, there is the possibility that groundwaters cool during recharge and then

are warmed up again at depth as the aquifer is 3 °C at ~ 100 m depth. Near Inuvik, permafrost is thicker (100 to 200 m) and flow of water is restricted to deeper aquifers (Smith and Burgess, 2002).

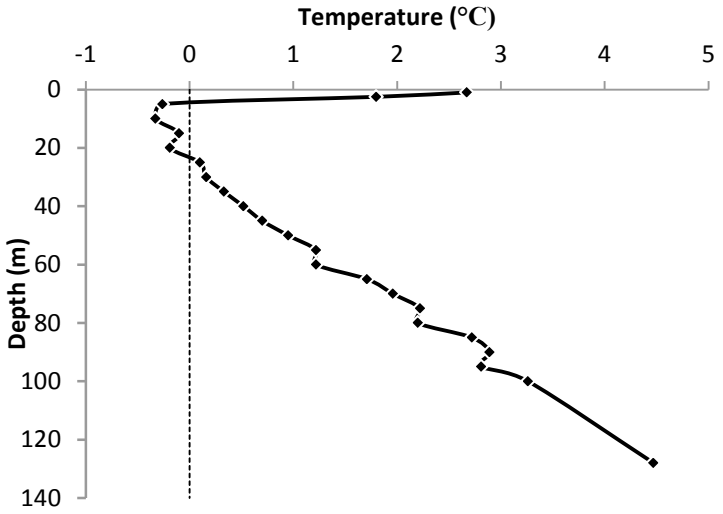

Figure 3- 32: Profile of temperature vs. depth from Canyon Creek (2A) borehole. Data courtesy S. Smith – Geological Survey of Canada - personal communication 2010.

Groundwater that discharges along Canyon Creek, White Sand Creek and Hodgson Creek flows through brecciated dolomite and limestone that has high porosity and permeability (Michel, 1977). Along Gayna River, groundwater discharges from the Rampart Formation; the Bear Rock Formation outcrops upstream (Aitken and Cook, 1974). The water chemistry from Gayna River groundwater is similar to Canyon Creek and White Sand Creek groundwater; based on the chemistry, water likely flows through the Bear Rock Formation. Using ^{3}H-^{3}He dating, the groundwaters along Gayna River and White Sand Creek were found to have residence times of 23.8 ± 2.4 and 30.5 ± 2.7 years respectively. These non-thermal groundwaters are modern, likely with a relatively shallow flow path in carbonate and evaporite rocks.

Smith Creek groundwater discharges from shale rocks of the Fort Simpson Formation; however it has been proposed that most of the flow path is through the Bear Rock Formation (Michel, 1977). Based on the very low tritium concentration in the Smith Creek groundwater, this water was found to have an age greater than 45 years. This is

consistent with the previous research by Michel, (1977) which also found Smith Creek groundwater to have low tritium (7± 8, 16 ± 8 TU). The low amount of tritium measured by Michel, (1977) may have been from some contamination with modern precipitation. Little Fish Creek groundwater water contained higher tritium (6.7 ± 0.5 TU) than Smith Creek and also high total helium concentrations. The presence of tritium suggests the water is likely younger than that from Smith Creek. Based on the tritium and helium concentrations the ^{3}H-^{3}He method is not appropriate, but it was concluded that these waters are likely less than ~ 45 years old. Little Fish Creek groundwater discharges from a small fault, and likely reaches the surface along some form of major discontinuity. Smith Creek and Little Fish Creek groundwaters both have deeper flow paths than the non-thermal springs, and have longer correspondingly residence times.

3.6.3 Groundwater Discharge

Different water sources contribute to river flow at different times of the year; these sources have unique flow pathways and take on unique chemistry. To trace the mixing of these components, Cl^- and SO_4^{2-} concentrations were used. Previously, three end members were identified along Little Fish Creek layer / runoff, deep thermal groundwater, and a shallow groundwater (Clark *et al.*, 2001). Along Little Fish Creek, Smith Creek, Canyon Creek and White Sand Creek samples were collected up and downstream of groundwater discharge zones. It was found that bedrock groundwater component represents up to 89% of flow in winter. During the summer river flow is diluted; however the bedrock groundwater component still represents 8% or more of river flow. These calculations show that groundwater discharge is important in maintaining flow along these rivers.

Along Little Fish Creek there is also a shallow groundwater system which does not discharge all year (Clark *et al.,* 2001). As outlined in the "results" section, a plot of Cl^- vs. SO_4^{2-} from Smith Creek, Canyon Creek and White Sand Creek samples also shows that creek water appears to contain a third end-member. In the results section, it was shown that the lowest TDS waters, with the lowest values of Cl^- and SO_4^{2-} are believed to be representative of runoff water. This is a best estimate of the composition of runoff. The highest TDS waters with the highest values of Cl^- and SO_4^{2-} were from bedrock

groundwater discharge, sampled from spring vents. It was noted that there was not linear mixing between the Cl^- and SO_4^{2-} components of bedrock groundwater and surface water, so it has been proposed that there must be a third end-member water (See Cl^- vs. SO_4^{2-}, Figure 3- 23, Figure 3- 24, Figure 3- 25). In March, creek water appears to be dominated by the mixing of bedrock groundwater and this third end-member. During the winter sampling there was water in these creeks which was not from deeper bedrock groundwater discharge. For example, during the March sampling there was water flowing along Smith Creek upstream of the groundwater springs. This water had lower TDS than the thermal groundwater; however this could not originate from overland runoff due to the extreme cold. Smith Creek water in June was interpreted to be dominated by a mix of low TDS surface runoff and third end member. The third end member is interpreted to be shallow groundwater similar to what is found along Little Fish Creek. Shallow groundwater system may flow through both bedrock and the alluvial sediments in the creek valleys. This water has higher ion concentrations than surface runoff, but lower concentrations than bedrock groundwater. Relative to linear mixing between bedrock groundwater and surface runoff, shallow groundwater has more SO_4^{2-} relative to the amount of Cl^-. This shallow groundwater system may be a supra-permafrost talik flow system. A shallow flow path would likely result in lower TDS water. In mixing calculations, the composition of shallow groundwater was found from completing the mixing triangle on graphs of Cl^- vs. SO_4^{2-}. While such a calculation is not ideal, it does provide a more accurate estimate of the bedrock groundwater discharge. Ideally the shallow groundwater would be sampled directly. Some water samples were very similar to the estimated composition of the shallow groundwater. Further sampling would have helped constrain this component.

Along Little Fish Creek, the shallow aquifer freezes during winter (Clark *et al.,* 2001). Along Smith Creek and Canyon Creek, the shallow aquifers contribute to creek flow during the winter. The role of shallow groundwater in winter along White Sand Creek is unknown due to insufficient sampling. Along Canyon Creek and Smith Creek in March 2008, creek water appears to be largely a mixture of bedrock groundwater and shallow groundwater. Many of the samples from June 2008 plotted along the surface runoff and shallow groundwater aquifer water mixing lines (Figure 3- 23, Figure 3- 24, Figure 3- 25).

3.6.4 Conceptual Model of Groundwater Discharge

Along the rivers studied, three types of groundwater are proposed: thermal bedrock groundwater, non-thermal bedrock groundwater and shallow groundwater. Along Little Fish Creek and Smith Creek there is thermal groundwater and shallow groundwater discharge. Figure 3- 33 shows a schematic diagram of the proposed conceptual model for the perennial thermal groundwater flow and shallow non-perennial groundwater flow systems present along Little Fish Creek. Thermal groundwater discharge occurs out of a fault in the bedrock. The shallow groundwater system flows only during the summer. Little Fish Creek is located in continuous permafrost that is colder and thicker than what is found adjacent to the other sampling sites.

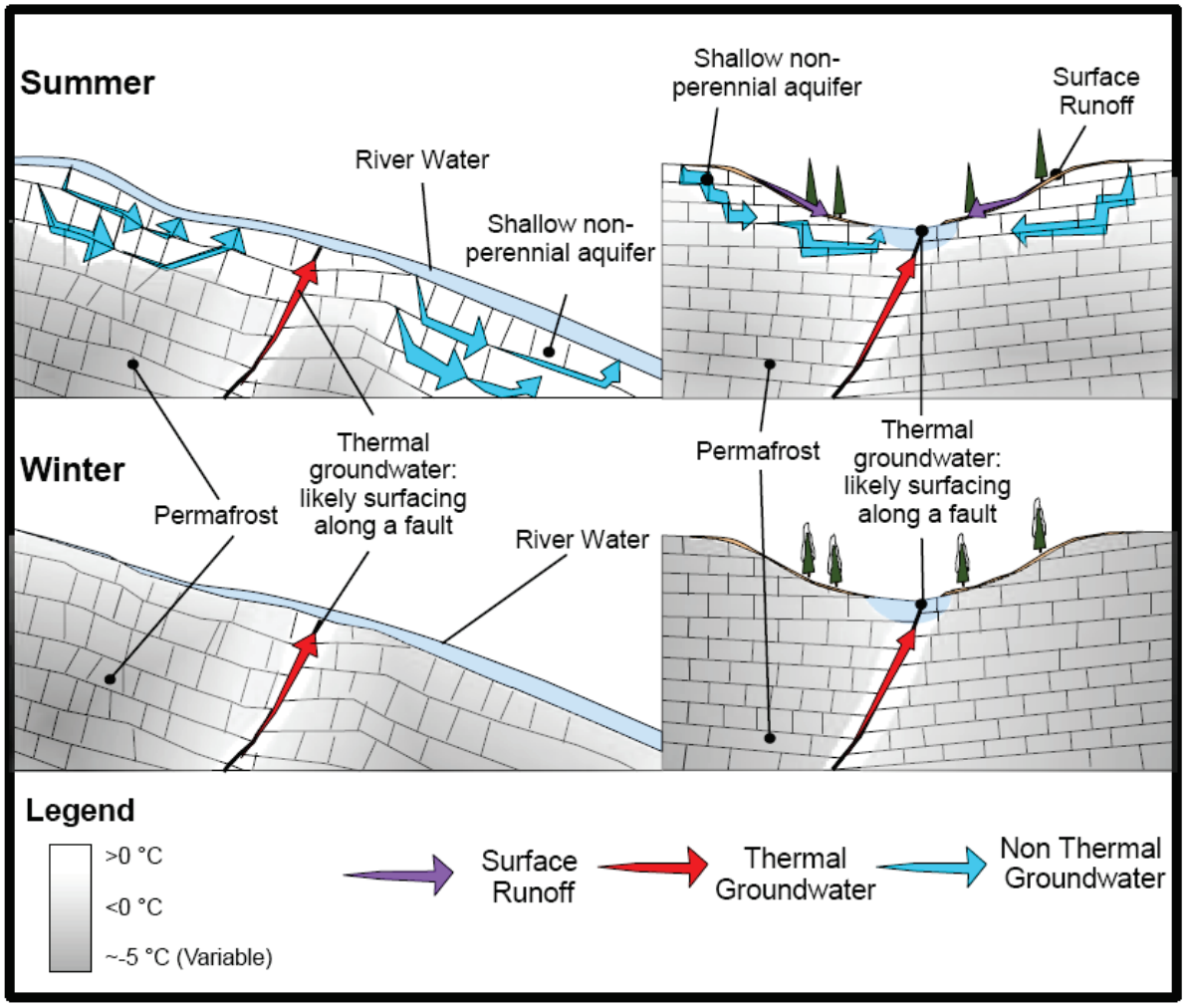

Figure 3- 33: Schematic diagram of proposed flow system along Little Fish Creek. Diagrams on left show longitudinal view, while on right transverse section is shown. Thermal groundwater discharges perennially, likely from discrete permeable zones such as faults and fissures in bedrock. Non-perennial groundwater flow occurs in shallow bedrock.

Along White Sand Creek, Canyon Creek, Hodgson Creek and Gayna River there are non-thermal bedrock groundwaters. Shallow groundwater discharge was also identified along Canyon Creek and White Sand creek. Similar shallow groundwater systems could exist along Hodson Creek and Gayna River; however there was insufficient sampling to determine this. Figure 3- 34 shows a schematic diagram of the proposed conceptual model of these discharge systems. The non-thermal bedrock groundwater systems studied in this chapter are located in the central Mackenzie Valley where permafrost is discontinuous, mean annual ground temperatures are > 0 to -2 °C and permafrost ranges in thickness from 10 m to 100 m. Bedrock groundwater flow may occur in intra or sub-permafrost talik

zones, and is likely concentrated in higher porosity zones. The Bear Rock Formation is a high porosity zone that may concentrate groundwater flow (Hamilton and Ford, 2002).

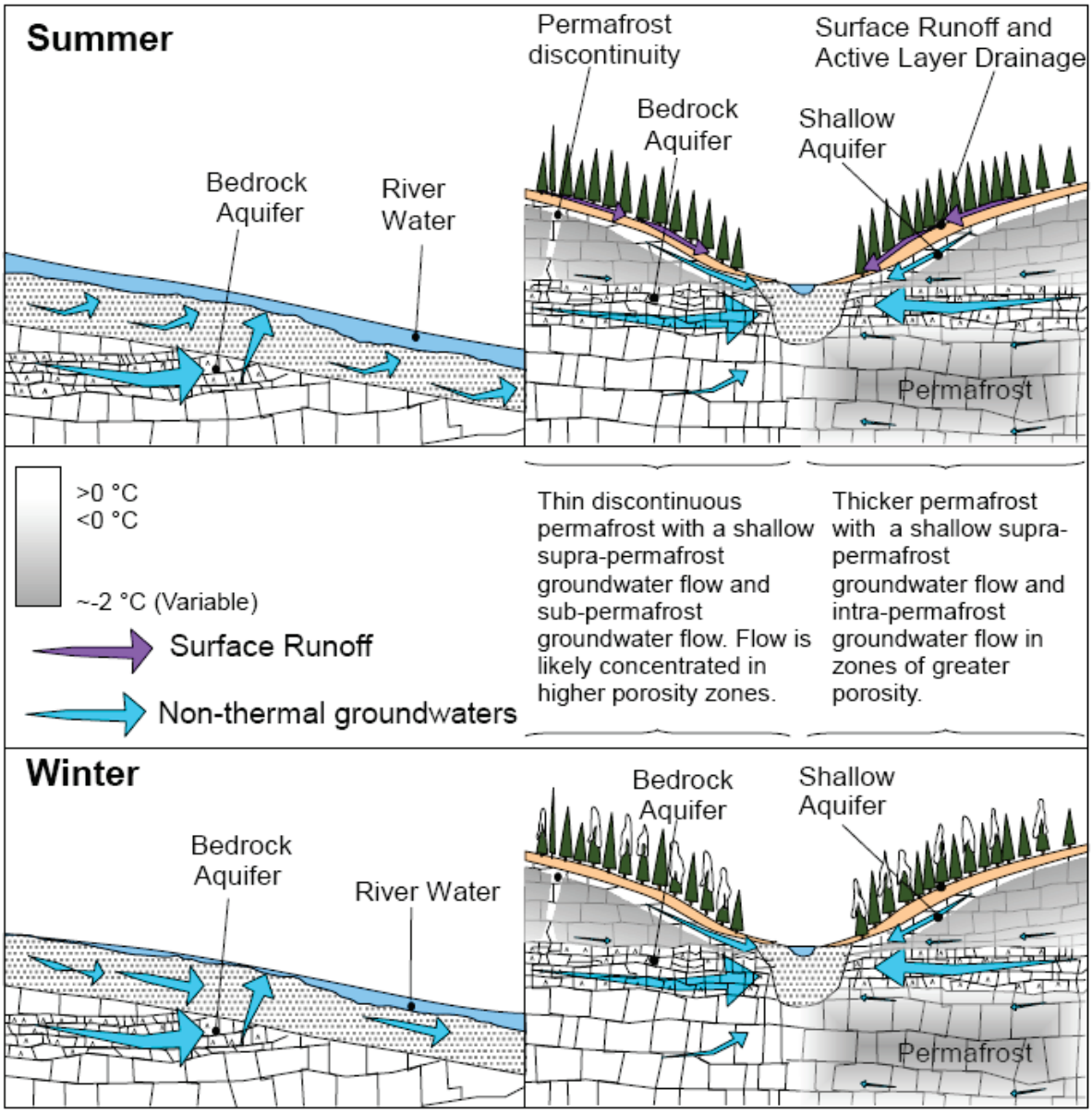

Figure 3- 34: Longitudinal (on left) and transverse (on right) schematic diagrams of watercourse which receives groundwater from a bedrock aquifer and a shallow aquifer. On transverse section two permafrost regimes are shown, on the left is thinner discontinuous permafrost with a sub-permafrost bedrock groundwater flow. On the right transverse is thicker permafrost (may be continuous or discontinuous) with an intra-permafrost bedrock groundwater flow. Bedrock groundwater flow in both models is likely in zones of greater porosity allowing for greater flow and maintenance of unfrozen conditions. The Bear Rock Formation is a primary conduit of groundwater flow, which is composed of dolomite and anhydrite and is susceptible to karstification. This represents the type of groundwater flow system along Canyon Creek and White Sand Creek. There is also a shallow groundwater flow system which may flow supra-permafrost.

3.7 Conclusion

The focus of this study was seven primary rivers and creeks (Little Fish Creek, Smith Creek, Gibson Creek, Canyon Creek, Hodgson Creek, Canyon Creek and Gayna River). These water courses were selected based on the presence of groundwater springs, which result in perennial open water. Groundwater discharge may result in an increase in TDS of surface water and open water in winter. There are both thermal and non-thermal bedrock groundwater aquifers which discharge along these rivers. Along Gibson Creek, Smith Creek and Little Fish Creek there is discharge of thermal groundwater. The occurrence of thermal groundwaters reaching the surface is less common, because the conditions for such flow are unique. Along Canyon Creek, Hodgson Creek, Canyon Creek and Gayna River non-thermal bedrock groundwater discharges. In addition to discharge from bedrock aquifers, shallow groundwater systems were discovered along four of these rivers. Along Little Fish Creek, the shallow groundwater system is non-perennial. Along Canyon Creek and Smith Creek, discharge from the shallow groundwater systems occurs all year. Non-thermal groundwater discharge is common along the creeks and rivers in the Mackenzie Valley. High porosity aquifers exist in karsted evaporite and carbonate rocks, allowing for flow all year.

Groundwater ages are related to groundwater flow path. The non-thermal groundwaters from White Sand Creek and Gayna River have ages between 20 and 30 years. The presence of tritium in the Little Fish Creek groundwater suggests that it is less than 45 years old. High helium concentrations in this water indicate a relatively deep flow path with waters most likely older than the non-thermal groundwaters. Thermal groundwaters along Smith Creek have been classified as sub-modern (>50 years) as they contain high helium and no tritium. Thermal groundwaters flow deeper into the crust and generally have a longer flow path than the non-thermal waters.

$\delta^{18}O$ and δD values in groundwaters are often slightly depleted, likely the result of recharge at a higher elevation. In March 2008, bedrock groundwater from Smith Creek, Gayna River and Gibson Creek had $\delta^{18}O$ values that were 0.6 to 1.6 ‰ depleted relative to the surface water in those creeks. These groundwaters are interpreted to recharge at higher

elevations. Along Canyon Creek no depletion was noted and insufficient samples were collected along White Sand and Hodgson Creek to assess this. Little Fish Creek thermal groundwaters are depleted relative to the shallow groundwater indicating that the thermal water recharge at a higher elevation.

The $\delta^{13}C_{DIC}$ signal in groundwater was used to assess recharge conditions. With the exception of Little Fish Creek, the $\delta^{13}C$ and P_{CO2} results indicate that the groundwater in most of these systems originates from recharge through organic soil, where it dissolves biogenic CO_2. Groundwaters from Smith Creek, Gibson Creek, Canyon Creek, White Sand Creek, Hodgson Creek and Gayna River have $\delta^{13}C_{DIC}$ values ranging from -7.4 to -12.8 ‰. These values are attributed to closed-systems weathering of marine carbonates with biogenic soil CO_2. Some samples showed minor enrichment which may be the result of exchange with the atmosphere. These results are similar to what would be expected for a carbonate watershed in non-permafrost terrain. Groundwater from Little Fish Creek had an average $\delta^{13}C_{DIC}$ of -3.8‰, which was more enriched than the other sites. This enrichment is interpreted to be due to incongruent dissolution of dolomite along the flow path.

Recharge temperatures were found using the noble gases recharge temperature method. Recharge temperatures were 0.0 ± 2.8, 1.3 ± 1.4 °C and 5.7 ± 1.5 °C from White Sand Creek, Gayna Creek and Little Fish Creek respectively. In general the noble gas temperatures, $\delta^{18}O$, δD and $\delta^{13}C_{DIC}$ of groundwater indicate that recharge is a mixture of precipitation throughout the year; however recharge occurs at different elevations. Recharge occurs during summer when soil CO_2 is being produced and recharge can occur when soil temperatures are > 0 °C. Most of these waters recharge through thin organic soils and subsequently flow through fractured and karsted bedrock.

In the Mackenzie valley tributaries, groundwater recharge is thought to occur in the local mountains and hills. This flow system may be similar to the mountain front recharge model used to understand recharge in arid regions. In mountainous arid regions there is limited groundwater recharge in valley bottoms due to limited precipitation (Wilson and Guan, 2002), while recharge in valley bottoms may be restricted by permafrost. In the mountain front recharge model, groundwater recharge occurs on the front flanks of

mountains, which is similar to what is predicted for recharge in the Mackenzie valley, due to the common phenomenon of thermal inversions that reduce permafrost depth near the tree line.

There is still much to be learned about groundwater flow in permafrost terrain, and how predicted future warmer climates would impact these systems. In the following chapter, a detailed study of an individual watershed provides additional understanding of groundwater flow in permafrost terrain.

Chapter 4: Origin and flow dynamics of perennial groundwater discharge in continuous permafrost terrain on the Fishing Branch River basin, northern Yukon, Canada: A case study using isotopes and noble gases

Article Submitted to: Permafrost and Periglacial Processes (Submission number: PPP-11-0015)

Nicholas Utting: Department of Earth Science, University of Ottawa, 140 Louis Pasteur, K1N 6N5 Ottawa, Canada

Ian Clark: Department of Earth Science, University of Ottawa, 140 Louis Pasteur, K1N 6N5 Ottawa, Canada

Bernard Lauriol: Department of Geography, University of Ottawa, 60 University, K1N 6N5 Ottawa, Canada

Martin Wieser: Institut für Umweltphysik, University of Heidelberg, Im Neuenheimer Feld 229, D-69120 Heidelberg, Germany

Werner Aeschbach-Hertig: Institut für Umweltphysik, University of Heidelberg, Im Neuenheimer Feld 229, D-69120 Heidelberg, Germany

This chapter is with some minor modifications the same as this article submitted to Permafrost and Periglacial Processes. The most significant difference is that this chapter includes Figure 4- 8 which was removed from the submitted article to keep within the allowable page limit.

This data interpretation and writing of the article were performed by Nicholas Utting. Co-authors contributed by assisting with laboratory analysis and providing assistance in the interpretation of results.

4.1 Introduction

The presence of permafrost in the Arctic has a profound effect on the hydrological cycle (e.g. Cederstrom *et al*, 1953; Ferrians *et al*, 1969; French, 1996). Areas of permafrost are often characterized by high surface runoff and little groundwater flow (Woo and Steer, 1983; McNamara *et al.,* 1997), although regions of extensive perennial groundwater discharge do exist in northern Canada. These regions include, among others, the Firth River catchment in the northern Yukon (Clark and Lauriol, 1997) and the Little Fish Creek catchment in the N.W.T. (Clark *et al.,* 2001). Also numerous rivers in the Norman Wells region of the N.W.T. are groundwater fed (Michel, 1986) as well as the Nahanni River Valley (Brook and Ford, 1980) and the Great Bear Lake region (van Everdigen, 1981). In eastern Canada, groundwater discharge from permafrost occurs on the Akpatok Island (Lauriol and Gray, 1990), and in the Canadian High Arctic, where brines discharge from evaporite on Axel Heiberg Island as studied by Pollard *et al.* (1999), Mckay *et al.* (2005), Omelon *et al.* (2006) and Pollard (2005).

Despite the widespread occurrence of permafrost in these catchments, seasonal hydrological responses and the geochemistry of discharge are not unlike those observed for temperate catchments. River flow in permafrost watersheds invariably reaches its peak in spring and early summer followed by decay towards baseflow in late summer and fall (e.g. Yang *et al*., 2002; Church, 1974; Quinton and Marsh, 1999). As the melt season progresses, the active layer thickens, allowing circulation of soil water and mineral dissolution of (Quinton and Pomery, 2006; Lacelle *et al.*, 2008). In areas where there are discontinuities in permafrost such that groundwater recharge can occur, the resulting hydrograph will have a less pronounced peak due to groundwater discharge to rivers throughout the year (Craig and McCart, 1975).

The occurrence of perennial groundwater discharge in permafrost regions demonstrates the presence of unfrozen permeable terrain, or talik. Taliks often occur along river channels (Cramtpon, 1979; French, 1996) but must also occur in the catchment where groundwater recharge takes place. Several studies have used GPR (ground-penetrating radar) to estimate the extent of unfrozen zones below rivers and creeks of different sizes

(Arcone *et al.,* 1998; Brosten *et al.,* 2006; Brosten *et al.*, 2009). The distribution of talik, and in particular the zones of recharge to talik, are likely controlled in part by geology, ground cover, and degree of southern exposure. The occurrence of talik and groundwater flow within the regions of continuous permafrost is closely associated with carbonate and evaporite karsts (Michel, 1986; van Everdingen, 1981; Clark and Lauriol, 1997).

Despite the important role that groundwater discharge plays in permafrost hydrology and ecosystem functioning, the origin and flow dynamics of these groundwater systems remains enigmatic due to a poor understanding of talik distribution and a lack of infrastructure (wells, discharge gauges) for measuring and sampling. However, valuable information regarding groundwater recharge and residence time can be obtained by combining isotope geochemistry and noble gas analyses. For example, the measurement of tritium, with its half-life of 12.3 years, combined with ^{3}He concentration measurements can be used to determine age for groundwater up to 45 years old (Clark and Fritz, 1997). Determining the concentration of the atmospheric noble gases (Ne, Ar, Kr and Xe), which are conservative in the subsurface, can be used to determine groundwater recharge temperature as they lock-in the temperature of surface water infiltration (Stute and Schlosser, 1993). To date, there has been little research on the use of noble gases related to permafrost hydrology. Of the few studies, McKay *et al*. (2005) analyzed noble gas concentrations in the cold saline groundwater springs on Axel Heiberg Island and found that the source of water consisted of a mixture of subglacial melt and lake water. In another study, Greene *et al.* (2008) used radiogenic and atmospheric noble gas concentrations to discriminate possible groundwater origins in proximity to the Con Mine near Yellowknife, NWT.

This study investigated the groundwater contributions to the Fishing Branch River situated in the zone of continuous permafrost in northern Yukon, Canada (66.5°N; 139.4°W). Extensive perennial groundwater discharge can be observed along the Fishing Branch River, near Bear Cave Mountain. Consequently, this reach of the river remains ice-free through the winter and provides important habitat for spawning salmon. The objectives of this study are to determine the groundwater contribution to total river discharge and to characterize the origin and flow dynamics of groundwater. These

objectives were reached by: i) measuring river flow and temperature of the spring water at various outlets; ii) using stable isotope geochemistry to provide information regarding groundwater recharge; iii) analyzing noble gas concentrations (Ne, Xe, Ar, Kr) to determine groundwater recharge temperature; and iv) using $^{3}H/^{3}He$ dating to constrain groundwater residence time. This study expands on a limited body of research on groundwater circulation in continuous permafrost terrain.

4.2 **Study Area**

The study area consists of the Fishing Branch watershed which is situated in the Ogilvie Mountains near the Arctic Circle in northern Yukon, Canada (Figure 4- 1). The Fishing Branch watershed drains an area of 1600 km^2 with elevation ranging between 400 to 1500 m.a.s.l. The summits correspond to an ancient peneplain that developed during the Tertiary in Devonian-age limestone and sandstone, faulted during the Laramide orogenesis (Norris, 1978). The lowlands are the result of erosion occurring during the Quaternary. Steep slopes connect the summits with the lowlands. The presence of numerous sinkholes and caves on the slopes suggests that there is an active karstic system below ground (Cinq-Mars and Lauriol, 1985; Thibaudeau *et al.,* 1988).

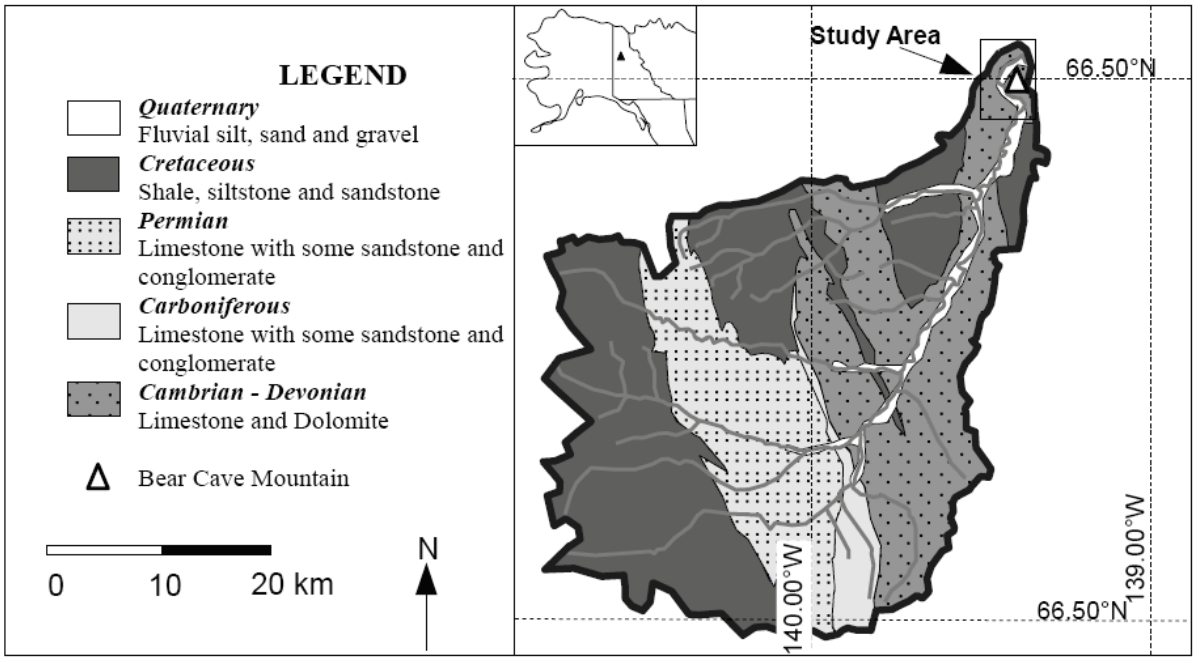

Figure 4- 1: Map of the Fishing Branch watershed and geological units exposed at the surface (map based on Norris, 1978).

The karst terrain in northern Yukon, and particularly in the Ogilvie Mountains, is characterized by an important subsurface drainage system. During summer, the ravines that cut the karst slopes are often dry, while those that cut sandstones or shale often have surface flow. In the case of the Fishing Branch River, its bed is often dry during summer upstream of Bear Cave Mountain (Figure 4- 1) while downstream perennial surface flow is observed in the river. This difference is related to the geology: upstream calcareous formations are present while downstream the area is composed of Cretaceous rocks comprising sandstones, siltstones and shales. Consequently, the lower reach of Fishing Branch River is characterized by perennial discharge which provide important habitat for salmon. Groundwater discharge along the Fishing Branch River keeps the river ice free during winter.

The regional climate can be estimated from meteorological stations located in the hamlet of Old Crow, 121 km north of the study site, and at Eagle Plains, 117 km east of the study site. The mean annual air temperature recorded at Old Crow is -8.9°C (July: 12°C; January: -22°C) and total precipitation amounts to 265 mm. However, the hamlet is situated at a lower elevation (250 m.a.s.l.) than the Fishing Branch watershed, and therefore, the air temperature represents maximum values. The Eagle Plains meteorological station is

situated at a similar elevation (700 m.a.sl.); however, climatic data are only available between 1984 and 1997, with some years missing data. During these years, the mean annual air temperature was -10.5°C with total precipitation amounting to 421 mm per year (Environment Canada, 2010). These climatic conditions ensure the presence of continuous permafrost with boreal vegetation in the valleys and alpine tundra in the mountains above 800 m.a.s.l. Although the exact thickness of permafrost is unknown, it is estimated to be 200-300 m thick based on calculations which take into account mean annual air temperature, snow cover and thermal conductivity of the rock (P. Bonnaventure, personal communication, 2009).

4.3 Studied sites and field sampling

Field sampling along the Fishing Branch River took place in June 2006, July 2007 and August 2008, and collaborators collected additional samples at opportune times. Groundwater springs for sampling were identified in the forest near the river and along the river bank. Fishing Branch River water and tributaries were sampled generally near spring locations. Locations of sampling sites are shown in Figure 4- 1. Groundwater springs are summarized in Table 4- 1. The most upstream sampling site is Upper Spring where springs discharge into a beaver pond. The Cabin site on the Fishing Branch River is located at the Yukon Parks cabin, with the BC Spring located in the forest approximately 700 m to the south west. S-4 is an ephemeral spring near a beaver pond on the east side of the Fishing Branch River opposite the Cabin site. Livingstone, Redd and Gossage springs are all located along the river bank downstream of the Cabin site. Groundwater discharge is from gravel sediments at Livingstone and Redd, and from bedrock at Gossage. The CS site includes a series of spring vents discharging at the base of limestone cliffs along a bend in the river. River waters were sampled at the Weir site where the Department of Fisheries and Oceans monitors the salmon run each fall.

The river, tributary creeks and groundwater springs were sampled for water chemistry and stable isotope measurements. Groundwater springs were also sampled for noble gas analysis. pH was measured using a Hanna instruments HI 9025 and temperature and conductivity were measured using a WTW COND 330i. Water samples were filtered

using 0.45 μm filters and collected in 30 ml HDPE bottles and dissolved organic and inorganic carbon samples were collected in 40 mL amber TraceClean vials with septa caps. Precipitation samples were collected in Old Crow from September 2007 to July 2008. A volunteer at the Natural Resources Department of the Vuntut Gwitchin Government filled a 30 mL bottle following each rain or snow event.

Table 4- 1: Table of spring description and sampling visits, number before letter indicates the number of spring vents sampled, D: indicates diffusion samples, P: piezometer with diffusion sample attached to end, W for copper tube water sample, CO stands for chemistry and isotopes only.

Spring	Sampled			Description	Approximate Discharge (m^3/s)
	June 12-20th 2006	July 1-5th 2007	August 1-8th 2008		
Upper Spring		3-D-1-P	CO	Most upstream spring, springs discharge into a series of pools, dammed by beavers	2007: 0.25 m^3/s
Livingstone	1-D	1-D		Located on river bank	
BC	1-W	1-P	CO	A sinkhole. Groundwater flowing in 2006, pool not spilling over in 2007	2008: 0.05 m^3/s
S-4	1-D			Spring behind beaver pond, no flow in 2007	Not perennial
Redd		1-P		Springs located in large salmon red (salmon spawning site)	
Gossage		1-D		Spring located by river, discharging from bedrock	
CS	2-D	2-W	CO	Several spring vents, one discharging directly from bedrock	2006: 1.6 m^3/s 2007: 0.7 m^3/s 2008: 0.8 m^3/s

Discharge measurements were made at four locations along the lower reaches of the Fishing Branch River: Upper Spring, Livingstone, Cabin and CS. The locations of these sites are shown in Figure 4- 1. Discharge was measured using the area-velocity method, where flow velocity and depth are measured across the river (Dingman, 2002). In 2006 flow velocity was measured using a GeoPacks FlowMeter and in 2007 and 2008 a Global Waters FP101 flow velocity probe was used.

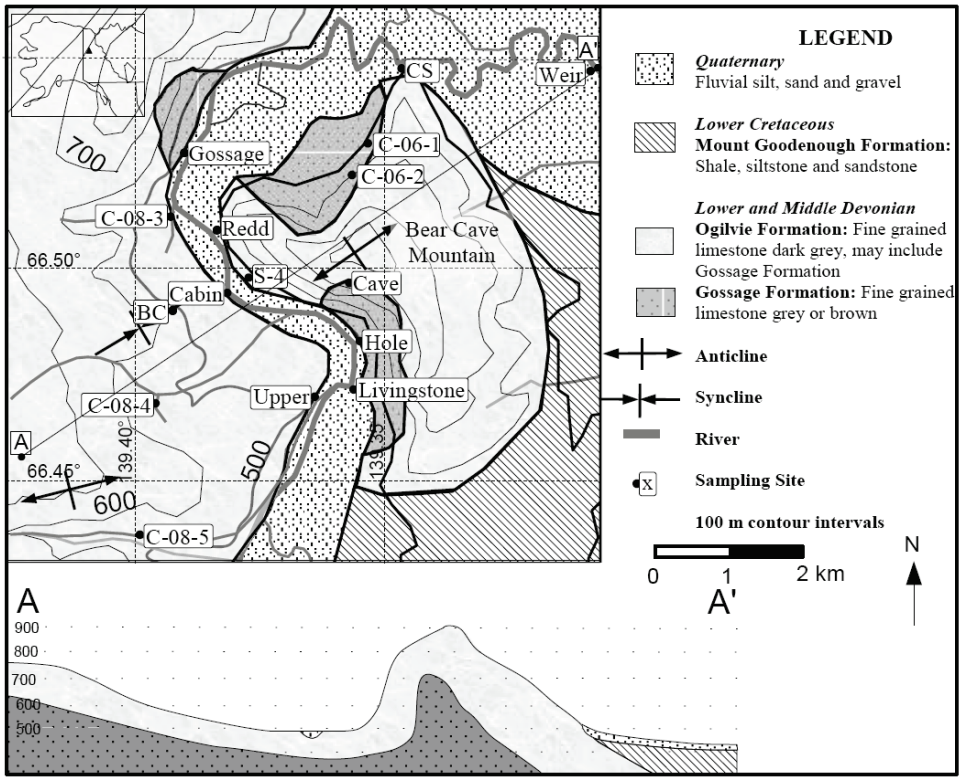

Figure 4- 2: Map of topography, geology and field sites in study area (Geology from Norris, 1978)

Hobo® Pendant Temperature Data Loggers were installed in the river at the Hole site, at the BC and Upper Springs as well as one logger to measure air temperature near Cabin site. The logger near Cabin site was deployed beneath a cache near the Parks cabin, at a height of 3 m. The data loggers recorded temperature every four hours between July 2007 and August 2008 with a precision of 0.1°C and an accuracy of ± 0.47 °C.

4.4 **Analytical methods**

4.4.1 Major Ion Chemistry and Isotopes

All water samples were analysed for major ion concentration, $\delta^{18}O$ and δD, and dissolved inorganic carbon concentration (DIC). Some samples were also analysed for $\delta^{13}C$ of DIC. Geochemistry measurements were conducted at the University of Ottawa, Department of Earth Science Geochemistry laboratory. Major cations were acidified and measured with a Varian radial Inductively Coupled Plasma Emission Spectroscopy (ICP-ES) and anions were measured using a Dionex DX-100 ion chromatograph. These analyses

are reproducible to within 1%. Based on the major ion geochemistry and pH, the P_{CO2} and calcite saturation were calculated using WATEQ (Ball, 1988).

Dissolved inorganic carbon and stable carbon isotope ratios were analysed at the G.G. Hatch Laboratory (University of Ottawa) using an OI Analytical Aurora Model 1030W TIC-TOC Analyser following the wet oxidation method described in St-Jean (2003). Alkalinity was then calculated from the DIC concentrations and pH measurements. The DIC concentrations were normalized using internal standards and the analytical precision was ± 2%. Most samples were analyzed for alkalinity by acid titration in the field. The $^{13}C/^{12}C$ ratios of the DIC are expressed in δ-notation, where δ represents the parts per thousand difference of $^{13}C/^{12}C$ in a sample with respect to the Vienna Pee-Dee Belemnite (VPDB) standard. Analytical precision is ± 0.2‰.

The $^{18}O/^{16}O$ ratio of the water samples was determined from CO_2 which had been isotopically equilibrated with the water sample at 25 °C (analytical reproducibility of ± 0.15‰). The D/H ratio was measured on H_2 which had been isotopically equilibrated with the water sample at 25 °C using a Pt catalyst (analytical reproducibility of ± 2.5‰). Both stable isotope measurements were made on the same sample using a Gas Bench II interfaced with a Finnigan Mat Delta+ XP isotope mass spectrometer at the G.G. Hatch Laboratory (University of Ottawa). Results are presented using the δ-notation, where δ represents the parts per thousand difference of $^{18}O/^{16}O$ or $^{D}H/^{1}H$ in a sample with respect to Vienna Standard Mean Ocean Water (VSMOW).

4.4.2 Noble gases

Ten groundwater springs were sampled for noble gas analysis. Eight samples were collected using passive diffusion gas samplers (Sanford *et al.*, 1996; Manning *et al.*, 2003) and two samples were collected using copper tube water samplers (Table 4- 1). Diffusion samplers allow for easier field sampling and simplified analysis in the lab. The silicon tubing between the copper tubes is permeable to non-polar gases, thus excluding water vapour. Diffusion gas samplers were deployed and left for a minimum of three days to allow equilibrium with dissolved gases in the surrounding water. Samples are then sealed

using a cold-welding crimping tool. At sites where groundwater springs were located in gravel sediments, piezometers with diffusion samplers on were hammered about 50 cm below surface to reduce degassing and surface influences. Where return sampling trips to retrieve diffusion samplers were not possible, two water samples were collected in copper tubes. For such samples, water is pumped through a $3/8^{th}$ inch tube and the tube is sealed with a cold weld using a crimping tool. At each site sampled for noble gases 500 ml, of water was also collected for tritium analysis by decay counting after electrolytic enrichment, which was conducted at the University of Waterloo.

Seven water samples were analysed for noble gas concentrations at the University of Heidelberg using a GV 5400 mass spectrometer, following the procedure based on Friedrich (2007). All gases are passed through a stainless steel Permanent Gas Trap (PGT), where Ar, Kr and Xe are trapped temporarily at a temperature of 25 K and the remaining helium and neon are trapped at 10 K on charcoal. Helium is released by heating to 42 K, followed by a release of neon after increasing the temperature to 90 K. For the analysis of argon, krypton and xenon, the PGT is heated up to 130 K to release the trapped gases. A pipette of this gas is extracted, gettered, and let into the mass spectrometer.

Three water samples were analysed at the University of Ottawa for helium and neon using a MAP 215-15. Gas was let into the line and was first trapped on charcoal cooled with liquid nitrogen to remove gases heavier than mass ~25 atomic mass units, this is followed by gettering with titanium to sorb N_2, O_2, CO_2 and CO and decompose hydrocarbons (Mohapatra, 1998), this is followed by gettering with SAES (ST 707) pellets to remove H_2, CO and N_2 (SAES, 2010). The remaining gas contains only He, Ne and residual Ar. After gettering, a 90K cold trap is used to remove argon. Helium and neon are then trapped at 10K and released by heating to 42K to first release He to the mass spectrometer, then to 90K to release and analyse Ne.

Eight of the samples analysed were diffusion samplers. Once the amount of gas in the tube was found (as cc_{stp}), the pressure of gas in the tube was calculated using the ideal gas law (Equation 4- 1) and the concentration of dissolved gas was corrected using the Bunsen coefficient (Equation 4- 2)(Weiss, 1970; Weiss, 1971, Weiss, 1978, Clever, 1979).

Equation 4- 1:

$$P = \frac{nRT_{spring}}{V} = \frac{(cc_{stp}/22.414L/mol)\cdot(0.082058atm\cdot L/mol/K)\cdot(T_{spring}+273.15)}{V}$$

In Equation 4- 1, P is the pressure of the gas in the tube, cc_{stp} is the amount (in cm^3 at standard conditions) of gas in the tube, R is the gas constant, T_{spring} is the temperature of water and V is the volume of the tube.

Equation 4- 2: $cc_{STP}/cc_{H2O} = B\cdot P$

In Equation 4- 2 cc_{stp}/cc_{H20} is the concentrations of gas in the water, B is the Bunsen coefficient and P is the pressure of the gas in the tube from (Equation 4- 1).

4.5 Results and Interpretation

4.5.1 Discharge Measurements

Perennial open water along the lower reach of the Fishing Branch River provides visual evidence of groundwater discharge. Along the river, between Upper and CS sites, there are numerous groundwater springs on the river bank and in the forest.

In June 2006, river flow increased from 10.4 m^3/s at Livingstone (about 400 m downstream of Upper spring) to 24.2 m^3/s at CS (refer to Figure 4- 2 for site locations and Table 4- 2 for flow measurements). Over the 1618 km^2 catchment area upstream of Livingstone, the river discharges 10.4 m^3/s, which represents a flux per unit area of 6.5 x 10^{-9} m/s. From Livingstone to CS, the river gains 13.8 m^3/s over a contributing area of 21 km^2, representing a flux per area of 6.6 x 10^{-7} m/s.

In July 2007, river flow increased from 0.9 m^3/s at Upper Spring to 7.7 m^3/s at CS. The associated flux for the headwater watershed area upstream of Upper Spring and that area between Upper Spring and CS were 5.6 x 10^{-10} m/s and 3.2 x 10^{-7}m/s per unit area respectively. On a helicopter fly-over during the sampling, it was noted that the river was dry less than 1 km upstream of the Upper Spring sampling station. This occurs during baseflow conditions and is consistent with traditional knowledge (Yukon Environment, 2010).

The August 2008 sampling took place after a period of heavy rains; in July 2008, Old Crow received 65 mm of precipitation while the average for this period is 36 mm. In August 2008 the discharge at Cabin site was 16.4 m^3/s. This was higher than measured in the previous two years where river discharge at Cabin ranged from 2.4 to 12.5 m^3/s. Due to the high discharge in 2008, it was unsafe to measure at other locations along the river. Results are summarized in Table 4- 2. The increase in river flow from the Upper sampling station and CS is greater than what could be attributed to contributions from the additional 21 km^2 catchment (normalized fluxes would be 100x greater than the full catchment). The substantial increase in discharge along this reach of the Fishing Branch River is attributed to groundwater discharge.

Table 4- 2: River discharge in m^3/s. Values ±10%.

Location	Discharge (m^3/s)		
	June 2006	**July 2007**	**August 2008**
Upstream		0.9	
Livingstone	10.4	1.9	
Cabin	12.5	2.4	16.4
CS	24.3	7.7	

4.5.2 Temperature Loggers

Temperature loggers recorded temperatures in groundwater springs, the river and air from July 2007 to August 2008. Four data loggers were installed, two in groundwater springs, one in the river and one to measure air temperature. Data logger results are presented in Figure 4- 3.

One data logger was installed at the Hole site in a deep pool of the river about 2 m from the bank and >1 m below the water's surface. This logger recorded temperatures below 0 °C from February 26, 2008 to March 26, 2008 (Figure 4- 3). Although the logger measured temperatures below zero during this time, it was likely packed below ice and snow at the river's edge as the temperature does not drop below -3 °C and it was buffered from air temperature variability. The data logger in the spring at Upper site had a constant temperature (4.2 °C) up until January 7th, 2008 and constant temperature flow resumed May

19th, 2008. The BC spring logger recorded a constant temperature of 3.9 °C until November 29th and logged marginally negative temperatures (0 to -0.21°C) from March 2nd to 9th, 2008.

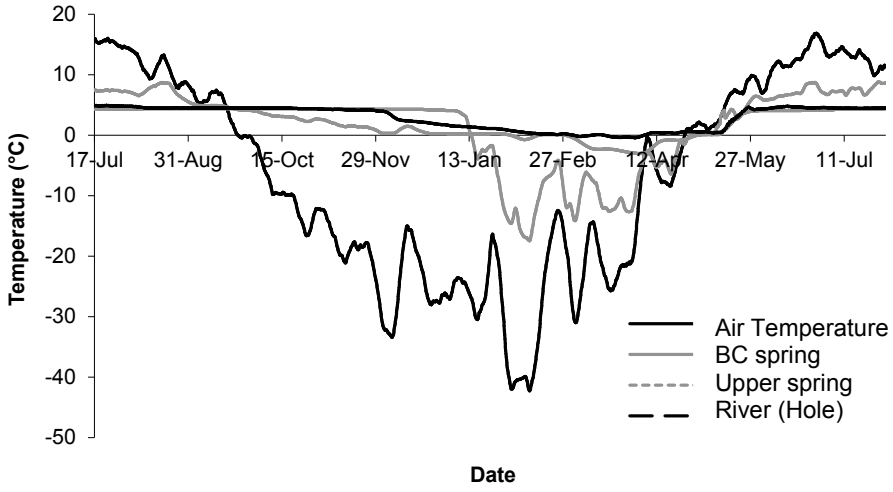

Figure 4- 3: Sixteen point moving average of 3 hour temperature logger data. Air temperature logger was left attached to the underside of an unheated tower (~3m above ground), BC spring is a logger in the groundwater spring at BC site, Upper is a logger in the Upper site spring and River logger is located in the river at the Hole site.

4.5.3 Major Ion Chemistry and Isotopes

Different contributions to river flow (i.e. snow melt water, precipitation, surface runoff and groundwater) result in different discharge water chemistry. Changes in solute concentrations (e.g. chloride, which represents groundwater inputs; Figure 4- 4-a) are due to differences in the contributions of groundwater and runoff to river flow at different locations along the river and throughout the year and between years. In 2006 and 2008, the river level was high and chloride concentrations were low (1.1 to 2.7 ppm). In 2007 the river level was low and chloride concentrations were high (3.5 to 4.7 ppm). Combining chloride and sulphate concentrations allows for a more complete differentiation of water sources by identifying mixing lines and end members (Figure 4- 4-b). Figure 4- 4-c shows sulphate vs. chloride in surface runoff samples. Most surface runoff samples have low concentrations of chloride and sulphate due to limited water-rock interaction. Two samples

up a tributary show low chloride and high sulphate, these concentrations are attributed to weathering of sulphate minerals in Cretaceous shales (C-08-3, C-08-4). At the upstream end of this tributary there had been a small recent forest fire (likely spring 2008) which is presumed to have caused deeper melting of the active layer and in turn weathering of previously frozen shales.

Along this same tributary, pH progressively increased downstream. Figure 4- 4-d shows sulphate vs. chloride concentrations in groundwater samples. Groundwaters from springs fall along a mixing line between those with higher sulphate and lower chloride concentrations and those with higher chloride and lower sulphate concentrations likely due to influence from different formations, as discussed later. Higher sulphate (~25 ppm)/lower chloride (~3 ppm) groundwaters were found at stations Upper Spring, BC and Gossage while lower sulphate (~15 ppm)/higher chloride (~7 ppm) waters were found at CS. Figure 4- 4-e shows the mixing of groundwater and surface water to generate different river chemistry through the three sampling years. Full geochemical results are listed in Table 4-3.

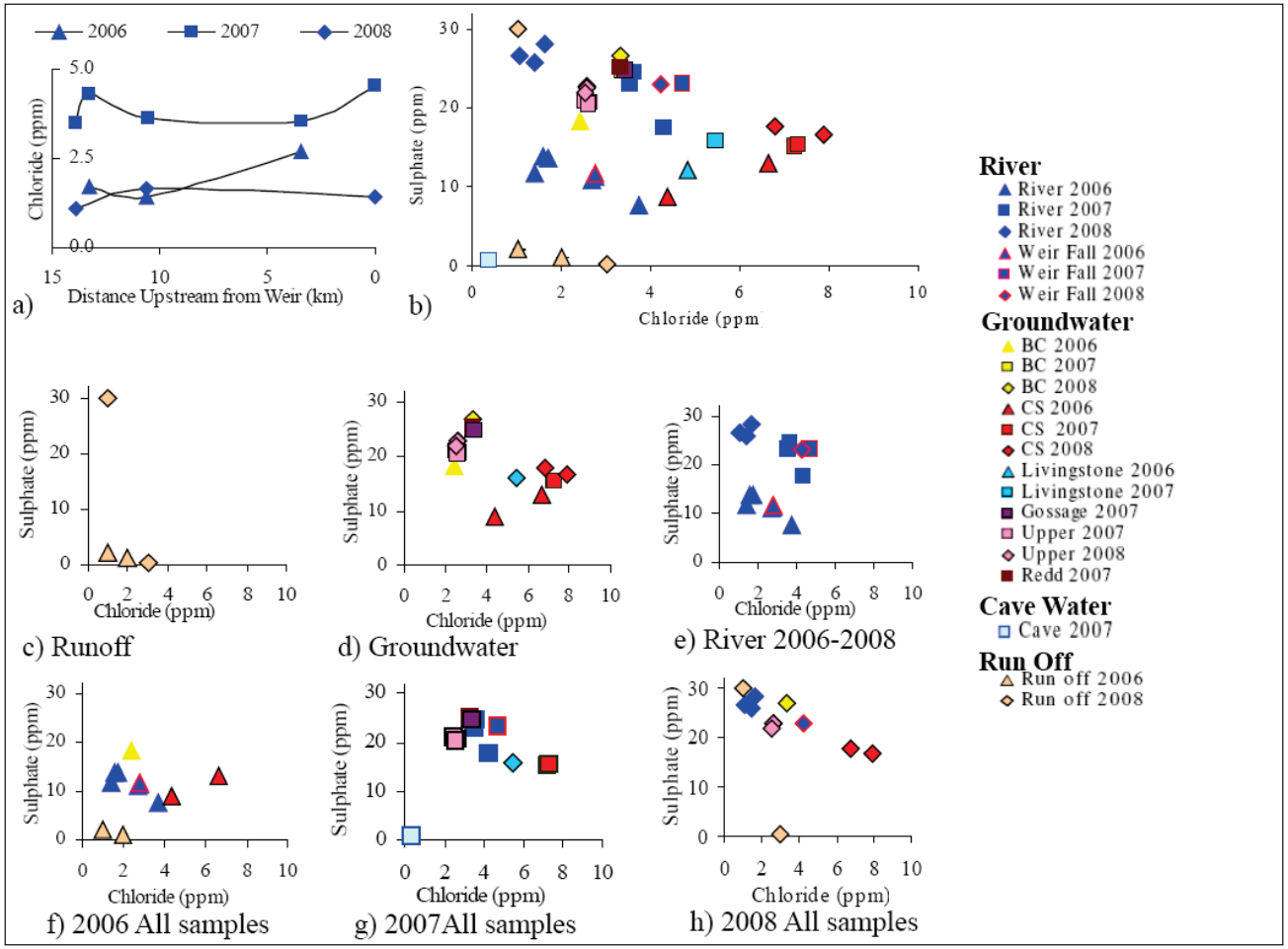

Figure 4- 4: a) Plot of chloride vs. distance upstream from weir in 2006, 2007 and 2008, b) Sulphate vs. chloride of all samples, c) Sulphate vs. chloride of runoff samples, d) Sulphate vs. chloride of groundwater samples, e) Sulphate vs. chloride of river samples from all years, f) Sulphate vs. chloride of 2006 samples, g) Sulphate vs. chloride of 2007 samples, h) Sulphate vs. chloride of 2008 samples. (error on analysis: ± 5.5% on sulphate, ± 2.8% on chloride).

Table 4- 3: Summary of geochemical data from groundwater springs, the river, cave water and run off. Weir Fall indicates samples that were collected in collaboration with the Department of Fisheries and Oceans, but were not discussed in this study. "--" indicates parameter not measured, xxx indicates parameter below detection limit (detection limits: Ca^{2+}: 0.009 ppm , K^{+}: 0.026 ppm, Mg^{2+}: 0.019 ppm, Na^{+}: 0.030 ppm, Si: 0.031, Sr: 0.00032 ppm, Cl^{-}: 0.1 ppm, NO_3^{-}:0.032 ppm, SO_4^{2-}: 0.012 ppm, DIC 1 ppm), (#) indicates value is an average of # samples.

Location	Lat. (°N)	Long. (°W)	pH	T °C	SC µS/cm	Ca^{2+}	K^{+}	Mg^{2+}	Na^{+}	Si	Sr	Cl^{-}	NO^{3-}	SO_4^{2-}	DIC	$\delta^{13}C$	$\delta^{2}H$	$\delta^{18}O$	log	SI
						Concentrations in ppm										$\delta^{13}C_{DIC\ VPDB}$	$\delta^{2}H_{VSMOW}$	$\delta^{18}O_{VSMOW}$	P_{CO2}	$SI_{Calcite}$
Springs 2006																				
Livingstone (2)	66.488	139.323	7.7	4.2	295	43.8	xxx	9.9	4.4	1.5	0.1	4.4	1.2	10.8	38	-11.3	-175	-22.5	-2.6	-0.13
S4	66.501	139.353	7.6	2.3	298	47.4	0.3	9.4	2.9	1.6	0.1	1.7	0.9	12.0	40	-10.8	-187	-23.2	-2.5	-0.22
Behind Cabin	66.500	139.371	7.8	4.7	312	47.2	0.3	10.2	3.9	1.7	0.1	2.4	0.6	18.3	25	-7.4	-164	-21.3	-2.8	-0.16
CS (2)	66.527	139.305	7.8	5.7	299	39.3	1.3	10.4	5.9	1.4	0.1	5.5	0.8	10.9	37	-9.8	-171	-22.3	-2.7	-0.06
Springs 2007																				
Upper (3)	66.518	139.371	--	4.3	301	45.7	0.3	9.3	2.6	1.6	0.1	2.6	1.0	20.7	38	-10.1	-169	-21.9	-2.7	0.09
BC	66.500	139.371	7.9	5.6	309	45.1	0.3	10.1	3.4	1.7	0.1	3.4	0.8	24.7	36	-9.7	-166	-21.5	-2.8	0.08
Redd	66.508	139.369	8.1	7.2	303	45.8	0.3	10.3	3.4	1.8	0.1	3.3	0.9	25.1	29	-9.4	-166	-21.5	-3.0	0.22
Gossage	66.512	139.379	7.9	7.8	310	46.4	0.3	10.5	3.4	1.8	0.1	3.4	0.9	24.7	28	-9.8	-168	-21.5	-2.9	0.03
Livingstone	66.488	139.323	7.7	4.3	302	43.1	0.4	10.6	4.1	1.5	0.1	5.5	1.0	15.9	30	-9.2	-171	-21.9	-2.7	-0.24
CS (2)	66.527	139.305	7.4	6.1	302	41.2	0.4	11.2	5.3	1.4	0.1	7.3	1.0	15.3	38	-8.7	-168	-21.8	-2.3	-0.45
Springs 2008																				
Upper (3)	66.518	139.371	--	4.2	304	49.7	0.3	10.0	2.8	1.7	0.1	2.6	0.6	22.5	29	--	-168	-21.7	-3.1	0.78
BC	66.500	139.371	8.3	4.9	312	50.3	0.3	11.2	3.8	1.8	0.1	3.3	0.8	26.8	27	--	-167	-21.6	-3.3	0.39
CS (2)	66.527	139.306	--	5.5	305	44.6	0.3	11.8	5.7	1.5	0.1	7.3	0.8	17.2	29	--	-170	-21.8	-3.6	0.67
River 2006																				
Livingstone	66.488	139.323	8.1	10.8	241	35.9	0.3	7.3	2.5	1.1	0.1	1.7	xxx	13.6	26	-10.1	-176	-23.0	-3.1	0.15
Cabin	66.501	139.364	8.1	6.7	311	47.3	0.3	10.2	3.6	1.6	0.1	1.4	xxx	11.7	38	-10.1	-169	-21.9	-2.9	0.34
Average at CS	66.527	139.305	8.1	8.6	284	41.4	0.3	9.7	4.2	1.3	0.1	2.7	xxx	11.0	27	-9.8	-172	-21.9	-3.1	0.19
Weir Fall (5)	66.527	139.247	7.9	--	--	43.5	0.3	9.4	3.1	1.8	0.1	2.8	xxx	23.2	33	--	-166	-21.4	-2.8	0.01
River 2007																				
Upper	66.484	139.335	8.1	9.4	303	45.1	0.5	9.6	3.2	1.2	0.1	3.5	0.7	17.3	41	-8.7	-165	-21.6	-2.9	0.40
Livingstone	66.488	139.323	8.4	10.0	298	44.2	0.3	10.1	3.5	1.3	0.1	4.3	0.7	17.5	35	-8.9	-172	-22.0	-3.3	0.63
Cabin	66.501	139.364	7.7	6.8	308	46.3	0.5	10.4	3.8	1.6	0.1	3.6	0.8	24.5	34	-2.6	-167	-21.3	-2.6	-0.12
CS (upstream)	66.527	139.307	7.7	7.9	305	46.1	0.3	10.3	3.4	1.3	0.1	3.6	0.6	23.0	39	-8.6	-169	-21.6	-2.5	-0.05
Weir	66.527	139.247	8.2	5.8	310	44.8	0.3	10.1	3.8	1.2	0.1	4.5	0.7	22.0	34	-8.9	-169	-21.7	-3.1	0.35
Weir Fall (3)	66.527	139.247	7.9	5.0	--	xxx	0.3	11.3	4.3	1.7	0.1	4.7	xxx	23.1	50	--	-167	-21.6	-2.6	0.18
River 2008																				
Upper	66.484	139.335	8.4	8.9	226	38.0	0.2	7.3	2.0	1.9	0.1	1.1	xxx	26.6	21	--	-161	-20.8	-3.5	0.34
Cabin (12)	66.501	139.364	8.5	6.6	255	42.1	0.2	8.4	2.3	1.8	0.1	1.6	xxx	28.2	23	--	-165	-20.9	-3.3	0.74
Weir	66.527	139.247	8.3	8.2	217	34.6	0.3	7.1	2.2	1.9	0.1	1.4	xxx	25.8	17	--	-160	-20.8	-3.5	0.11
Weir Fall (3)	66.527	139.247	7.8	--	--	29.5	0.3	10.9	4.2	1.6	0.1	4.2	0.8	23.0	25	--	-173	-21.8	-2.5	-0.10
Cave Water																				
2007	66.501	139.323	7.5	--	187	34.9	0.1	2.9	0.2	0.6	0.0	0.4	0.5	0.7	27	--	-166	-20.9	-2.5	-0.55
Run Off																				
C-06-1-	66.518	139.322	8.1	3.9	161	30.5	0.1	2.6	0.2	0.2	0.0	xxx	xxx	2.1	29	-11.0	-207	-25.4	-3.0	0.04
C-06-2	66.515	139.332	8.1	2.8	184	36.5	0.2	2.2	0.3	0.6	0.0	xxx	xxx	1.1	29	-11.0	-195	-23.6	-3.1	0.09
C-08-3	66.507	139.376	8.6	3.7	200	38.6	0.1	3.9	0.5	1.9	0.0	xxx	0.8	30.0	17	--	-166	-21.4	-3.5	0.64
C-08-4	66.485	139.373	8.4	4.5	265	57.7	0.0	1.6	0.5	1.9	0.0	0.0	xxx	47.5	22	--	-166	-20.8	-3.2	0.73
C-08-5	66.477	139.346	8.8	3.5	192	45.0	0.0	1.0	0.5	2.1	0.0	xxx	xxx	0.3	26	--	-167	-21.3	-3.5	1.08

Calcite saturation calculated using WATEQ is plotted vs. pH for each sample in Figure 4- 5-a (values listed in Table 4- 3). Most water samples are near or over calcite saturation, however they are under-saturated in dolomite, which also outcrops in the watershed. Groundwater samples were taken directly from spring vents and pH was measured in the spring vent. Any CO_2 degassing that happens likely does not occur until after groundwater discharge to the surface. Cave Water 2007 has the lowest saturation as this water has just passed through the soil where it would dissolve CO_2 (calculated $P_{CO2} = 10^{-2.5}$ atm.) and thus has the lowest pH (7.5). The groundwater samples vary in saturation and pH, which is likely due to variable degrees of weathering of the carbonate rocks, which increases the pH and calcite saturation index. Run-off samples from 2008 have higher calcite saturation indices and sulphate concentrations due to more extensive weathering of shale and limestone in shallow sediments. Figure 4- 5-b shows DIC concentrations vs. pH, along with open and closed system P_{CO2} scenarios and calcite and dolomite saturation curves.

The P_{CO2} of these waters ranges from $10^{-2.3}$ to $10^{-3.6}$ atm. Excess CO_2 is obtained during recharge when water flows through organic-rich soils, dissolving soil CO_2. Groundwater samples were also analyzed for $\delta^{13}C_{DIC}$ and had values between -9‰ and -10 ‰ (Table 4- 3). The $\delta^{13}C$ is a mix between -27 ‰ of soil CO_2 and 0 ‰ of limestone bedrock suggesting closed system dissolution of marine carbonate bedrock (Clark and Fritz, 1997). The P_{CO2}, calcite saturation and $\delta^{13}C_{DIC}$ suggest that recharge occurs through organic soils where water dissolved CO_2. This acidity is consumed along the flow path with the dissolution of marine limestone. After discharge waters likely degas CO_2 resulting in super-saturation in calcite and increases in pH.

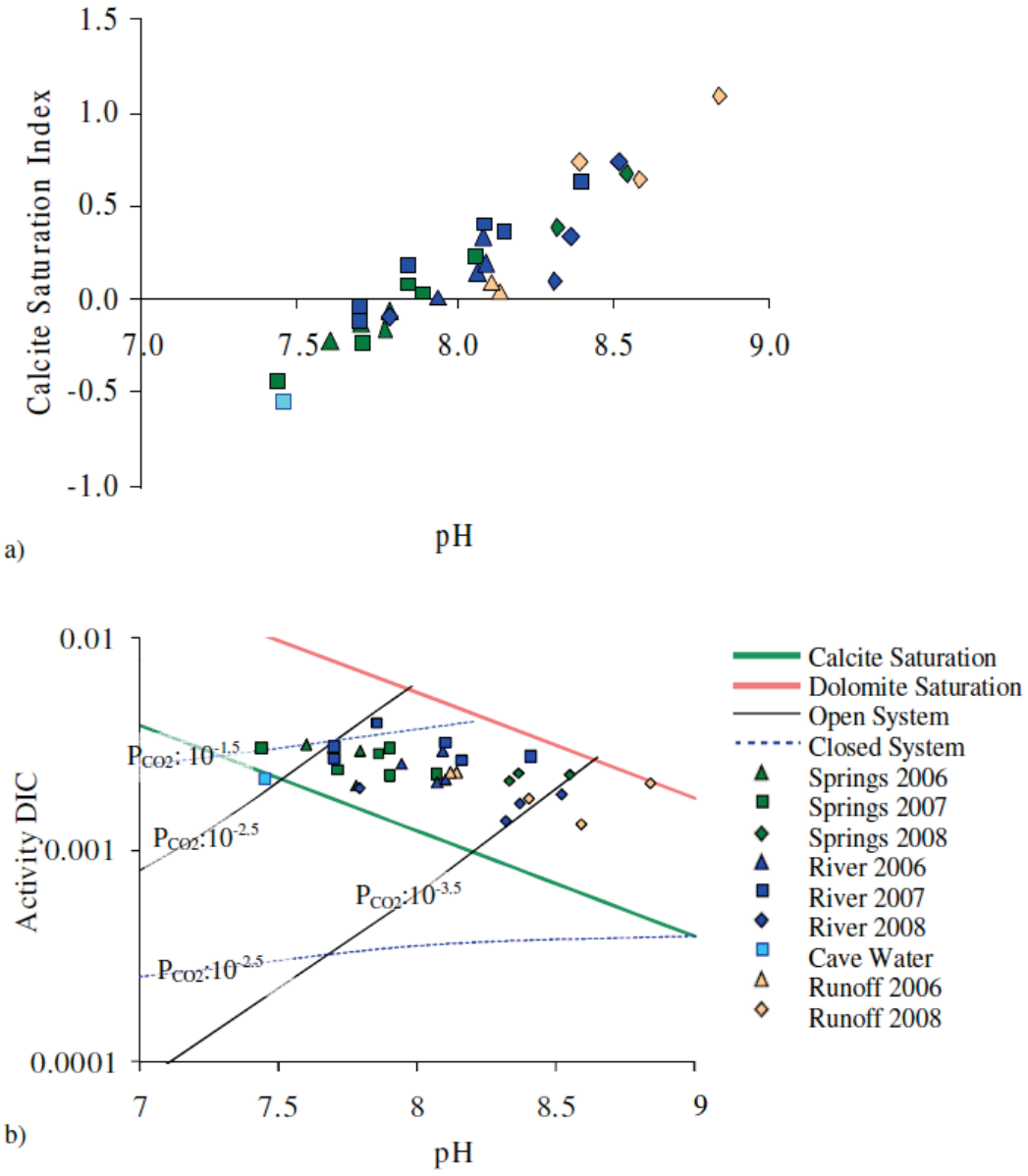

Figure 4- 5: a) Calcite saturation index vs. pH of all water samples. B) DIC activity vs. pH. Shows calcite and dolomite saturation at 5 °C, open and closed system weathering of calcite under different P_{CO2} conditions $10^{-1.5}$, $10^{-2.5}$, $10^{-3.5}$ atm.

There is limited variability in the δD and $\delta^{18}O$ results from the river over the three samplings seasons (2006, 2007, 2008) suggesting that groundwater is an important component of river flow (Figure 4- 6-a). Precipitation was collected from September 2007 to July 2008 in Old Crow, Yukon for measurement of δD and $\delta^{18}O$. In months where multiple samples were collected the average was determined. The δD and $\delta^{18}O$ values from each month were weighted using the average amount of precipitation during that month, to

determine the annual average δD and $\delta^{18}O$. These values are listed in Table 4- 4. Weighted averages were used in order to provide an estimate of the long term input from precipitations. This average value was corrected for elevation and latitude as Old Crow is approximately 110 km further north than the Fishing Branch River and has an elevation of 250 m a.s.l. while the Fishing Branch region ranges from 430 to 970 m a.s.l. (estimated average difference of 450 m). Based on these differences the average $\delta^{18}O$ value of precipitation at the Fishing Branch River should be more depleted. There are no local studies of isotopic depletion with elevation. A correction of -0.3 ‰/100m increase in elevation (Bortolami *et al.*, 1979) and +0.6‰/degree decrease in latitude were applied to correct $\delta^{18}O$. The value of δD was assumed to shift along the local meteoric water line, which has a slope of 6.8. Using these corrections the average value of δD and $\delta^{18}O$ for precipitation at the Fishing Branch shifts from -167.4 to -172 ‰ for δD and from -21.1 to -21.8‰ for $\delta^{18}O$. This correction is relatively small compared to the range of isotopic values measured, Figure 4- 6 -b shows only groundwater samples and corrected average precipitation. Average precipitation and groundwater have a similar δD and $\delta^{18}O$ signal indicating that groundwater recharge is a mix of precipitation through the year.

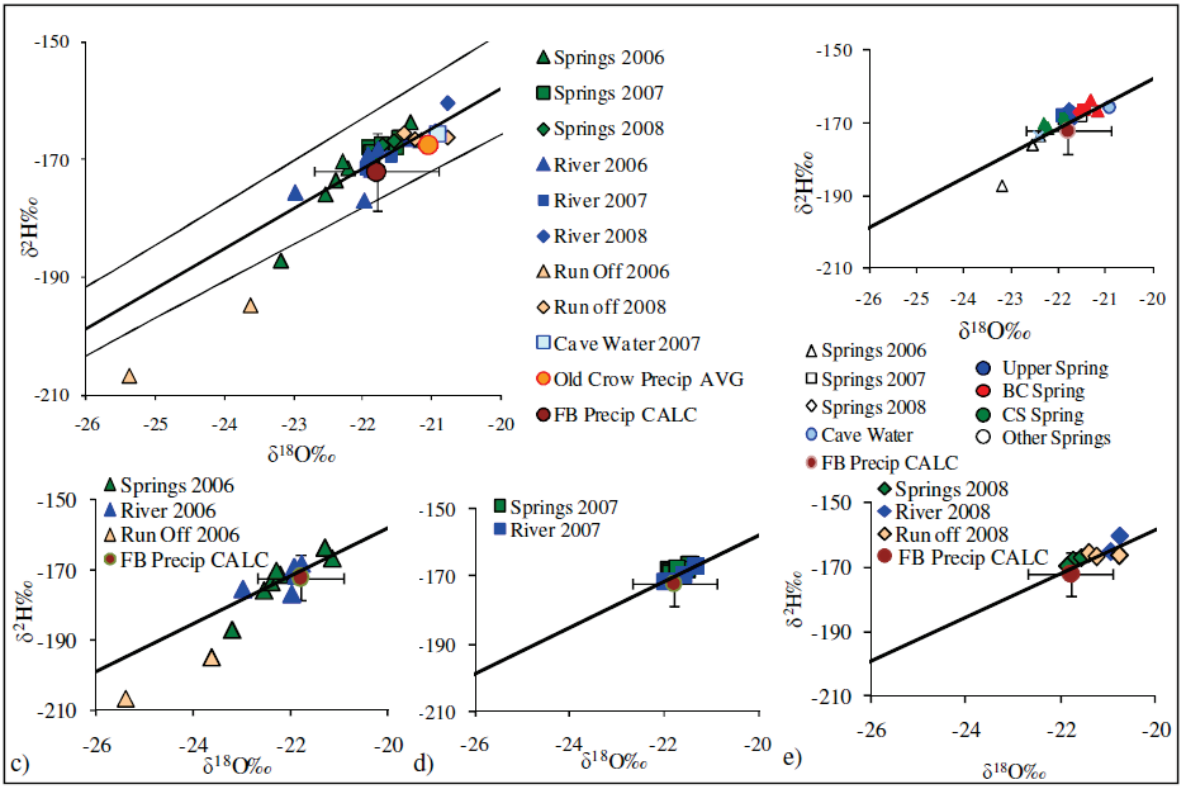

Figure 4- 6: Plot of δD vs. $\delta^{18}O$ of water samples from the Fishing Branch River with local meteoric water line determined from samples taken in Old Crow a) Shows all groundwater and river water samples, the weighted average of Old Crow Precipitation (Old Crow Precip AVG)(Table 4- 4) and the calculated average value for Fishing Branch Precipitation (Fishing Branch Precip CALC). The local meteoric water line is shown with the error envelope calculated on average Old Crow precipitation. b) Shows samples from groundwater springs along with water from caves, (meteoric water line from Old Crow) c-e) show river and groundwater springs from 2006 to 2009 (meteoric water line from Old Crow)(Error on individual analysis $\delta^{18}O$ ±0.15, δD ±2.5).

Table 4- 4: Table of isotope values from precipitation collected in Old Crow, Yukon. Average precipitation is used as groundwater is expected to reflect numerous years of precipitation and average precipitation will better reflect average input. Average is a weighted average with extrapolated values for $\delta^{18}O$ and $\delta^{2}H$ for missing months.

	δD	$\delta^{18}O$	Average Precipitation (mm)	Tritium (TU)	±
September 2007			24.4		
October Average 2007	-201.0	-27.5	17.8	7.6	0.7
November Average 2007	-213.0	-28.9	14	6.1	0.6
December 2007	-242.3	-32.7	11.9	6.9	0.7
January 2008	-238.9	-31.7	11.8	6.7	0.6
February 2008	-244.2	-31.7	11.9	12.7	1.0
March 2008	-232.8	-30.7	8.2	6.7	0.6
April 2008	-138.8	-17.7	14.7	13.2	1.1
May 2008			36.4		
June 2008			36		
July 2008	-153.9	-17.4	46.4		
August 2008	-105.0	-13.1	32		
Average	-167.4	-21.1	265.5	8.6	

As with water chemistry, the changes in δD and $\delta^{18}O$ in river water are related to mixing of different water sources. In June 2006 river water is depleted compared to average precipitation and the values are $\delta^{18}O$ (-21.8 ‰ to -23.0 ‰) and in δD (-168 ‰ to -177 ‰) (Figure 4- 6-c). The more depleted values are the result of snow melt entering the river as the samples were collected in the spring. In July 2007 there was less variability $\delta^{18}O$ (-21.3‰ to -22.0 ‰) and $\delta^{2}H$ (-167 ‰ to -171 ‰) (Figure 4- 6-d). The limited variability was interpreted to be because most river water was from groundwater. In 2008 the isotopic values in river water were more enriched in $\delta^{18}O$ (-20.8‰ to -20.9 ‰) and δD (-160 ‰ to -165 ‰) (Figure 4- 6-e) with minimal variability since the heavy summer precipitation was the dominant component of river flow.

4.5.4 Noble Gases

Based on the stable isotopes and geochemistry presented above, it is found that recharge occurs largely in the uplands and involves both snowmelt and summer precipitation. In an effort to determine the timing of recharge, noble gases were used to determine recharge temperature and groundwater age. The noble gas recharge temperature

is taken to represent the average temperature at the water table during recharge (Kipfer *et al.*, 2002). Springs in this study area had an average discharge temperature of 5.1°C and vary from 2.4 to 7.8°C. It is unknown if in the Fishing Branch watershed, groundwater recharge is a mechanism for the advective transport of heat into the subsurface. A gain in heat would suggest subpermafrost circulation and gain of geothermal heat while a loss would suggest transport of heat into the subsurface and permafrost degradation. Noble gas samples were collected at spring vents; these springs are used as an analogue for the recharge conditions that exists upstream in the watershed. Concentrations for all gases were measured in five samples, one sample was measured for helium and neon concentrations while two samples were only analysed for helium and neon ratios.

Groundwater recharge temperature

The large volume of groundwater discharge measured along the Bear Cave Mountain reach of the Fishing Branch River, must be sustained by an equally large volume of groundwater recharge. Changes in storage in the catchment, through melting of ground ice or changes in saturated water content can be reasonably discounted. The temperature recorded by noble gases during recharge then reflects the temperature at the water table. One complication in the application of noble gases to reconstruction of recharge temperatures is the incorporation of excess air (entrained bubbles) during recharge, which may in turn become chemically fractionated. Three models of excess air and fractionation are considered: i) unfractionated excess air, ii) partial re-equilibrium with the atmosphere, and iii) closed-system equilibrium with entrapped air (Kipfer *et al.*, 2002). To estimate groundwater recharge temperatures, noble gas concentrations have been analysed using the inverse modelling approach (Aeschbach-Hertig *et al.*, 1999). This analysis was conducted using the Mat Lab program Noble 90 which uses noble gas concentrations and elevation to vary the model parameters including temperature, excess air, and fractionation to find the best fit to the observed concentrations. The program minimises the error-weighted sum of the model – data deviations (χ^2) of the individual noble gases, which at the same time provides a measure of the goodness of the achieved fit (Aeschbach-Hertig *et al.*, 1999). The data set was best modelled using the closed-system equilibrium (CE) model, varying temperature, excess air and fractionation.

The recharge elevation is an input that helps to constrain the model. Due to the mountainous topography, the exact recharge elevation is unknown since recharge probably happens on the upper slopes of hills where bedrock fractures are exposed and elevation is variable. For noble gas calculations, the recharge elevation for the Fishing Branch watershed is assumed to be 700 m.a.s.l. The noble gas concentrations shown in Table 4- 5 were modelled under closed system equilibrium (as described above) using the MatLab program Noble 90 (Peeters *et al.*, 2003). This calculation returns recharge temperatures for the sampled springs between 0 and 5 °C (Table 4- 6).

Most of the samples fit with the CE model, although some samples do not match well. For example, a realistic recharge temperature for CS-1 2007 was found by modelling to include degassing, based on the model of Aeschbach-Hertig *et al.* (2008). A sample from the same spring taken a year before (CS-1 2006) did not display any degassing, and provides a recharge temperature of 5 ± 1 °C. The noble gas concentrations in the piezometer at the BC site (BC pizo) had a high χ^2 value indicating poor fit with the model; model results also indicated an unrealistically high value for the model parameter, A, describing the concentration of initially entrapped air. The recharge temperature calculated from the BC Pizo sample was at the lower limit of the expected range and had a relatively large uncertainty due to the high A value.

When comparing the recharge and discharge temperatures of springs, recharge temperatures are significantly cooler than the measured spring temperatures with a P value of <0.01. From data logger results, some springs are known to have stable temperatures (i.e. Upper); however others display more variability (i.e. BC). Groundwater temperatures may gain some heat in the subsurface; however as all noble gas samples were collected in the summer this may introduce a bias from heating of the spring vent area during summer. Those springs which may have a more variable temperature may be warmer in summer. The difference in discharge and recharge temperatures is small and it is not possible to conclusively state whether the water is warming.

Table 4- 5: Noble gas results. S is the sampler type where D is for diffusion and W is for water. H stands for samples analysed in Heidelberg and O for samples analysed in Ottawa. R/R_a is $^3He/^4He_{sample}/^3He/^4He_{air}$. Upper Spring and Upper Spring 2 are two different spring vents.

	Lab	S	^{4}He (cc/g) x10^{-7}	^{3}He/^{4}He x10^{-6}	R/R_a	Ne (cc/g) x10^{-7}	Ne/He	Ar (cc/g) x10^{-4}	Kr (cc/g) x10^{-7}	Xe (cc/g) x10^{-8}
2007										
Upper Spring	H	D	1.12±0.02	1.49±0.03	1.08	2.79±0.02	2.49	4.88±0.02	1.12±0.01	1.61±0.04
Upper Spring 2	H	D	1.21±0.02	1.52±0.03	1.10	2.87±0.02	2.37	5.03±0.02	1.15±0.01	1.71±0.04
CS 1	H	W	0.94±0.01	1.02±0.02	0.74	1.43±0.01	1.52	3.85±0.02	1.02±0.01	1.56±0.02
Livingstone	H	D	1.61±0.03	1.16±0.02	0.84	3.24±0.02	2.02	5.43±0.02	1.26±0.01	1.81±0.03
Redd Spring	H	D	1.01±0.02	1.05±0.01	0.76	2.56±0.02	2.53	5.15±0.02	1.21±0.01	1.76±0.03
BC Pizo	H	D	8.70±0.02	1.05±0.01	0.76	2.28±0.02	2.63	5.07±0.02	1.23±0.01	1.82±0.04
Gossage	O	D	1.81±0.01	1.37±0.02	0.75	1.79±0.01	0.99			
2006										
CS 1	H	W	1.53±0.03	1.06±0.01	0.77	2.32±0.02	1.52	4.73±0.02	1.15±0.01	1.66±0.03
Livingstone	O	D		1.14±na	0.83		2.90			
S-4	O	D		1.49±na	1.08		2.63			

Table 4- 6: Results of noble gas modelling using Noble90 and age calculations. Recharge is noble gas recharge temperature, A: the initial entrapped air according to the CE model, F: noble gas fractionation. Sample gas concentrations modelled using closed system equilibrium CE model, * denotes sample modelled with degassing.

	Measured Temperature	$\chi 2$	Noble Gas Recharge Temperature	±	ΔNe	A	±	F	±	^3H	^3He from ^3H	±	^3H-^3He Age	±
	(˚C)		(˚C)	(˚C)	%	(ccSTP/g)				(TU)	(TU)	(TU)	(years)	
2007														
Upper Spring	4.1	0.16	3.4	0.67	41	0.023	0.006	0.57	0.033	13.8	20.2	1.8	16.1	1.2
Upper Spring 2	4.5	0.97	2.5	0.55	43	0.023	0.005	0.56	0.03	14.1	23.9	1.9	17.7	1.2
CS-1 *	6.5	6.59	1.7	0.35	-29	0.005	0.002	2.37	0.43	13.8	6.4	1.0	6.8	1.0
Livingstone	4.3	2.40	0.4	0.42	58	0.020	0.003	0.43	0.032	14.2	12.5	2.1	11.3	1.5
Redd Spring	7.2	0.02	2.3	1.51	27	0.110	0.076	0.76	0.008	14.8	0.6	1.2	0.7	1.4
BC Pizo	5.6	9.63	0.0	2.7	11	0.263	0.96	0.89	0.02	12.3	0.0	1.2	0.0	1.7
Gossage										15.5				
2006														
CS-1	5.6	2.82	5.0	1.0	19	0.798	1.127	0.84	0.012	14.3	11.3	1.9	10.4	1.4
Livingstone	4.2									16.3				
S-4	2.3									10.7				

^3H-^3He: Groundwater residence time

Measured helium concentration (as total ^4He cc/cc) and isotope ratios (as $R/R_a = (^3He/^4He)_{sample}/(^3He/^4He)_{air}$) are given in Table 4- 5. For the spring samples, R/R_a ranged from 0.75 to 1.1. Determination of groundwater residence times requires correction of the measured ^3He and ^4He contents for crustal contributions. The in-growth of ^3He from tritium decay as well as from crustal sources is shown in Figure 4- 7. While the addition of ^3He from tritium decay increases the $^3He/^4He$ value, it does not contribute measurably to the total helium and so does not shift values to the left in this figure. The alpha decay of uranium and thorium in the crust results in the production of ^4He which is accompanied by production of ^3He through α-n induced fission of ^6Li, and an increase in the $^3He/^4He$ value. This $^3He/^4He$ signal is from crustal in-growth, R_{ter}. The value of the R_{ter} (6.25×10^{-7}) was determined with Figure 4- 7 and assumes that values for waters plotting along the ^4He and ^3He crustal in-growth line received helium only from crustal sources and not from tritium decay. This assumption yields a maximum estimate for R_{ter} and minimum estimates for the ^3H-^3He age. Using lower values for R_{ter} would produce ages greater by about 10 years. Unfortunately no independent estimate of R_{ter}, e.g. from an old, tritium-free groundwater is available. As such, ages are minimum groundwater ages; the water could be older if R_{ter} were found to be lower, which introduces some uncertainty in the age calculations.

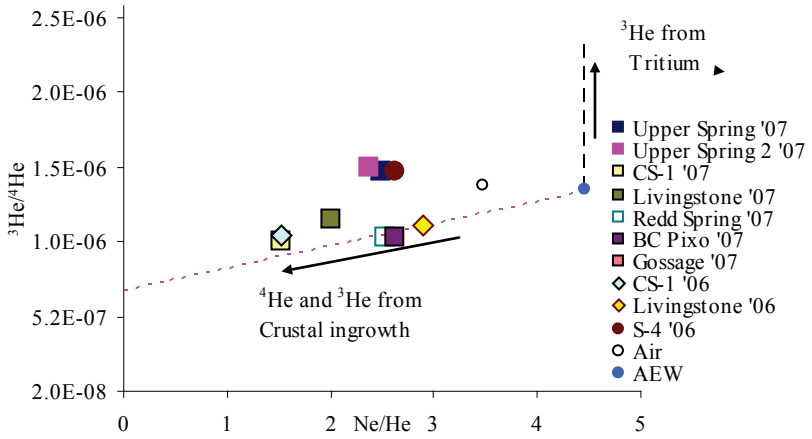

Figure 4- 7: $^3He/^4He$ vs. Ne/He of samples from groundwater springs. Pink dotted line represents crustal in-growth signature, while black dashed line is in-growth of ^3He solely from the decay of ^3H. AEW: Air equilibrated water.

The excess ^3He component from tritium in the groundwater has been calculated using Equation 4- 3,

Equation 4- 3:

$$^3He_{tri} = {}^4He_m\left(R_m - R_{ter}\right) - {}^4He_{eq}\left(R_{eq} - R_{ter}\right) - L_{ex}\left(Ne_m - Ne_{eq}\right)\left(R_{ex} - R_{ter}\right)$$ (Kipfer *et al.* 2002)

where:

- R_m is the measured $^3He/^4He$
- R_{eq} is the $^3He/^4He$ at atmospheric equilibrium (1.38×10^{-6})
- R_{ex} is the $^3He/^4He$ for excess air (1.40×10^{-6})
- R_{ter} is the $^3He/^4He$ from crustal sources
- L_{ex} is the He/Ne of the excess air component (2.88×10^{-1})
- ^4He_m is the measured amount of ^4He
- $^4He_{eq}$ is the amount of ^4He in air equilibrated water
- Ne_m is the measured neon
- Ne_{eq} is the equilibrium concentration of neon at recharge (Kipfer et al. 2002).

The amount of $^3He_{Tri}$ is then converted to tritium units (TU) by multiplying by 4.04×10^{14} TU/cc, which is then shown as $^3He_{TU}$.

The sampled groundwaters had tritium concentrations ranging from 10.7 to 15.5 TU, while average precipitation in Old Crow was 8.6 ± 3.0 TU. The groundwater tritium concentrations are combined with the $^3He_{Tri}$ obtained from Equation 4- 3 to determine groundwater age in Equation 4- 4 where 12.3 years is the half-life of tritium, $^3He_{TU}$ is tritogenic ^3He in tritium units, and $^3H_{TU}$ is the tritium concentration in tritium units (1 TU = 1 T per 10^{18} H in water.

Equation 4- 4: $$t = (12.3\text{yr})/\ln 2 \cdot \left(1 + \frac{^3He_{TU}}{^3H_{TU}}\right)$$

The groundwater spring ages ranged from 0 to 17 years (Table 4- 6). Water from Redd Spring and BC Pizo samples are very recent with an age of 0 to 1 year, these waters may have partially degassed or in the case of Redd Spring there could be a river water influence. These recent ages are supported by their locations as Redd Spring was located in the river gravel and may be hyporheic water, while BC pizo is from a spring in a karst sinkhole, which is known to flow all year. The noble gas age for CS-1 in 2007 is 6.8 ± 1.0 yrs which is younger than the value obtained in 2006 of 10.4 ± 1.4 yrs. The difference is explained by degassing of the 2007 sample; as such the 2007 sample likely does not represent a realistic groundwater age. In contrast, the geochemistry of the spring waters at the CS site over the two years was virtually identical (Figure 4- 4-D). The calculated initial tritium concentrations ($^3H_{TU}$ + $^3He_{TU}$) are consistent with the tritium in precipitation as shown in Figure 4- 8.

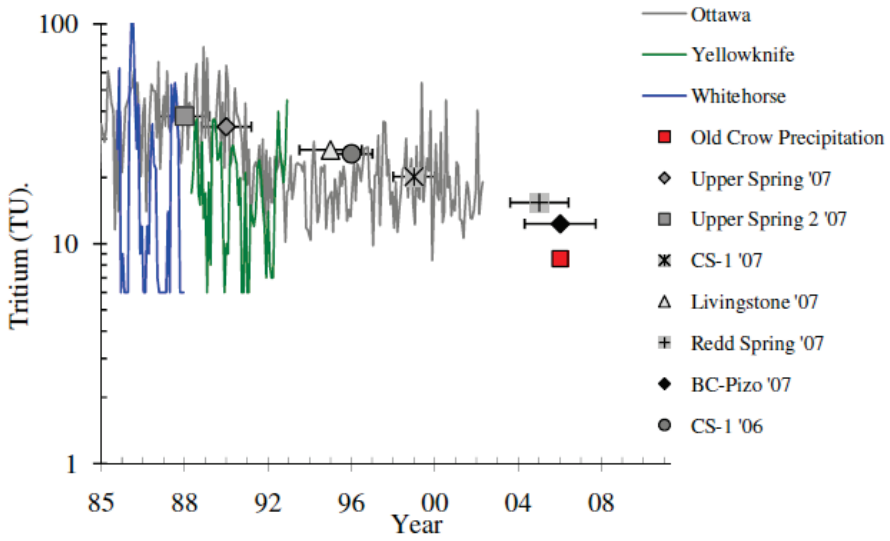

Figure 4- 8: Original tritium concentrations plotted vs. recharge year (calculated from the age), plotted with historical tritium record from Ottawa, Canada (from IAEA: GNIP database).

4.5.5 Estimation of Baseflow

It is known from both traditional knowledge and flights over the Fishing Branch River in winter that the river does not freeze over along the reach around Bear Cave Mountain (e.g. Schonewille and Anderton, 2006). Positive temperatures recorded by the

temperature loggers installed at groundwater springs and in the river also demonstrate that there is flow during winter. Bedrock groundwater discharge must be considered perennial as all but two groundwater samples represent water over 5 years old. An estimate of baseflow can be made based on summer flow measurements and photos taken of the river in winter.

The 2006 and 2007 samplings measured discharge at CS. In June 2006 river water was a mix of snow melt, spring rainfall and groundwater. Total river flow at that time was 24.3 m^3/s, and mixing calculations based on the chemical signature of groundwater determined that 15 m^3/s of river flow was discharge from the bedrock aquifer. In July 2007, the river was at baseflow, with a discharge of 7.7 m^3/s at CS; it is assumed that this flow is derived entirely from groundwater as discussed previously in the *Major ion chemistry and isotopes* section.

In February, 2006 photos were taken by EDS Dynamics during a low flyover, showing the river near the Cabin site (Figure 4- 9). The photos from the Cabin site in February 2006 and July 2007 can be compared to estimate the decrease in river flow over winter. Based on photos of the river in February 2006, the river is estimated to be ~16 m wide. The discharge in February, 2006 can be estimated based on a modified version of the Manning equation for open channel flow (Finnegar *et al.*, 2005). The flow and channel width were measured in July, 2006. The channel slope and Manning's roughness coefficient are assumed to be constant. It must be noted that this is an estimate of the flow, and winter flow gauging would greatly improve the accuracy of baseflow estimates. The equation is rearranged and the channel area term is added to determine the discharge (Equation 4- 5).

Figure 4- 9: Left: Photo of river in July 2007, during flow gauging river was ~21 m across. Right: Photo of river in February 2006, shows same section of river which is estimated to be ~ 16 m across at this time.

Equation 4- 5:
$$Q_F = \left(\frac{U_J}{\left(\frac{W_J}{D_J} + 2 \right)^{-2/3} W_J^{2/3}} \right) \cdot \left(\left(\frac{W_F}{D_F} + 2 \right)^{-2/3} W_F^{2/3} \right) \cdot A_F$$

In Equation 4- 5 U_J is the cross-section average water velocity in July (0.46 m/s), W_J is the channel width in July (21.5 m), D_J is the average depth in July (0.24 m), W_F is the channel width in February (14.0 m), D_F is the average depth in February (0.06 m), A_F is the area of flow in February (0.94 m^2) and the result is an estimated February, 2006 discharge of 0.77 m^3/s (A_F and D_F were estimated by decreasing the water level on the depth vs. distance profile that was previously measured in July, 2006). The estimated winter discharge is 31% of the summer discharge; it is assumed that the same decrease will occur at CS, the most downstream sample site. At CS, the February, 2006 estimated discharge (31% of summer discharge) is 2.4 m^3/s. The estimated February flow is used to estimate the baseflow hydrograph (Figure 4- 10). This hydrograph assumes flow gradually decreases over the summer, fall and winter. Decreasing river flow is assumed to occur until the spring freshet, and flow likely increases quickly to the flows measured in June. Based on this, the estimated annual average baseflow is 6.2 ± 1.0 m^3/s, which equates to a recharge rate of 121 ± 19 mm/yr over the catchment. This rough estimate of groundwater discharge is similar to what was found for the Firth River that is also within a karst watershed in

permafrost terrain and was found to have a recharge rate of 100 mm/yr (Clark and Lauriol, 1997).

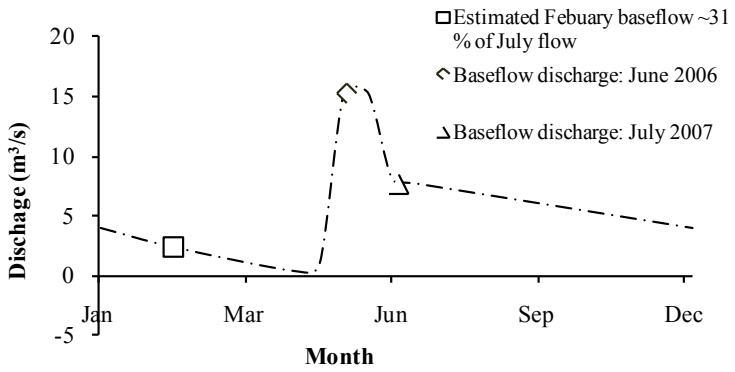

Figure 4- 10: Estimated baseflow hydrograph. Febuary flow is estimated based on the width of the river channel.

4.6 **Discussion**

The hills around the watershed have areas of exposed fractured bedrock. However the hilltops are mainly covered in thin organic soil estimated to range from 0 to 30 cm thick. Recharging water likely flows through these soils where it dissolves CO_2 from degrading organic matter and then through marine limestones. The range of $\delta^{13}C_{DIC}$ values suggest that weathering of marine carbonates occurs with biogenic CO_2 under closed system conditions. Along the flow path calcite is dissolved to saturation, although the water remains undersaturated in dolomite, likely because the aquifer is primarily calcite. The distribution of bicarbonate concentration and pH are similar to those found in other Paleozoic rock aquifers (e.g. Langmuir, 1971). The water may become over-saturated by the dissolution of calcite followed by exsolution of CO_2. Alternatively, calcite supersaturation may occur through the partial weathering of dolomite.

Recharge through organic soils can only happen when the soil is unfrozen. The noble gas recharge temperature was calculated to be between 0 and 5 °C. As recharge must clearly occur at temperatures much higher than the mean annual air temperature of -8.9 °C,

this differs from temperate regions where recharge temperatures may approximate mean annual air temperatures (e.g. Cey, 2009). Groundwater recharge in the Fishing Branch watershed must occur when soil temperatures are greater than 0 °C. The calculated recharge temperature likely reflects an average recharge temperature during the melt season when soils are thawed. Although recharge occurs only during summer the δD and $\delta^{18}O$ values suggest that the recharging water is a mix of snowmelt and summer rainfall.

The average annual baseflow was estimated based on flow measurements as well as photographs taken during winter. The estimated recharge rate is 121 ± 19 mm/yr. This rough estimate of recharge is similar to what was found for the Firth River that is also within a karst watershed in permafrost terrain and was found to have a recharge rate of 100 mm/yr (Clark and Lauriol, 1997).

Groundwater from this karstic aquifer discharges directly and indirectly to the Fishing Branch River. Minor groundwater discharge to the river happens at CS spring and Upper Spring. Along the river, there appears to be substantial discharge of groundwater below the river. As this was not observed to come from discrete zones along this reach of the river, it likely is derived from upwelling of groundwater from the alluvial aquifer. Groundwater most likely recharges the alluvial aquifer upstream. River water samples collected at baseflow show a mixed chemical signature of water from CS spring, Upper Spring and BC spring. Groundwater flow systems upstream of the sampling sites would be contributing water chemistry to the alluvial aquifer similar to those springs sampled and listed above. Groundwater discharge likely occurs at Bear Cave Mountain as the sub-river talik system is intersected by the large fold of Bear Cave Mountain which forces water up causing discharge along the river. This groundwater flow system is illustrated in Figure 4-11.

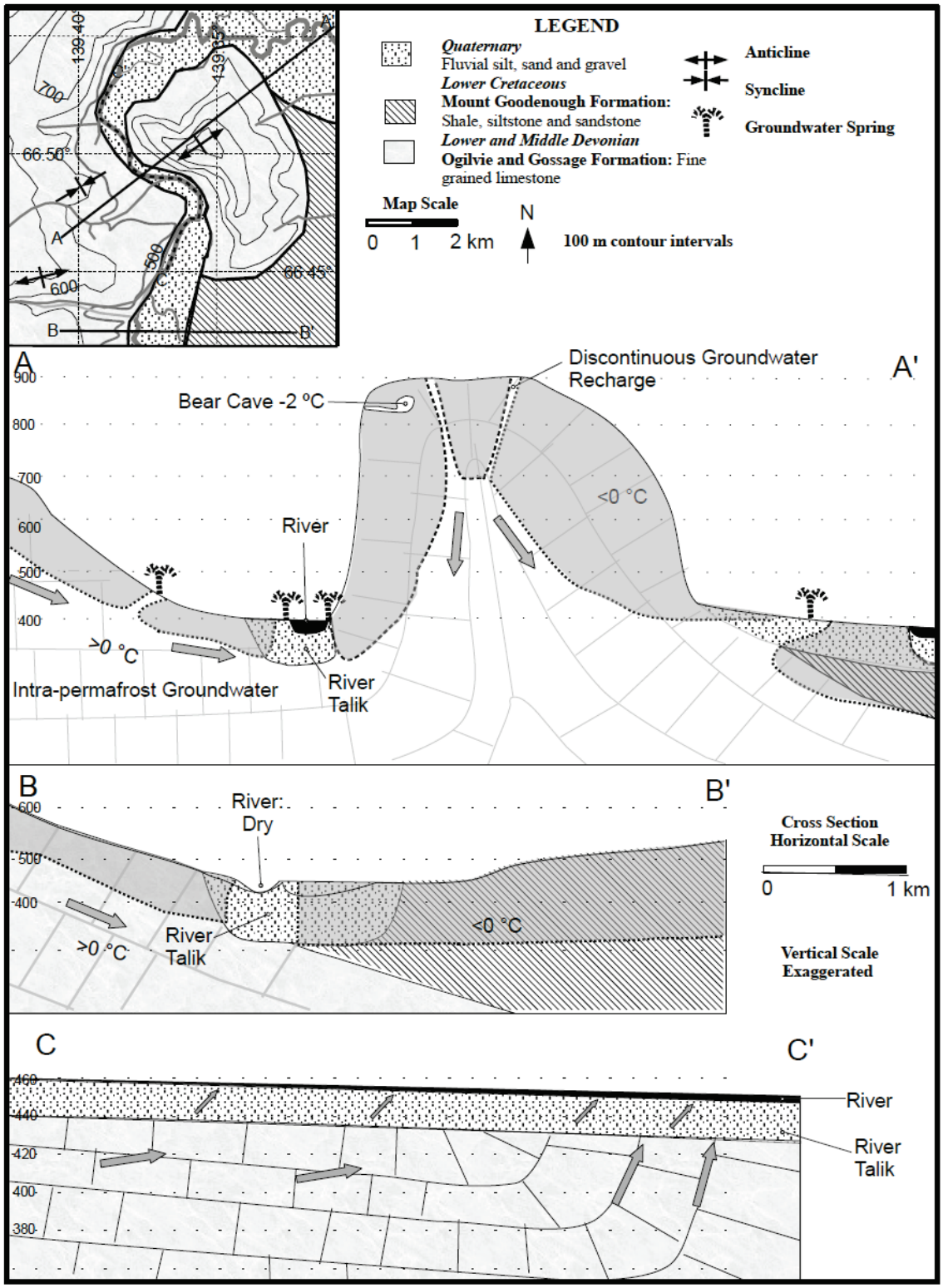

Figure 4- 11: Schematic diagram showing proposed groundwater flow system along Fishing Branch River. A-A' is a cross section of the proposed flow system which crosses through Bear Cave Mountain. B-B' shows upstream cross section of the proposed flow system. C-C' shows a longitudinal profile of how groundwater discharge is induced by changes in bedrock dip near Bear Cave Mountain.

4.7 Conclusions

The 10 km stretch of the Fishing Branch River near Bear Cave Mountain is a major groundwater discharge zone, with perennial open water and the presence of many groundwater springs along the river and in the surrounding forest. A baseflow hydrograph was estimated on the basis of discharge measurements coupled with geochemical and isotopic methods to distinguish groundwater discharge from runoff. The mean annual groundwater discharge from carbonate bedrock is estimated to be 6.2 ± 1.0 m^3/s which equates to a recharge rate of 121 ± 19 mm/yr.

Dissolved inorganic carbon concentrations and isotopes demonstrate that groundwater recharge is through karstic limestone in the catchment, and has mean transit times of up to a decade or more. Significant groundwater discharge occurs from alluvial gravels along the reach of the river around Bear Cave Mountain, where river gravels thin over a large anticline and forces groundwater discharge into the river.

The geochemistry of this groundwater component has evolved through carbonate weathering and retains the signature of the local geology. Groundwater from the Cretaceous bedrock is characterized by higher sulphate (25 ppm) and lower chloride (3 ppm), while groundwater that recharges solely in the Devonian limestone has higher chloride (7 ppm) and lower sulphate (15 ppm).

Groundwater recharge largely occurs in upland regions through organic soil overlying highly fractured bedrock as evidenced by the elevated P_{CO2} ($10^{-2.3}$ to $10^{-3.6}$) and $\delta^{13}C$ that indicate a biogenic source of CO_2 and results in the weathering of marine carbonates. Groundwater has a $\delta\ ^{18}O$ and $\delta\ ^{2}H$ signature similar to that of mean annual precipitation, indicating that recharge is a mixture of snowmelt and summer precipitation.

Noble gas results show that groundwater recharge temperatures are between 0°C and 5 °C, which indicates recharge during the summer months when soil temperatures are elevated above 0°C. Tritium-helium dating of the groundwater yields groundwater ages from 0 to 17 years.

Chapter 5: Using Noble Gas Ratios to Determine the Origin of Subsurface Ice in Permafrost

Article will be submitted to the journal Quaternary Research.

Nicholas Utting: Department of Earth Science, University of Ottawa, 140 Louis Pasteur, K1N 6N5 Ottawa, Canada

Ian Clark: Department of Earth Science, University of Ottawa, 140 Louis Pasteur, K1N 6N5 Ottawa, Canada

Bernard Lauriol: Department of Geography, University of Ottawa, 60 University, K1N 6N5 Ottawa, Canada

Denis Lacelle: Department of Geography, University of Ottawa, 60 University, K1N 6N5 Ottawa, Canada

A modified version of this chapter will be submitted to the journal Quaternary Research. Sample analysis, data interpretation and writing of the article were all performed by Nicholas Utting. Co-authors assisted with developing the interpretation of the results. The difference between this chapter and the article that will be submitted is that the discussion of the possible effects of ground ice on groundwater will be removed as this is likely of little interest to readers of Quaternary Research.

5.1 Introduction

In formerly glaciated permafrost regions, massive ground ice is preserved in the frozen terrain (French and Shur, 2010). Natural exposures of massive ground ice and icy sediments are found in the headwall of thermokarst slumps, and within eroding river banks and coastal cliffs (Mackay, 1966; Lewkowicz, 1987). The genesis of these ground-ice bodies have been attributed to a glacial origin (firnified or basal ice), buried lake ice, buried river ice or intrasedimental ice of a segregation / intrusive origin (Mackay, 1971; Rampton, 1982, Astakhow and Isayeva, 1988; Kaplyanskaya and Tarnogradskiy, 1986; Harry *et al.,* 1988, St-Onge and McMartin, 1999; Murton *et al.,* 2005; Waller *et al*., 2009, Froese *et al.,* 2008). Determining the ice emplacement mechanisms (e.g. glacial processes vs. periglacial) is fundamental to unlocking the paleoclimate, paleohydrology and stratigraphic implications of a particular ground ice body. For example the discovery of buried glacier ice may help constrain ice extent at different times (e.g. Lacelle *et al.*, 2007) or reveal the extent of permafrost melting during interglacials (Froese *et al.* 2008).

With the exception of wedge ice, with its classic V-shape profile (French, 1996), identifying the origin of massive ground ice bodies in exposed, permanently frozen sedimentary units using morphology alone is difficult. Other characteristics have been used to interpret ice origin including stratigraphic context, sediment content, bubble content, and crystallography (Murton *et al.,* 2005). Although these features are important for interpreting ice origin, they can be ambiguous. For example, both basal glacier ice and segregated ice may contain significant amounts of interbedded stratified sediment (Klassen and Shilts, 1987). As well, ice crystallography may also give clues to ice formations. However this can also be ambiguous, as segregated ice may have large anhedral equigranular crystals and buried snow bank ice may have smaller anhedral equigranular crystals (Pollard and French, 1985). Additionally the orientation of bubbles has been related to the mode of ice formation. However this may not be a definitive method, as both buried snow bank ice and ice formed by freezing of liquid water may contain vertically oriented bubble trains (Schumskii, 1964; Killawee *et al.*, 1998).

In response to these ambiguities, chemical-based techniques have been developed. $\delta^{18}O$ and δD isotopes have been used to exploit the fractionation processes related to freezing. If ice forms from an accumulation of snow, then when isotopic values from that snow are graphed, they should fall along the local meteoric waterline (Craig, 1961). Comparatively, ice which forms from the freezing of liquid water in closed system conditions, or where there is replenishment of the source water, will have a lower δD vs. $\delta^{18}O$ slope relative to the local meteoric water line (Jouzel and Souchez, 1982; Mackay and Dallimore, 1992). The limitation of this technique is that depending on the fractionation factor between water and ice, the regression slope of the ice can be similar to that of the local meteoric water line (Lacelle and Clark, 2011). As such, these analyses should be supplemented by other methods when attempting to identify ice origin.

Recent studies have used ratios of the gases trapped within bodies of massive ground ice to determine their origin (Cardyn *et al.,* 2007, Lacelle *et al.*, 2007, St.-Jean *et al.*, 2011). Cardyn *et al.* (2007) pioneered the use of molar gas ratios (N_2/Ar and O_2/Ar) to differentiate ground ice of glacial origin from ice formed by freezing of liquid water. Glacial ice will have molar gas ratios similar to those of atmospheric air incorporated during occlusion and transformation of the firn to ice, whereas the ratios in subsurface ice bodies originating from the freezing of water will be unique, because the solubility of gases in water is different from in air.

The analysis of occluded gases in subsurface ice has been found useful in the previous studies, although it can be complicated by the chemical and biological reactivity of certain gases (i.e. N_2, O_2, CO_2, CH_4). For example, the basal ice layers of GRIP and GISP2 ice cores in Greenland showed high CO_2 and CH_4 concentrations that cannot be attributed to climate-related changes (Price and Sowers, 2004; Tung *et al.*,2005). These spikes in gas were related to high microbial counts in basal layers of ice; as such the elevated CO_2 and CH_4 gas concentrations are due to *in situ* microbial activities of methanogens. In a study of N_2O concentration in portions of the Vostok ice core (Antarctica), Sowers (2001) found a 30% excess at a depth corresponding to the penultimate glacial maximum (135 Ka BP). The N_2O excess layer correlated with high bacteria counts and dust concentration, which led Sowers (2001) to suggest that the N_2O

had been produced in situ by nitrifying bacteria. Radtke *et al.* (2010) also presented evidence that O_2 and CO_2 gases in subsurface ice were modified by heterotrophic bacteria living within the ice matrix, thus making these gases useful biomarkers. As a result, the concentrations of O_2, N_2, CO_2 and CH_4 can be affected by biological reactions. While such reactions provide information on the geochemical and biological environment of the ice, they compromise the use of their ratios as a method to distinguish firnified ice (glaciers, snowbanks) from ice derived from the direct freezing of water.

Noble gases are inert and are affected only by physical processes, and may be a useful alternative to use in determining the origin of ground ice. Some previous studies have analysed noble gas concentrations in glacier ice (e.g. Serveringhaus *et al.*, 2003; Severinghaus and Battle, 2006; Ahn *et al.*, 2009). Ahn *et al.* (2009) used the greater solubility of Xe relative to Ar in water to identify glacier melt layers from non-melted layers.

In this study, the difference in solubilities of Ar, Kr and Xe was exploited to determine the origin of ground ice bodies in permafrost in the Canadian Arctic. To ensure efficacy of the method, ground ice of 'known origin', interpreted by other independent methods, was also analyzed from sites in the region. The method was found to work most effectively in assessing ice genesis and mechanisms of emplacement when complemented by other tools for characterizing ground ice.

5.2 Principles in Using Noble Gases to Determine Subsurface Ice Types

Noble gases (He, Ne, Ar, Kr, Xe) are inert gases, making up less than 1% of the atmosphere composition. This study has focused on Ar, Kr and Xe as a means of differentiating ground-ice bodies. Argon makes up 0.93% of the atmosphere, whereas Kr is 0.000114% and Xe is 0.0000086% (Andrews, 1992). In some ice bodies, He and Ne may be mobile (Kipfer *et al.,* 2002). Ar, Kr and Xe are less mobile making them suitable for this study. Although these concentrations have changed over geologic history, they have remained relatively constant over the last 1 million years (Serveringhaus and Battle, 2006). The concentration of Ar, Kr and Xe gases dissolved in water is dependent on their

concentration in the atmosphere, water salinity and the water temperature. The concentration of a given gas in fresh air equilibrated water can be determined using Equation 5- 1.

Equation 5- 1: $C_{(cc_{stp}/cc)} = B_{(cc_{stp}/cc/atm)} \cdot P_{(atm)}$

In Equation 5- 1, C is the concentration of gas in water, B is the Bunsen coefficient (at a given temperature) and P is the partial pressure of the gas of interest in the atmosphere. Table 5- 1 shows the concentrations of Ar, Kr and Xe in atmospheric air, the Bunsen coefficients at different water temperatures and the concentration in water at these temperatures and the associated gas ratios in δ notation. In δ notation, gas ratios are compared to the ratio in atmospheric air. The formula for calculating δ (Ar/Xe) is shown in Equation 5- 2 (Kr may replace Ar).

Equation 5- 2: $$\delta\left(\frac{Ar}{Xe}\right)_{Sample} = \left(\frac{\frac{Ar}{Xe}Sample}{\frac{Ar}{Xe}Atmosphere} - 1\right) \cdot 100$$

Using this notation, the value of δ(Ar/Xe) and δ(Kr/Xe) for air is 0.0 % and for air-equilibrated water at 0 °C is -75.5% for δ(Ar/Xe) and -50.7% for δ(Kr/Xe). There is a 3 % difference between gas ratios in air equilibrated water at 10 °C and 0 °C (Table 5- 1). This difference in δ(Ar/Xe) and δ(Kr/Xe) between atmosphere and air equilibrated water can be exploited in determining the origin of ground ice bodies. For example, if a ground ice body originates from the firnification of snow, as with glacial ice and buried snow pack, the gas ratios in that ice will be similar to the atmospheric values. Conversely, ground ice that forms from the freezing of water is expected to have noble gas ratios similar to those dissolved in water at recharge.

Table 5- 1: Concentrations of gases in atmosphere and water at 0 °C, 1 °C, 2 °C, 5°C and 10°C and associated Bunsen coefficients and δ values. (Bunsen coefficient as per: Weiss, 1970; Weiss, 1978; Clever, 1979, Concentrations in air equilibrated water calculated using Equation 5- 1)

	Bunsen Coefficient (cc/cc/atm)			**Concentration** (cc_{stp}/cc)				
	Ar	**Kr**	**Xe**	**Ar** ($\times 10^{-4}$)	**Kr** ($\times 10^{-8}$)	**Xe** ($\times 10^{-8}$)	**δ(Ar/Xe) %**	**δ(Kr/Xe) %**
Atmosphere				93.4	114.0	8.6	0.0	0.0
Concentration in Water								
0 °C	0.054	0.11	0.22	5.0	12.5	1.91	-75.9	-50.7
1 °C	0.052	0.11	0.21	4.9	12.1	1.84	-75.6	-50.3
2 °C	0.051	0.10	0.21	4.8	11.7	1.77	-75.3	-50.0
5 °C	0.047	0.09	0.18	4.4	10.7	1.58	-74.3	-48.9
10 °C	0.042	0.08	0.15	3.9	9.2	1.32	-72.7	-47.2

Noble gases are inert and cannot be altered by biological or chemical reactions as is observed for O_2, N_2 and CO_2 (e.g. Sowers, 2001; Tung *et al.*, 2005; Radtke *et al.*, 2010). The concentrations of noble gases can be affected by physical process during the formation of ice. Glacial ice originates as snow which over numerous years is transformed into ice. Snow which has begun to turn into ice and has survived one melt season is known as firn (Paterson, 1994). Firn is considered ice once the spaces between grains have been closed-off and there are bubbles. The air between the grains of snow is initially just that, atmospheric air; however it may be altered during the transformation from snow to ice. In firn there are three zones where different gas processes can occur: the convection zone, the diffuse zone and the non-diffuse zone of occlusion (Schwander, 1989). In the convection zone, air can be moved through the firn due to changes in air pressure. In the diffuse zone, gas may migrate by diffusion. In the non-diffuse zone there is porosity but limited permeability resulting in limited diffusion.

In firn, physical fractionation may occur with the heavier gases settling to the bottom of the column of gas (Craig *et al.,* 1988; Schwander, 1989). The heavier gases will also migrate to colder areas resulting in cold-trap fractionation (Grew and Ibbs, 1952). During the occlusion of gas bubbles in the ice, lighter gases such as Ne and Ar are preferentially excluded and may then re-exchange through the firn air column with the

atmosphere (Sowers *et al.*, 1989; Bender *et al.*, 1995). Another process which may alter the noble gas composition of the ice is the presence of micro-fractures which may allow for smaller atoms such as Ar to migrate (Craig *et al.,* 1988). Many of the above processes can occur during metamorphism of snow to ice as there may be up to several decades between the initial precipitation and full gas occlusion in ice (Barnola *et al.*, 1991; Clark *et al.*, 2007). Melt layers in ice may form more quickly. As these form from liquid water, the gas ratios of Kr/Ar and Xe/Ar will be greater than in air (Ahn *et al.*, 2009).

It is unknown if intrasedimental ice would experience changes in gas concentration during freezing. If bubbles form during freezing and some are able to escape, there will be a fractionation of noble gases as is observed during recharge at the water table (Kipfer *et al*., 2002).

The greater difference between the solubilities of Ar and Xe mean the value of δ(Ar/Xe) may be more diagnostic of ice formation processes. However as Ar may be mobile in some cases, the value of δ(Kr/Xe) is also useful in attempting to identify different ice formation processes. In this study, we have combined both δ(Ar/Xe) and δ(Kr/Xe) to determine ice emplacement processes.

5.3 Site Descriptions

Samples of polar ice and bodies of massive ground ice of different origins have been collected at 10 sites in the Canadian Arctic (Figure 5- 1). These sites are located from 64° to 80.7° N within the discontinuous and continuous permafrost zones. There are a limited number of meteorological stations in the region. Mean annual air temperature in the region varies latitudinally from -3.1°C measured in Mayo (south of all sites) to -8.9°C in Old Crow (north of all mainland sites) to -18.0 °C for Alert (near Agassiz ice cap) and -9.8 °C at Iqaluit (closest station to Penny Ice Cap) (Environment Canada, 2010). Previous studies have measured the ratios of $\delta(O_2/Ar)$ and $\delta(N_2/Ar)$ from five of the ice bodies analysed in this study. Those results are summarized in Figure 5- 1, and briefly discussed below as it will serve for comparison purposes with our noble gas measurements.

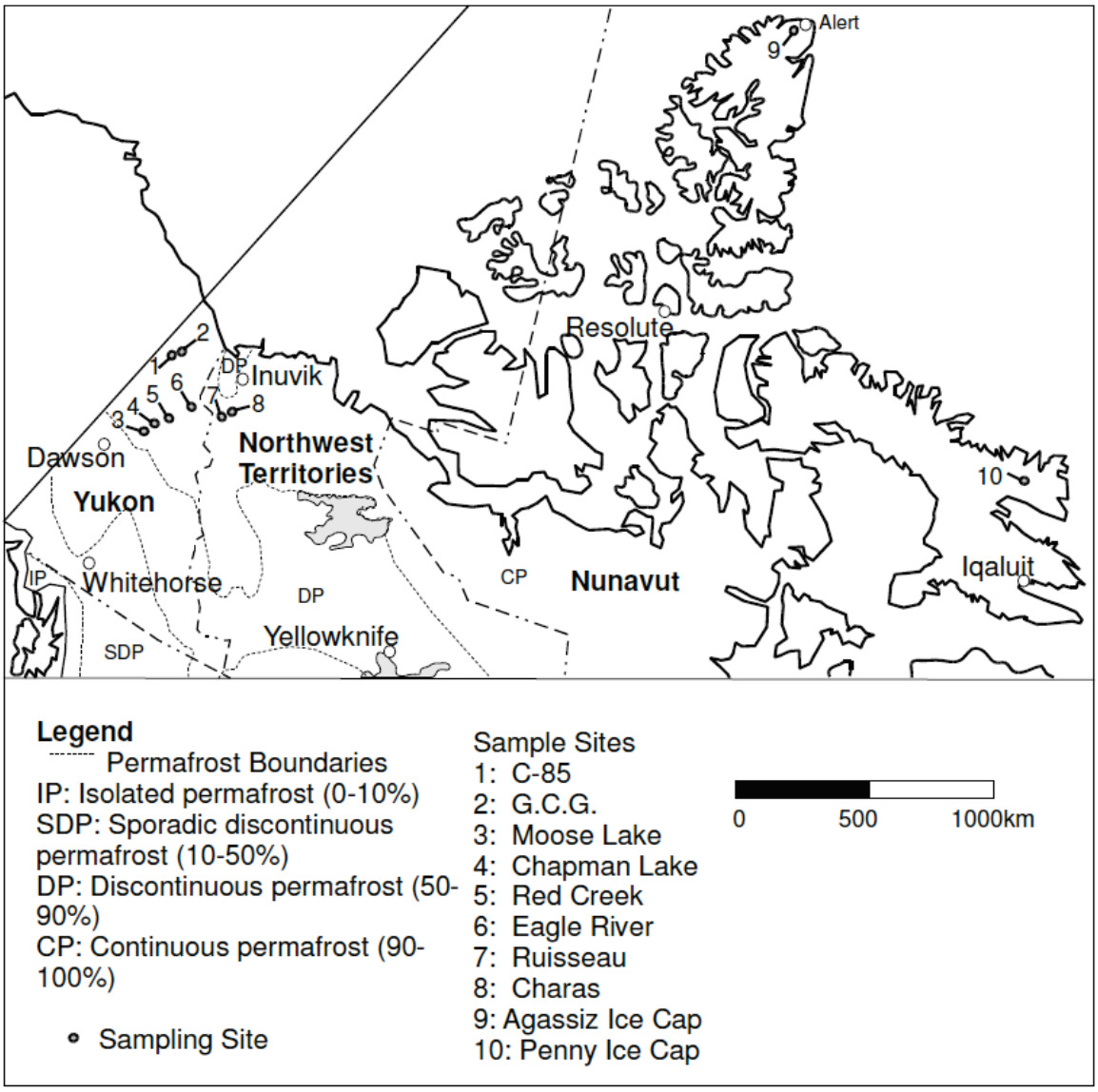

Figure 5- 1: Map of sampling sites and distribution of permafrost. (Permafrost distribution from NRCan, 2003)

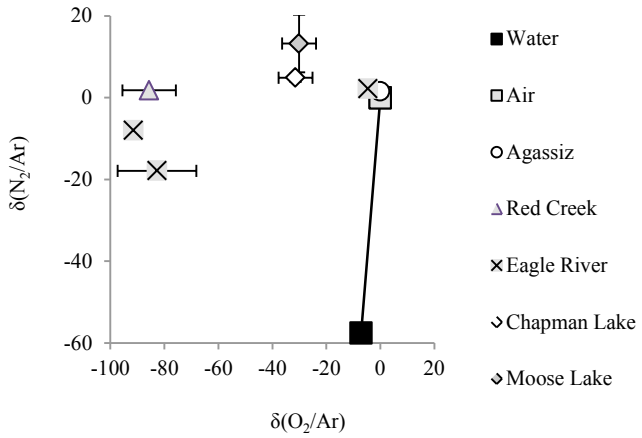

Figure 5- 2: Average values of $\delta(N_2/Ar)$ vs. $\delta(O_2/Ar)$ from previous studies. Average values ± 1 standard deviation (error bars shown when larger than symbols). Eagle River shows 3 points as 3 different blocks of ice were sampled. Values from previous publications as follows: Agassiz: Cardyn *et al.* (2007), Red Creek: Lacelle *et al.* (2009b) Eagle: Lauriol *et al.* (2010) Chapman: Lacelle *et al.* (2007), Moose Lake: St-Jean *et al.* (2011).

5.3.1 Agassiz Ice Cap, Nunavut (80.7 °N, 73.1 °W)

The 16 000 km^2 Agassiz Ice Cap is located on Ellesmere Island at an elevation of 1730 m a.s.l. The ice cap was cored in 1977 using a mechanical corer to a depth of ~186 m. The ice analyzed in this study comes from a depth of 186m, corresponding to an age of approximately 375 AD according to the age-depth scale for this site (Fisher *et al.*, 1995). During this period, there was minimal summer melting of the ice and consequently the ice sample analyzed consists of firnified ice. Cardyn *et al.* (2007) measured the O_2/Ar and N_2/Ar of ice from depths of 107 to 112 m (corresponding to the Late Pleistocene – Early Holocene transition period) and the results yielded atmospheric values. The core used in this study was from a different core used by Cardyn *et al.* (2007) resulting in a different depth-age relationships. This ice is used as a control in the noble gas study, as its origin is known and as such it is predicted that it should have gas ratios near atmospheric air.

5.3.2 Penny Ice Cap, Nunavut (67.2 °N, 65.7 °W)

Penny Ice Cap is located on Baffin Island, Nunavut. A sample of ice was retrieved at a depth of 3 m from a 20 m deep core collected in April 1995 (Fisher *et al.,* 1998). Based on ice layer counting, the sample represents precipitation from 1993 or 1994. It is estimated

that 40% of the sample corresponds to a summer melt contribution. This ice was from a melt layer and was expected to have gas ratios enriched in Xe relative to atmospheric air (Ahn *et al.*, 2009). This ice was also used as a control in the noble gas study, as the genesis of this ice is known.

5.3.3 Buried Perennial Snowbank, Red Creek, Yukon (65.157 °N, 138.370 °W)

The Red Creek site is located beyond the limit of the Reid and McConnell glacial limits and at the limit of the oldest glaciation in central Yukon (Duk-Rodkin, 1999). A tributary stream of Red Creek recently exposed a tabular body of massive ground ice over a 10 m wide and 4-6 m high section. Lacelle *et al.* (2009) measured the stable δD - $\delta^{18}O$ isotope composition of the ice (δD -224 ± 23‰; $\delta^{18}O$ -28 ± 3‰) and occluded O_2, N_2 and Ar gases ($\delta(O_2/Ar)$ = –86 ± 10%; $\delta(N_2/Ar)$ = 1.8 ± 0.5%,) and determined the ice originated as a buried snowbank. The timing of deposition of the perennial snowbank was constrained by the presence of Dawson tephra overlying the ice (dated to 25,300 ^{14}C BP) and the presence of a muck deposit inside the ice, dated to 30,720 ^{14}C BP (Lacelle *et al.* 2009). This sample was analysed for δ(Ar/Xe) and δ(Kr/Xe) to resolve the discrepancy between $\delta(O_2/Ar)$ and $\delta(N_2/Ar)$ values.

5.3.4 Intrusive Ice, Eagle River, Yukon (66.566 °N, 136.966 °W)

Massive ice is exposed at a site along the Eagle River, located within fluvial Quaternary sediments underlain by Devonian gypsiferous shale (Norris, 1985). Based on the cryostratigraphy and radiocarbon dating of buried organic material, it was found that the ice post-dates the drainage of glacial Lake Old Crow, which flooded the valley around 18 000 -15 000 ^{14}C BP (Kennedy *et al*., 2010; Lauriol *et al*., 2010). The $\delta(O_2/Ar)$ and $\delta(N_2/Ar)$ values of occluded gases in the ice yielded variable results with two blocks having values below the value of atmospheric air ($\delta O_2/Ar$: -91 ± 3%, -82 ± 15% and $\delta N_2/Ar$: -8.0±0.5%, -18 ± 3%) and one block with values close to atmospheric air ($\delta O_2/Ar$: -5 ± 1%, $\delta N_2/Ar$: 2.2±0.1%). In this study an ice sample from this site was analysed for δ(Ar/Xe) and δ(Kr/Xe) to resolve the discrepancy between $\delta(O_2/Ar)$ and $\delta(N_2/Ar)$ values which were observed in some of the samples previously analysed.

5.3.5 Wedge Ice, Moose Lake, North Fork Pass, Yukon (64.686 °N, 138.406 °W):

Moose Lake, North Fork Pass is situated in central Yukon, in a proglacial outwash plain where an ice wedge is exposed (St-Jean *et al.,* 2011). These ice wedges are found in ice-rich silt sediments which have been dated as late Holocene. St-Jean *et al.* (2011) measured the $\delta(O_2/Ar)$ and $\delta(N_2/Ar)$ composition of occluded gases in the wedge ice and obtained values of -30 ± 13% and -1 ± 1% respectively. This ice wedge was interpreted to be filled in by snow or hoar frost resulting in an atmospheric signal. However, there is a discrepancy between the $\delta(O_2/Ar)$ and $\delta(N_2/Ar)$. In this study ice from this site was analysed for δ(Ar/Xe) and δ(Kr/Xe) to resolve this discrepancy.

5.3.6 Buried Glacial Ice, Chapman Lake, Yukon (64.764 °N, 138.364 °W):

Chapman Lake is located in North Fork Pass, central Yukon. The site is located within the Reid glacial limit (dated to MIS4/6) (Westgate *et al.*, 2008; Briner *et al.,* 2005) and beyond the McConnell glacial limits (dated to MIS2) (Matthews *et al.,* 1990). At the site, a tabular body of massive ground ice was found exposed in the headwall of a thaw slump along the Dempster Highway. Previous work used stable $\delta^{18}O$- δD isotopes and occluded gases (N_2, O_2 and Ar) to determine that this ice was a remnant of glacial ice dating from the Reid glaciation (Lacelle *et al.*, 2007). In this previous research, the ice was found to have an average $\delta(N_2/Ar)$ value of -3 ± 3%, which is similar to atmospheric composition; the average $\delta(O_2/Ar)$ ratio of the ice was -25 ± 4%, which is lower than atmospheric composition. In this study, ice from this site was analysed for δ(Ar/Xe) and δ(Kr/Xe) to resolve this discrepancy.

5.3.7 Unknown Ice Type, Ruisseau, NWT (67.129 °N, 135.929 °W):

This site is located in the Richardson Mountains and is underlain by Cretaceous bedrock from the Arctic Red Formation composed of shale and siltstone (Norris, 1974). This site is located at the maximum westward limit of the Laurentide ice sheet (Duk-Rodkin and Hughes, 1992). At this location, ground ice is melting, creating a thaw slump. Ice is covered by 1-2 m of till at the surface. Replicate analysis showed that ice had a δ^2H of -226.2 ± 3.1 ‰ and $\delta^{18}O$ -28.7 ± 0.1 ‰. Bubbles in the ice contain abundant

calcium carbonate concretions (~5mg/L) of unknown origin. These concretions return a ^{14}C age of 29 090+/-200 BP, but this age is outside the calibration range and should likely be divided by two, as approximately half the carbon is estimated to be from dead carbon sources. No previous studies have investigated the origin of this ice and the objective of the analysis of this ice is to constrain its origin.

5.3.8 Unknown Ice Type, Charas, NWT (67.255 °N, 135.230 °W):

This site is located in the foothills east of the Richardson Mountains close to Fort McPherson. The area is underlain by Cretaceous bedrock from the Arctic Red Formation composed of shale and siltstone (Norris, 1974). The site was glaciated by the Laurentide ice sheet and the ice body is located within glacial till deposits. About 5 km to the west of the site is a glacial standstill limit (Duk-Rodkin and Hughes, 1992). At this location, ground ice is melting forming a giant thaw slump. In till overlying the ice, organic material was dated using radiocarbon providing an age of 9560 ±50 yr. B.P. (Beta: 263 919), which correlates to the timing of regional deglaciation (Rampton, 1982). This ice has a δD of -244 ± 2 ‰ and $\delta^{18}O$ -30.7 ± 0.2 ‰. No previous studies have analysed the origin of this ice. The objective of analysis of this sample was to determine its origin.

5.3.9 Ice Plugs, Grande Caverne Glacée (GCG) (66.698 °N, 139.314 °W) and Caverne 85 (C-85), Yukon (66.723 °N, 139.278 °W):

Grande Caverne Glacée (G.C.G.) and Caverne-85 (C-85) are located in Tsi-it-toh-Choh Mountain, in the northern Nahoni Range extension of the Ogilvie Mountains. The mountain is composed of Cambrian to Devonian limestone. These caves developed during the Tertiary when the climate was warmer, and were exposed by mechanical erosion during the Pleistocene (Lauriol *et al.,* 1997). This site was not glaciated during the last glaciations (Hughes, 1972). The entrance to G.C.G. is at the top of a scree slope below the face of a north-facing cliff. The main passage is about 4 m wide and 3 m tall and meanders to the southwest. The cave floor is covered by up to 50 cm of ice formed by freezing dripwater from melting frost on the roof during inflow of warm summer air. Ninety metres into the cave passage the cave is blocked by an ice plug. A sample was

collected in August 2009 from near the base of that plug (Figure 5- 3). This ice has a δD of -138 ± 4 ‰ and $\delta^{18}O$ -18.6 ± 0.1 ‰. The plug is interpreted to be from a massive accumulation of hoar frost crystals on the cave walls, which over time turned to solid ice (Lauriol *et al.,* 1988).

The entrance to C-85 is located in a cliff face on a north-facing slope 3.2 km north of G.C.G. A rock passage about 2 m wide and 4 m high was followed about 40 m into the cave to a point where ice fills the cave from floor to ceiling. Here an ice sample was taken in August 2009 at a height of about 1 m (Figure 5- 3). This ice has a $\delta^{2}H$ of -149.6 ± 0.7 ‰ and $\delta^{18}O$ -20.3 ± 0.1‰. The ice has been interpreted to be stratified ice, which includes layers of summer melt frozen over winter ice accumulations (Lauriol *et al.,* 1988).

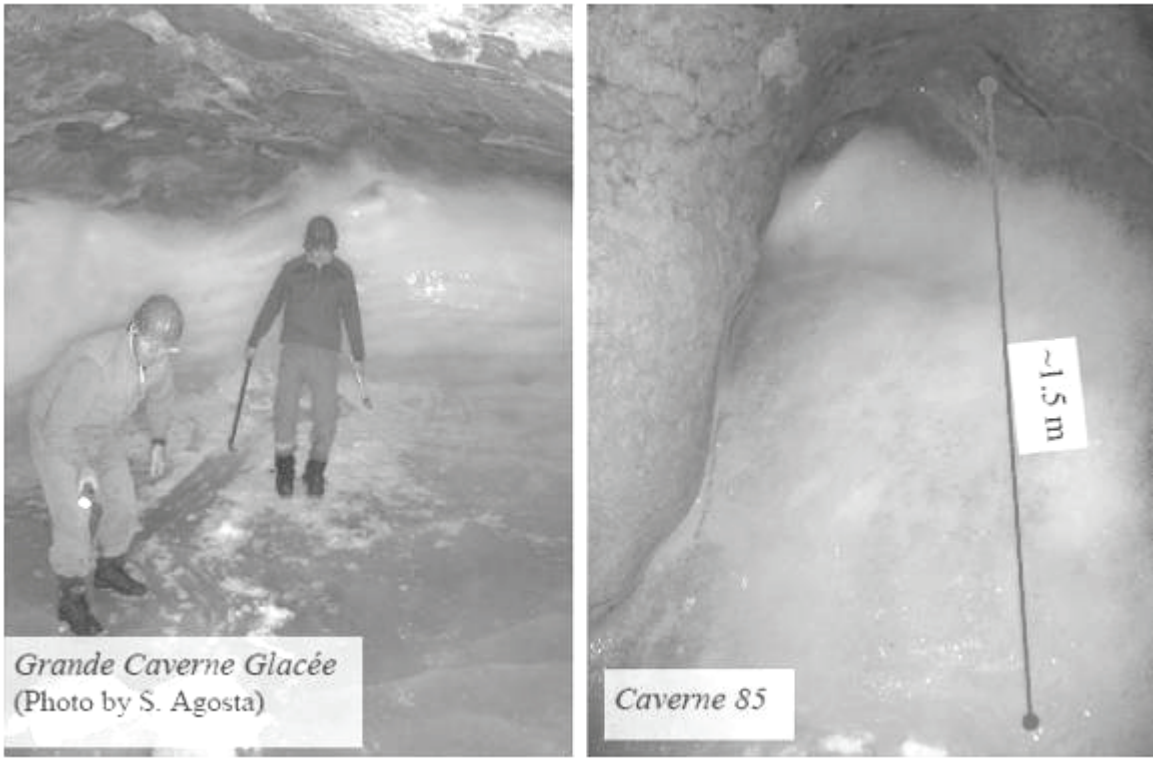

Figure 5- 3: Photos of GCG (Photo by S. Agosta) and C-85. In GCG sample was collected at base of back wall behind individual on right. In C-85 sample was taken at base of photo.

The objective of the analysis of samples from both caves was to confirm or refute the methods of ice formation proposed by Lauriol *et al.* (1988).

5.4 **Methods**

5.4.1 Sample Collection and Preparation

Ground ice was sampled in caves and at retrogressive thaw slumps. Glacier ice was obtained from the Geological Survey of Canada collection of ice cores. In the field, samples were collected from areas of the ice body where the ice appears to be most continuous. At each site a cube of ice roughly 30 cm on each side was cut out using a hammer and chisel or a chain saw. Samples were kept frozen in coolers, shipped to Ottawa and stored at -15 °C. To minimize surface contamination, samples were cut a few days before analysis with a band saw in a cold room at the Geological Survey of Canada Snow and Ice Core laboratory. The outer 5 - 10 cm of ice was removed from samples and individual ice samples were trimmed to ~ 2.5 cm x. 2.5 cm x 10 cm rectangular blocks, providing 50 to 70 g of ice. To reduce exposure to the atmosphere, samples were wrapped in aluminium foil and plastic wrap that was removed just before gas extraction and analysis. In this study, fresh ice samples were collected in August 2009 from G.C.G., C-85, Charas and Ruisseau, whereas all other samples were from previous sampling campaigns which were collected and treated in the same manner.

5.4.2 Noble Gases Measurement

The extraction of occluded gases was based partly on the method of Severinghaus *et al.* (2003) whereas the gas analysis technique was performed using a quadrupole mass spectrometer on an isotope dilution noble gas line based on the design of Poole *et al.* (1997). The method used in this study is explained in brief below and in more detail in Appendix A.

The noble gas spike contains the rare isotopes ^{3}He, ^{22}Ne, ^{36}Ar, ^{78}Kr and ^{136}Xe, however in this study only Ar, Kr and Xe were of interest. The volume of gas in the spike is determined by air standard analysis. During an air standard, the spike is mixed with a known volume of atmospheric air. As the volume of atmospheric air is known the volume of the spike can be calculated from this analysis. The error on air standard analysis was 6% for Ar, 8% for Kr, 11% for Xe, 6% for δ(Ar/Xe) and 5% δ(Kr/Xe). The error on gas ratios

is lower than the error on volumes because the volume is the main source of error and this cancels when determining the ratios. The volume of gas in the spike and in air is listed in Table 5- 2 based on the composition of the spike at the start of sample measurements. The volume of the spike progressively decreases and was determined by regression of values over multiple analysis (More details in Appendix B). During sample analysis the volume of the spike is known from the standards and used to determine the volume of sample.

Table 5- 2: Isotopic composition of spike, volume of spike at start of sample measurements, air standard volume and associated measured ratio.

Noble Gas	Composition of Spike		Volume of spike (cc)	Volume of air standard (cc)	Measured Ratio	
	Isotope	Fraction				
Argon	^{36}Ar	0.997	1.44×10^{-4}	1.45×10^{-5}	$^{36}Ar/^{40}Ar$	0.036
	^{40}Ar	0	0	4.28×10^{-3}		
Krypton	^{78}Kr	0.689	3.15×10^{-6}	1.88×10^{-9}	$^{78}Kr/^{84}Kr$	9.47
	^{84}Kr	0.006	2.74×10^{-8}	3.05×10^{-7}		
Xenon	^{132}Xe	0	0	1.09×10^{-8}	$^{132}Xe/^{136}Xe$	2.77
	^{136}Xe	1	2.66×10^{-8}	3.60×10^{-9}		

Samples were placed in glass vessels that were kept between -20 ˚C and -30 ˚C using an ethanol bath. The sample was evacuated for 30 min to allow the sublimation of outer surface contamination. Due to sublimation, the pressure during this process is ~5 Torr. After sublimation, the pump was closed and an aliquot of spike was introduced. The sample was then melted by submerging the glass vessel in water. To reduce vapour pressure and induce further degassing, the sample was refrozen with the ethanol bath. Once vapour pressure was reduced, the gas was expanded to the entire line and was closed to the extraction vessel. Full gas recovery is not necessary after the spike has been mixed with the sample. After the line was isolated from the extraction vessel, gas was exposed to a hot titanium getter at 600˚C. At this point an aliquot of gas was taken and let into the SRS RGA200 quadrupole mass spectrometer for analysis of argon on the Faraday collector. Krypton and xenon were then trapped on charcoal cooled to -78 ˚C. The line was then evacuated and krypton and xenon are desorbed by heating to 150 ˚C. The gas was then let in to the mass spectrometer and krypton and xenon were analysed on the multiplier collector.

5.5 **Results**

5.5.1 Noble Gas

All analysed samples of ice contained air trapped in bubbles that ranged in size from < 1 to ~5 mm. The morphology of the bubbles in each sample was variable, from rounded to elliptical. Gas concentrations found in the analysed ice were variable with Ar ranging from 0.9 to 5.0 x 10^{-4} cc_{stp}/g_{ice}, Kr from 1.2 to 4.9 x 10^{-8} cc_{stp}/g_{ice} and Xe from 0.6 to 4.2 x 10^{-9} cc_{stp}/g_{ice} (concentrations listed in Table 5- 3). For each sample, the values from each individual replicate are reported along with the average of the replicates and one standard deviation of this measurement. This was done to account for instrumental error, extraction error and variability within the sample. Ice from Agassiz Ice Cap has some of the highest gas concentrations while Chapman Lake ice generally has the lowest gas concentrations. If gas concentrations were diagnostic of origin it would be expected that these ice bodies would have similar concentrations as both are from known or suspected glacial ice.

In response to variability in gas concentrations, the values of δ(Ar/Xe) and δ(Kr/Xe) were used to determine the origin of ice bodies. The results of δ(Ar/Xe) and δ(Kr/Xe) are listed in Table 5- 3. For each sample, two or more replicates were analysed. From these replicates the average and the standard deviation are calculated accordingly, as such the standard deviation is variable for each sample. Eagle River ice has a standard deviation of less than 3% for δ(Ar/Xe) and δ(Kr/Xe), while Chapman Lake ice has an standard deviation of 35 % for δ(Ar/Xe). Six samples have standard deviations over 10% for δ(Ar/Xe) and three greater than 10% for δ(Kr/Xe). This difference is attributed to greater mobility of Ar in ice relative to Kr. During the initial sublimation and pumping phase of analysis, Ar may be lost preferentially. It is likely during the sublimation and pumping phase that heterogeneities in the ice may affect gas loss. For example the ice from Chapman Lake has δ(Ar/Xe) values of 49.8% and 98.7%. The Chapman Lake ice most likely had many small fractures in it as when melting of the sample started it was noted that the sample quickly fractured into several pieces. This also occurred with C-85 ice. The process occurred with some other samples, however incomplete notes were taken of this occurrence as it was not initially anticipated to be important. Despite these errors results are still within the necessary range for interpretation purposes.

Table 5- 3 : Concentrations of Ar, Kr, Xe in cc_{stp}/g_{ice} and gas ratios in δ notation. In bold are averages of sample replicates and the standard deviation of the mean.

	Sample Runs	Ar ($x10^{-4}$) (cc_{spt}/g)	Kr ($x10^{-8}$) (cc_{spt}/g)	Xe ($x10^{-9}$) (cc_{spt}/g)	δ(Ar/Xe) %	δ(Kr/Xe) %
Charas		3.2	4.6	3.2	-6.7	9.8
		4.2	4.8	3.5	9.3	4.3
		4.4	5.1	3.4	21.3	14.4
Average	**3**	**3.9**	**4.9**	**3.3**	**8**	**10**
Standard Deviation		**0.6**	**0.3**	**0.2**	**14**	**5**
Ruisseau		5.0	8.0	6.1	-29.5	-1.5
		1.4	1.7	1.5	-21.5	-14.7
Average	**2**	**3**	**5**	**4**	**-25**	**-8**
Standard Deviation		**2**	**4**	**3**	**6**	**9**
Red Creek		2.1	2.3	1.5	20.8	11.8
		2.2	2.7	1.8	2.5	10.2
Average	**2**	**2.0**	**2.5**	**1.7**	**12**	**11**
Standard Deviation		**0.03**	**0.3**	**0.2**	**13**	**1**
Eagle River		2.5	4.0	4.3	-51.0	-30.2
		2.5	4.0	4.2	-48.6	-26.8
Average	**2**	**2.3**	**4.0**	**4.2**	**-50**	**-29**
Standard Deviation		**0.01**	**0.02**	**0.1**	**2**	**2**
C-85		1.1	1.7	1.5	-34.9	-18.3
		1.1	2.1	2.1	-53.7	-25.0
		0.9	1.7	1.6	-49.3	-18.9
Average	**4**	**1.0**	**2.2**	**1.7**	**-46**	**-21**
Standard Deviation		**0.1**	**0.8**	**0.3**	**10**	**4**
Chapman Lake		1.3	1.3	0.8	49.8	31.1
		1.1	1.1	0.5	98.7	61.1
Average	**2**	**1.2**	**1.2**	**0.6**	**74**	**46**
Standard Deviation		**0.1**	**0.2**	**0.2**	**35**	**21**
GCG		1.7	2.3	2.0	-28.0	-16.2
		1.0	1.5	1.2	-31.8	-6.8
Average	**2**	**1.3**	**1.9**	**1.6**	**-30**	**-12**
Standard Deviation		**0.5**	**0.5**	**0.6**	**3**	**7**
Moose Lake		1.5	2.0	1.5	-15.3	-1.9
		1.6	2.0	1.3	9.8	20.5
Average	**2**	**1.5**	**2.0**	**1.4**	**-3**	**9**
Standard Deviation		**0.1**	**0.05**	**0.2**	**18**	**16**
Agassiz Ice		3.3	4.9	3.1	-8.7	18.6
		3.5	5.1	2.8	6.2	36.3
Average	**2**	**3.2**	**5.0**	**3.0**	**-1**	**27**
Standard Deviation		**0.2**	**0.2**	**0.2**	**11**	**13**
Penny Ice		0.9	1.4	1.4	-42.6	-23.8
		1.1	1.4	1.2	-22.8	-10.5
Average	**2**	**0.9**	**1.4**	**1.3**	**-33**	**-17**
Standard Deviation		**0.1**	**0.0**	**0.1**	**14**	**9**

Figure 5- 4 shows the δ (Kr/Xe) and δ (Ar/Xe) values of the various ice types. The Red Creek buried snowbank, Moose Lake wedge ice, Agassiz glacial ice and Charas stratified ice (unknown ice type) all have δ(Ar/Xe) and δ(Kr/Xe) ratios close to the atmospheric value. The GCG and C-85 ice plugs, Eagle River intrusive ice, Penny glacial ice and Ruisseau (unknown ice type) have δ(Ar/Xe) and δ(Kr/Xe) ratios that fall mid-way between the air equilibrated water at 0 ºC and atmospheric ratios. The Chapman Lake buried glacial ice has higher gas ratios than the other sites with δ(Kr/Xe) of 46 ± 22 and δ(Ar/Xe) of 74 ± 35 above the atmospheric value.

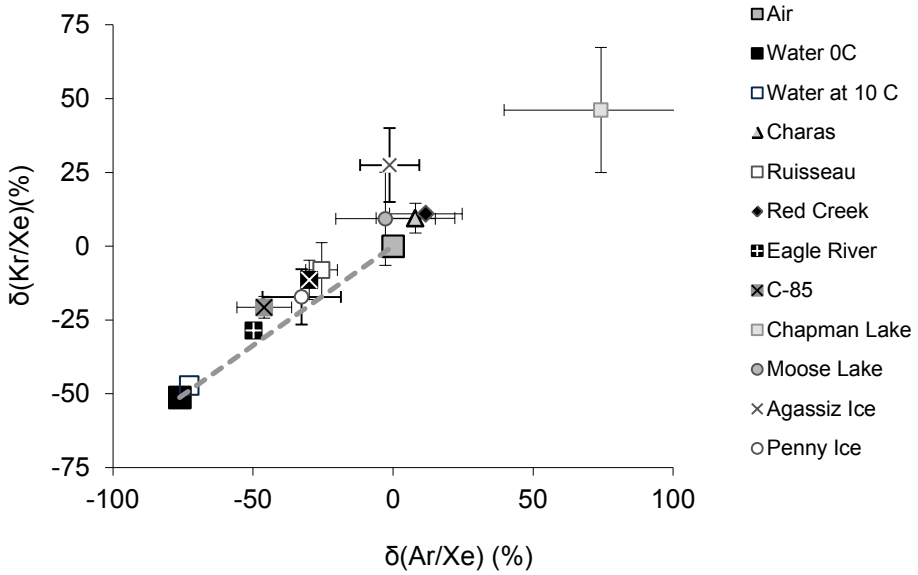

Figure 5- 4: δ(Kr/Xe) vs. δ(Ar/Xe) for ice samples. The large black square represents the gas ratio of air equilibrated water at 0 ºC, while the hollow white square represents air equilibrated water at 10 ºC, and the large grey square is the atmospheric ratio; these two squares are connected by a dotted mixing line.

5.6 **Discussion**

5.6.1 Agassiz and Penny Ice Cap

Ice from Agassiz and Penny Ice Caps was measured because the formation of these ice bodies is well understood and should give predictable values. Firnified glacier ice from Agassiz Ice Cap was expected to yield gas ratios similar to atmospheric air. The δ(Ar/Xe) of Agassiz Ice was -1 ± 11 %, which is the same as atmospheric air, however the δ(Kr/Xe) was 28 ± 13 %, which is enriched relative to atmospheric air. The cause of this deviation is unknown.

Ice from a melt layer in Penny Ice Cap was measured. The δ(Ar/Xe) of this ice was -33 ± 14 % and the δ(Kr/Xe) was -17 ± 9 %. These values fall between the values for atmospheric air and air equilibrated water. Melt layers are expected to have gas ratios showing an enrichment trend of Xe > Kr > Ar, due to the greater solubility of the heavier gases in water. This is consistent with other studies that have measured these ratios in melt layers (Headly *et al.*, 2005; Ahn *et al.*, 2009).

5.6.2 Previously Studied Ground Ice: Red Creek, Eagle River, Moose Lake and Chapman Lake

Ground ice along Red Creek was previously interpreted to be a buried snowbank and had $\delta(N_2/Ar)$ near atmospheric air, however the $\delta(O_2/Ar)$ was depleted (Lacelle *et al.,* 2009). In this study, it was found that δ(Ar/Xe) was 12 ± 13 % and δ(Kr/Xe) was 11 ± 1 %. These values confirm that dissolved gases are most likely of atmospheric origin and that O_2 may have been consumed by bacteria in the ice matrix as suggested by Radtke *et al.* (2010).

Along the Eagle River, there is ground ice exposed which was previously studied using $\delta(N_2/Ar)$, $\delta(O_2/Ar)$ and stable isotopes (Lauriol *et al.,* 2010). Based on those analyses the ice was interpreted to originate from frozen groundwater with excess air, resulting in a mixed air equilibrated water / atmospheric air signal. In this study the δ(Ar/Xe) of ice was -50 ± 2% and the δ(Kr/Xe) of ice was -29 ± 2%. These results suggest that the ice formed from the freezing of liquid water with potential entraining of excess air during groundwater recharge. This is consistent with the previous interpretation of this ice body by Lauriol *et al.* (2010).

The Moose Lake ice wedge, previously studied was found to have $\delta(N_2/Ar)$ near atmospheric air, however it also had a depleted $\delta(O_2/Ar)$ signal (St. Jean *et al.,* 2011). In this study, it was found that the ice has a δ(Ar/Xe) of -3 ± 18% and a δ(Kr/Xe) of 9 ± 16%. These atmospheric gas ratios are consistent with infilling of this ice wedge with snow or hoar frost, as suggested by St. Jean *et al.* (2011).

Chapman Lake was previously studied and found to have $\delta(N_2/Ar)$ near atmospheric air values and depleted values of $\delta(O_2/Ar)$ (Lacelle *et al.,* 2007). The previous work

concluded that this ice body was buried glacier ice from the Reid glaciation. In this study, it was found that the ice contained a δ(Ar/Xe) of 74 ± 35 % and a δ(Kr/Xe) was 46 ± 21 %. It was expected that this ice would have noble gas ratios similar to atmospheric air like the ice from Agassiz Ice Cap; however Chapman Lake ice was found to be more enriched than expected in both Ar and Kr relative to Xe. The cause of this enrichment is unknown. It is possible that this enrichment is due to physical changes in the ice; however this ice had the lowest gas concentrations and high error. While there was no reason to discard this sample completely, limited conclusions about ice origin can be made based on these results.

5.6.3 Unknown Ground Ice Bodies: Ruisseau and Charas

The ice at Ruisseau was found to have a δ(Ar/Xe) value of -25 ± 6 % and a δ(Kr/Xe) value of -8 ± 9. These values are between air equilibrated water and atmospheric air, but are much closer to those of atmospheric air. This ice is proposed to be from accumulations of snow or hoar frost which has been altered by some melting.

Ice from Charas was found to have a δ(Kr/Xe) value of 8 ± 14 % and a δ(Ar/Xe) value of 10 ± 5%, both of which are close to atmospheric air. Field observations show that this ice is encased in till, which was dated near the time of deglaciation (9560 ±50 yr. B.P.). Based on the noble gas ratios and the stratigraphic position, this ice is most likely a remnant of the Laurentide Ice Sheet.

5.6.4 Ice Plugs: Grande Caverne Glacée and Caverne 85

Ice from CGC had a δ(Ar/Xe) value of -30 ± 3 % and a δ(Kr/Xe) value of -12 ± 7 %. These gas ratios fall between atmospheric air and air equilibrated water. Lauriol *et al.* (1988) propose that this ice is from the accumulation of hoar frost on cave walls which partially melted in summer and slowly accumulated. This proposed mechanism is consistent with the gas ratios measured in this study.

Ice from C-85 had a δ(Ar/Xe) value of -46 ± 10 % and a δ(Kr/Xe) value of -21 ± 4 %. Like CGC these values fall between those of atmospheric air and air equilibrated water. Lauriol *et al.* (1988) interpreted this ice formation to be stratified ice, which includes

layers of summer melt, frozen over winter ice accumulations. In winter, hoar frost may accumulate. In summer there would be some melting of the hoar frost, which would result in a mixed gas ratio.

5.6.5 Effects of Ice on Gas Composition of Recharging Groundwater

In this chapter, noble gases in ground ice have been used to determine the origin of ground ice bodies. In the previous two chapters noble gases have been used to determine groundwater recharge temperature and groundwater age, which raises the question of whether the formation and melting of ground ice in permafrost terrain affect noble gas concentrations in associated groundwaters. As presented in this chapter, noble gas ratios are related to formation of ice. As such, the melting of a ground ice body could introduce water with different gas compositions to groundwater. As discussed in Chapter 3 and 4, groundwater recharge in permafrost terrain often occurs on hilltops where fractured bedrock is exposed. C-85 and G.C.G. are examples of caves in permafrost karst, with associated groundwater flow systems such as found near Bear Cave Mountain and Fishing Branch River. The results of this study show that noble gas ratios in these cave-ice formations are the result of thawing and refreezing of hoar ice. In the event that the melting of such waters contributed to groundwater recharge, then this would confound the use of noble gases as a record of recharge temperature. In other cases some ground ice bodies (e.g. Eagle River) are interpreted to be frozen groundwater, with excess air, which, if incorporated into groundwater flow, would be corrected for by the neon excess air calculations. In any case, the contributions of melting ground ice are unlikely to be volumetrically significant to adversely affect the use of noble gases in tracing groundwater recharge temperatures for permafrost catchments.

5.7 **Conclusion**

Ground ice in permafrost terrain may originate from a number of formational scenarios from burial of firnified (glacial) ice to segregation ice. The occluded gases in each generally fall on a line between origins as incorporated air during occlusion or exsolution of dissolved gas during freezing of water. This work shows that the contrasting

solubilities of Kr and Xe can be used to distinguish between an origin as buried air or freezing-exsolution. The method involves measuring the ratios of Kr/Ar and Xe/Ar, and was tested using a firnified layer of ice from the Agassiz Ice Cap and a melt layer from the Penny Ice Cap. As expected firnified Agassiz Ice Cap ice has gas ratios near atmospheric air and the melt layer from Penny Ice Cap was enriched in Xe due to partial melting of the ice. Ground ice samples from Red Creek and Moose Lake all had gas ratios near atmospheric air, which supports an origin from buried snow or hoar frost of these ice bodies. Eagle River ice was found to have gas ratios midway between atmospheric air and air equilibrated water, which is consistent with it having an origin as groundwater. Chapman Lake has gas ratios for both δ(Kr/Xe) and δ(Ar/Xe) greater than atmospheric air, which may be the result of experimental error. Samples were analysed from two unknown sites, where Charas was found to be buried glacier ice and Ruisseau was interpreted to be buried snow which has undergone melting. Ice from two caves was analysed and found to have gas ratios between atmospheric air and air equilibrated water, which was consistent with modes of formation previously proposed. Noble gases are non-reactive, and only affected by physical processes, and so are diagnostic of cryogenic origins of ground ice features. This adds a complementary tool to the measurement of reactive gas ratios (CO_2, O_2 and N_2) which can be useful as tracers of biogeochemical processes involved in the generation of ground ice formations.

Chapter 6: Conclusions

6.1 Research Synthesis and Context

6.1.1 Introduction

In Yukon and Northwest Territories, there are numerous creeks and rivers that are groundwater fed. These watercourses are located in a region underlain by permafrost where there are also ground ice bodies. This thesis examines the nature of groundwater recharge, flow and amounts of groundwater discharge to rivers and creeks as well as the origin of ground ice formations. Climate change and resource development may impact aquifers in permafrost terrain; this may have implications on permafrost degradation, contaminant migration and water supply (Dyke, 2001; Frey *et al.,* 2007; Muskett and Romanovsky, 2009). It is therefore timely to study the flow of groundwater in permafrost.

6.1.2 Permafrost Hydrogeology

Woo *et al.* (2000), Woo and Marsh (2005) and Woo *et al.* (2008) outline the limited research on groundwater in permafrost terrain. For example in Woo *et al.* (2008) eight groundwater articles are cited. These articles focus on three geographic areas, two of which are probably unusual groundwater flow regimes (e.g. thermal springs and non-thermal saline springs). This thesis has presented unique findings in the study of permafrost hydrogeology and links the features of frozen ground to non-frozen hydraulic processes. This research studied both thermal and non-thermal groundwaters, the non-thermal waters likely more representative of most permafrost groundwater flow systems.

Figure 6- 1 presents a schematic diagram of groundwater and ground ice in permafrost terrain of Yukon and NWT to synthesize the findings of the three case study chapters and previous research. The characteristics of different components of permafrost hydrology are noted on the diagram. This work has shown that groundwaters are generally at thermal equilibrium with the bedrock. Stable isotope data show that recharge may occur on hills and mountains where there is often a thin layer of organic-rich soil. During recharge, water passes through this soil where it dissolves soil CO_2. This water subsequently weathers marine carbonates. The non-thermal groundwaters studied had

groundwater residence times of up to 30 yrs. Thermal groundwaters are presumed to be older based on the abundant crustal helium and in one case very low tritium suggesting a sub-modern age. The noble gas recharge temperature method was used to find the recharge temperatures of groundwater. Thermal groundwater has evidently been warmed, while the non-thermal waters appear to remain at or slightly above the water temperature at recharge. This suggests that groundwater recharge is not degrading permafrost.

Groundwater discharge along the studied rivers has long been known and studied (e.g. Hume, 1954; Mutch and McCart, 1974; Clark *et al.,* 2001). These discharge areas are evidenced by the presence of open water in winter, which exists because there is considerable groundwater discharge, which means the water does not freeze immediately. This research has used geochemistry of springs and surface waters for evidence of groundwater discharge and its fractional contribution to river flow in winter. The discharge of groundwater into rivers provides a source of solutes to rivers, especially in the case of thermal waters which contribute high TDS water. The studied groundwaters are generally near calcite saturation and degassing at the surface renders surface waters super-saturated in calcite. The non-thermal groundwater springs studied appear to be more common as previous researchers have documented other known groundwater systems like these in the Mackenzie Valley and northern Yukon. Some of these other non-thermal groundwater systems have been previously described (e.g. van Everdingen, 1981; Michel, 1986; Clark and Lauriol, 1997). These types of perennial groundwaters will likely be found to some degree in many other places in the Mackenzie Valley and northern Yukon where the appropriate geologic conditions exist. If the climate warms, groundwater systems in permafrost terrain are likely to expand (Bense *et al.,* 2009).

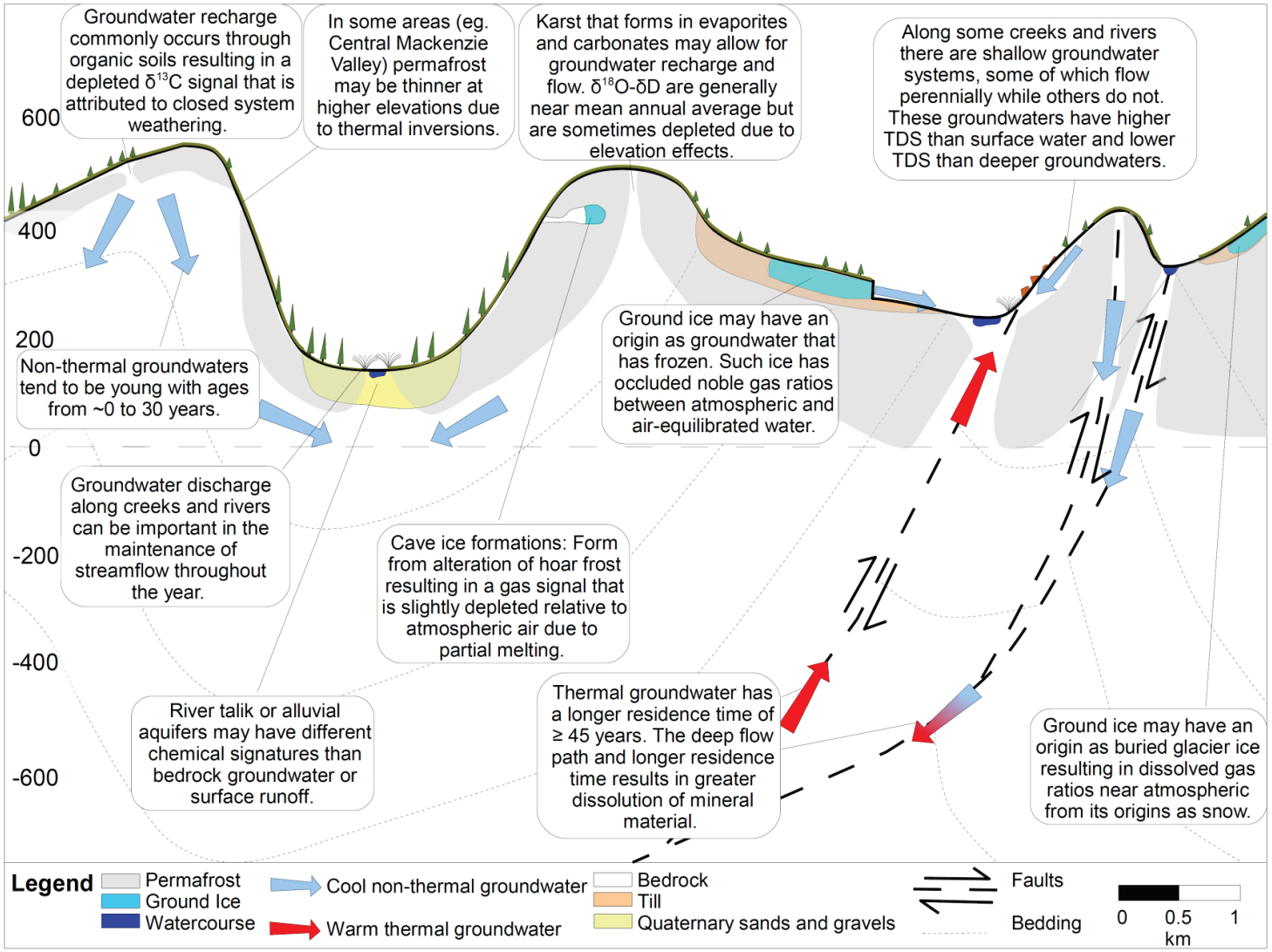

Figure 6- 1: Schematic diagram to depict groundwater and ground ice in a permafrost environment of Yukon and NWT, Canada. Horizontal and vertical scales are approximate.

6.1.3 Noble Gas Methods in Permafrost Research

Noble gas methods have been applied in this work to advance the understanding of groundwater and ground ice in permafrost terrain. Noble gas concentrations are only affected by physical processes; as such they are useful tracers for the study of recharge and circulation in permafrost terrain. This thesis has applied noble gas methods to the determination of groundwater age, groundwater recharge temperatures and the origin of ground ice in permafrost terrain.

The ^{3}H-^{3}He dating method was used to determine groundwater residence times. This method was applied with apparent success to non-thermal groundwaters which have relatively shallow flowpaths. Thermal groundwaters have high concentrations of crustal helium, which limit the usefulness of ^{3}H-^{3}He dating. Little Fish Creek thermal groundwater is the warmest sampled and has the highest concentration of crustal helium. Smith Creek is the second warmest and also has high crustal helium. The calculated ages of samples with higher ^{4}He have greater uncertainty because the local value of $^{3}He/^{4}He$ for crustal helium is poorly constrained. The value of $^{3}He/^{4}He$ can be determined from groundwaters that recharged prior to atmospheric testing of nuclear weapons and have a deep flow path. Groundwater from Smith Creek had very low tritium concentrations and it is therefore believed to meet these criteria. Its measured $^{3}He/^{4}He$ ratio of $3.01 \pm 0.14 \times 10^{-8}$, is close to the average crustal value ($\sim 2.0 \times 10^{-8}$) (Kipfer *et al.,* 2002). This value of crustal helium is likely applicable to other areas along the east side of the Mackenzie River with similar local geology.

Noble gas concentrations have been used to determine groundwater recharge temperatures. Most of the groundwaters sampled have recharge temperatures between 0 and 5 °C. In this work, it was considered that melting and refreezing of ground ice along the groundwater flow path could distort the noble gas signature. This possibility prompted the investigation of noble gas ratios in ground ice bodies. The result of this investigation is a novel method for the determination of the origin of ground ice bodies. The dissolved noble gas ratios in ground ice bodies were found to be related to the formation of the given ground ice body. Most samples had gas ratios between the expected mixing of air

equilibrated water and atmospheric air. Some ground ice bodies do form from the freezing of groundwater; however in this study the noble gas concentrations do not suggest that groundwaters were systematically altered by freezing processes. It was anticipated that groundwaters might have high excess air due to incorporation from melting ice or snow. Although some samples did have high excess air, a systematic incorporation of excess air was not observed. The sampled groundwaters generally had discharge temperatures > 0.5 °C, with many of the groundwater temperatures near 4 °C; hence the water in these systems that is above 0 °C has likely not been affected by freezing processes. The freeze-thaw action that occurs in the active layer could result in an altered gas composition; however this was not investigated in this study.

6.1.4 $\delta^{13}C_{DIC}$ in the Study of Permafrost Groundwaters

$\delta^{13}C_{DIC}$ can be used to study groundwater recharge conditions. During recharge, groundwater may dissolve CO_2 from the soil. This CO_2 makes the water more acidic and allows for increased weathering of mineral material. The resulting values of $\delta^{13}C_{DIC}$ reflect the type of soil through which recharge occurs (e.g. organic rich soil vs. mineral soil), the $\delta^{13}C$ of the rock material, and whether there is a continual supply of CO_2 during weathering (open vs. closed system). This research has shown that these methods can be applied to permafrost groundwaters in a similar way to which they are applied to groundwaters in temperate regions. This is a novel tool that helps in determining where groundwater recharge occurs.

6.2 **Summary of Findings**

The findings of this thesis respond to three objectives outlined in 1.4 Objectives: 1) isolate major ion contributions to Arctic creeks and rivers and to determine amounts of groundwater discharge; 2) determine recharge conditions and groundwater ages; and 3) determine the origin of ground ice bodies in permafrost using noble gas techniques. These objectives address the identified need to better characterize the groundwater component of permafrost hydrology, with relevance to changes in hydrology associated with changing climate and development in the north.

1) In Chapters 3 and 4, the chemistry of groundwaters and surface waters was characterized and used to determine relative contributions of groundwater discharge to surface water.

- The sampling of groundwater and surface water shows that groundwater has higher TDS than local surface water. Furthermore groundwaters can be divided into two groups. Non-thermal groundwaters are cooler than 5 °C and have lower TDS (less than 1000 ppm) whereas thermal springs have temperatures higher than 5 °C and higher TDS (greater than 1000 ppm) due to a deeper flowpath. Groundwater chemistry is variable with samples falling into three general facies Ca^{2+}-HCO_3^{2-}, Ca^{2+}-SO_4^{2-} and Na^{+}-Cl^{-}. These facies are related to the dissolution of calcite, gypsum and halite respectively. In general, these groundwaters are close to calcite saturation with saturation indices ranging from -0.136 to 0.366. These minerals are part of the dominant bedrock geology in the studied catchments and dissolution of these minerals has formed much of the aquifer porosity. Calcite is abundant in the watershed. Gypsum is present in the Bear Rock Formation and there is halite in the Saline River Formation.
- This work adds to previous geochemical research on these springs (Michel, 1977; 1986) by linking spring water geochemistry with that of the watershed discharge as a first attempt for hydrograph separation.
- The geochemical characterization of groundwater and surface water has been used to estimate groundwater contributions along five rivers in Yukon and NWT (Fishing Branch River, Little Fish Creek, Smith Creek, White Sand Creek and Canyon Creek). While these are punctual measurements, these results show that with continually-monitored discharges, this approach can be used to quantify the relative contributions of groundwater to discharge from permafrost watersheds on a seasonal to inter-annual basis. Such calculations, correlated with prevailing meteorological conditions, will provide insights to permafrost stability and evolution in the context of changing climates.

2) In Chapters 3 and 4, stable isotope and noble gas methods are developed that bring new insights to recharge conditions and groundwater circulation rates. These methods are novel in the field of permafrost hydrogeology, and together with the geochemical methods for hydrograph separation, provide new approaches to understanding the groundwater component of the hydrological cycle in permafrost catchments. Again, in view of changing climatic conditions, understanding this component is relevant to northern issues of water resources, freshwater fisheries and contaminant migration. A review of these methods is summarized in the following points.

    - $\delta^{18}O$- δD can be used to determine the sources of groundwater recharge throughout the year (e.g. snow melt vs. summer precipitation) and constrain the elevation of recharge. As examples, groundwater from the Fishing Branch watershed had ratios similar to the mean annual δD-$\delta^{18}O$ of all precipitation, indicating recharge water was a mix of precipitation throughout the year. Bedrock groundwater along Little Fish Creek, Smith Creek, Gayna River and Gibson Creek is slightly depleted in $\delta^{18}O$- δD relative to creek water. In March the creek water is interpreted to be derived from shallow groundwater at these locations; this depletion suggests that bedrock groundwater recharge either occurs at higher elevations or is composed of winter precipitation.
    - Recharge temperatures can be recorded by noble gas concentrations in groundwaters. Contrary to recharge in temperate environments where recharge temperatures are taken to represent mean annual air temperatures, recharge temperatures in permafrost regions must be biased towards soil temperatures during the melt season and therefore can provide information on the advection of enthalpy into the subsurface. This work shows that noble gas recharge temperatures along the Fishing Branch River in Yukon ranged from 0°C to 5 °C. Recharge temperatures from non-thermal groundwater springs along White Sand Creek and Gayna River in NWT had recharge temperatures of 0.0 ± 2.8 °C and 1.3 ± 1.4 °C respectively, while Little Fish Creek groundwater had a recharge temperature of 5.7 ± 1.5 °C. The higher

recharge temperature of Little Fish Creek groundwater may be due to recharge later in the summer. From the comparison of the calculated recharge temperatures with the measured temperature of groundwater at discharge from springs, we may conclude that water has either not changed in temperature or that water has warmed up (as in the case of thermal groundwaters) along the flow path and does not appear to be contributing to permafrost degradation. While of limited scope, these findings are the first attempt at measuring recharge temperatures and provide a promising approach to pursue in future research.

- Advances in the use of DIC and $\delta^{13}C$ to establish groundwater recharge conditions are similarly promising for permafrost hydrogeology. Results of $\delta^{13}C_{DIC}$ from groundwaters sampled in all creeks and rivers show that summertime groundwater recharge occurs through organic soils where water dissolves CO_2 (groundwater P_{CO2} $10^{-2.0}$ to $10^{-3.6}$). With the increased acidity that comes from the dissolution of CO_2, the water subsequently weathers carbonate along the flow path. Groundwater recharge in many of the watersheds likely occurs on hills where there is a thin veneer of organic-rich soil and then flows mostly through carbonate and evaporite rocks.
- Groundwater ages of springs in these systems are shown to be an important parameter in understanding groundwater dynamics in these permafrost watersheds. Michel (1977, 1986) made some estimates of groundwater age using ^{3}H and ^{14}C. This thesis has employed the ^{3}H-^{3}He method to further refine the dating of young groundwaters. Groundwater ages were found to range from very recent to submodern. Remarkably, the 16°C thermal groundwaters along Little Fish Creek, considered to be deeply circulating from recharge higher in the Richardson Mountains, have tritium concentrations well above detection (6.3 and 7.0 TU in two different samples), and are estimated to be less than ~45 years old. This shows that such systems may either be actively circulating or comprise a mixture of two groundwaters, one deeply circulating over a much longer time period, and an intrapermafrost groundwater. By contrast other shallower (cooler)

groundwaters have tritium concentrations below detection, making it difficult to reconcile with a single conceptual model for subpermafrost groundwater circulation. For example, the Smith Creek thermal groundwater (10.3°C) had tritium concentrations below detection and is classified as submodern. Meanwhile, non-thermal groundwaters (T < 5°C; springs along Fishing Branch River, White Sand Creek and Gayna River) were younger, ranging from 0 to 30 years (8.6 to 9.2 TU), likely reflecting shallower flow paths. The thermal groundwater likely discharges at a fairly constant rate throughout the year; however there is probably more variability in discharge from non-thermal springs as these groundwaters are younger and more susceptible to short-term changes in recharge.

3) Massive ground ice formations are common in permafrost and their genesis and degradation are important in the overall hydrologic cycle of permafrost terrain (French, 1996). Moreover, ground ice formations can be formed from the freezing of groundwater. As such noble gas methods for addressing the origin of ground ice and its relationship to groundwater have been developed in this thesis. A novel method using the noble gas ratios of Kr/Xe and Ar/Xe was used to determine the origin of ice bodies. The method was developed around the central tenet that gas in ice originating from occluded snow or hoar frost will have ratios similar to atmospheric air and gas in ice from liquid water will have ratios similar to air-equilibrate water. The gas ratios of Kr/Xe and Ar/Xe were measured from ice bodies of known and unknown origin. The method is complementary to the previously developed method using reactive gases (δO_2/Ar and δN_2/Ar) which can incorporate artefacts of the local geochemical environment prior to freezing.

6.3 Future Work

Based on this work, several aspects of permafrost hydrology and Quaternary history should be investigated to further refine the conclusions made in this thesis and to improve the understanding of how groundwater flows in permafrost and predict how climate warming may affect these systems. In this study, efforts were made to capture winter flow

conditions by conducting sampling and using temperature data loggers. Despite this, much more needs to be done to better understand the components of river flow through the winter. To advance such work, a detailed study encompassing all seasons of a single watershed is suggested. This was begun along the Fishing Branch River, however actual winter flow conditions were not directly measured. White Sand Creek, Hodgson Creek or Canyon Creek are candidates for further work as these sites are near towns and easier to access. If river flow and water chemistry throughout the year could be further quantified and characterized, the amount that groundwater discharge changes through winter could be elucidated. Flow of shallow groundwater should also be further quantified to better constrain their role in streamflow generation. Once these different components have been further constrained, thermal modelling should be conducted to predict how climate warming may impact the groundwater system. Such modeling will require further constraint on groundwater ages using the ^{3}H-^{3}He method, with some additional constrain on the value of $^{3}He/^{4}He$ for crustal helium.

Chapter 5 describes a novel method using noble gases to determine the origin of ground ice bodies. To address some of the uncertainties in this method, ice bodies should be further sampled to collect ice across different parts of a single ice face as well as cutting deeper into the ice face to determine variability within a given formation. Such sampling should be carried out on both ground ice bodies as and modern glacier ice. It would also be of interest to sample proglacial groundwaters that recharge sub-glacially for noble gases to determine how melting of glacial ice may fractionate the gases. It would also be of interest to measure ratios of multiple isotopes of each noble gas on a magnetic sector instrument to determine what type of fractionation processes may occur during ice metamorphosis. To better apply the use of noble gas methods in permafrost, sampling of noble gases from active layer water and the underlying permafrost should be conducted. This would help further constrain the gas composition of recharging water and show how freezing processes may affect gas concentrations.

References

Aeschbach-Hertig, W., Peeters, F., Beyerle, U. and Kipfer, R. (1999). Interpretation of dissolved atmospheric noble gases in natural waters. *Water Resources Research* **35,** 2779-2792.

Aeschbach-Hertig, W., Clark. J.F. Reuter, R.F. and Schlosseri, P. (2002) A paleotemperature record derived from dissolved noble gases in groundwater of the Aquia Aquifer (Maryland, USA). *Geochimica et Cosmochimica Acta* **66**, 797–817.

Aeschbach-Hertig, W., El-Gamal, H., Wieser, M. and Palcsu, L. (2008). Modeling excess air and degassing in groundwater by equilibrium partitioning with a gas phase. *Water Resources Research* **44,** 1-12.

Ahn, J., Headly, M., Wahlen, M., Brook, E., Mayewski, P. and Taylor, K. (2009). CO_2 diffusion in polar ice: observations from naturally formed CO_2 spikes in the Siple Dome (Antarctica) ice core. *Journal of Glaciology* **54,** 685-695.

Aitken, J. and Cook, D. (1974). Sans Sault Rapids Map 1453A. Geological Survey of Canada.

Akerman, H. and Johansson, M. (2008). Thawing permafrost and thicker active layers in sub-arctic Sweden. *Permafrost and Periglacial Processes* **19,** 279-292.

Anderson, D.T., Pollard, W.H., McKay, C.P. and Heldman, J. (2002) Cold springs on Earth and Mars. *Journal of Geophysical Research* **107,** E3 5015.

Andrews, J. N. (1992). Mechanisms for noble gas dissolution by groundwaters. Isotopes of Noble Gases as Tracers in Environmental Studies, International Atomic Energy Agency, Vienna, 87-109.

Anisimova, N., Nikitina, N., Piguzova, V. and Shepelyev, V. (1973). Water sources in Central Yakutia. *In* "Second International Conference on Permafrost ", Yakutia, USSR.

Appelo, C. and Postma, D. (1993). Geochemistry, Groundwater and Pollution. Balkema, New York.

Arcone, S., Chacho, E. and Delaney, A. (1998). Seasonal Structure of talik beneath arctic streams determined with ground-penetrating radar. *In* "Permafrost: Seventh International Conference Proceedings." pp. 19-24., Yellowknife, NWT, Canada.

Astakhov, V. and Isayeva, L. (1988). The 'Ice Hill': An example of 'retarded deglaciation' in

Siberia *Quaternary Science Reviews* **7,** 29-40.

Ball, J. (1988). WATEQ4F, United States Geological Survey.

Ballentine, C. and Burnard, P. (2002). Production, release and transport of noble gases in the continental crust. *In* "Noble Gases in Geochemistry and Cosmochemistry." (Editors: D. Porcelli, C. J. Ballentine, and R. Wieler). Mineralogical Society of America, Washington D.C.

Barnola, J. M., Pimienta, P., Raynaud, D. and Korotkevich, Y. S. (1991). CO_2 climate relationship as deducted from the Vostok ice core: a re-examination based on new measurements and on re-evaluation of the air dating. *Tellus* **43,** 83-90.

Battye, N. (2002).M.Sc. Thesis, "Noble Gases in Canadian Shield Groundwaters from the Con Mine, Yellowknife, N.W.T." University of Ottawa.

Bender, M. L., Sowers, T. and Lipenkov, V. (1995). On the concentrations of O_2, N_2, and Ar in trapped gases from ice cores. *Journal of Geophysical Research* **100,** 18 561-18 660.

Bennett, M., Huddart, D., Hambrey, M. and Chienne, J. (1998). Modification of braided outwash surfaces by aufeis: An example from Pedersenbreen, Svalbard. *Zeitschrift für Geomorphologie* **42,** 1-20

Bense, V., Ferguson, G. and Kooi, H. (2009). Evolution of shallow groundwater flow systems in areas of degrading permafrost. *Geophysical Research Letters* **36,** 1-6.

Birks, S. J., Edwards, T. W. D., Gibson, J. J., Michel, F. A., Drimmie, R. J. and MacTavish, D. (2003). Canadian Network for Isotopes in Precipitation. University of Waterloo/Meteorological Service of Canada.

Bonnaventure, P. (2009). Personal Communication: Ph.D. Candidate: Environmental Geocryology, Department of Geography, University of Ottawa, Canada.

Bortolami, G., Ricci, B., Susella, G. and Zuppi, G. (1979). Isotope hydrology of the Val Corsaglia, Maritime Alps, Piedmont, Italy. *In* "Isotope Hydrology." IAEA Symposium 228, Vienna.

Briner, J., Kaufman, D., Manley, W., Finkel, R. and Caffee, M. (2005). Cosmogenic exposure dating of late Pleistocene moraine stabilization in Alaska. *Geological Society of America Bulletin* **117,** 1108-1120.

Brook, G. and Ford, D. (1980). Hydrology of the Nahanni Karst, Northern Canada and the importance of extreme summer storms. *Journal of Hydrology* **46,** 103-121.

Brosten, T., Bradford, J., McNamara, J., Zarnetske, J., Gooseff, M. and Bowden, B. (2006).

Profiles of temporal thaw depths beneath two arctic stream types using ground-penetrating radar. *Permafrost and Periglacial Processes* **17,** 341-355.

Brosten, T., Bradford, J., McNamara, J., Gooseff, M., Zarnetske, J., Bowden, B. and Johnston, M. (2009). Estimating 3D variation in active-layer thickness beneath arctic streams using ground-penetrating radar. *Journal of Hydrology* **373,** 479-486.

Brown, R. (1961). Hydrology of tritium in the Ottawa Valley. *Geochemica et Cosmochimica Acta* **21,** 199-216.

Brown, R. (1971). Distribution and the Environmental Relationship of Permafrost. *In* "Permafrost Hydrology." (Editor: J. Demers). Environment Canada, Ottawa.

Brown, R. (1975). "Permafrost in Canada." Toronto: University of Toronto Press.

Burt, T. and Williams, P. (1976). Hydraulic conductivity in frozen soils. *Earth Surface Processes* **1,** 349-360.

Cardyn, R., Clark, I. D., Lacelle, D., Lauriol, B., Zdanowicz, C. and Camels, F. (2007). Molar gas ratios of air entrapped in ice: A new tool to determine the origin of relict massive ground ice bodies in permafrost. *Quaternary Research* **68,** 239-248.

Carey, S. and Woo, M. (2000). The role of soil pipes as a slope runoff mechanism, subarctic Yukon, Canada. *Journal of Hydrology* **233,** 206-222.

Carey, S. and Quinton, W. (2004). Evaluating snowmelt runoff generation in a discontinuous permafrost catchment using stable isotope, hydrochemical and hydrometric data. *Nordic Hydrology* **35,** 309–324.

Carey, S. and Quinton, W. (2005). Evaluation of runoff generation during summer using hydrometric, stable isotope and hydrochemical methods in a discontinuous permafrost environment. *Hydrological Processes* **19,** 95-114.

Cederstrom, D. J., Johnston, P. M. and Subitzky, S. (1953). Occurrence and development of ground water in permafrost regions, United States Geological Survey Circular, p. 276.

Cey, B. D. (2009). On the accuracy of noble gas recharge temperatures as a paleoclimate proxy. *Journal of Geophysical Research* **114,** 1-9.

Church, M. (1974). Hydrology and Permafrost with Reference to Northern North America. *In* "Permafrost Hydrology, Proceedings of workshop seminar." pp. 7-19, Calgary, Canada.

Cinq-Mars, J. and Lauriol , B. (1985). Le karst de Tsi-it-toh-Choh: notes préliminaires sur quelques phénomènes kastiques de Yukon septentrional. *Annales de la Société*

Géologique de Belgique **107,** 185-195.

Clark, I. and Fritz, P. (1997). Environmental Isotopes in Hydrogeology. Lewis Publishing, New York.

Clark, I. and Lauriol, B. (1997). Aufeis of the Firth River Basin, Northern Yukon, Canada: Insights into permafrost hydrology and karst. *Arctic and Alpine Research* **2,** 240-252.

Clark, I. D., Lauriol, B., Harwood, L. and Marschner, M. (2001). Groundwater contributions to discharge in a permafrost setting: Big Fish River, N.W.T. *Arctic, Antarctic and Alpine Research* **33,** 62-69.

Clark, I. D., Henderson, L., Chappelaz, J., Fisher, D., Koerner, R., Worthy, D. E. J., Kotzer, T., Norman, A. L. and Barnola, J. M. (2007). CO_2 isotopes as tracers of firn air diffusion and age in an Arctic ice cap with summer melting, Devon Island, Canada. *Journal of Geophysical Research* **112,** 1-13.

Clark, J., Lee Davidson, M., Hudson, G. and Macfarlane, P. (1998). Noble gases, stable isotopes, and radiocarbon as tracers of flow in the Dakota aquifer, Colorado and Kansas. *Journal of Hydrology* **211,** 151–167.

Clever, H.L. (1979). "IUPAC Solubilities: Krypton, Xenon, Radon." Pergamon Press, Oxford.

Craig, H. (1961) Isotopic variations in meteoric waters. *Science* **133**, 1833-1834.

Craig, H., Horibe, Y. and Sowers, T. (1988). Gravitational separation of gases and isotopes in polar ice caps. *Science* **242,** 1675-1678.

Craig, P. and McCart, P. (1975). Classification of stream types in Beaufort Sea drainages between Prudhoe Bay, Alaska, and the Mackenzie delta, N.W.T., Canada. *Arctic and Alpine Research* **7,** 183-198.

Crampton, C. B. (1979). Changes in permafrost distribution produced by a migrating river meander in the Northern, Yukon, Canada. *Arctic* **32,** 148-151.

Davis, N. (2001). "Permafrost: A guide to frozen ground in transition." University of Alaska Press, Fairbanks.

Dingman, L. (2002). Physical Hydrology, pp. 373-375. Prentice Hall, New York.

Douglas, R. J. W. and Norris, D. K. (1973). Geology Wrigley (1373A), Geological Survey of Canada.

Dragon, K. and Marciniak, M. (2010). Chemical composition of groundwater and surface

water in the Arctic environment (Petuniabukta region, central Spitsbergen). *Permafrost and Periglacial Processes* **10,** 137-149.

Duk-Rodkin, A. (1993). Surficial Geology: Sans Sault Rapids (Map 1784A), Geological Survey of Canada.

Duk-Rodkin, A. (1999). Glacial limits map of Yukon Territory (Open File 3694), Geological Survey of Canada

Duk-Rodkin, A. and Hughes, O.L. (1992). Fort McPherson - Bell River Surficial Geology (Map 1742A), Geological Survey of Canada.

Dyke, L.D. (2001). Contaminant migration through the permafrost active layer, Mackenzie Delta area, Northwest Territories, Canada. *Polar Record*. **37**, 215–228.

Eley, F. (1974). Mesoscale climatic study of Norman Wells, NWT Canada, Environmental-Social Committee, Northern Pipeline, pp. 56, Department of Indian and Northern Affairs.

Environment Canada. (2010) National Climate Data and Information Archive.

Farrera, I., Harrison, S., Prentice , I., Ramstein, G., Guiot , J., Bartlein, P., Bonnefille, R., Bush, M., Cramer, W., von Grafenstein, U., Holmgren, K., Hooghiemstra, H., Hope, G., Jolly, D., Lauritzen, S.-E., Ono, Y., Pinot, S., Stute, M. and Yu, G. (1999). Tropical climates at the Last Glacial Maximum: a new synthesis of terrestrial palaeoclimate data I. Vegetation, lake-levels and geochemistry. *Climate Dynamics* **15**, 823-856.

Ferrians, O. J., Jr., Kachadoorian, R. and Green, G. W. (1969). Permafrost and related engineering problems in Alaska (Professional paper), pp. 37, United States Geological Survey.

Finnegar, N., Roe, G., Montgomery, D. and Hallet, B. (2005). Controls on the channel width of rivers: Implications for modeling fluvial incision of bedrock. *Geology* **33,** 229-232.

Fisher, D., Koerner, R. and Reeh, N. (1995). Holocene climatic records from Agassiz Ice Cap, Ellesmere Island, NWT, Canada. *The Holocene* **5,** 195-24.

Fisher, D.C., Koerner, R., Bourgeois, J., Zielinski, G., Wake, C., Hammer, C., Clausen, H., Gundestrup, N., Johnson, S., Gota-Azuma, K., Hondoh, T., Blake, E. and Gerasinoff, M. (1998). Penny Ice Cap cores, Baffin Island, Canada, and the Wisconsinan Foxe Dome Connection: Two states of Hudson Bay ice cover. *Science* **279,** 692-695.

Ford, D.C. (1983). The physiography of the Castleguard Karst and Columbia Icefields area,

Alberta, Canada. *Arctic and Alpine Research* **15,** 427-436.

Ford, D. and William, P. (2007). "Karst Hydrogeology and Geomorphology." John Wiley and Sons Ltd, West Sussex, England.

French, H. (1996). "The Periglacial Environment." Addison Wesley Longman Limited., Canada.

French, H. and Egginton, P. (1973). Thermokarst development, Banks Island, Western Canadian Arctic. In Permafrost: North American contribution. *In* "Second International Permafrost Conference." pp. 203-212. National Academy of Science, Yakutsk, Russia.

French, H. and Shur, Y. (2010). The principles of cryostratigraphy. *Earth-Science Reviews* **101,** 190-206.

Frey, K., Siegel, D. and Smith, L. (2007). Geochemistry of west Siberian streams and their potential response to permafrost degradation. *Water Resources Research* **43,** 1-15.

Friedrich, R. (2007). Ph.D. Thesis: "Grundwassercharakterisierung mit Umwelttracern: Erkundung des Grundwassers der Odenwald-Region sowie Implementierung eines neuen Edelgas-Massenspektrometersystems." University of Heidelberg, Germany.

Froese, D., Westgate, J., Reyes, A., Enkin, R. and Preece, S. (2008). Ancient permafrost and a future, warmer arctic. *Science* **321,** 1648.

Glotov, V. and Glotova, L. (2008). Hydrogeology of the northern sea of Okhotsk Coast. *Russian Journal of Pacific Geology* **27,** 31-42.

Glotov, V. E. (2009). "Hydrogeology of sedimentary basins in northeastern Russia (Russian)." Moscow, Russian Federation.

Grasby, S. (2003). Supraglacial sulfur springs and associated biological activity in the Canadian High Arctic—Signs of life beneath the ice. *Astrobiology* **3,** 583-596.

Greene, S. (2005). M.Sc. Thesis: "Noble gases of the Canadian Shield from the Lupin and Con mines, Canada, as indicators of deep ground ", University of Ottawa Canada.

Greene, S., Battye, N., Clark, I., Kotzer, T. and Bottomley, D. (2008). Canadian shield brine from the Con Mine, Yellowknife, NT, Canada: Noble gas evidence for an evaporated Palaeozoic seawater origin mixed with glacial meltwater and Holocene recharge. *Geochimica et Cosmochimica Acta* **72,** 4008-4019.

Grew, K. E., and Ibbs, T. L. (1952). "Thermal diffusion of gases." Cambridge University Press, New York.

Haldorsen, S., and Heim, M. (1999). An Arctic Groundwater System and its dependence upon climatic change: An example from Svalbard. *Permafrost & Periglacial Processes* **10,** 137-149.

Haldorsen, S., Heim, M., Dale, B., Landvik, J.Y., van der Ploeg, M., Leijnse, A., Salvigsen, O., Ove Hagen, J. and Banks, D. (2010) Sensitivity to long-term climate change of subpermafrost groundwater systems in Svalbard. Quaternary Research **73**, 393–402.

Hamilton, J. and Ford, D. (2002). Karst geomorphology and hydrogeology of the bear rock formation — a remarkable dolostone and gypsum megabreccia in the continuous permafrost zone of Northwest Territories, Canada. *Carbonates and Evaporites* **17,** 114-115.

Harry, D., French, H. and Pollard, W. (1988). Massive Ground Ice and ice-cored terrain near Sabine Point, Yukon coastal Plain. *Canadian Journal of Earth Science* **25,** 1846-1856.

Hayashi, M., Quinton, W. L., Pietroniro, A. and Gibson, J. J. (2004). Hydrologic functions of wetlands in a discontinuous permafrost basin indicated by isotopic and chemical signatures. *Journal of Hydrology* **296,** 81-97.

Headly, M., Ahn, J. and Severinghaus, J. (2005). Using Kr/Ar and Xe/Ar Ratios to Identify Melt Layers in ice Cores. *In* "American Geophysical Union: Fall Meeting 2005." San Francisco.

Heldmann, J.L., Pollard, W.H., Mckay, C.P., Andersen, D.T. and Toon, O.B. (2005). Annual development cycle of an icing deposit and associated perennial spring activity on Axel Heiberg Island, Canadian high Arctic. *Arctic, Antarctic and Alpine Research* **37,** 127–135.

Hinzman, L.D., Kane, D.L., Yoshikawa, K., Carr, A., Bolton, W.R. and Fraver, M. (2003). Hydrological variations among watersheds with varying degrees of permafrost. In "Proceedings 8th International Conference on Permafrost", 407–411, Zurich, Switzerland.

Hoefs, J. (2009). Stable isotope geochemistry, 6th Edition. Springer-Verlarg, Berlin, Heidelberg.

Hu, X. and Pollard, W. (1997). The hydrologic analysis and modelling of river icing growth, North Fork Pass, Yukon Territory, Canada. *Permafrost & Periglacial Processes* **8,** 279-294.

Hume, G.S. (1954). The Lower Mackenzie River area, Northwest Territories and Yukon (Memoire 173) Geological Survey of Canada, p118.

Hughes, O. (1972). Surficial geology of the Northern Yukon Territory and Northwestern District of the Mackenzie, Northwest Territories, Geological Survey of Canada.

Hughes, O., Viellette, J.J., Pilon, J., Hanley, P.T. and van Everdingen, R.O. (1973). Terrain Evaluation with respect to pipeline constructions, Mackenzie Transportation Corridor, Central Part, Lat 64 °N to 68 °N. Environmental Social Committee, Northern Pipelines, Report 73-37.

IAEA (International Atomic Energy Agency). (2010) Global Network of Isotopes in Precipitation & Isotope Hydrology Information System (GNIP/ ISOHIS).

IPA (International Permafrost Association). (2010). Data map of permafrost distribution.

Jouzel, J. and Souchez, R. (1982). Melting-refreezing at the glacier sole and isotopic composition of the ice. *Journal of Glaciology* **28,** 35-41.

Kaplyanskaya, F. and Tarnogradskiy, V. (1986). Remnants of the Pleistocene ice sheets in the permafrost zone as an object for paleoglaciological research. *Polar Geography and Geology* **10,** 65-72.

Kaufman, S. and Libby, W. (1954). The natural distribution of tritium. *Physical Review* **93,** 338-340.

Kennedy, K., Froese, D., Zazula, G. and Lauriol, B. (2010). Last Glacial Maximum age for the northwest Laurentide maximum from the Eagle River spillway and delta complex, northern Yukon *Quaternary Science Reviews* **29,** 1288-1300.

Killawee, J., Fairchild, J., Tison, J., Janssens, L. and Lorrain, R. (1998). Segregation of solutes and gases in experimental freezing of dilute solutions: Implications for natural glacial systems. *Geochimica et Cosmochimica Acta* **62,** 3637-3655.

Kipfer, R., Aeschback-Hertig, W., Peeters, F. and Stute, M. (2002). Noble gases in lakes and groundwaters. *In* "Noble Gases in Geochemistry and Cosmochemistry." (Porcelli, D, Ballentine, C.J. and Wieler, R.), pp. 642. Mineralogical Society of America, Washington D.C.

Klassen, R. and Shilts, W. (1987). "Bylot Island, Eastern Canada Arctic XII INQUA Congress Field Excusion A.I. Guidebook." National Research Council of Canada, Ottawa.

Kokelj, S. V. and Burn, C. R. (2005). Geochemistry of the active layer and near-surface permafrsot, Mackenzie delta region, Northwest Territories, Canada. *Canadian Journal of Earth Sciences* **42,** 37-49.

Kulongoski, J. and Hilton, D. (2002). A quadrupole-based mass spectrometric system for the determination of noble gas abundances in fluids. *Geochemistry Geophysics Geosystems* **3,** 1-10.

Lacelle, D., Bjornson, J., Lauriol, B., Clark, I. and Troutet, Y. (2004). Segregated-intrusive

ice of subglacial meltwater origin in retrogressive thaw flow headwalls, Richardson Mountains, N.W.T Canada. *Quaternary Science Reviews* **23,** 681-696.

Lacelle, D., Lauriol, B. and Clark, I. (2006). Effect of chemical composition of water on the oxygen-18 and carbon-13 signature preserved in cryogenic carbonates, Arctic Canada: Implications in paleoclimatic studies. *Chemical Geology* **234,** 1-16.

Lacelle, D., Lauriol, B., Clark, I. D., Cardyn, R. and Zdanowicz, C. (2007). Nature and origin of a Pleistocene-age massive ground-ice body exposed in the Chapman Lake moraine complex, central Yukon Territory. *Quaternary Research* **68,** 249-260.

Lacelle, D., Juneau, V., Pellerin, A., Lauriol, B. and Clark, I. (2008). Weathering regime and geochemical conditions in a polar desert environment, Haughton impact structure region, Devon Island, Canada. *Canadian Journal of Earth Sciences* **45,** 1139-1157.

Lacelle, D., Lauriol, B. and Clark, I. (2009a). Formation of seasonal ice bodies and associated cryogenic carbonates in Caverne de l'Ours, Quebec, Canada: Kinetic isotope effects and pseudo-biogenic crystal structures. *Journal of Cave and Karst Studies* **71,** 48-62.

Lacelle, D., St-Jean, M., Lauriol, B., Clark, I. D., Lewkowicz, A., Froese, D., Kuehn, S. and Zazula, G. (2009b). Burial and preservation of a 30,000 year old perennial snowbank in Red Creek valley, Ogilvie Mountains, central Yukon, Canada. *Quaternary Research Reviews* **28,** 3401-3413.

Lacelle, D., Bjornson, J. and Lauriol, B. (2010). Climatic and geomorphic factors affecting contemporary (1950-2004) activity of retrogressive thaw slumps on the Aklavik plateau, Richardson mountains, NWT, Canada. *Permafrost and Periglacial Processes* **21,** 1-15

Lacelle, D. and Clark, I. D. (2011). On the $\delta^{18}O$, δD and D-excess relations in meteoric precipitation and during equilibrium freezing: theoretical approach and field examples. *Permafrost and Periglacial Processes,* **22,** 13–25.

Langmuir, D. (1971). The geochemistry of some carbonate ground waters in central Pennsylvania. *Geochimica et Cosmochimica Acta* **35,** 1023-1045.

Lantuit, H. and Pollard, W. (2008). Fifty years of coastal erosion and retrogressive thaw slump activity on Herschel Island, southern Beaufort Sea, Yukon Territory, Canada. *Geomorphology* **95,** 84-102.

Lauriol, B., Carrier, L and Thibaudeau, P. (1968) Topoclimatic zones and dynamics in the caves of the northern Yukon, Canada. *Arctic* **41**, 215-220.

Lauriol, B., Carrier, L. and Thibaudeau, P. (1988). Topoclimatic zones and ice dynamics in the caves of the northern Yukon, Canada. *Arctic* **41,** 215-220.

Lauriol, B. and Clark, I. (1993). An approach to determine the origin and age of massive Ice blockages in two Arctic caves. *Permafrost and Periglacial Processes* **4,** 77-85.

Lauriol, B. and Gray, J. (1990). Karst drainage in permafrost environments: the case of Akpatok Island, NWT Canada *Permafrost & Periglacial Processes* **1,** 129-144.

Lauriol, B., Ford, D., Cinq-Mars, J. and Morris, W. (1997). The chronology of speleothem deposition in Northern Yukon and its relationship to permafrost. . *Canadian Journal of Earth Sciences* **23,** 902-911.

Lauriol, B., Lacelle, D., St-Jean, M., Clark, I. D. and Zazula, G. (2010). Late Quaternary paleoenvironments and growth of intrusive ice revealved by a thaw slump in the Eagle River Valley, northern Yukon, Canada. *Canadian Journal of Earth Sciences* **47,** 941-955.

Lawrence, D. and Slater, A. (2005). A projection of severe near-surface permafrost degradation during the 21st century. *Geophysical Research Letters* **32,** 1-5.

Leibman, M. (1996). Results of chemical testing for various types of water and ice, Yamal Peninsula, Russia. *Permafrost and Periglacial Processes* **7,** 287-296.

Lewkowicz, A. (1987). Nature and importance of thermokarst processes, Sandhills moraine, Banks Island, Canada. *Geografiska Annaler* 67A, 1077-1085.

Lippmann, J., Stute, M., Torgersen, T., Moser, D. P., Hall., J. A., Lin, L., Borcsik, M., Bellamy, R. E. S. and Onstott, T. C. (2003). Dating untra deep mine waters with noble gases and ^{36}Cl, Witwatersrand Basin, South Africa. *Geochemica et Cosmochimica Acta* **67,** 4597-4619.

Lorrain, R. and Demeur, P. (1985). Isotopic evidence for relic Pleistocene glacier ice on Victoria Island. *Arctic and Alpine Research* **17,** 89-98.

Mackay, J. (1966). Segregated epigenetic ice and slumps in permafrost, Mackenzie Delta area, N.W.T. *Geographical Bulletin* **8,** 59-80

Mackay, J. (1971). The origin of massive icy beds in permafrost, western Arctic coast, Canada. *Canadian Journal of Earth Sciences* **8,** 397-422.

Mackay, J. (1989) A Classification of massive ground ice, Geological Survey of Canada workshop .

Mackay, J. and Dallimore, R. (1992). Massive ice of the Tuktoyaktuk area, western Arctic coast, Canada. *Canadian Journal of Earth Sciences* **29,** 1235-1249.

Manning, A.H., Solomon, D.K. and Sheldon, A.L. (2003) Applications of a total dissolved gas pressure probe in ground water studies. *Ground Water* **41**, 440-448.

Manning, A. and Caine, J. (2007). Groundwater noble gas age and temperature signatures in an Alpine watershed: Valuable tools in conceptual model development. *Water Resources Research* **43,** 1-16.

March, R. and Todd, J. (2005). Quadrupole Ion Trap Mass Spectrometry. p. 2. Second Edition, John Wiley and Sons Inc. New Jersey.

Matthews, J., Schweger, C. and Hughes, O. (1990). Plant and insect fossils from the Mayo Indian Village Section (central Yukon): new data on middle Wisconsinan environments and glaciations. *Géographie physique et Quaternaire* **44,** 15-26.

Mazor, E. (1991). "Applied Chemical and Isotopic Groundwater Hydrology." Halsted Press a division of John Wiley & Sons, Toronto.

McCracken, A., Poulton, T., Macey, E., Monro Gray, J. and Nowlan, G. (2007). Popular Geoscience: Energy: Arctic Oil and Gas <http://www.gac.ca/PopularGeoscience/factsheets/ArcticOilandGas_e.pdf> Geological Survey of Canada.

McFadden, T. (1990). Kilpisjaervi project. Case study of cold-regions research in Finland. *Journal of Cold Regions Engineering* **4,** 69-84

McKay, C., Anderson, D., Pollard, W. H., Heldman, J. L., Doran, P. T., Fritsen, C. and Priscu, J. (2005). Polar lakes, streams and springs as analogs for the hydrological cycle on Mars. *In* "Water on Mars and Life, Advances in Astrobiology and Biogeophysics." pp. 219–233. Springer, Berlin.

McNamara, J. P., Kane, D. L. and Hinzman, L. D. (1997). Hydrograph separation in an Arctic watershed using mixing model and graphical techniques. *Water Resources Research* **33,** 1707-1919.

Michel, F. A. (1977). M.Sc. Thesis: "Hydrogeologic studies of springs in the Central Mackenzie Valley, Northwest Territories, Canada." University of Waterloo, Canada.

Michel, F. A. (1986). Hydrogeology of the Central Mackenzie Valley. *Journal of Hydrology* **86,** 379-405.

Mochnacz, N. (2008). Personal Communication. Fisheries Research Biologist, Department of Fisheries and Oceans, Winnipeg, Canada.

Mohapatra, R. K. (1998). Ph.D. Thesis:"Study of the abundance and isotopic composition of nitrogen in Earth's Mantle." Maharaja Sayajirao University of Baroda, India.

Mohapatra, R. K. and Murty, S. V. S. (2000). Search for the mantle nitrogen in the ultramafic xenoliths from San Carlos, Arizona. *Chemical Geology* **164,** 305–320

Müller, F. (1959). Beobachtungenüber Pingos. *Meddelelser om Gronland* **153,** 127.

Muller, S. (1947). "Permafrost or permanently frozen ground and related engineering problems." Military Intelligence Division, Ann Arbor, Michigan.

Murton, J., Whiteman, C., Waller, R., Pollard, W., Clark, I. and Dallimore, S. (2005). Basal ice facies and supraglacial melt-out till of the Laurentide Ice Sheet, Tuktoyaktuk Coastlands, Western Arctic Canada. *Quaternary Science Reviews* **24,** 681-708.

Muskett, R. and Romanovsky, V. (2009). Groundwater storage changes in arctic permafrost watersheds from GRACE and in situ measurements. *Environmental Research Letters* **4,** 1-8.

Mutch, R. A. and McCart, P. (1974). Springs within the northern Yukon drainage system (Beaufort Sea Drainage). *In* "Fisheries research associated with proposed gas pipeline routes in Alaska, Yukon and Northwest Territories." (P. McCart, Ed.), pp. 34. Canadian Arctic Gas Study Limited.

Norris, D. K. (1974). Geology Fort McPherson (Map 1520A). Geological Survey of Canada.

Norris, D. K. (1977). Blow River and Davidson Mountains (Map 1516A). Government of Canada.

Norris, D. K. (1978). Geology, Porcupine River, Yukon Territory (Map 1522A). Geological Survey of Canada.

Norris, D. K. (1985). Geology of the northern Yukon and Northwestern district of Mackenzie (1581A). Geological Survey of Canada.

NRCan (Natural Resources Canada). (2003). The Atlas of Canada: Permafrost, Government of Canada.

NRCan (Natural Resources Canada). (2004). The Atlas of Canada: Geological Provinces, Government of Canada.

NRC (National Research Council of Canada). (1988). Glossary of permafrost and related ground ice terms, Associate Committee on Geotechnical Research, Permafrost Subcommittee, pp. 156 Government of Canada.

Omelon, C., Pollard, W. and Andersen, D. (2006). A geochemical evaluation of perennial spring activity and associated mineral precipitates at Expedition Fjord, Axel Heiberg Island, Canadian High Arctic. *Applied Geochemistry* **21,** 1-15.

Paterson, W. (1994). "The Physics of Glaciers 3rd Edition." Pergamon, Oxford.

Peeters, F., Beyerle, U., Aeschbach-Hertig, W., Holocher, J., Brennwald, M. S. and Kipfer, R. (2003). Improving noble gas based paleoclimate reconstruction and groundwater dating using $^{20}Ne/^{22}Ne$ ratios. *Geochimica et Cosmochimica Acta,* **67,** 587-600.

Péwé, T. (1982). Geologic Hazards of the Fairbanks Area, Alaska, Special Report #15, Alaska Division of Geological and Geophysical Surveys p. 109.

Pollard, W. and French, H. (1985). The internal structure and ice crystalography of seasonal frost mounds. *Journal of glaciology* **31,** 157-162.

Pollard, W. H., Omelon, C., Anderson, D. and Mckay, C. (1999). Perennial spring occurrence in the Expedition Fiord area of the western Axel Heiberg Island, Canadian High Arctic. *Canadian Journal of Earth Science* **36,** 105-120.

Pollard, W. H. (2005). Icing processes associated with high Arctic perennial springs, Axel Heiberg Island, Nunavut, Canada. *Permafrost and Periglacial Processes* **16,** 51-68.

Poole, J. C., McNeill, G. W., Langman, S. R. and Dennis, F. (1997). Analysis of noble gases in water using a quadrapole mass spectrometer in static mode. *Applied Geochemistry* **12,** 707-714.

Porcelli, D., Ballentine, C. J. and Wieler, D. (2002). Noble Gases in Geochemisty and Cosmochemisty. *In* "Reviews in Minerology and Geochemistry." (Editors: J. J. Rosso and P. H. Ribbe). Minerological Society of America, Washington D.C.

PMO. (2010). PM announces high Arctic research station coming to Cambridge Bay, Government of Canada.

Price, P. and Sowers, T. (2004). Temperature dependence of metabolic rates for microbial growth, maintenance and survival. *Proceedings of the National Academy of Sciences of the United States of America* **101,** 4631-4636

Quinton, W. and Marsh, P. (1999). A conceptual framework for runoff generation in a permafrost environment. *Hydrological Processes* **13,** 2563-2581.

Quinton, W. L. and Pomeroy, J. W. (2006). Transformation of runoff chemistry in the Arctic tundra, Northwest Territories, Canada. *Hydrological Processes* **20,** 2901-2919.

Radtke, K., Lacelle, D., Greer, C. and Whyte, L. (2010). Subsurface ice bodies in the Canadian Arctic: analogue environment for astrobiology. *In* "13th International Symposium on Microbial Ecology." Seattle, Washington, USA.

Rampton, V. (1982). Quaternary geology of the Yukon Coastal Plain (Bulletin 317), Geological Survey of Canada.

Rozanski, K., Araguas-Araguas, L., and Gonfiantini, R. (1993). Isotopic patterns in modern

global precipitation. In: Climate change in continental isotopic records (Editors: Swart, P.K., Lohmann, K.C.; McKenzie, J.A.; Savin, S.) AGU Monograph, 78, 1-36.

Sano, Y. and Takahata, N. (2005). Measurement of noble gas solubility in seawater using a quadrupole mass spectrometer. *Journal of Oceanography* **61,** 465-473.

Schonewille, B. and Anderton, I. (2006). 2005 Porcupine River Coho radio tagging/telemetry pilot project. EDI Environmental Dynamics Inc., Whitehorse.

Schumskii, P. (1964). "Principles of structural Glaciology." Dover Publications, New York.

Schwander, J. (1989). The transformation of snow to ice and the occlusion of gases. *In* "The environmental record in glaciers and ice sheets." (Editors: Oeschger, H and Langway, C.C.), pp. 53-67. John Wiley, New York.

Serreze, M. C. and Barry, R. G. (2005). "The arctic climate system." Cambridge Univ Pr, Cambridge.

Serveringhaus, J. and Battle, M. (2006). Fractionation of gases in polar ice during bubble close-off: New constraints from firn air Ne, Kr and Xe observations. *Earth and Planetary Science Letters* **244,** 474-500.

Severinghaus, J., Grachev, A., Luz, B. and Caillon, N. (2003). A method for precise measurement of argon 40/36 and krypton/argon ratios in trapped air in polar ice with applications to past firn thickness and abrupt climate change in Greenland and at Siple Dome, Antarctica. *Geochimica et Cosmochimica Acta* **67,** 325-343.

Smith, S. (2010). Personal Communication. Permafrost Research Scientist, Geological Survey of Canada, Ottawa, Canada.

Smith, S. and Burgess, M. (2002). A digital database of permafrost thickness in Canada (Open File 4173), Geological Survey of Canada.

Smith, S., Burgess, M., Riseborough, D. and Nixon, F. (2005). Recent trends from Canadian Permafrost Thermal Monitoring Network Sites. *Permafrost & Periglacial Processes* **16,** 19-30.

Smith, S., Romanovsky, V., Lewkowicz, A., Burn, C., Allard, M., Clow, G., Yokikawa, K. and Throop, J. (2010). Thermal state of permafrost in North America: A contribution to the International Polar Year. *Permafrost and Periglacial Process* **21,** 117-135.

Sowers, T. (2001). N_2O record spanning the penultimate deglaciation from the Vostok ice core. *Journal of Geophysical Research: Atmospheres (D)* **106,** 31903-31914.

Sowers, T., Bender, M. L. and Raynaud, D. (1989). Elemental and isotopic composition of occluded O_2 and N_2 in polar ice. *Journal of Geophyciscal Research* **94,** 5137-5150.

St-Jean, G. (2003) Automated quantitative and isotopic (^{13}C) analysis of dissolved inorganic carbon and organic carbon in continuous-flow using a total organic carbon analyser. *Rapid Communication in Mass Spectrometry* **17**, 418-428.

St-Jean, M., Lauriol , B., Clark, I., Lacelle, D. and Zdanowicz, C. (2011). Investigation of ice-wedge infilling processes using stable oxygen and hydrogen isotopes, crystallography and occluded gases (O_2, N_2, Ar). *Permafrost and Periglacial Processes,* **22**, 49–64.

St-Onge, D. and McMartin, I. (1999). The Bluenose Lake Moraine, a moraine with a glacier ice core. *Geographie Physique et Quaternaire* **53,** 287-295.

Sanford, W.E., Shropshire, R.G. and Solomon, D.K. (1996). Dissolved gas tracers in groundwater: Simplified injection, sampling and analysis. *Water Resources Research* **32,** 1635-1642.

Stute, M., Clark, J., Schlosser, P., Broecker, W. and Bonani, G. (1995). A 30,000 yr continental paleotemperature record derived from noble gases dissolved in groundwater from the San Juan Basin, New Mexico. *Quaternary Research* **43,** 209-220.

Stute, M. and Schlosser, P. (1993). Principles and applications of the noble gas paleothermometer. *In* "Climate Change in Continental Isotopic Records." pp. 89-100. American Geophysical Union, Washington DC.

Taylor, A., Nixon, M., Eley, J., Burgess, M. and Egginton, P. (1998). Effects of atmospheric inversions on ground surface temperatures and discontinuous permafrost, Norman Wells, Mackenzie valley, Canada. *In* "Proceedings of the 7th International Conference on Permafrost." (Lewkowicz, A. and Allard, M.), pp. 1043-1047, Yellowknife.

Thibaudeau, P., Roberge, J. and Lauriol, B. (1988). Agressivité chimique des eaux dans les massifs calcaires du Nord du Yukon - Canada. *Revue de Geomorphologie Dynamique* **37,** 61-71.

Tolstikhin, N. and Tolstikhin, O. (1976). Groundwater and surface water in the permafrost region (Translation) Inland Waters Directorate, pp. 22, Government of Canada.

Tung, H., Bramall, N. and Price, P. (2005). Microbial origin of excess methane in glacial ice and implications for life on Mars. *Proceedings of the National Academy of Sciences of the United States of America* **102,** 18292-18296.

van Everdingen, R. (1974). Groundwater in Permafrost Regions of Canada. *In* "Canadian National Committee: The International Hydrological Decade: Permafrost Hydrology." Environment Canada.

van Everdingen, R. (1976). Geocryology terminology. *Canadian Journal of Earth Sciences*

13, 862-867.

van Everdingen, R. O. (1981). Morphology, hydrology and hydrochemistry of karst in permafrost terrain near Great Bear Lake, Northwest Territories, Government of Canada p. 53.

Venzke, J. (1988). Observation on icings phenomena in the Icelandic subarctic-oceanic environment. *Geookodynamik* **9,** 207-220

Vogel, J.C. (1993). Variablity of carbon isotope fractionation during photosynthesis. *In* "Stable Isotopes and Plant Carbon- Water Relations" (Editors: J.R. Ehleringer, A.E. Hall and G.D. Farquhar) Academic Press, San Diego, California, pp 29-38.

Waller, R., Murton, J. and Knight, P. (2009). Basal glacier ice and massive ground ice: different scientists, same science? *Geological Society Special Publication: Glaciology & Permafrost* **320,** 57-69.

Walter, D. J. (1981). Geological Map of the Northern Interior Plains (1497A). Geological Survey of Canada.

Washburn, A. (1980). "Geocryology." John Wiley & Sons, New York.

Weiss, R. (1970). The solubility of nitrogen, oxygen and argon in water and seawater. *Deep-sea research* **17,** 721-735.

Weiss, R. (1971). Solubility of helium and neon in water and seawater. *Journal of chemical and engineering data* **16,** 235–241.

Weiss, R. (1978). Solubility of krypton in water and sea water. *Journal of chemical and engineering data* **23,** 69-72.

Westgate, J., Preece, S., Froese, D., Pearce, N., Roberts, N., Demuro, D., Hart, W. and Perkins, W. (2008). Changing ideas on the identity and stratigraphic significance of the Sheep Creek tephra beds in Alaska and the Yukon Territory, northwestern North America. *Quaternary international* **178** 183-209.

White, D.E. (1957). Thermal waters of Volcanic Origin. *Geologic Society of America Bulletin* **68**, 237-239.

Wilson, J. and Guan, H. (2004). Mountain-Block Hydrology and Mountain-Front Recharge. *In* "Groundwater Recharge in a Desert Environment: The Southwestern United States." (Editor: Phillips, F, Hogan, J and Scanlon, B.). AGU, Washington, DC.

Woo, M. and Steer, P. (1983). Slope hydrology as influenced by thawing of the active layer, Resolute, NWT. *Canadian Journal of Earth Sciences* **20,** 978-986.

Woo, M., Marsh, P. and Pomeroy, J. (2000). Snow, frozen soils and permafrost hydrology in Canada. *Hydrological Processes* **14,** 1480-1611.

Woo, M. and Marsh, P. (2005) Snow, frozen soils and permafrost hydrology in Canada, 1999–2002. *Hydrological Processes* **19,** 215-229.

Woo, M.K., Kane, D., Carey, S.K. and Yang, D. (2008). Progress in permafrost hydrology in the new millennium, *Permafrost and Periglacial Processes* **19**, 237-254.

Wrangel, F. (1841). "A journey to the northern shores of Siberia and along the Arctic Ocean Made in 1820-1924." Harper and Brothers, St. Petersburg, Russia.

Yang, D., Kane, D. L., Hinzman, L. D., Zhang, X., Zhang, T. and Ye, H. (2002). Siberian Lena River hydrologic regime and recent change *Journal of Geophysical Research D: Atmospheres* **107,** 14-1- to 4-10.

Yukon Environment. (2010). Ni'iinlii'Njik (Fishing Branch) Wilderness Preserve & Habitat Protection Area Management Plan.

Yoshikawa, K., Hinzman, L. and Kane, D. (2007). Spring and aufeis (icing) hydrology in Brooks Range, Alaska. *Journal of Geophysical Research* **112,** 1-14.

Zhao-ping, Y., Hua, O., Xing-liang, X., Lin, Z., Ming-hua, S. and Cai-ping, Z. (2010). Effects of permafrost degradation on ecosystems. *Acta Ecologica Sinica* **30,** 33-39.

Appendix A: Noble Gas Extraction and Analysis Methods

The isotope dilution method for the determination of noble gas concentrations has been described and used in various research programs (e.g. Poole *et al.*, 1997; Kulongoski and Hilton, 2002; Sano and Takahata, 2005; Battye, 2002; Greene, 2005). The noble gas extraction from ice design has been modified slightly from Severinghaus *et al.* (2003).

Principle: The objective of this method is to determine the concentration of gases in the sample. A spike dominated by rare-isotopes of each gas of interest is used; the isotopic concentration is known from the manufacturer. The volume of the spike is determined by measuring the isotopic ratio of the spike gas vs. major isotope of that gas compared with air of a known volume and isotopic composition. With the calibrated spike samples are by adding spike to the sample and measuring the isotopic ratio.

Design: The noble gas line used in this study is based on the design of Poole *et al.* (1997) and this specific line has been mostly described in Battye, (2002) and Greene, (2005). The mass spectrometer used is a SRS RGA 200. To improve the repeatability of Kr-Xe trapping on charcoal the trap has been modified to include a heating element surrounded by lead pellets and an outer cover which is all submerged in liquid nitrogen. Ice samples are placed in a glass vessel which has a volume of ~ 425 cc.

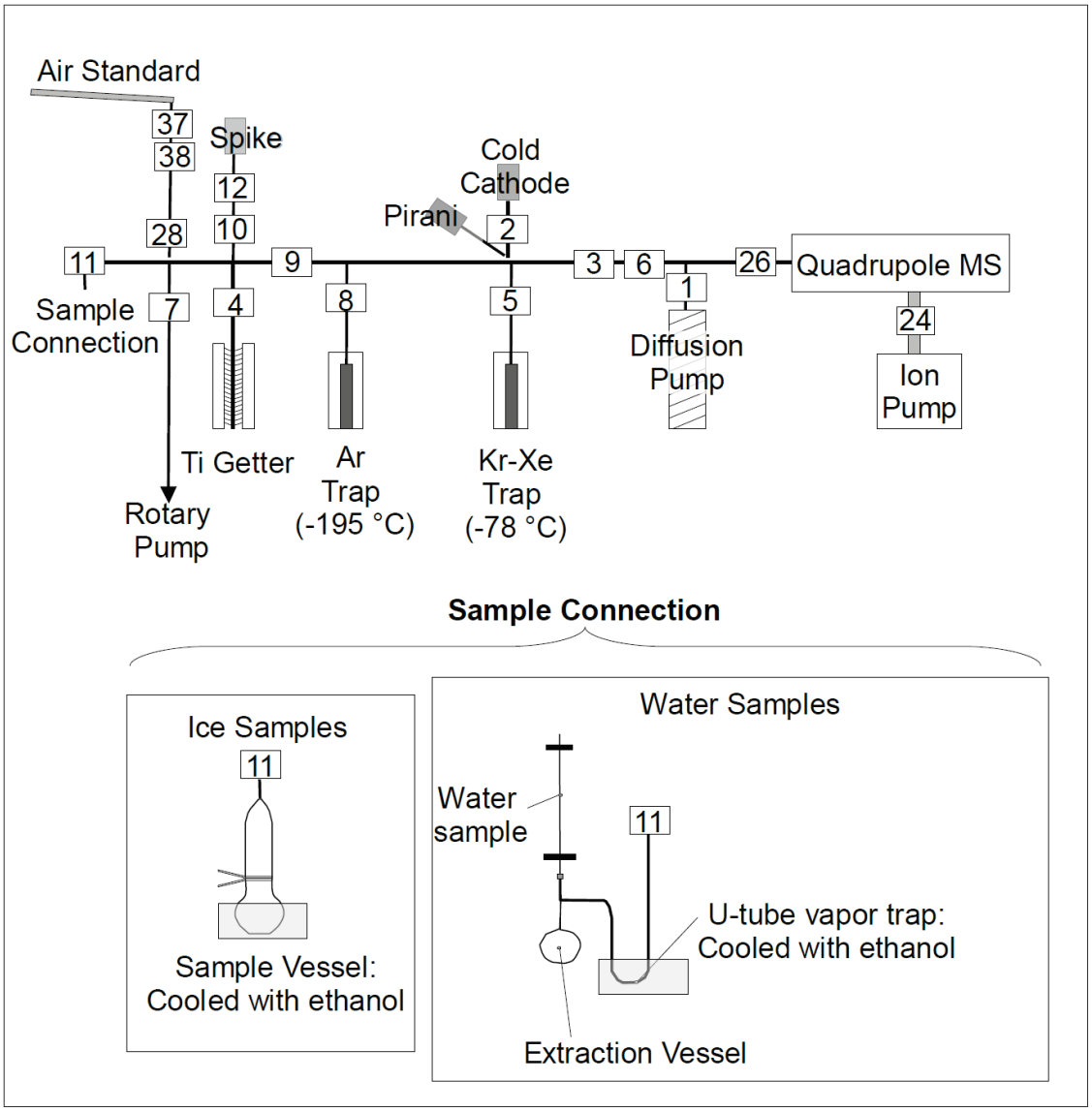

Figure A 1: Isotope dilution noble gas line. Squares with numbers in are valves.

Methods: [denotes open valve]

Extraction: Ice: Approximately 50 g (weighed for each sample) of ice was placed in glass sample vessel (See Figure A 1: Ice Samples). The extraction vessel with the ice in is cooled to -20 ˚C to -30 ˚C using a cooled ethanol bath. At -20 ˚C to -30 ˚C the sample was kept pumped under vacuum for 30 min to allow the sublimation of surface contamination [11, 7]. Once pumping was stopped, spike was mixed with the sample and the sample was melted by submerging the glass vessel in water [11, 10]. Once fully melted the ice water is

frozen again with the ethanol bath inducing degassing and reducing vapour pressure in the line.

Extraction: Water: Copper tube water sample is attached to line with a glass extraction vessel below the tube and connected to the noble gas line via a stainless steel U-tube (See Figure A 1: Water Samples). Line is evacuated to 7 x 10^{-5} Torr and U-tube is cooled to -30 ˚C by an ethanol bath. Once line is at 7 x 10^{-5} Torr, spike is introduced to the sample extraction portion of the line and the sample is opened mixing it with the spike. Water vapour is trapped on the U-tube trap.

Purification and Separation: Once the sample has been refrozen it is expanded further into the line and the sample vessel is isolated from the line, the gas is then exposed to a hot titanium getter at 600˚C for 10 minutes to remove reactive gases [4, 9, 10]. At this point an aliquot of gas is taken between valves 3 and 6 and inlet to the mass spectrometer to measure argon (^{36}Ar and ^{40}Ar). Krypton and xenon are then trapped on charcoal cooled to -78 ˚C for 15 minutes [4, 9, 10, 5]. After 15 minutes gas remaining in the line is pumped away until the pressure is 7 x 10^{-5} Torr (usually about 1 minute) [4, 9, 10, 5, 3, 6, 1]. After this the line was closed to pumping and the charcoal trap was heated to 150 ˚C for 15 minutes [4, 9, 10, 5]. The gas released from this trap is continually exposed to the titanium getter to remove any contamination which was not already gettered. After 15 minutes the gas is inlet into the mass spec and krypton (^{78}Kr, ^{84}Kr) and xenon (^{132}Xe, ^{136}Xe) are measured on the multiplier collector [4, 9, 10, 5]. Standards are run regularly to calibrate the volume of spike. The method used is the same as describe above, but the gas inlet through the calibrated air standard aliquot.

Calculations:

When spike and sample are mixed the isotopic ratios in the mixed sample is dependent on the amount of spike and its isotopic ratio as well as the amount of sample and its isotopic ratio. The isotopic composition of the spike is known and the isotopic composition of the sample is assumed to be the same as atmospheric. When running a standard, the amount of atmospheric gas is known and is used to calibrate the volume of spike, when running a sample the calibrated volume of spike is used to determine the

amount of gas in the sample. The mole ratios of the spike and air as well as the volume of gases for air standards are shown in Table 1 .When a mixed of spike and sample are analysed the isotopic ratio is a result of the parameters shown in Equation A 1 (Argon used as an example, the same format is used for the other gases).

Table 1: Table of mole ratios of air and spike as well as volumes of gases in air standard.

	^{36}Ar	^{40}Ar	^{78}Kr	^{84}Kr	^{132}Xe	^{136}Xe
Mole ratio of Air	0.0033	0.996	0.0035	0.569	0.2689	0.0889
Mole ratio of spike	0.997	0	0.689	0.006	0	1

Volume of air in Standard	**Total (cc)**	**Ar**	**Kr**	**Xe**
$\mathbf{V_{aliqout(cc)}}$	0.471	0.0044	3.08E-07	1.44E-08

Equation A 1:

$$R = \frac{^{36}\mathrm{Ar}}{^{40}\mathrm{Ar}} = \frac{^{36}\mathrm{X}_{at} \cdot \mathrm{V}_{at(Ar)} + ^{36}\mathrm{X}_{(t)} \cdot \mathrm{V}_{t(Ar)}}{^{40}\mathrm{X}_{at} \cdot \mathrm{V}_{at(Ar)} + ^{40}\mathrm{X}_{(t)} \cdot \mathrm{V}_{t(Ar)}}$$

Where ^{36}Ar is the spike gas and ^{40}Ar is the dominant isotope in air. The value of R is ^{36}Ar/^{40}Ar measured using the mass spectrometer, $^{40}X_{(t)}$ is the mole fraction of spike isotope, $^{36}X_{at}$ is the mole fraction of ^{36}Ar in the sample, $V_{t(Ar)}$ is the volume of Ar in the spike at STP and $V_{at(Ar)}$ is the volume of Ar in the sample STP.

To determine the amount of gas in a standard Equation A 1 is rearranged to give Equation A 2. Each standard or sample uses a small amount of $V_{t(Ar)}$ and the decrease in spike volume is corrected for each sample. Spike extractions are recorded and $V_{t(Ar)}$ is plotted vs. the number of spike extractions to develop a continually variable calibration line to determine the most accurate $V_{t(Ar)}$ for a given sample run (Figure A 2).

Equation A 2:

$$\mathrm{V}_{t(Ar)} = \mathrm{V}_{at(Ar)}\left(\frac{^{36}\mathrm{Ar}_{at} - \mathrm{R}\cdot ^{40}\mathrm{X}_{at}}{R\cdot ^{40}\mathrm{X}_{t} - ^{36}X_{t}}\right)$$

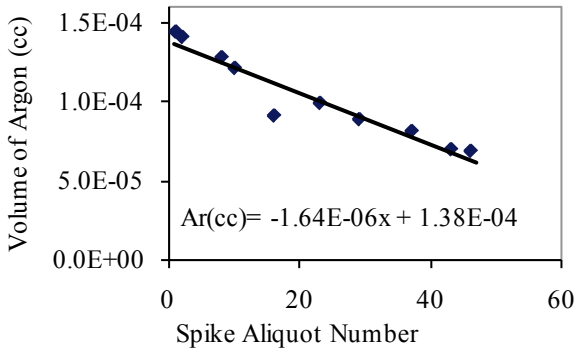

Figure A 2: Volume of argon in spike vs. spike aliquot number. Over time amount of spike in aliquot decreases as more and more aliquots are removed.

To determine the amount of gas in a sample the equation is arranged slightly differently (Equation A 3).

Equation A 3:
$$V_{at(Ar)} = V_{t(Ar)}\left(\frac{{}^{36}Ar_t - R\cdot{}^{40}X_t}{R\cdot{}^{40}X_{at} - {}^{36}X_{at}}\right)$$

Blank Correction for Ice Samples

The line black is less than 1% for each isotope. The extraction process for ice samples involves a glass extraction vessel which has a rubber gasket which does not hold vacuum as well as the metal fittings used with water samples. This results in an appreciable background for ice samples that must be corrected. (For water samples the extraction background is negligible, as extraction takes place through pipes with metal fittings and does not take as long.) For ice samples the blank has an atmospheric composition and was determined the same way as other samples. The correction is made using Equation A 4, where $C_{cc/cc}$ is the concentration of gas in the ice, V_{gas} is the measured volume of gas from a sample, V_{blank} is the measured volume of gas in a blank, V_{ice} is the volume of ice determined by weighing the ice.

Equation A 4: $C_{cc/cc} = \frac{(V_{gas} - V_{blank})}{V_{ice}}$

To convert concentrations in cc/cc to ccSTP/cc Equation A 5 is used, where T_{STP} is 273.15 K and T_{Lab} is ~291.15 K.

Equation A 5: $C_{ccSTP/cc} = \frac{C_{cc/cc} \cdot T_{STP}}{T_{Lab}}$

Appendix B: NWT Water Samples Data

Legend:

Sampling Location Names are listed in this appendix give meaning to their location (this system is only used for the focus river and not other rivers or permafrost slumps).

Sample Number: SCW08-3-R (Location))Sampling)-(Sample Site)-(Sample Type)

Location

SC: Smith Creek

HC: Hodgson Creek

BFF: Little Fish Creek on Big fish river

GP: Gibson Creek

WS: White Sand

GR: Gayna River

CC: Canyon Creek

Sampling

F07: Fall 2007 Sampling (August and September)

W08: Winter 2008

J08: June 2008 Sampling

F08: Fall 2008 Sampling

Sample Site

#'s sequentially moving upstream. Decimal values are given for multiple samples at same location.

Sample Type

R: river sample

S: spring

ST: thermal spring

P: pool

T: tributary

SC: side channel

Sample Information

SO_4^{2-} : Concentrations with [1] were determined from the concentration of elemental sulphur.

xxx indicates samples below detection limit.

Detection Limits:

B: 0.012 ppm, Ba: 0.00038 ppm, Ca: 0.0093 ppm, Cu: 0.0011 ppm, Fe: 0.0073 ppm, K: 0.026 ppm, Mg: 0.019ppm, Mn: 0.00043 ppm, Na: 0.030 ppm, Ni: 0.0073ppm, S: 0.013ppm, Si: 0.031 ppm, Sr: 0.00032 ppm, Zn: 0.0035 ppm, F^-:0.0876 ppm, Cl^-:0.1195 ppm, NO_2^{2-}: 0.1098 ppm, Br^-: 0.0629 ppm, NO_3^-: 0.0319 ppm, PO_4^{3-}: 0.0628 ppm, SO_4^{2-}: 0.0119 ppm HCO_3^{1-}: 0.1 ppm

Creek and Sampling	Description	Date	Latitude (N)	Longitude (W)	pH	T °C	Cond. µS/Cm
Smith Creek							
SCW08-3.1-HS-P	Groundwater pool by river	03/03/2008	63°10.806'	123°20.125'	7.25	13.8	3120
SCW08-3.2-HS-P	Upper groundwater pool	03/03/2008	63° 10.822'	123° 20.170'	7.53	7.9	3880
SCW08-3-R	Creek down stream of springs	03/03/2008	63° 10.792'	123° 20.099'	7.40	3.2	1496
SCW08-4-R	Creek where it appears out of ice (upstream)	03/03/2008	63°10.883'	123°20.204'	7.14	1.9	887
SCW08-4.1-HS	Spring where open water starts	03/03/2008	63°10.875'	123°20.178'	7.13	10.3	2540
SCW08-4.2-HS	Groundwater spring	06/03/2008	63°10.875'	123°20.178'	7.35	5.5	2120
SCW08-1-R	Creek close to where it enters the Mackenzie	06/03/2008	63°10.132'	123°20.245'	8.01	1.5	1535
SCF07-4-R	Creek	24/08/2007	63° 10.893'	123° 20.199'	7.96	--	--
SCF07-3-R	Creek	24/08/2007	63° 10.795'	123° 20.116'	7.83	--	--
SCJ08-6-R	Creek	24/06/2008	63°10.851'	123°17.549'	7.93	--	307
SCJ08-2-R	Creek	24/06/2008	63°10.435'	123°20.288'	8.07	--	629
SCJ08-3-R	Creek	24/06/2008	63°10.796'	123°20.113'	7.78	--	802
SCJ08-1-R	Creek	24/06/2008	63°10.154'	123°20.230'		--	
SCJ08-4-R	Creek	24/06/2008	63°10.882'	123°20.288'	8.12	--	346
SCJ08-5-R	Creek	24/06/2008	63°10.907'	123°19.10'	7.95	--	310
SCJ08-3-R	Creek	24/06/2008	63°10.812'	123°20.105'	8.03	--	535
Whitesand Creek							
WSW08-3-S	Groundwater spring	03/03/2008	63°37.157'	123°36.426'	7.62	3.8	466
WSW08-3-R	Creek near groundwater spring	03/03/2008	63°37.157'	123°36.426'	7.76	--	463
WSJ08-5-R	Downstream creek	25/06/2008	63°33.161'	123°39.381'	8.22	--	369
WSJ08-3.1-R	Creek	25/06/2008	63°37.144'	123°36.411'	8.07	--	362
WSJ08-4-R	Creek	25/06/2008	63° 37.099'	123° 36.755'	8.25	--	368
WSJ08-3.4-R	Creek	25/06/2008	63° 37.161'	123° 36.381'	8.19	--	321
WSJ08-1.1-R	Creek	25/06/2008	63°37.345	123°35.452'	8.16	--	375
WSJ08-3.2-R	Creek	25/06/2008	63°37.142'	123°36.408'	8.12	--	325
WSF07-3.3-R	Creek	25/06/2008	63°37.142'	123°36.415'	8.12	--	370

Creek and Sampling	Description	Date	Latitude (N)	Longitude (W)	pH	T °C	Cond. µS/Cm
Hodgson Creek							
HCW08-2-S	Groundwater spring	03/03/2008	63°20.027'	123°26.536'	7.54	2.2	535
HCF07-2-R	Creek	24/08/2007	63° 20.337'	123° 25.889'	7.99	--	
HCJ08-3-R	Creek	26/06/2008	63°20.377'	123°25.877'	8.28	--	405
HCJ08-2-R	Creek	26/06/2008	63°20.313'	123°25.703'	8.21	--	402
HCJ08-1-R	Creek	26/06/2008	63°20.255'	123° 25.874'	8.27	--	401
Canyon Creek							
CCW08-3.1-R	Ice with creek water overflowing	04/03/2008	65°14.696'	126°29.666'	7.67	0.0	309
CCW08-3.2-R	Ice with creek water overflowing	04/03/2008	65°14.696'	126°29.666'	7.55	0.1	876
CCW08-1-R	Creek (below winter road)	04/03/2008	65°13.196'	126°31.715'	7.40	0.5	903
CCW08-1-S	Groundwater spring	04/03/2008	65°13.226'	126°31.700'	7.40	0.5	953
CCW08-6-R	Creek at base of canyon	04/03/2008	65°15.490'	126°27.772'	8.52	0.1	809
CCF07-2-R	Creek	27/08/2007	65° 15.013'	126° 28.876'	8.03	--	--
CCF07-3-R	Creek	28/08/2007	65° 15.219'	126°28.258'	7.61	--	--
CCJ08-7-R	Creek above falls	30/06/2008	65°15.509'	126°27.743'	8.24	--	629
CCJ08-5-R	Creek	30/06/2008	65°15.217'	126°28.260'	8.24	--	578
CCJ08-4-R	Creek	30/06/2008	65°15.013'	126°28.882'	8.18	--	605
CCJ08-9-R	Creek	01/07/2008	65°15.196'	126°31.715'	8.29	--	659
CCJ08-2-R	Creek	01/07/2008	65°14.601'	126°31.341'	8.16	--	675
CCJ08-6-R	Creek	30/06/2008	65°15.462'	126°27.859'	8.18	--	567
CCJ08-8-R	Creek	30/06/2008	65°14.721'	126°26.714'	8.40	--	640
Gibson Creek							
GPW08-5-HS-P	Groundwater pool	04/03/2008	65°42.475'	127°53.147'	7.33	8.2	1607
GPW08-3-R	Creek (downstream)	04/03/2008	65°42.526'	127°53.389'	7.94	0.9	871
GPW08-4-R	Creek (upstream)	04/03/2008	65°42.810'	127°53.680'	8.03	2.1	690
GPF07-1-R	Creek	29/08/2007	65° 41.989'	127°53.719'	7.86	--	--
GPJ08-2.1-R	Creek	01/07/2008	65°42.557'	127°53.421'	7.87	--	551
GPJ08-2.2-R	Creek	01/07/2008	65°42.470'	127°53.310'	7.61	--	570
GPJ08-2.3-R	Creek	01/07/2008	65°42.516'	127°53.368'	7.86	--	574

Creek and Sampling	Description	Date	Latitude (N)	Longitude (W)	pH	T °C	Cond. µS/Cm
Gayna River							
GRW08-1-S	Groundwater spring	06/03/2008	65° 17.837'	129° 21.413'	7.47	3.1	519
GRW08-1-R	River	06/03/2008	65° 17.837'	129° 21.413'	8.33	0.5	456
GRF07-1-R	River	04/09/2007	65°17.861'	129°21.376'	7.72	--	--
GRF07-2-R	River	04/09/2007	65°17.464'	129°21.481'	7.80	--	--
Little Fish River							
BFF08-9-R	Creek	20/09/2008	68°17.022'	136°22.392'	8.52	1.0	1165
BFF08-5-R	Creek	20/09/2008	68° 17.385'	136° 22.183'	8.56	6.2	2310
BFF08-6-HS	Warm groundwater spring	20/09/2008	68° 17.346'	136° 22.234'	7.53	15.9	4770
BFF08-6-R	Creek	20/09/2008	68° 17.345'	136° 22.239'	8.47	6.5	2330
BFF08-7-R	Creek	20/09/2008	68° 17.324'	136° 22.207'	8.43	6.2	2230
BFF08-7-HS	Warm groundwater spring	20/09/2008	68° 17.326'	136° 22.212'	7.38	8.6	4210
BFF08-3-R	Creek	20/09/2008	68°18.097'	136°21.393'	8.56	6.9	2300
BFF08-9-HS	Warm groundwater spring	20/09/2008	68°17.022'	136°22.392'	7.36	15.0	4430
BFF08-9-HS	Warm groundwater spring	20/09/2008	68°17.022'	136°22.392'	7.45	16.0	4550
BFF08-8.1-S	Cool groundwater spring	20/09/2008	68° 17.054'	136° 22.228'	--	9.4	2120
BFF08-8.2-S	Warm groundwater spring	20/09/2008	68° 17.050'	136° 22.262'	--	15.1	4190
BFF08-8.3-S	Warm groundwater spring	20/09/2008	68° 16.998'	136° 22.354'	--	15.2	4250
BFF08-10-T	Creek: Tributary upstream	20/09/2008	68° 16.840'	136° 23.862'	8.62	2.1	977
BFF08-10-R	Creek: Upstream	20/09/2008	68° 16.843'	136° 23.856'	8.67	4.1	3740
BFF08-1-R	Creek (downstream)	20/09/2008	68° 19.514'	136° 14.900'	8.43	--	--
BFF08-3-R	Creek	22/09/2008	68° 18.082'	136° 21.410'	8.52	3.0	1258
BFF08-9-HS	Creek	22/09/2008	68°17.022'	136°22.392'	8.09	1.8	981
BFF08-5-R	Creek	22/09/2008	68° 17.379'	136° 22.184'	--	--	lab
BFF08-1-R	Creek	22/09/2008	68° 19.514'	136° 14.900'	8.32	3.0	1295
BFF08-4-R	Pool by river	22/09/2008	68° 17.652'	136° 21.568'	8.13	5.7	2000
BFF08-4-P	River by above pool	22/09/2008	68° 17.652'	136° 21.568'	8.42	3.4	1300
BFF08-2-R	Creek	22/09/2008	68° 18.106'	136° 21.225'	8.09	4.1	1840

Creek and Sampling	Description	Date	Latitude (N)	Longitude (W)	pH	T °C	Cond. µS/Cm
Other Creeks and Rivers							
Rat River		23/09/2008	67° 49.864'	136° 16.114'	8.28	2.7	511
Rat River		23/09/2008	67° 46.992'	136° 19.163'	8.29	2.5	485
Rat River		23/09/2008	67° 43.706'	136° 15.650'	8.47	2.4	485
Rat River		23/09/2008	67° 43.692'	136° 15.635'	8.47	2.5	491
Rat River		23/09/2008	67° 43.691'	136° 15.634'	8.22	4.0	498
Bluefish Creek		29/06/2008	63°51.133'	126°05.430'	8.15	--	343
Cacajou River		01/09/2007	64°42.024'	126°57.895'	7.89	--	
Chick Creek		02/07/2008	65°51.750'	128°08.079'	7.94	--	396
Chick Creek		02/07/2008	65°51.200'	128°08.128'	8.13	--	393
Chick Creek		02/07/2008	65°51.314'	128°07.987'	8.02	--	393
Dam Creek		26/06/2008	63°47.431'	123°47.809'	7.75	--	252
Dam Creek		02/07/2008	63°47.750'	123°57.976'	7.58	--	258
Dam Creek		26/07/2008	63°47.419'	123°57.626'	7.80	--	251
Elliot Creek		02/07/2008	65°31.353'	127°37.092'	7.89	--	997
Elliot Creek		02/07/2008	65°31.271'	127°37.069'	7.90	--	1006
Elliot Creek		02/07/2008	65°31.432'	127°37.132'	7.99	--	995
Elliot Creek Reach 1		29/08/2007	65°31.435'	127°37.123'	7.90	--	
Francis Creek		01/07/2008	65°12.234'	126°27.431'	8.06	--	838
Francis Creek			65°12.324'	126°27.379'	8.22	--	843
Heleva Creek		01/07/2008	65°11.919'	126°24.370'	8.24	--	554
Heleva Creek		01/07/2008	65°12.087'	126°24.156'	8.23	--	574
Helleva Creek		01/07/2008	65°12.017'	126°24.325'	8.12	--	579
Jungle Ridge		02/07/2008	65°03.654'	126°03.615'	8.06	--	934
Jungle Ridge		02/07/2008	65°03.722'	126°03.772'	7.71	--	934
Jungle Ridge Creek		28/08/2007	65° 02.887'	126°01.238'	7.95	--	
Jungle Ridge Creek		30/06/2008	--	--	8.08	--	924
Little Keel River		01/09/2007	64°42.566'	126°58.207'	7.94	--	
Trout Creek		01/09/2007	64°11.691'	126°14.285'	7.80	--	

Creek and Sampling	TDS	$\delta^{2}H$	$\delta^{18}O$	B	Ba	Ca	Cu	Fe	K	Mg	Mn	Na	Ni	S	Si	Sr	Zn
	ppm	(VSMOW)		Concentrations in ppm													
Smith Creek																	
SCW08-3.1-HS-P	2356	-179.0	-23.0	0.12	0.01	261	xxx	0.1	7.1	82	0.1	400	xxx	263	5.5	12.1	xxx
SCW08-3.2-HS-P	2817	-178.5	-23.1	0.14	0.02	324	xxx	xxx	8.3	99	0.1	472	xxx	336	5.7	12.2	xxx
SCW08-3-R	1143	-171.6	-21.5	xxx	0.06	149	xxx	xxx	4.1	51	0.2	134	xxx	115	4.8	7.4	xxx
SCW08-4-R	1191	-170.8	-21.5	xxx	0.05	155	xxx	0.1	4.2	52	0.2	141	xxx	122	4.9	7.5	xxx
SCW08-4.1-HS	1874	-181.5	-23.2	0.11	0.02	226	xxx	0.2	5.8	68	0.1	283	xxx	222	5.6	10.3	xxx
SCW08-4.2-HS	1215	-171.6	-21.6	xxx	0.05	157	xxx	0.1	3.8	50	0.2	150	xxx	124	4.7	7.2	xxx
SCW08-1-R	1166	-172.5	-21.5	xxx	0.05	141	xxx	xxx	3.7	48	0.1	143	xxx	109	4.7	7.0	xxx
SCF07-4-R	367	-165.6	-20.8	xxx	0.10	78	xxx	xxx	1.0	21	xxx	7.0	xxx	13	2.9	1.9	xxx
SCF07-3-R	1362	-173.2	-22.0	xxx	0.06	172	xxx	xxx	3.8	50	xxx	207	xxx	146	4.2	7.0	xxx
SCJ08-6-R	257	-168.9	-21.0	xxx	0.10	52	xxx	0.0	0.3	12	xxx	1.0	xxx	3	1.8	0.4	xxx
SCJ08-2-R	465	-169.5	-21.4	0.02	0.09	74	0.0	0.0	1.3	20	0.0	39.9	0.0	29	2.5	2.1	xxx
SCJ08-3-R	589	-172.5	-21.4	0.02	0.08	86	xxx	0.0	1.6	24	xxx	61.2	xxx	45	2.8	2.8	xxx
SCJ08-1-R	287	-171.6	-21.4	0.01	0.08	74	xxx	0.0	1.3	20	xxx	39.2	0.0	29	2.4	2.1	xxx
SCJ08-4-R	346	-167.2	-21.3	0.00	0.09	57	xxx	0.0	0.6	14	xxx	3.7	xxx	7	2.1	1.0	xxx
SCJ08-5-R	263	-166.3	-21.1	xxx	0.10	54	xxx	0.0	0.4	13	xxx	1.6	xxx	3	1.9	0.4	xxx
SCJ08-3-R	425	-169.7	-21.4	0.01	0.09	70	xxx	0.0	1.0	18	xxx	26.2	xxx	23	2.3	1.7	xxx
Whitesand Creek																	
WSW08-3-S	371	-174.3	-22.4	xxx	0.05	47	xxx	xxx	0.9	25	xxx	13.9	xxx	19	2.4	4.4	xxx
WSW08-3-R	375	-178.1	-22.4	xxx	0.05	47	xxx	xxx	0.9	25	xxx	13.4	xxx	18	2.4	4.5	xxx
WSJ08-5-R	313	-173.2	-20.9	xxx	0.08	54	0.0	xxx	0.8	18	xxx	4.9	xxx	8	1.9	1.8	xxx
WSJ08-3.1-R	297	-171.3	-21.2	0.00	0.08	57	0.0	0.0	0.7	16	xxx	3.5	xxx	7	1.8	1.3	0.0
WSJ08-4-R	328	-172.2	-21.0	0.01	0.09	57	0.0	0.0	0.8	19	0.0	4.6	xxx	9	1.9	1.8	0.0
WSJ08-3.4-R	293	-170.4	-20.6	0.00	0.09	60	0.0	0.0	0.7	15	xxx	0.8	xxx	4	1.7	0.1	xxx
WSJ08-1.1-R	315	-171.5	-20.9	0.00	0.08	56	0.0	xxx	0.8	19	xxx	4.8	xxx	9	1.9	1.8	xxx
WSJ08-3.2-R	288	-170.5	-21.5	xxx	0.09	67	0.0	0.0	0.4	12	xxx	0.6	xxx	2	1.6	0.1	xxx
WSF07-3.3-R	318	-170.0	-21.1	0.00	0.08	57	0.0	0.0	0.8	18	xxx	4.4	xxx	8	1.9	1.6	xxx

Creek and Sampling	TDS	$\delta^{2}H$	$\delta^{18}O$	B	Ba	Ca	Cu	Fe	K	Mg	Mn	Na	Ni	S	Si	Sr	Zn
	ppm	(VSMOW)		Concentrations in ppm													
Hodgson Creek																	
HCW08-2-S	428	-181.8	-23.1	xxx	0.04	67	xxx	xxx	1.0	28	xxx	4.4	xxx	25	2.4	2.8	xxx
HCF07-2-R	492	-170.7	-22.2	xxx	0.11	70	xxx	xxx	0.7	18	xxx	0.8	xxx	7	2.2	0.1	xxx
HCJ08-3-R	353	-174.1	-21.7	xxx	0.11	73	0.0	xxx	0.9	17	xxx	0.9	xxx	7	2.2	0.1	xxx
HCJ08-2-R	346	-173.1	-21.9	xxx	0.11	72	0.0	xxx	0.9	17	xxx	0.9	0.0	7	2.2	0.1	xxx
HCJ08-1-R	348	-169.9	-21.7	xxx	0.11	73	0.0	xxx	0.9	17	xxx	0.9	xxx	7	2.3	0.1	xxx
Canyon Creek																	
CCW08-3.1-R	749	-179.2	-22.7	xxx	0.07	124	xxx	xxx	2.2	44	xxx	6.6	xxx	86	2.4	2.6	xxx
CCW08-3.2-R	751	-176.8	-22.8	xxx	0.07	136	xxx	xxx	1.8	44	xxx	6.6	xxx	94	2.4	2.6	xxx
CCW08-1-R	800	-175.8	-22.0			152		xxx	2.9	62	0	12.77		117	2.4	4.43	xxx
CCW08-1-S	811	-176.8	-22.0	xxx	0.07	140	xxx	xxx	1.5	51	xxx	9.3	xxx	111	2.1	3.6	xxx
CCW08-6-R	695	-174.1	-22.6	xxx	xxx	120	xxx	xxx	1.3	42	xxx	4.8	xxx	81	2.2	2.9	xxx
CCF07-2-R	748	-173.2	-22.3	xxx	xxx	108	xxx	xxx	1.3	41	xxx	5.1	xxx	73	2.2	2.4	xxx
CCF07-3-R	685	-174.9	-22.3	xxx	xxx	116	xxx	xxx	1.2	40	xxx	4.3	xxx	103	2.2	2.3	xxx
CCJ08-7-R	484	-166.9	-21.6	0.00	0.05	85	xxx	xxx	1.1	28	xxx	2.9	0.0	39	2.0	1.7	xxx
CCJ08-5-R	482	-167.2	-21.0	0.00	0.05	89	xxx	xxx	1.2	29	xxx	3.1	0.0	42	2.1	1.7	xxx
CCJ08-4-R	519	-169.9	-21.2	0.00	0.05	93	0.0	xxx	1.2	30	xxx	3.7	0.0	48	2.1	1.8	xxx
CCJ08-9-R	542	-167.8	-20.8	0.01	0.06	93	xxx	xxx	1.6	36	xxx	7.9	0.0	62	2.2	2.7	xxx
CCJ08-2-R	588	-159.9	-19.5	0.01	0.07	90	xxx	xxx	1.9	40	xxx	5.6	0.0	69	2.6	4.0	xxx
CCJ08-6-R	572	-169.4	-21.2	0.00	0.05	98	0.0	xxx	1.3	33	xxx	4.4	0.0	55	2.0	2.0	xxx
CCJ08-8-R	499	-171.8	-21.3	0.00	0.05	87	0.0	xxx	1.1	28	xxx	2.9	0.0	40	2.1	1.6	xxx
Gibson Creek																	
GPW08-5-HS-P	1769	-188.5	-24.2	0.06	xxx	316	xxx	0.1	2.1	103	0.1	15.5	xxx	348	3.8	4.4	xxx
GPW08-3-R	745	-182.8	-23.3	xxx	xxx	135	xxx	xxx	1.5	46	xxx	5.3	xxx	113	2.8	1.5	xxx
GPW08-4-R	616	-179.7	-23.3	xxx	xxx	133	xxx	xxx	1.1	35	xxx	3.6	xxx	97	2.6	1.0	xxx
GPF07-1-R	1075	-184.7	-23.2	xxx	xxx	188	xxx	xxx	1.5	58	xxx	8.8	xxx	179	2.9	2.2	xxx
GPJ08-2.1-R	415	-165.1	-21.8	0.01	0.06	79	xxx	0.0	0.9	27	xxx	3.1	xxx	56	2.0	0.8	xxx
GPJ08-2.2-R	438	-172.7	-21.8	0.02	0.06	82	xxx	0.0	0.9	28	xxx	3.2	0.0	59	2.0	0.8	xxx
GPJ08-2.3-R	445	-162.8	-21.8	0.02	0.06	82	xxx	0.0	0.9	28	xxx	3.2	0.0	58	2.0	0.8	xxx

Creek and Sampling	TDS	$\delta^{2}H$	$\delta^{18}O$	B	Ba	Ca	Cu	Fe	K	Mg	Mn	Na	Ni	S	Si	Sr	Zn
	ppm	(VSMOW)		Concentrations in ppm													
Gayna River																	
GRW08-1-S	437	-174.5	-22.3	xxx	0.28	72	xxx	0.2	0.6	23	0.1	11.9	xxx	30	2.0	0.4	xxx
GRW08-1-R	422	-171.6	-21.7	xxx	0.09	65	xxx	xxx	0.9	22	xxx	3.9	xxx	38	2.5	0.4	xxx
GRF07-1-R	406	-168.1	-21.5	xxx	0.07	50	xxx	xxx	0.7	19	xxx	1.7	xxx	28	1.4	0.2	xxx
GRF07-2-R	345	-169.5	-21.6	xxx	0.07	49	xxx	xxx	0.7	19	xxx	1.6	xxx	28	1.4	0.1	xxx
Little Fish River																	
BFF08-9-R	1017	-164.9	-21.4	0.07	0.03	127	xxx	xxx	2.4	38	xxx	69.87	xxx	146	2.1	0.83	xxx
BFF08-5-R	1708	-160.5	-21.4	0.25	0.02	148	xxx	0.315	7.3	45	xxx	300.2	0.039	192	3.9	1.653	xxx
BFF08-6-HS	3012	-164.8	-21.4	0.66	0.03	77	xxx	0.013	20.3	27	xxx	848	xxx	163	8.7	3.022	0.068
BFF08-6-R	1749	-165.9	-21.9	0.26	0.02	154	xxx	xxx	7.6	47	xxx	317.3	xxx	196	3.9	1.7	xxx
BFF08-7-R	1682	-164.7	-21.2	0.24	0.02	153	xxx	xxx	7.0	47	xxx	288.8	xxx	195	3.7	1.629	xxx
BFF08-7-HS	2674	-165.3	-21.8	0.59	0.02	85	xxx	xxx	17.3	27	xxx	754.6	xxx	156	7.4	2.695	xxx
BFF08-3-R	1603	-162.7	-21.3	0.22	0.04	142	xxx	xxx	6.9	44	xxx	287.2	xxx	179	3.5	1.592	xxx
BFF08-9-HS	2851	-162.1	-21.8	0.59	0.05	118	xxx	xxx	18.1	30	xxx	802.2	xxx	169	8.1	3.064	xxx
BFF08-9-HS	2989	-167.6	-21.8	0.63	0.03	107	xxx	xxx	19.6	31	xxx	882	xxx	179	8.6	3.214	xxx
BFF08-8.1-S	1534	-167.8	-21.7	0.26	0.02	114	xxx	xxx	8.0	27	xxx	310.2	0.013	128	4.9	1.451	xxx
BFF08-8.2-S		--	--	--	--	--	--	--	--	--	--	--	--	--	--	--	--
BFF08-8.3-S		--	--	--	--	--	--	--	--	--	--	--	--	--	--	--	--
BFF08-10-T	846	-160.0	-21.2	0.03	0.03	128	xxx	xxx	1.7	56	xxx	7.467	xxx	176	1.6	0.364	0.008
BFF08-10-R	1103	-163.1	-21.2	0.04	0.02	180	xxx	0.076	1.4	57	xxx	34.26	xxx	213	1.5	1.027	xxx
BFF08-1-R		--	--	--	--	--	--	--	--	--	--	--	--	--	--	--	--
BFF08-3-R	1043	-158.7	-21.2	0.09	0.03	123	xxx	xxx	2.9	44	0.019	91.78	0.027	165	2.3	0.857	0.005
BFF08-9-HS	855	-159.6	-21.2	0.04	0.03	130	xxx	xxx	1.3	48	0.024	23.04	xxx	170	1.6	0.691	0.017
BFF08-5-R	1021	-160.6	-21.3	0.09	0.03	129	xxx	xxx	2.8	46	0.019	90.83	0.009	170	2.2	0.879	xxx
BFF08-1-R	1005	-160.0	-21.2	0.11	0.02	108	xxx	xxx	3.2	38	0.017	114.4	0.035	152	2.2	0.864	0.002
BFF08-4-R	1323	-163.3	-21.4	0.21	0.02	113	xxx	xxx	6.5	34	xxx	221.6	xxx	167	3.1	1.367	xxx
BFF08-4-P	1068	-157.2	-21.2	0.09	0.03	131	xxx	xxx	2.9	46	0.019	97.66	0.031	172	2.3	0.903	0.006
BFF08-2-R	1455	-162.0	-21.3	0.18	0.02	130	xxx	xxx	5.9	38	xxx	225.8	xxx	181	2.8	1.506	xxx

Creek and Sampling	TDS	$\delta^{2}H$	$\delta^{18}O$	B	Ba	Ca	Cu	Fe	K	Mg	Mn	Na	Ni	S	Si	Sr	Zn
	ppm	(VSMOW)		Concentrations in ppm													
Other Creeks and Rivers																	
Rat River	467	-165.4	-21.9	0.00	0.07	81	xxx	xxx	0.7	17	xxx	9.2	xxx	52	1.3	0.2	xxx
Rat River	445	-167.0	-21.9	0.00	0.06	76	xxx	xxx	0.6	16	0.0	9.1	xxx	46	1.0	0.2	xxx
Rat River	428	-167.8	-21.9	0.00	0.06	73	xxx	xxx	0.6	18	0.0	8.6	xxx	50	1.1	0.2	xxx
Rat River	433	-168.2	-22.0	0.00	0.05	75	xxx	xxx	0.7	17	0.0	8.6	xxx	50	1.0	0.2	xxx
Rat River	458	-162.9	-21.9	0.00	0.06	79	xxx	xxx	0.8	16	xxx	8.5	0.0	47	1.4	0.2	xxx
Bluefish Creek	287	--	--	xxx	0.07	56	xxx	xxx	0.3	17	xxx	0.4	0.0	1	1.6	0.7	xxx
Cacajou River	339	--	--	xxx	0.12	40	xxx	xxx	0.6	18	xxx	16.5	xxx	12	1.2	0.3	xxx
Chick Creek	332	--	--	xxx	0.08	69	0.0	0.0	0.7	16	xxx	2.0	xxx	11	1.3	0.1	xxx
Chick Creek	334	--	--	xxx	0.08	69	0.0	0.0	0.7	16	xxx	2.1	xxx	11	1.4	0.1	xxx
Chick Creek	321	--	--	xxx	0.08	68	0.0	0.0	0.7	16	xxx	2.0	0.0	11	1.3	0.1	xxx
Dam Creek	209	--	--	xxx	0.05	46	xxx	0.0	0.5	11	xxx	0.9	xxx	4	1.6	0.1	xxx
Dam Creek	212	--	--	xxx	0.06	47	0.0	0.1	0.6	11	xxx	0.9	xxx	4	1.6	0.1	xxx
Dam Creek	209	--	--	xxx	0.06	45	0.0	0.1	0.6	10	xxx	0.9	0.0	4	1.5	0.1	xxx
Elliot Creek	980	--	--	0.07	0.02	214	xxx	0.01	0.7	21	xxx	8.2	0.0	167	1.5	2.0	xxx
Elliot Creek	1051	--	--	0.06	0.02	206	xxx	xxx	0.7	20	xxx	7.9	xxx	162	1.5	2.0	xxx
Elliot Creek	958	--	--	0.06	0.02	207	xxx	0.02	0.7	21	xxx	7.9	xxx	163	1.5	2.0	xxx
Elliot Creek Reach 1		--	--	xxx	xxx	284	xxx	xxx	0.9	29	xxx	5.7	xxx	235	1.8	3.1	xxx
Francis Creek	696	--	--	0.02	0.04	125	xxx	xxx	1.6	44	xxx	9.1	0.0	104	2.3	0.9	xxx
Francis Creek	778	--	--	0.02	0.04	123	xxx	xxx	1.7	44	xxx	9.3	xxx	104	2.3	0.9	xxx
Heleva Creek	495	--	--	0.02	0.06	91	0.0	0.0	1.1	24	0.0	11.0	0.0	44	2.4	0.3	xxx
Heleva Creek	597	--	--	0.02	0.06	91	0.0	xxx	1.1	24	xxx	10.8	xxx	44	2.4	0.3	xxx
Helleva Creek	474	--	--	0.01	0.06	91	0.0	xxx	1.1	24	xxx	11.0	0.0	44	2.4	0.3	xxx
Jungle Ridge	742	--	--	0.02	0.09	113	0.0	0.0	1.1	32	0.0	61.5	0.0	67	1.9	1.3	xxx
Jungle Ridge	717	--	--	0.01	0.09	112	0.0	0.0	1.1	32	xxx	60.0	xxx	66	1.9	1.3	0.0
Jungle Ridge Creek	1049	--	--			143		xxx	1.7	45	0	105.5		85	2.0	2.1	xxx
Jungle Ridge Creek	731	--	--	0.01	0.09	113	0.0	0.0	1.1	32	xxx	60.5	0.0	68	2.0	1.3	xxx
Little Keel River	409	--	--	xxx	0.11	40	xxx	xxx	0.5	17	xxx	31.1	xxx	9	1.0	0.4	xxx
Trout Creek	264	--	--	xxx	0.09	37	xxx	xxx	0.6	13	xxx	0.6	xxx	19	1.2	0.3	xxx

Creek and Sampling	F^-	Cl^-	NO_2^{2-}	Br^-	NO^{3-}	PO_4^{3-}	SO_4^{2-}	HCO_3^{1-}	DOC	$\delta^{13}C$ DOC	$\delta^{13}C$ DIC	pCO_2	$SI_{Calcite}$	SI_{Gypsum}
									ppm	vpdb	vpdb			
Smith Creek														
SCW08-3.1-HS-P	xxx	560	xxx	xxx	xxx	xxx	790[1]	238	1.5	-26.1	-7.8	1.0E-02	0.12	-0.535
SCW08-3.2-HS-P	xxx	651	xxx	xxx	xxx	xxx	1008[1]	237	1.2	-26.5	-6.8	4.8E-03	0.37	-0.381
SCW08-3-R	xxx	173	xxx	xxx	xxx	xxx	346[1]	274	10.0	-26.5	-8.8	7.7E-03	0.06	-0.949
SCW08-4-R	xxx	190	xxx	xxx	xxx	xxx	385	250	9.0	-26.6	-9.0	1.3E-02	-0.26	-0.86
SCW08-4.1-HS	xxx	348	xxx	xxx	xxx	xxx	667[1]	258	1.2	-26.1	-8.1	1.4E-02	-0.03	-0.643
SCW08-4.2-HS	xxx	189	xxx	xxx	xxx	xxx	380	273	11.0	-26.9	-8.8	8.8E-03	0.05	-0.87
SCW08-1-R	xxx	187	xxx	xxx	xxx	xxx	347	284	6.6	-26.8	-8.1	1.9E-03	0.62	-0.93
SCF07-4-R	xxx	5	xxx	xxx	xxx	xxx	38	213	10.3	--	--	2.8E-03	0.21	-1.914
SCF07-3-R	xxx	280	xxx	xxx	xxx	xxx	445	193	5.5	--	--	2.0E-03	0.39	-0.792
SCJ08-6-R	xxx	0	xxx	xxx	xxx	xxx	7	182	15.8	--	--	1.6E-03	0.18	-2.74
SCJ08-2-R	xxx	47	xxx	xxx	xxx	xxx	82	196	14.5	--	--	1.2E-03	0.43	-1.631
SCJ08-3-R	xxx	85	xxx	xxx	xxx	xxx	135	191	13.6	--	--	2.4E-03	0.16	-1.399
SCJ08-1-R	xxx	55	xxx	xxx	xxx	xxx	92		14.5	--				
SCJ08-4-R	xxx	2	xxx	xxx	xxx	xxx	21	244	15.4	--	--	1.4E-03	0.51	-2.259
SCJ08-5-R	xxx	0	xxx	xxx	xxx	xxx	10	182	16.8	--	--	1.6E-03	0.21	-2.578
SCJ08-3-R	xxx	35	xxx	xxx	xxx	xxx	69	201	15.3	--	--	1.4E-03	0.30	-1.7
Whitesand Creek														
WSW08-3-S	xxx	7	xxx	xxx	xxx	xxx	53	216	2.1	-26.2	-8.4	3.9E-03	-0.16	-1.963
WSW08-3-R	xxx	7	xxx	xxx	xxx	xxx	53	222	1.5	-25.8	-8.2	2.9E-03	0.01	-1.967
WSJ08-5-R	xxx	2.0	xxx	xxx	xxx	xxx	25	203	8.3	--	--	9.2E-04	0.50	-2.208
WSJ08-3.1-R	xxx	1.6	xxx	xxx	xxx	xxx	19	196	9.3	--	--	1.3E-03	0.37	-2.298
WSJ08-4-R	xxx	2.2	xxx	xxx	xxx	xxx	25	216	8.3	--	--	9.1E-04	0.58	-2.194
WSJ08-3.4-R	xxx	0.4	xxx	xxx	xxx	xxx	11	203	11.7	--	--	9.9E-04	0.53	-2.511
WSJ08-1.1-R	xxx	2.0	xxx	xxx	xxx	xxx	25	203	7.7	--	--	1.1E-03	0.46	-2.197
WSJ08-3.2-R	xxx	0.3	xxx	xxx	xxx	xxx	4	202	13.8	--	--	1.2E-03	0.51	-2.902
WSF07-3.3-R	xxx	1.9	xxx	xxx	xxx	xxx	24	208	7.5	--	--	1.2E-03	0.44	-2.206

Creek and Sampling	F^-	Cl^-	NO_2^{2-}	Br^-	NO^{3-}	PO_4^{3-}	SO_4^{2-}	HCO_3^{1-}	DOC	$\delta^{13}C$ DOC	$\delta^{13}C$ DIC	pCO_2	$SI_{Calcite}$	SI_{Gypsum}
									ppm	vpdb	vpdb			
Hodgson Creek														
HCW08-2-S	xxx	2.1	xxx	xxx	xxx	xxx	71	249	1.6	-25.8	-9.9	5.3E-03	-0.07	-1.719
HCF07-2-R	xxx	0.5	xxx	xxx	xxx	xxx	20	379	4.4	--	--	2.9E-03	0.63	-2.237
HCJ08-3-R	xxx	0.0	xxx	xxx	xxx	xxx	19	240	4.4	--	--	9.4E-04	0.75	-2.224
HCJ08-2-R	xxx	0.0	xxx	xxx	xxx	xxx	19	233	5.0	--	--	1.1E-03	0.67	-2.227
HCJ08-1-R	xxx	0.0	xxx	xxx	xxx	xxx	19	234	5.6	--	--	9.3E-04	0.73	-2.223
Canyon Creek														
CCW08-3.1-R	xxx	4.3	xxx	xxx	xxx	xxx	290	273	4.5	-26.8	-6.5	4.3E-03	0.31	-0.999
CCW08-3.2-R	xxx	3.3	xxx	xxx	xxx	xxx	291	263	3.2	-26.5	-6.4	5.2E-03	0.14	-0.953
CCW08-1-R	xxx	6.4	xxx	xxx	xxx	xxx	310	247	3.8	-27.1	-7.6	6.9E-03	0.00	-0.913
CCW08-1-S	xxx	6.2	xxx	xxx	xxx	xxx	348	249	2.9	-26.1	-7.4	7.0E-03	-0.04	-0.887
CCW08-6-R	xxx	3.3	xxx	xxx	xxx	xxx	250	269	1.8	-26.2	-6.4	5.5E-04	1.05	-1.054
CCF07-2-R	xxx	3.0	xxx	xxx	xxx	xxx	226	360	2.9	--	--	2.4E-03	0.74	-1.143
CCF07-3-R	xxx	2.8	xxx	xxx	xxx	xxx	217	300	2.7	--	--	5.4E-03	0.29	-1.124
CCJ08-7-R	xxx	1.4	xxx	xxx	xxx	xxx	123	239	6.8	--	--	1.0E-03	0.72	-1.426
CCJ08-5-R	xxx	1.7	xxx	xxx	xxx	xxx	134	221	6.0	--	--	9.3E-04	0.70	-1.376
CCJ08-4-R	xxx	1.7	xxx	xxx	xxx	xxx	153	232	6.0	--	--	1.1E-03	0.67	-1.313
CCJ08-9-R	xxx	2.7	xxx	xxx	xxx	xxx	181	215	5.3	--	--	8.0E-04	0.74	-1.258
CCJ08-2-R	xxx	3.0	xxx	xxx	xxx	xxx	227	214	4.3	--	--	1.1E-03	0.58	-1.191
CCJ08-6-R	xxx	1.9	xxx	xxx	xxx	xxx	204	226	6.1	--	--	1.1E-03	0.67	-1.191
CCJ08-8-R	xxx	1.4	xxx	xxx	xxx	xxx	128	246	4.8	--	--	7.1E-04	0.89	-1.405
Gibson Creek														
GPW08-5-HS-P	xxx	13.8	xxx	xxx	xxx	xxx	1127	184	1.7	-26.3	-7.7	6.1E-03	0.08	-0.286
GPW08-3-R	xxx	4.3	xxx	xxx	xxx	xxx	342	207	1.2	-27.7	-9.3	1.7E-03	0.42	-0.898
GPW08-4-R	xxx	2.5	xxx	xxx	xxx	xxx	226	211	1.5	-26.2	-10.0	1.4E-03	0.56	-1.043
GPF07-1-R	xxx	8.1	xxx	xxx	xxx	xxx	510	295	2.4	--	--	2.9E-03	0.64	-0.679
GPJ08-2.1-R	xxx	1.3	xxx	xxx	xxx	xxx	179	123	11.4	--	--	1.2E-03	0.03	-1.291
GPJ08-2.2-R	xxx	1.5	xxx	xxx	xxx	xxx	190	130	12.5	--	--	2.4E-03	-0.19	-1.259
GPJ08-2.3-R	xxx	1.5	xxx	xxx	xxx	xxx	193	134	12.4	--	--	1.4E-03	0.07	-1.254

Creek and Sampling	F^-	Cl^-	NO_2^{2-}	Br^-	NO^{3-}	PO_4^{3-}	SO_4^{2-}	HCO_3^{1-}	DOC	$\delta^{13}C$ DOC	$\delta^{13}C$ DIC	pCO_2	$SI_{Calcite}$	SI_{Gypsum}
									ppm	vpdb	vpdb			
Gayna River														
GRW08-1-S	xxx	1.1	xxx	xxx	xxx	xxx	90	235	4.3	-27.3	-12.8	5.9E-03	-0.13	-1.592
GRW08-1-R	xxx	5.4	xxx	xxx	xxx	xxx	166	156	2.3	-28.0	-7.6	5.2E-04	0.44	-1.378
GRF07-1-R	xxx	1.3	xxx	xxx	xxx	xxx	93	238	4.4	--	--	3.5E-03	0.01	-1.704
GRF07-2-R	xxx	1.2	xxx	xxx	xxx	xxx	95	176	10.3	--	--	2.1E-03	-0.04	-1.694
Little Fish River														
BFF08-9-R	xxx	75.4	xxx	xxx	0.5	xxx	483	219	6.0	-25.4	-5.0	4.4E-04	0.93	-0.821
BFF08-5-R	xxx	392	xxx	xxx	0.5	xxx	565	244	6.5	-24.9	-3.4	4.5E-04	1.10	-0.793
BFF08-6-HS	xxx	1182	xxx	xxx	xxx	xxx	495	351	6.0	-22.4	-2.8	8.0E-03	0.09	-1.213
BFF08-6-R	xxx	401	xxx	xxx	0.5	xxx	572	245	6.6	-24.4	-3.5	5.6E-04	1.04	-0.778
BFF08-7-R	xxx	365	xxx	xxx	0.5	xxx	571	244	6.5	-24.9	-3.9	6.1E-04	1.00	-0.774
BFF08-7-HS	xxx	983	xxx	xxx	0.7	xxx	467	330	6.2	-25.1	-2.7	9.9E-03	-0.14	-1.259
BFF08-3-R	xxx	360	xxx	xxx	0.6	xxx	519	238	6.3	-21.9	-3.0	4.4E-04	1.10	-0.833
BFF08-9-HS	xxx	1058	xxx	xxx	1.4	xxx	496	315	5.9	-23.1	-3.0	1.1E-02	0.05	-1.029
BFF08-9-HS	xxx	1112	xxx	xxx	xxx	xxx	498	326	6.0	-22.8	-6.9	8.9E-03	0.12	-1.08
BFF08-8.1-S	xxx	434	xxx	xxx	0.6	xxx	420	214	5.2	-24.2	-4.4	1.6E-02	-0.50	-0.98
BFF08-8.2-S	--	--	--	--	--	--	--	--	--	--	--	--	--	--
BFF08-8.3-S	--	--	--	--	--	--	--	--	--	--	--	--	--	--
BFF08-10-T	xxx	xxx	xxx	xxx	0.9	xxx	551	99	7.7	-27.0	-6.4	1.6E-04	0.70	-0.767
BFF08-10-R	xxx	xxx	xxx	xxx	0.8	xxx	628	200	6.7	-26.2	-4.3	2.8E-04	1.25	-0.637
BFF08-1-R	--	--	--	--	--	--	--	--	--	--	--			
BFF08-3-R	xxx	107	xxx	xxx	0.7	xxx	524	147	7.2	-26.4	-4.1	3.0E-04	0.77	-0.817
BFF08-9-HS	xxx	xxx	xxx	xxx	0.9	xxx	518	131	6.4	-26.9	-4.6	7.4E-04	0.32	-0.776
BFF08-5-R	xxx	102	xxx	xxx	0.6	xxx	529	117	7.9	-26.7	-4.2	8.5E-03	-0.77	-0.797
BFF08-1-R	xxx	126	xxx	xxx	0.6	xxx	469	143	8.0	-26.6	-3.3	4.7E-04	0.52	-0.899
BFF08-4-R	xxx	213	xxx	xxx	0.7	xxx	499	231	7.0	-25.9	-5.0	1.2E-03	0.58	-0.897
BFF08-4-P	xxx	107	xxx	xxx	0.6	xxx	524	155	7.6	-26.4	-3.9	4.0E-04	0.73	-0.798
BFF08-2-R	xxx	259	xxx	xxx	0.8	xxx	564	226	5.9	-25.5	-4.7	1.3E-03	0.55	-0.808

Creek and Sampling	F^-	Cl^-	NO_2^{2-}	Br^-	NO^{3-}	PO_4^{3-}	SO_4^{2-}	HCO_3^{1-}	DOC ppm	$\delta^{13}C$ DOC vpdb	$\delta^{13}C$ DIC vpdb	pCO_2	$SI_{Calcite}$	SI_{Gypsum}
Other Creeks and Rivers														
Rat River	xxx	3.4	xxx	xxx	xxx	xxx	156	199	5.6	-26.0	-8.4	7.6E-04	0.62	-1.326
Rat River	xxx	3.2	xxx	xxx	xxx	xxx	136	203	5.5	-25.6	-8.8	7.5E-04	0.62	-1.398
Rat River	xxx	2.8	xxx	xxx	xxx	xxx	144	181	6.6	-26.3	-8.6	4.4E-04	0.72	-1.392
Rat River	xxx	3.0	xxx	xxx	xxx	xxx	140	188	6.0	-25.9	-8.1	4.7E-04	-0.22	-2.311
Rat River	xxx	3.3	xxx	xxx	0.3	xxx	140	209	5.3	-25.8	-8.9	9.0E-04	0.59	-1.376
Bluefish Creek	xxx	xxx	xxx	xxx	xxx	xxx	2	209	5.2	--	--	1.1E-03	0.48	-3.275
Cacajou River	xxx	24.3	xxx	xxx	xxx	xxx	34	205	1.5	--	--	2.0E-03	0.05	-2.196
Chick Creek	xxx	xxx	xxx	xxx	xxx	xxx	30	212	11.3	--	--	1.8E-03	0.35	-2.041
Chick Creek	xxx	xxx	xxx	xxx	xxx	xxx	31	214	9.7	--	--	1.2E-03	0.53	-2.028
Chick Creek	xxx	xxx	xxx	xxx	xxx	xxx	31	201	10.2	--	--	1.5E-03	0.40	-2.03
Dam Creek	xxx	xxx	xxx	xxx	xxx	xxx	11	138	22.9	--	--	1.9E-03	-0.16	-2.577
Dam Creek	xxx	xxx	xxx	xxx	xxx	xxx	11	140	22.2	--	--	2.9E-03	-0.32	-2.57
Dam Creek	xxx	xxx	xxx	xxx	xxx	xxx	10	139	22.8	--	--	1.7E-03	-0.12	-2.623
Elliot Creek	xxx	xxx	xxx	xxx	xxx	xxx	610	123	15.8	--	--	1.1E-03	0.35	-0.536
Elliot Creek	xxx	xxx	xxx	xxx	xxx	xxx	607	205	15.6	--	--	1.9E-03	0.56	-0.555
Elliot Creek	xxx	xxx	xxx	xxx	xxx	xxx	571	148	14.0	--	--	1.1E-03	0.52	-0.569
Elliot Creek Reach 1	xxx	1.6	xxx	xxx	xxx	xxx	766	275	7.1	--	--	2.4E-03	0.78	-0.39
Francis Creek	xxx	2.0	xxx	xxx	xxx	xxx	298	213	6.1	--	--	1.3E-03	0.59	-0.983
Francis Creek	xxx	1.8	xxx	xxx	xxx	xxx	296	299	4.7	--	--	1.3E-03	0.88	-1.000
Heleva Creek	xxx	2.9	xxx	xxx	xxx	xxx	129	233	12.1	--	--	9.8E-04	0.74	-1.379
Heleva Creek	xxx	2.9	xxx	xxx	xxx	xxx	207	257	11.8	--	--	1.1E-03	0.74	-1.205
Helleva Creek	xxx	2.7	xxx	xxx	xxx	xxx	132	208	13.5	--	--	1.2E-03	0.57	-1.366
Jungle Ridge	xxx	86	xxx	xxx	xxx	xxx	197	249	12.7	--	--	1.6E-03	0.64	-1.179
Jungle Ridge	xxx	83	xxx	xxx	xxx	xxx	191	235	13.1	--	--	3.4E-03	0.27	-1.19
Jungle Ridge Creek	xxx	132	xxx	xxx	xxx	xxx	227	390	11.2	--	--	3.1E-03	0.79	-1.084
Jungle Ridge Creek	xxx	79	xxx	xxx	xxx	xxx	192	249	13.0	--	--	1.5E-03	0.66	-1.188
Little Keel River	xxx	49	xxx	xxx	xxx	xxx	28	242	2.0	--	--	2.1E-03	0.16	-2.292
Trout Creek	xxx	0.4	xxx	xxx	xxx	xxx	52	159	1.5	--	--	2.0E-03	-0.17	-2.017